Vol. 279, No. 1, July 1, 1993

ISSN 000

Special Issue

ANALYTICA CHIMICA ACTA

An international journal devoted to all branches of analytical chemistry

ANABIOTEC '92

Papers presented at the 4th International Symposium on Analytical Methods, Systems and Strategies in Biotechnology

Noordwijkerhout, The Netherlands
September 21–23, 1992

EDITORS

HARRY L. PARDUE (West Lafayette, IN, U.S.A.)
ALAN TOWNSHEND (Hull, Great Britain)
J.T. CLERC (Berne, Switzerland)
WILLEM E. VAN DER LINDEN (Enschede, The Netherlands)
PAUL J. WORSFOLD (Plymouth, Great Britain)

ELSEVIER

ANALYTICA CHIMICA ACTA

Scope. *Analytica Chimica Acta* publishes original papers, preliminary communications and reviews dealing with every aspect of modern analytical chemistry. Reviews are normally written by invitation of the editors, who welcome suggestions for subjects. Preliminary communications of important urgent work can be printed within four months of submission, if the authors are prepared to forego proofs.

Submission of Papers

Americas

Prof. Harry L. Pardue
Department of Chemistry
1393 BRWN Bldg, Purdue University
West Lafayette, IN 47907-1393
USA
Tel:(+1-317) 494 5320
Fax:(+1-317) 496 1200

Computer Techniques

Prof. J.T. Clerc
Universität Bern
Pharmazeutisches Institut
Baltzerstrasse 5, CH-3012 Bern
Switzerland
Tel:(+41-31) 654171
Fax:(+41-31) 654198

Other Papers

Prof. Alan Townshend
Department of Chemistry
The University
Hull HU6 7RX
Great Britain

Tel:(+44-482) 465027
Fax:(+44-482) 466410

Prof. Willem E. van der Linden
Laboratory for Chemical Analysis
Department of Chemical Technology
Twente University of Technology
P.O. Box 217, 7500 AE Enschede
The Netherlands
Tel:(+31-53) 892629
Fax:(+31-53) 356024

Prof. Paul Worsfold
Dept. of Environmental Sciences
University of Plymouth
Plymouth PL4 8AA
Great Britain

Tel:(+44-752) 233006
Fax:(+44-752) 233009

Submission of an article is understood to imply that the article is original and unpublished and is not being considered for publication elsewhere. *Anal. Chim. Acta* accepts papers in English only. There are no page charges. Manuscripts should conform in layout and style to the papers published in this issue. See inside back cover for "Information for Authors".

Publication. *Analytica Chimica Acta* appears in 14 volumes in 1993. The subscription price for 1993 (Vols. 267-280) is Dfl. 4214.00 plus Dfl. 462.00 (p.p.h.) (total approx. US$ 2597.75). *Vibrational Spectroscopy* appears in 2 volumes in 1993. The subscription price for *Vibrational Spectroscopy* (Vols. 4 and 5) is Dfl. 700.00 plus Dfl. 66.00 (p.p.h.) (total approx. US$ 407.50). The price of a combined subscription (*Anal. Chim. Acta* and *Vib. Spectrosc.*) is Dfl. 4592.00 plus Dfl. 528.00 (p.p.h.) (total approx. US$ 2844.50). All earlier volumes (Vols. 1-266) except Vols. 23 and 28 are available at Dfl. 259.50 (US$ 144.00), plus Dfl. 18.00 (US$ 10.00) p.p.h., per volume. The Dutch guilder price is definitive. The U.S. dollar price is subject to exchange-rate fluctuations and is given only as a guide. Subscriptions are accepted on a prepaid basis only, unless different terms have been previously agreed upon.
Our p.p.h. (postage, packing and handling) charge includes surface delivery of all issues, except to subscribers in the U.S.A., Canada, Australia, New Zealand, China, India, Israel, South Africa, Malaysia, Thailand, Singapore, South Korea, Taiwan, Pakistan, Hong Kong, Brazil, Argentina and Mexico, who receive all issues by air delivery (S.A.L.-Surface Air Lifted) at no extra cost. For Japan, air delivery requires 25% additional charge of the normal postage and handling charge; for all other countries airmail and S.A.L. charges are available upon request.

Subscription orders. Subscription orders can be entered only by calendar year and should be sent to: Elsevier Science Publishers B.V., Journals Department, P.O. Box 211, 1000 AE Amsterdam, The Netherlands. Tel: (+31-20) 5803 642, Telex: 18582, Telefax: (+31-20) 5803598, to which requests for sample copies can also be sent. Claims for issues not received should be made within six months of publication of the issues. If not they cannot be honoured free of charge. Readers in the U.S.A. and Canada can contact the following address: Elsevier Science Publishing Co. Inc., Journal Information Center, 655 Avenue of the Americas, New York, NY 10010, U.S.A. Tel: (+1-212) 6333750, Telefax: (+1-212) 6333990, for further information, or a free sample copy of this or any other Elsevier Science Publishers journal.
Advertisements. Advertisement rates are available from the publisher on request.

Detailed "Instructions to Authors" for *Analytica Chimica Acta* was published in Volume 256, No. 2, pp. 373-376. Free reprints of the "Instructions to Authors" of *Analytica Chimica Acta* and *Vibrational Spectroscopy* are available from the Editors or from: Elsevier Science Publishers B.V., P.O. Box 330, 1000 AH Amsterdam, The Netherlands. Telefax: (+31-20) 5862845.

US mailing notice - Analytica Chimica Acta (ISSN 0003-2670) is published biweekly by Elsevier Science Publishers (Molenwerf 1, Postbus 211, 1000 AE Amsterdam). Annual subscription price in the USA US$ 2597.75 (subject to change), including air speed delivery. Second class postage paid at Jamaica, NY 11431. *USA Postmasters*: Send address changes to Anal. Chim. Acta, Publications Expediting, Inc., 200 Meacham Av., Elmont, NY 11003. Airfreight and mailing in the USA by Publication Expediting.

ANALYTICA CHIMICA ACTA

An international journal devoted to all branches of analytical chemistry

(Full texts are incorporated in CJELSEVIER, a file in the Chemical Journals Online database available on STN International; Abstracted, indexed in: Aluminum Abstracts; Anal. Abstr.; Biol. Abstr.; BIOSIS; Chem. Abstr.; Curr. Contents Phys. Chem. Earth Sci.; Engineered Materials Abstracts; Excerpta Medica; Index Med.; Life Sci.; Mass Spectrom. Bull.; Material Business Alerts; Metals Abstracts; Sci. Citation Index)

VOL. 279 NO. 1 CONTENTS JULY 1, 1993

Papers presented at the 4th International Symposium on Analytical Methods, Systems and Strategies in Biotechnology—ANABIOTEC '92, Noordwijkerhout, The Netherlands, September 21–23, 1992

Preface 1

Process Control

Monitoring and control of recombinant protein production
K. Schügerl, L. Brandes, X. Wu, J. Bode, J. Il Ree, J. Brandt and B. Hitzmann (Hannover, Germany) 3

Rapid and quantitative analysis of bioprocesses using pyrolysis mass spectrometry and neural networks: application to indole production
R. Goodacre and D.B. Kell (Aberystwyth, UK) 17

Characterization of a sampling unit based on tangential flow filtration for on-line bioprocess monitoring
T. Buttler, L. Gorton and G. Marko-Varga (Lund, Sweden) 27

Automated monitoring of biotechnological processes using on-line ultrafiltration and column liquid chromatography
N.C. Van de Merbel, H. Lingeman, U.A.Th. Brinkman (Amsterdam, Netherlands), A. Kolhorn (Glasgow, UK) and L.C. De Rijke (Woerden, Netherlands) 39

On-line monitoring of penicillin V during penicillin fermentations: a comparison of two different methods based on flow-injection analysis
M. Carlsen, C. Johansen, R.W. Min, J. Nielsen (Lyngby, Denmark), H. Meier and F. Lantreibecq (Saint-Etienne, France) 51

Development of an on-line method for the monitoring of vicinal diketones and their precursors in beer fermentation
C. Mathis, M.N. Pons, J.M. Engasser (Nancy, France) and M. Lenoel (Strasbourg, France) 59

Monitoring of fermentation by infrared spectrometry. Alcoholic and lactic fermentations
D. Picque (Thiverval-Grignon, France), D. Lefier, R. Grappin (Poligny, France) and G. Corrieu (Thiverval-Grignon, France) 67

Chromatography and other Separation Techniques

Chromatographic analysis of biopolymers distribution in "poly-hemoglobin", an intermolecularly crosslinked hemoglobin solution
J. Simoni, G. Simoni and M. Feola (Lubbock, TX, USA) 73

Applications of HY-APATITE in liquid chromatography
G.W. Boers, J.J. Kettenes-van den Bosch and A. Bult (Utrecht, Netherlands) 89

In situ thermal monitoring of adsorption column performance
Y. Meng-Yang, R.R. Rathbone, J. Hubble and A.D. Lockett (Bath, UK) 95

Retention characteristics of a β-cyclodextrin polymer-coated liquid chromatographic column
T. Cserháti, E. Forgács and A. Ujházy (Budapest, Hungary) 107

Application of multivariate mathematical–statistical methods for the comparison of the retention behaviour of porous graphitized carbon and octadecylsilica columns
E. Forgács, T. Cserháti and B. Bordás (Budapest, Hungary) 115

High-performance size-exclusion chromatography of proteoglycans extracted from bovine articular cartilage
P.M. Dekeyser, S. De Smedt, K. Vercruysse, J. Demeester and A. Lauwers (Ghent, Belgium) 123

Antibodies

Catalytic antibodies: new developments
R. Hilhorst (Wageningen, Netherlands) 129

(Continued overleaf)

Contents (continued)

Biosensors

Measurements of nitric oxide in biological materials using a porphyrinic microsensor
T. Malinski, Z. Taha, S. Grunfeld, A. Burewicz, P. Tomboulian (Rochester, MI, USA) and F. Kiechle (Royal Oak, MI, USA) 135

Reusable fiber-optic-based immunosensor for rapid detection of imazethapyr herbicide
R.B. Wong (Princeton, NJ, USA), N. Anis and M.E. Eldefrawi (Baltimore, MD, USA) 141

Biosensor monitoring of blood lactate during open-heart surgery
M. Kyröläinen, H. Håkanson, R. Ekroth and B. Mattiasson (Lund, Sweden) 149

Instrumental Techniques

Introduction to the dielectric estimation of cellular biomass in real time, with special emphasis on measurements at high volume fractions
C.L. Davey, H.M. Davey, D.B. Kell and R.W. Todd (Aberystwyth, UK) 155

Application of fast atom bombardment mass spectrometry for the analysis of biologically active compounds
L. Fourie (Potchefstroom, South Africa), K.J. Van der Merwe, P. Swart and S.S. De Kock (Stellenbosch, South Africa) 163

Spectral analysis of interactions between proteins and dye ligands
J. Hubble, A.G. Mayes and R. Eisenthal (Bath, UK) 167

Oxyheamoglobin degradation and radiolysis analysed by Mössbauer and positron annihilation techniques
M.I. Oshtrakh, E.A. Kopelyan and V.A. Semionkin (Sverdlovsk, Russian Federation) 179

Enzymatic Analysis

Preservation of shelf life of enzyme based analytical systems using a combination of sugars, sugar alcohols and cationic polymers or zinc ions
T.D. Gibson, J.N. Hulbert (Leeds, UK) and J.R. Woodward (Yellow Springs, OH, USA) 185

ANALYTICA CHIMICA ACTA
VOL. 279 (1993)

ANALYTICA CHIMICA ACTA

An international journal devoted to all branches of analytical chemistry
Revue internationale consacrée à tous les domaines de la chimie analytique
Internationale Zeitschrift für alle Gebiete der analytischen Chemie

Anal. Chim. Acta, Vol. 279 (1993)

ELSEVIER, Amsterdam–London–New York–Tokyo

0003-2670/93/$06.00

SPECIAL ISSUE

PAPERS PRESENTED AT THE 4th INTERNATIONAL SYMPOSIUM ON ANALYTICAL METHODS, SYSTEMS AND STRATEGIES IN BIOTECHNOLOGY

ANABIOTEC '92

NOORDWIJKERHOUT, THE NETHERLANDS SEPTEMBER 21–23, 1992

Analytica Chimica Acta, 279 (1993) 1
Elsevier Science Publishers B.V., Amsterdam

PREFACE

Anabiotec '92, the *Fourth International Symposium on Analytical Methods, Systems and Strategies in Biotechnology*, was held in Noordwijkerhout, The Netherlands from September 21 to 23, 1992. After being held in California in 1990 this meeting was located for the third time in The Netherlands. With nearly 200 attendees representing 15 countries this meeting was truly internationally oriented. In total there were over 30 oral presentations in parallel sessions and 53 posters. Discussion sessions on specific hot topics augmented the paper presentations. The relatively small size of Anabiotec provided an ambience of informality leading to open discussions. In conjunction with the Symposium a small exhibition was run in parallel emphasising the interactions between research in the integrated fields of analysis and biotechnology at one hand and their applications at the other hand.

Like its predecessors, the Symposium was focused on the further integration of biotechnology and analytical chemistry. The results of Anabiotec '92 clearly demonstrated that a substantial progress could be reported in the application of both conventional and new analytical techniques, the latter essentially based on natural analytical tools such as biomolecules.

Due to the required integration of biotechnology and analytical chemistry, the number of practising analytical chemists feeling at ease upon working with proteins, peptides, and carbohydrates is steadily increasing. Also biotechnologists are themselves applying sophisticated analytical methodologies in their own laboratories. The main themes covered during this meeting can be allocated to the following integrated fields of analysis in biotechnology: fermentation monitoring, chromatography, instrumental analysis, biosensors and bioanalysis. In comparison with the previous Anabiotec symposia relatively new areas of research and application were mentioned. The general tendency was deepening and broadening of research and their applications in the above mentioned areas.

As Chairman of Anabiotec '92, I wish to express my personal appreciation to all those individuals whose efforts help to ensure the success of the Symposium. The help, suggestions, and the undertaking of the time-consuming abstract review process by the Scientific Committee was appreciated. Special thanks go to Bauke te Nijenhuis and Joost Holthuis for their invaluable help and guidance during the organization of Anabiotec.

In addition my thanks also go to the session organizers, chairpersons and discussion leaders for their contribution to the meeting.

Finally, I want to thank all of the delegates, both presenters and non-presenters, who attended and participated in Anabiotec '92. Without your active participation and support, such international meetings would not have a fertile basis.

This issue of *Analytica Chimica Acta* includes most of the papers submitted for publication after presentation as oral or poster contributions to the Symposium. The next Anabiotec meeting is scheduled to be held in 1994 in Canada.

Cees van Dijk
Symposium Chairman

Analytica Chimica Acta, 279 (1993) 3–16
Elsevier Science Publishers B.V., Amsterdam

Monitoring and control of recombinant protein production

Karl Schügerl, Lutz Brandes, Xiaoan Wu, Jens Bode, Jong Il Ree, Jens Brandt and Bernd Hitzmann

Institut für Technische Chemie, Universität Hannover, Callinstr. 3, D-3000 Hannover (Germany)

(Received 1st October 1992; revised manuscript received 8th December 1992)

Abstract

For better control of the production of a toxic product by recombinant *Escherichia coli* carrying three different types of multicopy plasmids, the total and viable cell concentration, total cell count (TCC), number of colony-forming units (CFU), plasmid copy numbers, intracellular enzyme activity and the concentrations of the cell metabolites in the cultivation medium were monitored. This was performed during the growth phase and after chemical induction with IPTG and temperature induction, respectively. Gene expression was carried out in a small stirred-tank reactor and in a 60-l tower loop reactor equipped with a draught tube. Cell concentration was determined with an in situ turbidometer, TCC by off-line counting, cell viability by culture fluorescence, CFU also by off-line counting, the concentration of metabolites with off-line and on-line liquid chromatography and with off-line and on-line flow-injection analysis (FIA) and intracellular enzyme concentrations by off-line and on-line FIA. The evaluated data allowed an improvement of the production process, and increases in cell concentration and volumetric and specific productivity.

Keywords: Flow injection; Liquid chromatography; Process analysis; Cell cultivation; Proteins; Recombinant *Escherichia coli*

The combination of conventional biotechnology with genetic engineering has opened up new possibilities for the production of proteins (enzymes, blood factors and other pharmaceutical products). Genetic engineering is based on the DNA recombination technique and extends the synthesis capacity of the cells significantly.

The transfer of new genes to cells is mainly used for the manufacture of proteins, i.e. direct gene products. Transfer of new genes to the host is usually performed by plasmids. Construction of expression systems for the production of recombinant proteins is frequently realized by plasmid host systems. The necessary expression plasmids are coded for the protein product, the transcription control of which is often accomplished with inducible promotors. The production of recombinant proteins with these expression systems consists of two stages: growth and propagation of the host cells; and induction of the gene expression and product formation. Monitoring of cell growth and gene expression makes possible the optimization of the production (cell propagation and gene expression) process.

In this paper, the evaluation of the optimum cultivation and gene expression conditions by means of monitoring cell and medium properties are considered, and also the control of the

Correspondence to: K. Schügerl, Institut für Technische Chemie, Universität Hannover, Callinstr. 3, D-3000 Hannover (Germany)

medium composition by the example of the production of an enzyme and a fusion protein with *Escherichi coli*.

EXPERIMENTAL AND RESULTS

Biological system

Escherichia coli JM103 (DSM, Braunschweig) was employed for the production of the restriction endonuclease EcoRI having the following genotype: *end*A, delta[*lac*,*pro*] thi-1, *str*A, *scb*B15, *hsd*R4, *sup*E, lambda-, [F'*tra*D36, *pro*A$^+$B$^+$, *lac*I^q_z, delta [M15]. On account of EcoRI being highly toxic to the host, the bacteria are cultivated without gene expression and, after the cell concentration has been attained, the gene expression is induced by means of a suitable promoter–repressor system. Further, the host is protected by a DNA methylase. Three different systems were compared (Table 1). In system A, no protection plasmid was used and the plasmid stability and productivity were very low. In systems B and C, the stabilities were satisfactory. The highest productivity was attained in system C [1,2].

TABLE 1

Plasmid combinations used during cultivation

Biological system	Expression plasmid	Repressor plasmid	Protection plasmid	Product
A	pRIF309+	pcI857	–	EcoRI
B	pRIF309+	pRK248cI	pEcoR4	EcoRI
C	pMTC48	pRK248cI	pEcoR4	SPA::EcoRI

In situ monitoring and control of operation variables

Temperature (30°C) and pH (7.0) were kept constant and the aeration rate (Brooks mass flow meter) and stirrer speed were varied to maintain an adequate dissolved oxygen concentration.

The feeding rate of the substrate was open-loop controlled by measuring the weight of the substrate storage by a load cell. Foam (electrical conductivity probe), head pressure, O_2 (Oxygor, Maihak) and CO_2 (Unor 6N, Maihak) were monitored in the off-gas.

Monitoring of cell concentration and properties

The cell concentration was measured in situ with a turbidity probe (MEX 2 EUR-Control, BTG) and fluorescence probe (Fluoromeasure, Ingold), which were integrated into a loop of cell-containing medium, which was furnished with a degasser to avoid disturbances caused by bubbles. Cell concentrations measured by weight (X) and with a turbidometer agreed well (Fig. 1).

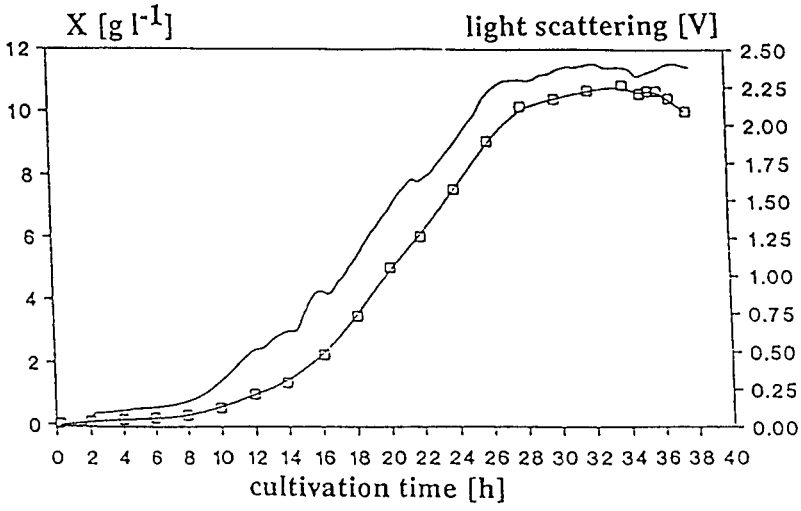

Fig. 1. Comparison of cell concentrations measured by (solid line) light scattering (MEX 2, EUR Control) and (□) weight (X) [1].

As long as a balanced growth was maintained, the cell concentrations measured by weight and culture fluorescence agreed well. Alternations in cell environment caused deviations of the cell concentrations calculated by the culture fluorescence signal and measured by weight or by a turbidometer (Fig. 2).

The total cell count (TCC) was determined in a Neubauer counting chamber with a microscope. The number of colony-forming units (CFU) was evaluated by plating a 100-μl sample on Luria–Bertani (LB) agar plates. By diluting with 0.9% NaCl solution, the number of colonies was kept between 50 and 100. Counting took place during the night after incubation at 30°C.

For the evaluation of the plasmid copy numbers and the intracellular product, the cells must be disintegrated. This was performed enzymatically by treating the sample with lysozyme–ETDA.

For the determination of the plasmid copy number, the plasmid DNA was isolated from 1.5 ml of cell suspension (minipreparation according to Horowicz and Burke [3]) and transferred to linear fragments by restriction decomposition, separated by agarose gel electrophoresis; the copy number was evaluated from the intensity and molecular weight of the bands [4].

The product concentration, i.e., the EcoRI enzyme activity, was determined by the lambda-DNA splicing activity of the sample at the recognizing sequence G/AATTC. The cell debris was separated from the supernatant by centrifuging at 15 000 g, and the latter was diluted with RE-buffering solution under ice cooling. A 5-μl volume of this solution was reacted with 1 μl of DNA solution (250 mg), 1 μl of 10 × RE-buffering solution and 3 μl of water and was incubated for 15 min at 37°C. After adding 5 μl of stop solution, the DNA fragments were separated by gel electrophoresis, then stained with ethidium bromide and photographed on a 360-nm transluminator. The negative was scanned (Camac TLC Scanner II) and integrated (Spectra-Physics integrator). The enzyme activity was calculated by comparing the integral of the sample with that of a standard [4].

The plasmid stability was evaluated by replica plating: a print was made from the first LB agar plate by means of the aseptic stamp covered with velvet and transferred to a second LB agar plate containing antibiotics. After incubation at 30°C, the difference in the number of colonies on the first and second LB plates was evaluated.

On-line monitoring of medium composition

The concentrations of substrate glucose and the metabolites pyruvate, succinate, lactate, glyc-

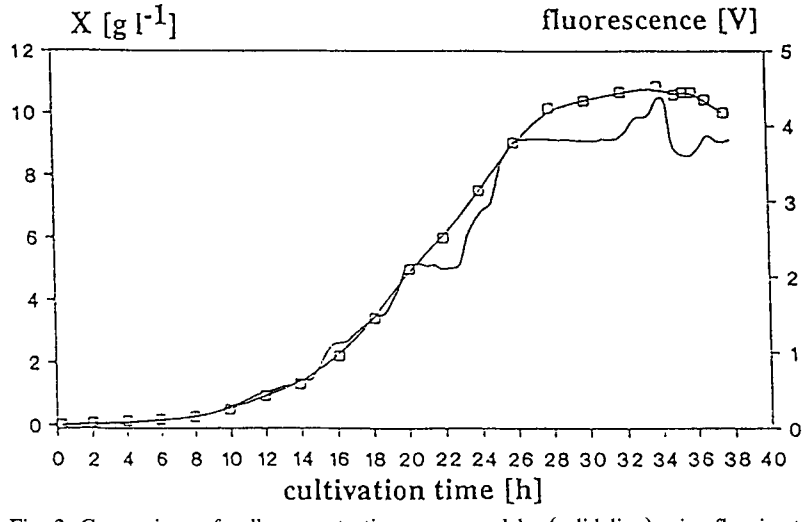

Fig. 2. Comparison of cell concentrations measured by (solid line) microfluorimeter (Fluoromeasure, Ingold) (Fluor) and (□) weight (X) [1].

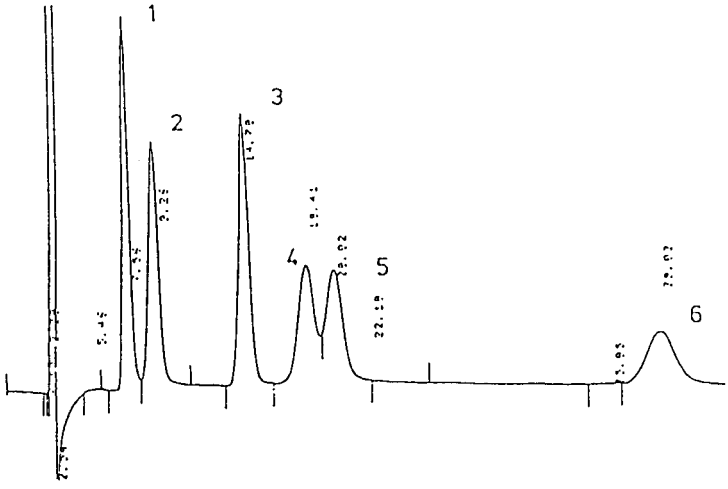

Fig. 3. Chromatogram of a standard solution with an amino-bonded column, Nucleosil 1005 NH_2 (250 mm × 4.6 mm i.d.), at 28°C. Eluent, 77.5% acetonitrile–22.5% 0.003 M phosphate buffer containing 0.004 mol l^{-1} TBAHS (pH 7.2). Peaks: 1 = fructose; 2 = glucose; 3 = sucrose; 4 = maltose; 5 = lactose; 6 = maltotriose.

erol, acetate, methanol and ethanol were monitored with off-line and on-line liquid chromatography (LC), using an ERC 3120 degasser (ERMA), Consta Metric Model III LC pump (LDC/Milton Roy), Shodex DP-1 (pulse damper), Model 231 autosampler with Model 401 diluter (ABIMED), ERC 7511 refractive index detector (ERMA), Shodex Ionpak S-801 gel permeation column (Macherey–Nagel) with frit, precolumn and thermostat (Julabo), and integrator (Spectra-Physics). The sample was taken on-line with a tubular filtration module (ABC, Puchheim) by employing a peristaltic pump (Skalar).

The different sugar components were analysed with the same equipment, but with a Nucleosil 100-5 NH_2 column under the following conditions: eluent, 77.5% acetonitrile and 22.5% 0.003 M phosphate buffer solution supplemented with 0.004 mol l^{-1} tetrabutyl ammonium hydrogensulphate (TBAHS); flow-rate, 1.0–1.2 ml min^{-1}; and temperature, 28°C.

Chromatograms of standard solutions with an amino phase column (Fig. 3) and with a gel permeation column (Fig. 4) are shown. The set-up of the LC system is shown in Fig. 5.

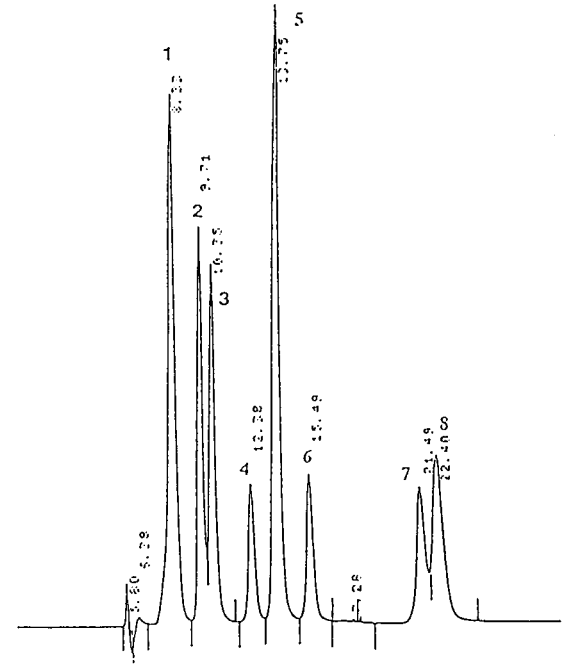

Fig. 4. Chromatogram of a standard solution with a gel permeation column, IONpak S-801 (250 mm×8 mm i.d.) at 60°C. Eluent, 0.0009 M H_2SO_4. Peaks: 1 = pyruvate; 2 = glucose; 3 = galactose; 4 = succinate; 5 = glucerol; 6 = acetate; 7 = ethanol; 8 = butyric acid.

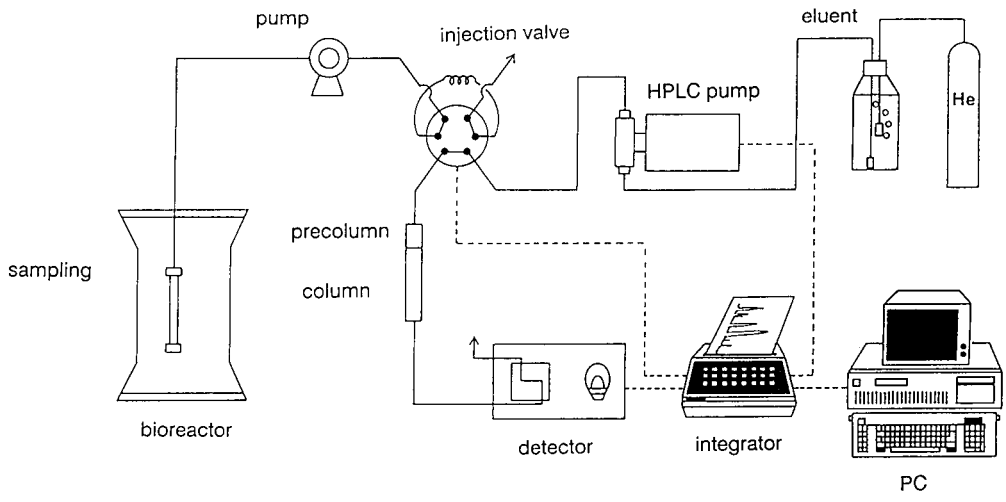

Fig. 5. Set-up of the LC system.

The different sugar components were also analysed with the following enzyme–flow-injection analysis (FIA) systems:

$$\beta\text{-D-glucose} + O_2 \xrightarrow{GOD} H_2O_2 + \text{D-glucono-}\delta\text{-lactone} \quad (1a)$$

$$\text{D-glucono-}\delta\text{-lactone} \longrightarrow \text{gluconic acid} \quad (1b)$$

$$\text{maltose} \xrightarrow{\alpha\text{-glucosidase}} \alpha\text{-D-glucose} + \beta\text{-D-glucose} \quad (2)$$

$$\text{sucrose} \xrightarrow{\text{invertase}} \alpha\text{-D-glucose} + \beta\text{-D-fructose} \quad (3)$$

$$\alpha\text{-D-glucose} \xrightleftharpoons{\text{mutarotase}} \beta\text{-D-glucose} \quad (4)$$

In contrast to earlier investigations [5], the enzymes were co-immobilized (on VA-Epoxy Biosynth carrier, Riedel-de Haën) and placed in 0.8-ml cartridges. The dissolved oxygen concentration in Eqn. 1a was measured with an amperometric oxygen electrode.

In order to measure disaccharides and glucose in the medium at the same time, two cartridges were combined [6]: in the first cartridge immobilized α-glucosidase and/or invertase–mutarotase were used, and in the second cartridge immobilized glucose oxidase (GOD) was employed. The sample was injected into the carrier flow preceding the first cartridge and simultaneously between the first and second cartridges. Two peaks appeared: the first was the glucose peak and the second the disaccharide peak (Fig. 6). Special software was used to separate the two peaks [7].

For off-line measurement of the glucose concentrations, a YSI Model 27 industrial analyser was used. For oxidases, an alternative transducer is the pH sensor. Field-effect transistors with pH-sensitive $Si/SiO_2/Si_3N_4/Ti_2O_5$ gates were used as transducers. On the surface of the gate, GOD (for glucose analysis) [8,9], α-glucosidase and GOD (for maltose analysis), β-galactosidase and GOD (for lactose analysis) and invertase, mutarotase and GOD (for sucrose analysis) were co-immobilized [10]. These biosensors were integrated into a flow cell together with an Ag/AgCl reference electrode and were used as detectors in FIA systems [8,9]. The disadvantage of these biosensors is that the signal height depends on the pH and buffering capacity of the cultivation medium. The pH and buffering capacity dependence was reduced by the sample dilution in the carrier flow, but could not be eliminated completely.

The pH dependence was compensated for by using sensor arrays (combination of bio- and pH sensors) [8,9]. The buffering capacity dependence was taken into account by determining the buffering capacity of the cultivation medium as a function of the pH value. For each pH value, a particular calibration graph holds true. By moni-

toring the pH value, the corresponding calibration graph is used for the evaluation of the analyte concentration. Figures 7 and 8 show how the agreement between LC and FIA measurements improves if a bio–pH sensor array is used in the FIA system for the measurements.

The quality of the measurements depends on the dilution rate and the injection time (Figs. 9 and 10). The key components were monitored with two independent methods. This redundancy is necessary to control the results of the analyses for greater reliability of the process control.

On-line monitoring of intracellular products

The investigation indicated that sometimes the intracellular product concentration increases, passes through a maximum and quickly decreases. The productivity depends on the harvest time. To maintain the highest productivity, the cultivation must be stopped when the intracellular product concentration is at its maximum. In this instance, it is recommended to form a fusion protein of the product with a tag (enzyme) that can be easily detected; β-galactosidase was used. The β-galactosidase activity was determined with

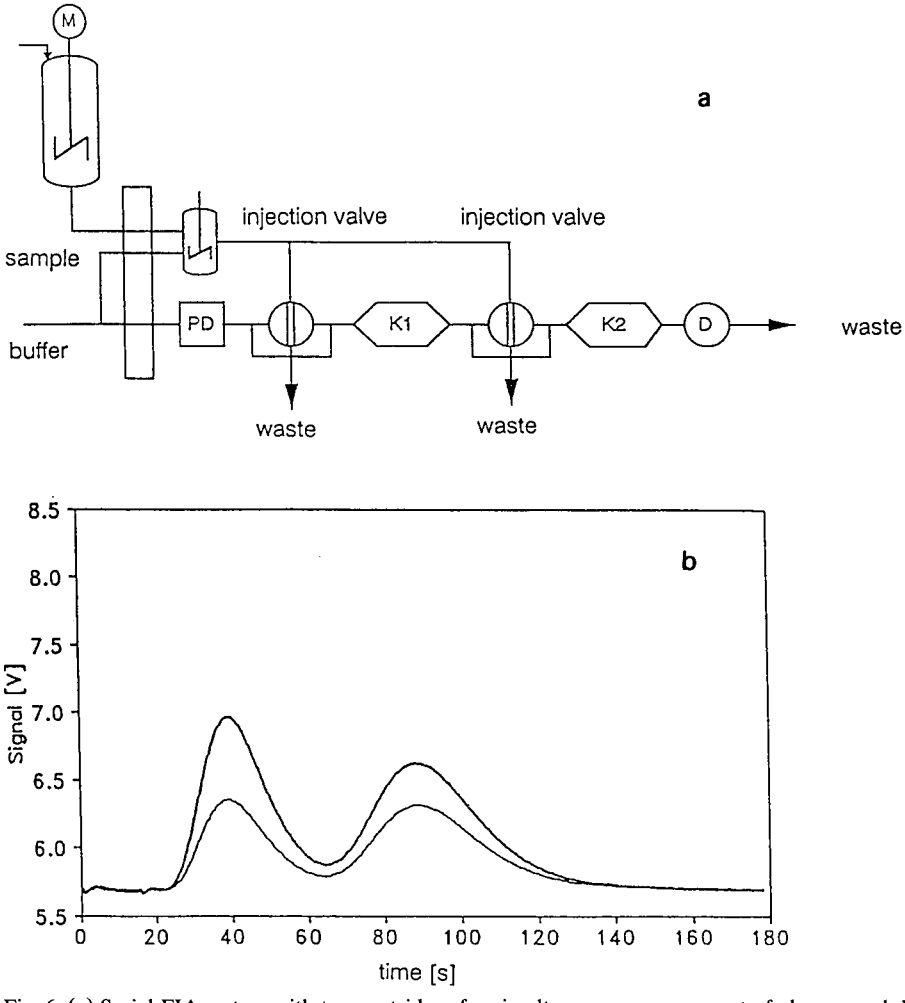

Fig. 6. (a) Serial FIA system with two cartridges for simultaneous measurement of glucose and disaccharides [6]. K1 = mutarose + invertase for sucrose; K2 = GOD for glucose. (b,c) Detector signal with serial FIA system [6]. (b) Constant sucrose. (c) Constant glucose.

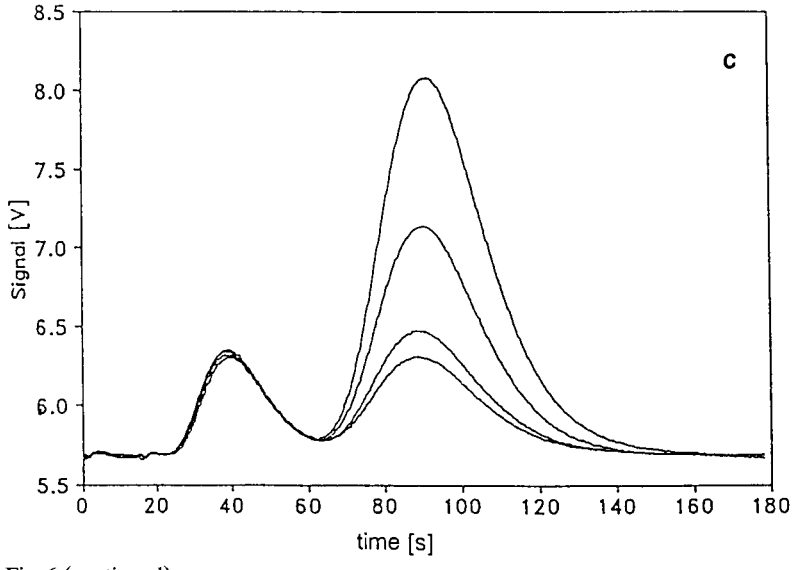

Fig. 6 (continued).

o-nitrophenyl-β-D-galactopyranoside (ONPG) according to Miller [11]. The diluted sample was treated with ultrasound (Labsonic, Braun, Melsungen) at 4°C, diluted and injected into the FIA system with ONPG in the carrier buffer. The yellow colour of *o*-nitrophenol was measured with a spectrophotometer (Fig. 11) [12].

Examples of the monitoring of the batch process

The cells were cultivated in a 60-l working volume airlift tower loop (ATL) reactor [13] on M9 minimal medium (Table 2) at 30°C. The gene expression was induced by temperature shift from 30 to 38°C, which proved to be the optimum for the gene expression. At the same time, 4 l of Luria Bertani (LB) concentrate [100 g l^{-1} casein peptone, 50 g l^{-1} NaCl and 100 g l^{-1} yeast extract (pH 7)] were added to the culture medium. The plasmid stability was satisfactory in biological systems B and C.

In Fig. 12, the concentrations of cell mass (X), glucose (GLU) and acetate (Ac) are shown dur-

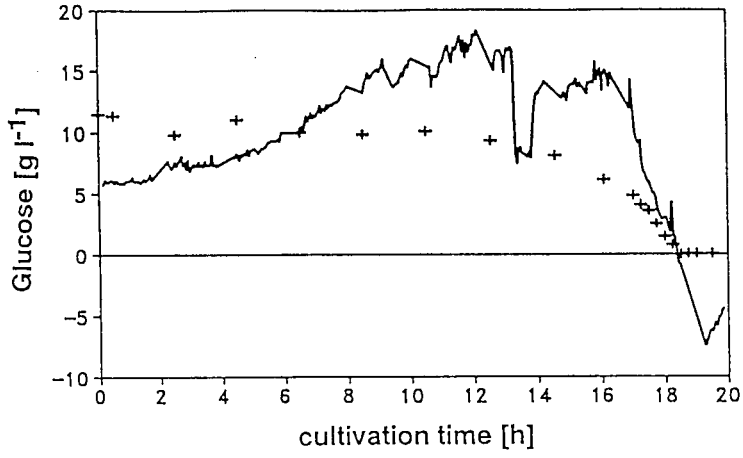

Fig. 7. Glucose concentration in recombinant *Escherichia coli* JM103 culture measured with (solid line) GOD field-effect transistor FIA on-line without pH correction and by (+) LC off-line as a function of the cultivation time [8,9].

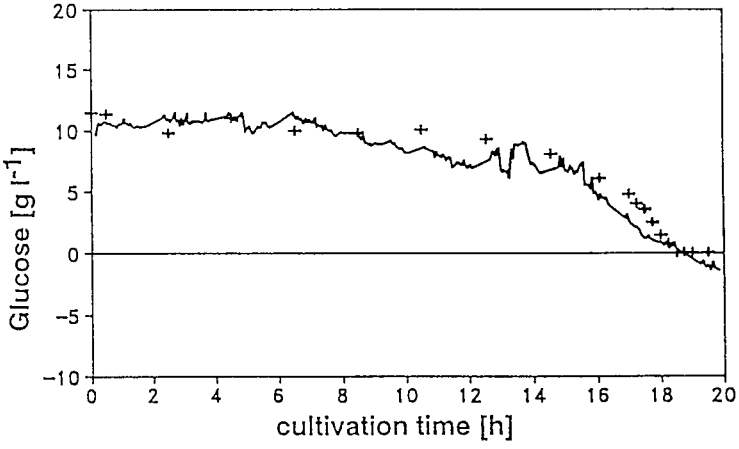

Fig. 8. Glucose concentration in recombinant *Escherichia coli* JM103 cultivation measured with (solid line) GOD-FET-FIA–pH-FET-FIA on-line with pH correction and by (+) LC off-line as a function of the cultivation time [8,9].

ing a typical batch cultivation. At $t = 19$ h, gene expression was induced by a temperature shift to 38°C. The courses of X and GLU changed only slightly during the temperature shift and gene expression, but Ac increased from 1.5 to 2.8 g l^{-1}. Also, the concentrations of other primary metabolites, such as ethanol, pyruvate, and lactate, increased considerably during gene expression, but the concentration of succinate changed only slightly (Fig. 13). The TCC and CFU exhibited a dramatic change during gene expression (Fig. 14). The dissolved concentration pO_2 and the O_2 concentration in the off-gas passed through a sharp minimum and the CO_2 concentration in the off-gas passed through a sharp maximum during gene expression. Accordingly, the oxygen utilization rate (OUR) and CO_2 production rate (CPR) increased steeply and then dropped, but the respiratory quotient RQ = CPR/OUR did not change.

The intracellular enzyme activity increased to

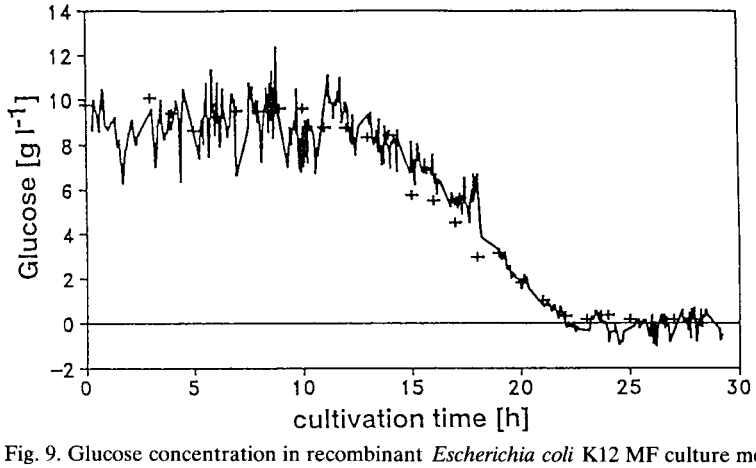

Fig. 9. Glucose concentration in recombinant *Escherichia coli* K12 MF culture measured with (solid line) GOD-FET-FIA on-line at a dilution ratio of 1 : 26 with a change in the injection time from 8 to 30 s below 6 g l^{-1} and by (+) LC off-line as a function of the cultivation time [8,9].

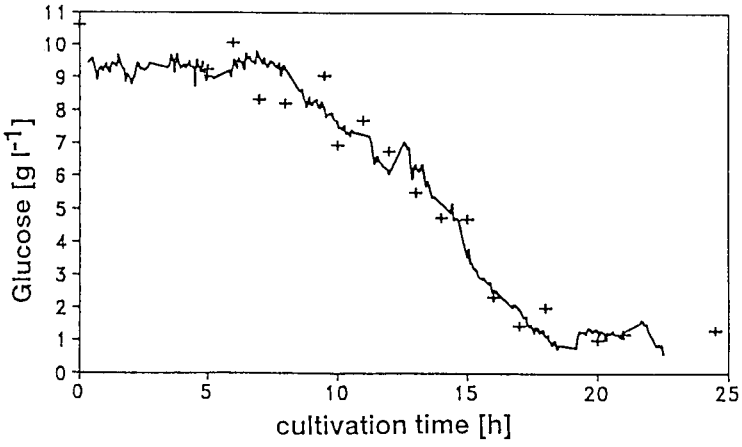

Fig. 10. Glucose concentration in recombinant *Escherichia coli* K12 MF culture measured with (solid line) DOD-FET-FIA on-line with a change in the dilution ratio from 1:52 at an injection time of 1 min to 1:26 at an injection time of 30 s below 6 g l^{-1} and by (+) LC off-line as a function of the cultivation time [8,9].

7500 U ml^{-1} during gene expression at a cell mass concentration of 4 g l^{-1}.

Examples of monitoring and control of the fed-batch process

These investigations were carried out with biosystem C, the host carrying the expression plasmid pMTC48, which has two promoters: temperature-inducible lambda promoter P_R and isopropyl thiogalactoside (IPTG)-inducible lac-promoter P_{LacUV5}. They were induced both singly and together.

Formation of primary metabolites and their

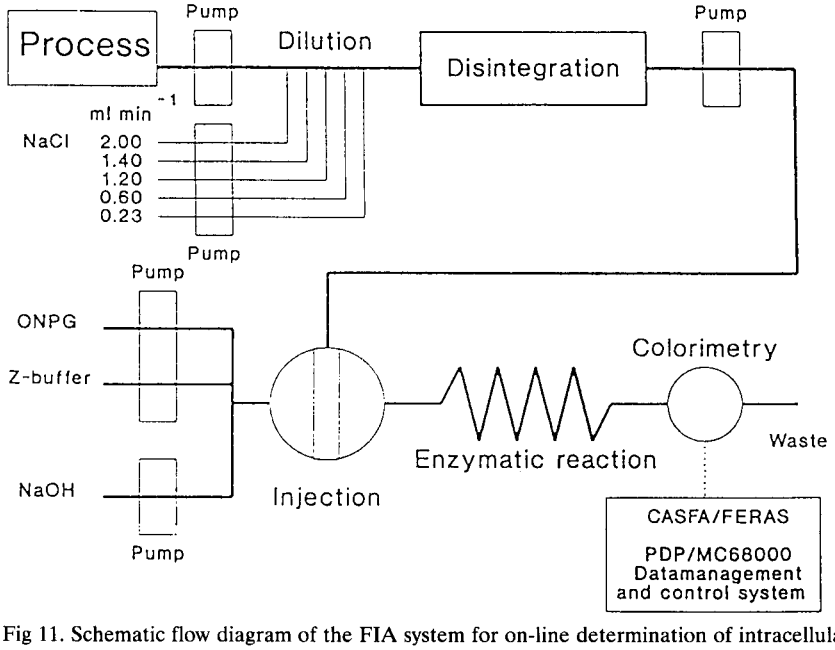

Fig 11. Schematic flow diagram of the FIA system for on-line determination of intracellular β-galactosidase activity in recombinant *Escherichia coli* K12 MF. The assay is divided into five steps: dilution of the samples, cell disintegration, flow injection of the sample, enzymatic reaction and spectrophotometry at 420 nm [12].

TABLE 2

Composition of the M9 minimal medium

100 ml l^{-1} salt solution	21 g l^{-1} Na_2HPO_4, 25 g l^{-1} KH_2PO_4, 5 g l^{-1} NaCl, 25 g l^{-1} $(NH_4)_2SO_4$
1 ml l^{-1}	0.1 M $CaCl_2$
1 ml l^{-1}	1.0 M $MgCl_2$
100 ml l^{-1} glucose solution	100 g l^{-1}
0.2 ml l^{-1} vitamin solution	5 mg l^{-1} thiamine, 5 mg l^{-1} biotin
1 ml l^{-1} trace element solution	1.38 g l^{-1} $ZnSO_4 \cdot 7H_2O$, 5.40 g l^{-1} $FeCl_3 \cdot 6H_2O$, 1.650 g l^{-1} $MnSO_4$, 0.17 g l^{-1} $CuCl_2$, 0.56 g l^{-1}, $CoSO_4 \cdot 7H_2O$, 0.06 g l^{-1} H_3BO_3, 10 ml l^{-1} conc. HCl

20 l salt solution, 10 l glucose solution, 3.5 l $MgCl_2$–$CaCl_2$ solution and 2.5 l trace element solutions were autoclaved separately.

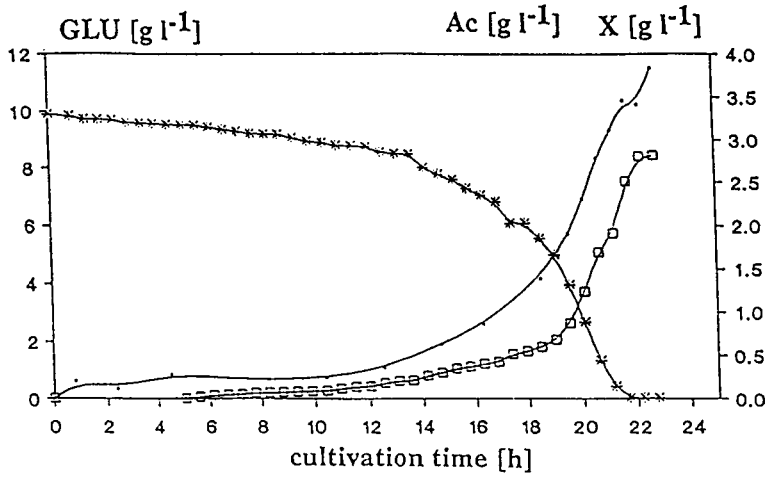

Fig. 12. Concentrations of (●) cell mass (X), (∗) glucose (GLU) and (□) acetate (Ac) as a function of time during batch cultivation of *Escherichia coli* JM103 (run 9101) [1].

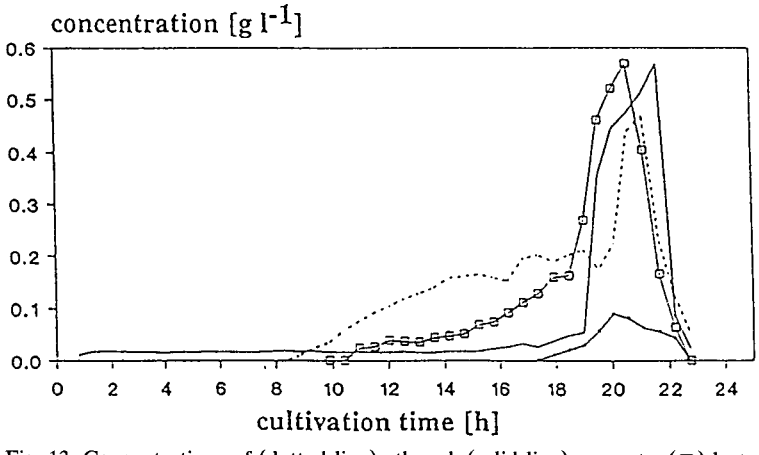

Fig. 13. Concentrations of (dotted line) ethanol, (solid line) pyruvate, (□) lactate, and (●) succinate as a function of time during cultivation of *Escherichia coli* JM103 (run 9101) [1].

excretion into the cultivation medium decreases the yield coefficients of cell growth and product formation. The main by-product is acetate. Its presence in the cultivation medium impairs cell growth and product formation. The aim of the cultivation is to have a high growth rate and cell concentration, but a low acetate formation rate. This can be attained by suitable control of the glucose feed rate (F_S) and oxygen transfer rate.

Two control strategies were used. In the first, the cell concentration X was measured in situ, the specific growth rate μ was evaluated in real time and the feed rate F_S was calculated by the equation

$$F_s = \frac{V_0 \mu X_0}{Y_{X/GLU} S_F} \cdot \exp(\mu t) \quad (5)$$

where V_0 is the medium volume at the beginning of the fed-batch operation, X_0 is the dry cell concentration at the beginning of the fed-batch operation, $Y_{X/GLU}$ is the yield coefficient, S_F is the substrate (GLU) concentration in the feed and t is the fed-batch cultivation time. The actual volume V was also calculated and was taken into account:

$$V = V_0 \exp(\mu t) \quad (6)$$

In the second strategy, the feed rate was closed-loop controlled by on-line monitoring of the glucose concentration to keep the glucose concentration at a particular level.

When using the in situ measured cell concentration, a constant yield coefficient of the cell growth with regard to the substrate $Y_{X/GLU}$ was assumed. During the fed-batch operation, the dissolved oxygen concentration diminished gradually with increasing cell concentration, and after about 11–16 h it dropped to zero. This caused a decrease in $Y_{X/GLU}$ and an increase in the glucose concentration. Therefore, in most runs, the feed rate was controlled by means of glucose concentration monitoring.

The dissolved oxygen concentration was not closely controlled. Its value, therefore, usually decreased with increasing cell concentration, because the oxygen demand was higher than the attainable oxygen transfer rate with air sparging. Oxygen limitation was avoided only during run 9109 by using a mixture of oxygen and air for the aeration of the medium.

At high glucose and low dissolved oxygen concentrations, the enzyme productivity was very low. With decreasing glucose concentration during the fed-batch operation, the acetate concentration diminished and the enzyme activity increased. For example, at 8 g l^{-1} glucose concentration and at an oxygen transfer limitation after 11 h, a maximum enzyme activity of 32 000 U ml^{-1} was obtained. If the glucose concentration was kept at

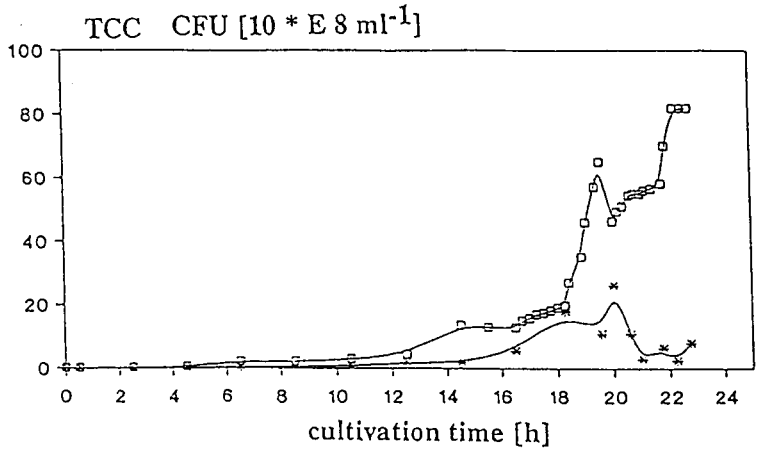

Fig. 14. (□) Total cell count (TCC) and (*) number of colony-forming units (CFU) as a function of time during cultivation of *Escherichia coli* JM103 (run 9101) [1].

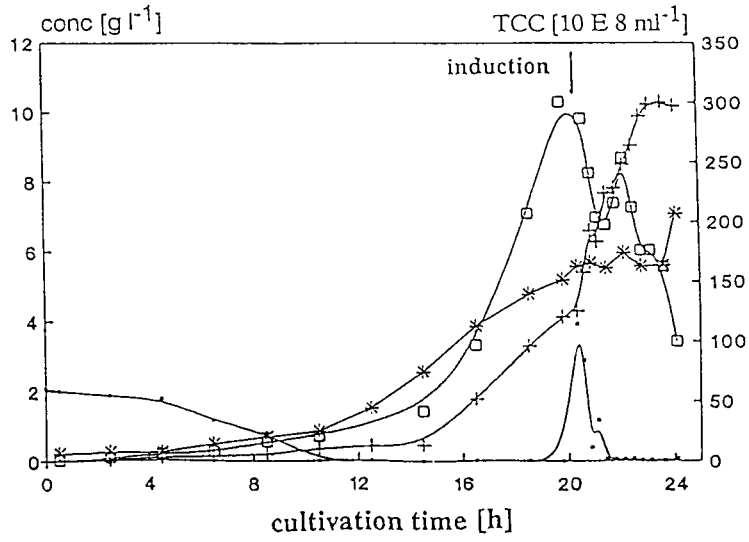

Fig. 15. Concentrations of (∗) dry cell mass, (□) TCC, (●) glucose and (×) acetate as a function of time during fed-batch cultivation of *Escherichia coli* JM103. Influence of the induction of gene expression by IPTG and temperature shift on process performance (run 9108) [1].

0.5 g l^{-1} during the fed-batch operation and the dissolved oxygen concentration dropped to zero after 16 h, it was possible to obtain a higher enzyme activity. Figure 15 shows the cell mass, TCC, CFU and acetate concentrations for this run (run 9108). After induction, X remained constant, TCC and CFU decreased, but the metabolite concentrations increased (Fig. 16). A maximum enzyme activity of 80 000 U ml^{-1} (Fig. 17) was obtained at a cell concentration of 7 g l^{-1}.

On keeping the dissolved oxygen at 16% of its saturation and the glucose concentration at 0.1 g l^{-1}, high TCC and CFU values (Fig. 18) and a maximum enzyme activity of 270 000 U ml^{-1} (Fig.

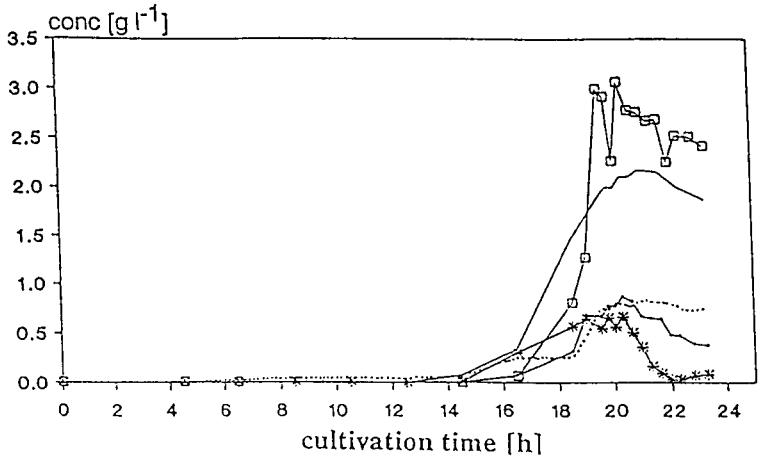

Fig. 16. Concentrations of the metabolites as a function of time during fed-batch cultivation of *Escherichia coli* JM103. Dotted line = ethanol; solid line = pyruvate; □ = lactate; ● = succinate; ∗ = glycerol (run 9108) [1].

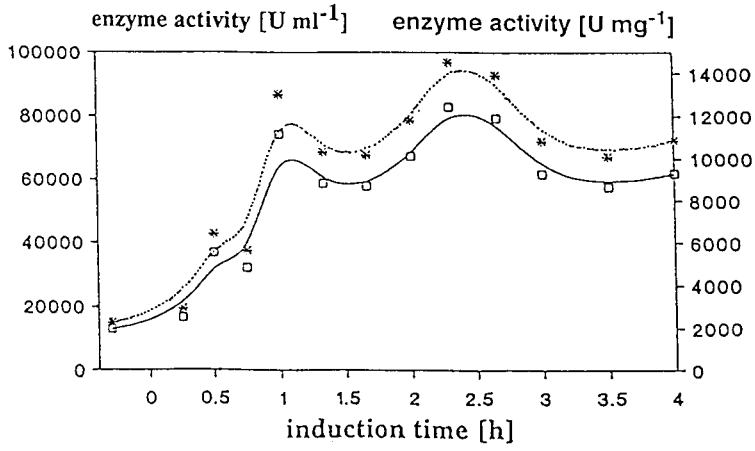

Fig. 17. Variation of (□) volumetric enzyme activity and (*) specific enzyme activity with respect to cell mass as a function of induction time. Induction of gene expression of *Escherichia coli* JM103 by temperature shift and IPTG (run 9108). [1].

19) could be obtained at a cell concentration of 10 g l^{-1}. Except for acetate, no other metabolite was excreted. The process performance was improved considerably.

Conclusion

A production process with recombinant *Escherichia coli* was investigated. Optimization of cell growth and induction of gene expression are possible only if the concentrations of substrate S and dissolved oxygene pO_2 are monitored and controlled. By monitoring cell concentrations X, TCC, CFU, the concentrations of product and by-product, O_2 and CO_2 in the off-gas, the influence of cell environment and induction of gene expression on cell metabolisms can be understood more thoroughly, which is a prerequisite for process improvement.

On-line FIA was used for closed-loop process control and on-line and off-line LC analysis for

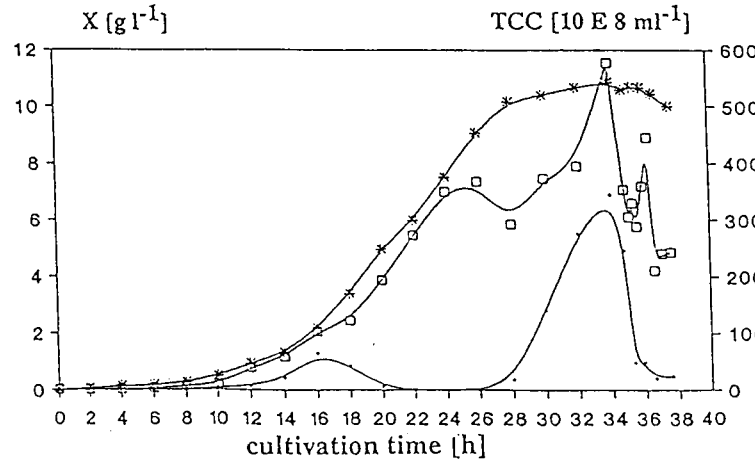

Fig. 18. (*) Concentration of dry cell mass X, (□) TCC and (●) CFU as a function of time during fed-batch cultivation of *Escherichia coli* JM103. Induction of gene expression by temperature shift was started at 34.5 h (run 9109) [1].

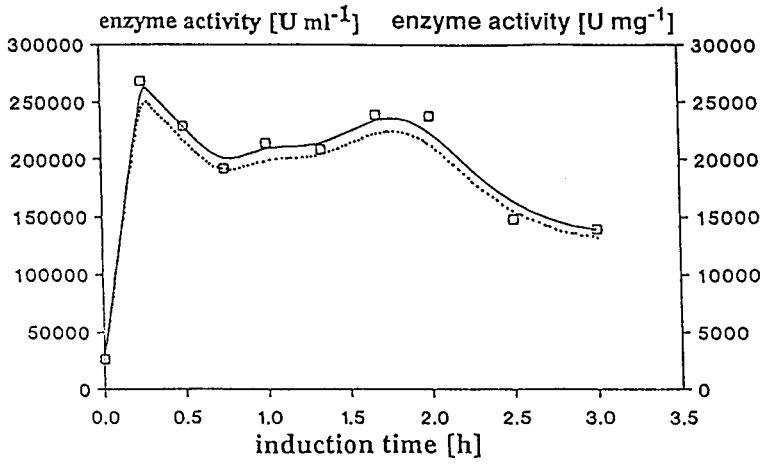

Fig. 19. (□) Volumetric enzyme activity and (dotted line) specific activity with respect to dry cell mass as a function of time of induction by temperature shift (run 9109) [1].

checking the FIA by comparison of the data. This redundancy is necessary, because the reliability of FIA is not yet adequate for process control.

The authors express their gratitude to Hoechst for their support and X. Wu thanks DAAD, Bonn, for a scholarship.

REFERENCES

1 L. Brandes, Dissertation, University of Hannover, Hannover, 1991.
2 X. Wu, Dissertation, University of Hannover, Hannover, 1992.
3 D.I. Horowicz and J.R. Burke, Nucleic Acids Res., 16 (1981) 2989.
4 H.-E. Maschke, Dissertation, University of Hannover, Hannover, 1991.
5 K. Schügerl, L. Brandes, T. Dullau, K. Holzhauer-Rieger, S. Hotop, U. Hübner, X. Wu and W. Zhou, Anal. Chim. Acta, 249 (1991) 87.
6 B. Weigel, Diploma Thesis, University of Hannover, Hannover, 1992.
7 J. Brandt, Dissertation, University of Hannover, Hannover, in preparation.
8 B. Reinhardt, Dissertation, University of Hannover, Hannover, 1991.
9 U. Brand, L. Brandes, V. Koch, T. Kullick, B. Reinhardt, F. Rüther, T. Scheper, K. Schügerl, S. Wand, X. Wu, R. Ferretti, S. Prasad and D. Wilhelm, Appl. Microbiol. Biotechnol., 36 (1991) 167.
10 T. Kullick, Dissertation, University of Hannover, Hannover, in preparation.
11 J.M. Miller, Experiments in Molecular Genetics, Cold Spring Harbour Laboratory, 1982.
12 H.-A. Kracke-Helm, L. Brandes, B. Hitzmann, U. Rinas and K. Schügerl, J. Biotechnol., 20 (1991) 95.
13 H.-A. Kracke-Helm, U. Rinas, B. Hitzmann and K. Schügerl, Enzyme Microb. Technol., 13 (1991) 554.

Analytica Chimica Acta, 279 (1993) 17–26
Elsevier Science Publishers B.V., Amsterdam

Rapid and quantitative analysis of bioprocesses using pyrolysis mass spectrometry and neural networks: application to indole production

Royston Goodacre and Douglas B. Kell

Department of Biological Sciences, University of Wales, Aberystwyth, Dyfed SY23 3DA (UK)

(Received 27th September 1992; revised manuscript received 1st December 1992)

Abstract

In pure form indole, when subjected to pyrolysis mass spectrometry (PyMS), gave a pattern of peaks at m/z 117, 90, 89 and a murmur at 63. Significant differences in the magnitudes of these peaks were observed between strains of *Escherichia coli* which were grown on nutrient agar and which differed solely in whether a transposon had been inserted into the tryptophanase gene or elsewhere within the genome. We applied artificial neural networks (ANNs) to the deconvolution of pyrolysis mass spectra. The combination of ANNs and PyMS was able quantitatively to detect the component indole when a single strain of *E. coli*, containing the tryptophanase gene, was grown on a minimal supplemented salts medium incorporating various amount of tryptophan, in the range 0–253 mg/l. This approach constitutes a novel, powerful and interesting technology for the analysis of the concentrations of appropriate substrates, metabolites and products in chemical and bioprocesses generally.

Keywords: Mass spectrometry; Artificial neural networks; Indoles; Neural networks; Pyrolysis MS

Pyrolysis is the thermal degradation of complex material in an inert atmosphere or a vacuum. It causes molecules to cleave at their weakest points to produce smaller, volatile fragments called pyrolysate [1,2]. A mass spectrometer can then be used to separate the components of the pyrolysate on the basis of their mass-to-charge ratio (m/z) so as to produce a pyrolysis mass spectrum, which can then be used as a "chemical profile" or fingerprint of the complex material analysed.

Within microbiology, this technique, called pyrolysis mass spectrometry (PyMS), has largely been applied to the characterisation of *bacterial* systems (for reviews see Refs. 3–5). In particular, PyMS, because of its high discriminatory ability, has been successfully applied to the inter-strain comparison of a wide range of bacterial species and groups, including: *Bacillus* [6], *Corynebacterium* [3], *Escherichia coli* [7,8], *Legionella* [9], mycobacteria [10–12], salmonellae [13] and streptococci [14], highlighting the usefulness of this technique in the detection of small differences between microbial samples. Furthermore, one of the major advantages that PyMS has over other diagnostic methods, such as ELISA [15] and nucleic acid probing [16], is that it is rapid, both for a single sample and with respect to the (automated) throughput of samples. Typical sample time is less than 2 min.

PyMS of complex organic mixtures can be expressed in subpatterns of spectra describing the pure components of the mixtures and their relative concentrations [17]; here the authors success-

Correspondence to: R. Goodacre, Department of Biological Sciences, University of Wales, Aberystwyth, Dyfed SY23 3DA (UK).

fully used factor and discriminant analyses [18,19] to uncover the concentration of components (expressed in the form of "variance diagrams") from various sets of simulated mixtures (biopolymers, lignites and grass leaves). It is plausible that such an approach would be successful in estimating the concentrations of biochemical components from pyrolysis mass spectra of microorganisms (simply another form of complex mixture).

Chemometrics is the discipline concerned with the application of statistical and mathematical methods to chemical data, typically via the transformation of multivariate spectral inputs into the concentrations of target determinands [20,21]. A related approach is the use of (artificial) neural networks (ANNs), which are, by now, a well-known means of uncovering complex, nonlinear relationships in multivariate data. ANNs can be considered as collections of very simple "computational units" which can take a numerical input and transform it (usually via summation) into an output (see Refs. 22–27 for excellent introductions). The relevant principle of supervised learning in ANNs is that the ANNs take numerical inputs (the training data) and transform them into desired predetermined outputs. The input and output nodes may be connected to the "external world" and to other nodes within the network. The way in which each node transforms its input depends on the so-called "connection weights" (or "connection strength") and "bias" of the node, which are modifiable. The output of each node to another node or the external world then depends on both its weight strength and bias and on the weighted sum of all its inputs, which are then transformed by a (normally) nonlinear weighting function referred to as its activation function. For present purposes, the great power of neural networks stems from the fact that it is possible to "train" them. Training is effected by continually presenting the networks with the "known" inputs and outputs and modifying the connection weights between the individual nodes and the biases, typically according to some kind of back-propagation algorithm [28], until the output nodes of the network match the desired outputs to a stated degree of accuracy. The network, the effectiveness of whose training is usually determined in terms of the root mean square (RMS) error between the actual and the desired outputs averaged over the training set, may then be exposed to "unknown" inputs and will then immediately" output the globally optimal best fit to the outputs.

The reason this method is so attractive for the quantitative analysis of PyMS data is that it has been shown mathematically [29–31] that a neural network consisting of only one hidden layer, with an arbitrarily large number of nodes, can learn any, arbitrary (and hence nonlinear) mapping to an arbitrary degree of accuracy. ANNs are also considered to be robust to noisy data, such as those which may be generated by PyMS.

In this study the combination of PyMS and ANNs was evaluated for the possible use of these techniques quantitatively to analyse biological samples for the presence of unknown concentrations of determinands. Although ANNs have been applied to analyses for the presence of functional groups in the mass spectra of purified compounds [32], we believe this to be the first demonstration of the ability of ANNs quantitatively to analysis pyrolysis mass spectra in terms of the concentrations of target determinands.

EXPERIMENTAL

Bacterial strains

The three strains used in this study were *E. coli* W3110, a laboratory strain [33], ECO861 and ECO883. ECO861 and ECO883 have the common *E. coli* parent strain ECO80, a nalidixic acid-resistant mutant of a natural isolate from chicken litter, ECO70 [34], into which the transposon Tn1732 [35] was inserted [36]. In the case of ECO883, Tn1732 was inserted into the tryptophanase gene (tnaA), inactivating the gene, thus making this strain indole-negative. In ECO861, Tn1732 was inserted into another chromosomal region and the strain remained an indole producer. Strains were maintained on nutrient agar slopes (LabM) at 4°C.

Growth conditions

For the preliminary analyses of strains by PyMS cultures were grown on nutrient agar (LabM) for

16 h at 37°C. In the experiment investigating the production of indole, strains were grown for 16 h at 37°C on a minimal salts supplemented media [MSSM: K_2PO_4 (BDH), 7.0 g; KH_2PO_4 (BDH), 3.0 g; $(NH_4)_2SO_4$ (BDH), 1.0 g; sodium citrate (BDH), 0.5 g; $MgSO_4 \cdot 7H_2O$ (BDH), 0.25 g; casamino acids (Difco), 5.0 g; glucose (BDH), 4.0 g; agar (Oxoid), 16.5 g; H_2O, 1 l] with increasing amounts of DL-tryptophan (BDH) incorporated, ranging from 0 to 253 mg/l (0, 19, 38, 56, 74, 92,

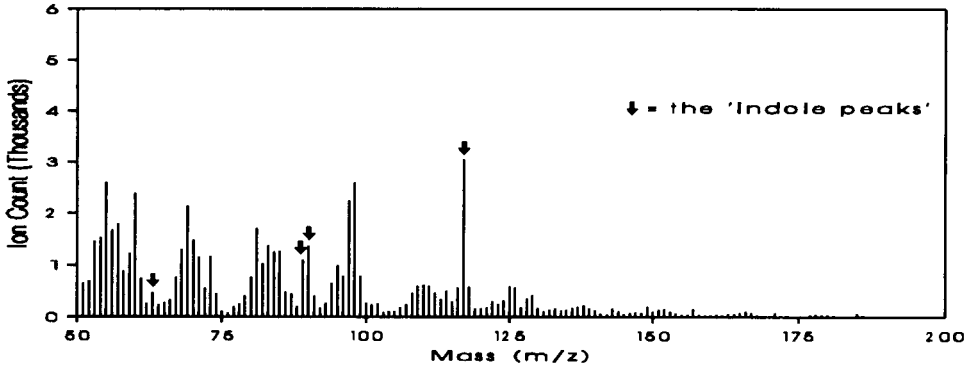

A

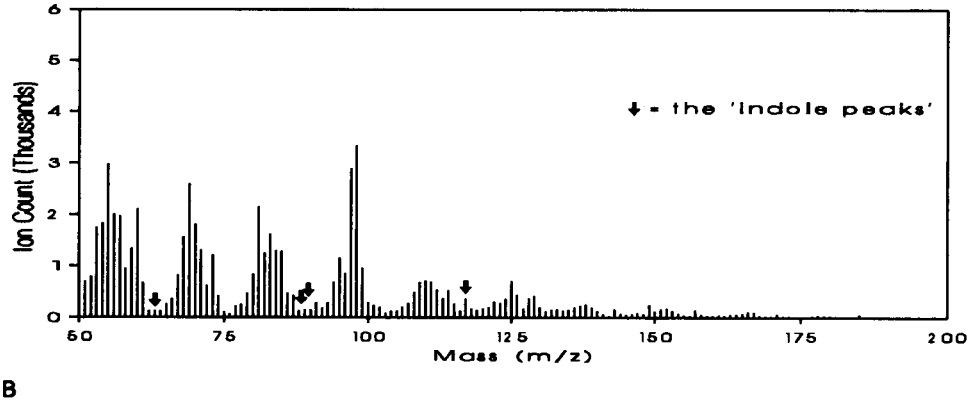

B

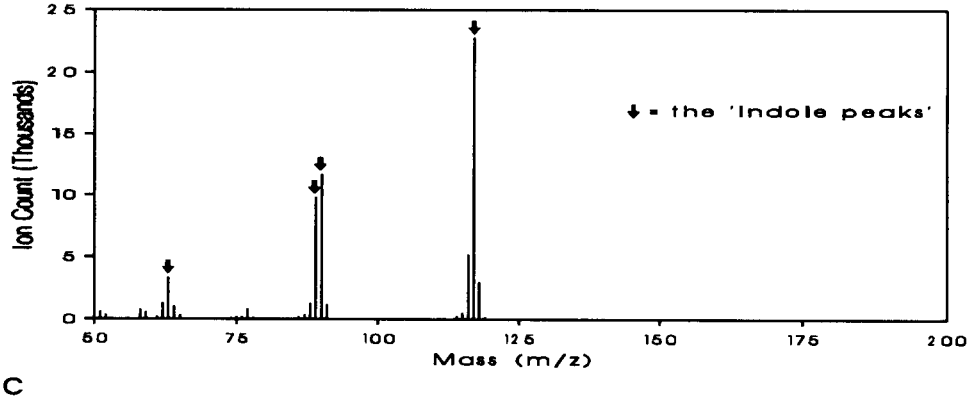

C

Fig. 1. Pyrolysis mass spectra of (A) *E. coli* ECO861, (B) *E. coli* ECO883, (C) and indole.

109, 127, 143, 160, 176, 192, 208, 223, 238 and 253 mg/l).

Sample preparation for pyrolysis mass spectrometry

Clean iron–nickel foils (Horizon Instruments, Heathfield) were inserted, using clean forceps, into clean pyrolysis tubes (Horizon Instruments), so that 6 mm was protruding from the mouth of the tube. After incubation, bacteria were picked up carefully from the top of one or more well-isolated colonies, avoiding the plate surface, by means of disposable plastic loops and smeared on 5 mm of a protruding foil to give a thin uniform surface coating. The samples were dried by vacuum desiccation for 20 min, then the foils were pushed into the tube using a stainless steel depth gauge so as to lie 10 mm from the mouth of the tube. Finally, viton 'O'-rings (Horizon Instruments) were placed on the tubes. Cultures to be analysed were grown in duplicate and two samples were prepared from each, giving four replicates for each culture. The samples were then analysed immediately. For the analysis of indole by PyMS: indole was dissolved in warm (50°C) distilled water, to an unknown concentration, and a 5 ml aliquot applied to a pyrolysis foil.

Pyrolysis mass spectrometry

The pyrolysis mass spectrometer used in this study was the Horizon Instruments PYMS-200X as described by Aries et al. [37]. The pyrolysate was generated in a vacuum by the heating of a ferro-magnetic foil carrying the sample. Heating was achieved by passing a radiofrequency current for 3 s through a pyrolysis coil which surrounds the sample-coated alloy foil. The foil and sample heated rapidly, 0.5 s, to the temperature corresponding to the Curie-point of the iron–nickel foil. At this temperature, 530°C, the alloy ceased to exhibit ferro-magnetic properties and heating finished; on cooling below the Curie-point, inductive heating resumed, so that the foil-pyrolyser system acted as a thermostatic switch maintaining the sample at the Curie-point, until current ceased to flow through the pyrolysis coil. The pyrolysate then entered a gold-plated expansion chamber heated to 150°C, whence it diffused down a molecular beam tube to the ionisation chamber of the mass spectrometer.

The pyrolysate was bombarded with low energy electrons (25 eV) producing both molecular and fragment ions (because low energy was used the majority carried only a single positive charge). Non-ionised molecules were deposited on a cold trap, cooled by liquid nitrogen. The ionised fragments were focussed by the electrostatic lens of a set of source electrodes, accelerated and directed into a quadrupole mass filter. The ions were separated by the quadrupole, on the basis of their mass-to-charge ratio, and detected and amplified with an electron multiplier. The mass spectrometer scans the ionised pyrolysate 160 times at 0.2 s intervals following pyrolysis. Data were collected over the m/z range 51 to 200, in one tenth of a mass-unit intervals. These were then integrated to give unit mass. Given that the charge of the fragment was unity the mass-to-charge ratio can be accepted as a measure of the mass of pyrolysate fragments. The IBM-compatible PC used to control the PYMS-200X, was also programmed (using software provided by the manufacturers) to record spectral information on ion count for the individual masses scanned and the total ion count for each sample analysed.

Data analysis

The data from PyMS may be displayed as quantitative pyrolysis mass spectra (Fig. 1). The x-axis represents the m/z ratio and the y-axis contains information on the ion count for any particular m/z value ranging from 51 to 200. Data were normalised to a total ion count of 2^{16}.

All ANN analyses were carried out using a user-friendly, neural network simulation program, NeuralDesk (Neural Computer Sciences, Southampton), which runs under Microsoft Windows/3.1 on an IBM-compatible PC. To ensure maximum speed, an accelerator board for the PC (NeuSprint) based on the AT&T DSP32C chip, which effects a speed enhancement of some 100-fold, permitting the analysis (and updating) of some 400 000 weights per second, was used. Data were also manipulated prior to analysis using the Microsoft Excel 4.0 spreadsheet.

For training the ANN, the inputs were the

averages of the four normalised replicate pyrolysis mass spectra derived from *E. coli* W3110 grown on MSSM containing tryptophan at concentrations of 0, 38, 74, 109, 143, 176, 208, 238 and 253 mg/l, with the output nodes being the actual (true) initial tryptophan concentration.

The primary algorithm used was standard back-propagation (BP) [28], running on the accelerator board. As indicated above this algorithm employs processing nodes (neurons or units), connected using abstract interconnections (connections or synapses). The format (topology) of the network is that of a directed acyclic graph. Connections each have an associated real value, termed the weight, that scale signals passing through them. Nodes sum the signals feeding to them and output this sum to each driven connection scaled by a "squashing" function with a sigmoidal shape.

The training of the network consists of the preparation of a set of pairs of patterns where one half of the pair is input to the network and the other represents the known or expected response. The stimulus pattern is applied to the network, which is allowed to run until an output is produced at each output node. The differences between the actual output and that expected, taken over the entire set of patterns are fed back through the network in the reverse direction to signal flow (hence back-propagation) modifying the weights as they go. This process is repeated until a suitable level of error is achieved.

For any given network, set of weight values, and set of training patterns there exists an overall RMS error value. If one dimension in a multidimensional space is put aside for each weight, and one more for the RMS error, one can construct an error surface. The BP algorithm performs gradient descent on this error surface by modifying each weight in proportion to the gradient of the surface at its location. Two parameters, *learning rate* and *momentum*, control this process. Learning rate scales the size of the step down the error surface taken each iteration, and momentum acts like a low pass filter, smoothing out progress over small bumps in the error surface.

It is known that gradient descent can cause the network to get "stuck" in a depression in the error surface should such a depression exist. These are termed "local minima" [24,26]. However, it has been found empirically that these are seldom problematic for larger networks, since the chances of encountering a multidimensional depression that is bounded in every dimension are small.

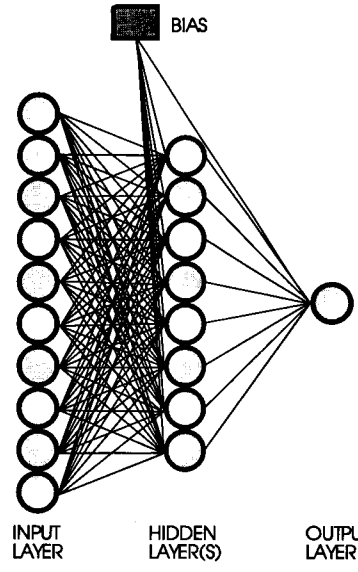

Fig. 2. A neural network consisting of 10 inputs (data herein actually consisted of 150 inputs/masses) and 1 output (tryptophan concentration) connected to each other by 1 hidden layer consisting of 8 nodes. In the architecture shown, adjacent layers of the network are fully interconnected, although other architectures are possible.

The structure of the ANN used in this study therefore consisted of 3 layers containing 159 nodes made up of the 150 input nodes (normalised pyrolysis mass spectra), 1 output node (initial tryptophan concentration), and one "hidden" layer containing 8 nodes. Each of the 150 input nodes was connected to the 8 nodes of the hidden layer which in turn were connected to the output node. In addition, the hidden layer and output node were connected to the bias, making a total of 1217 connections, whose weights will be altered during training (for a diagrammatic representation see Fig. 2). Before training commenced the input and output nodes were normalised between 0 and +1, and the connection weights were set to small random values, except the bias

which was always set to +1 [24]. Each epoch (one complete calculation in the network) represented 1217 connection weight updatings and a recalculation of the root mean squared (RMS) error between the true and desired outputs over the entire training set. A plot of the RMS error vs. the number of epochs represents the "learning curve", and was used to estimate the extent of training. Finally during training, all the 16 spectra (the averages of the four normalised replicate spectra) from *E. coli* W3110 grown on MSSM containing tryptophan (0–253 mg/l) (a mixture of seen and unseen data) were used as the "unknown" inputs (test data); the network then output its estimate (best fit) in terms of the initial tryptophan concentrations.

RESULTS AND DISCUSSION

Pyrolysis mass spectral fingerprints of *E. coli* ECO861, *E. coli* ECO883 and indole are shown in Fig. 1. When indole was analysed by PyMS, peaks at *m/z* 117, 90, 89 and a "murmur" at 63 can be seen (Fig. 1C). These we designate the "indole peaks". The analysis of an indole-producing strain of *E. coli*, ECO861, showed that these "indole peaks" were present in its pyrolysis mass spectrum (Fig. 1A), but were absent, or at least marginal, in spectra from ECO883, an indole-negative strain (Fig. 1B).

The significance of these changes is clear from Fig. 3 which shows a simple subtraction of the normalised averages of four spectra of ECO883 from ECO861. The positive half of the graph indicates the peaks that are more intense in ECO861 and shows many similarities to the pyrolysis mass spectrum of pure indole (Fig. 1C). ECO861 and ECO883 are genotypically very similar; they both arise from the same ECO80 parent strain and both have the Tn1732 transposon inserted, so they contain the same DNA. Genotypically they differ only in that ECO861 has an active tryptophanase gene (when this strain is cultivated on tryptophan-containing media it has the indole-positive phenotype), which in ECO883 has been inactivated by insertion of Tn1732, giving an indole-negative phenotype.

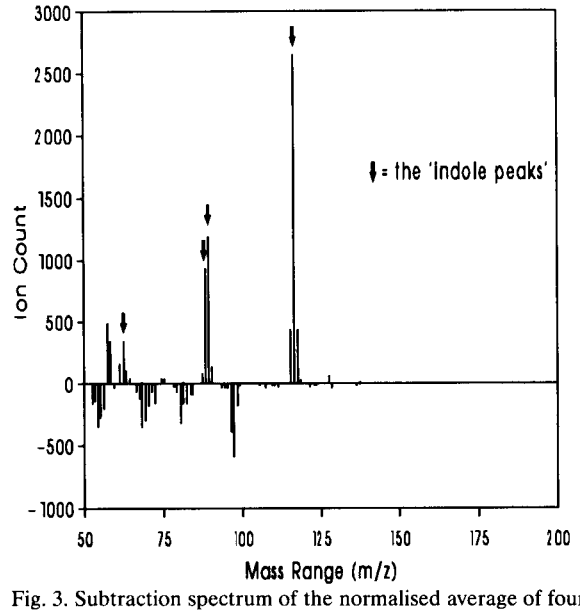

Fig. 3. Subtraction spectrum of the normalised average of four *E. coli* ECO883 pyrolysis mass spectra from the average of four *E. coli* ECO861 spectra, showing the masses that are more intense in *E. coli* ECO861 (positive half) and ECO883 (negative half).

This demonstrates that the presence of the single cellular component indole gives a large and clearly visible spectral change. It is plausible that indole gives such an easily detectable signal because it is preferentially vaporized on pyrolysis. Indole boils at 253°C *without* decomposition, a temperature which is lower than the Curie-point used (530°C). When indole was introduced by evaporation into the mass spectrometer without pyrolysis (a blank tube, with no foil, was loaded with 5 μl of indole solution, which will "sublime" when exposed to a vacuum) the same spectrum as that shown in Fig. 1C was observed (data not shown). Since the molecular weight of indole is 117.15, the peak at *m/z* 117 corresponds to the molecular ion. The peaks at *m/z* 90, 89 and 63 are likely to be produced by electron impact fragments, but the structures of these ions have not been elucidated.

The relationship between the relative amount of indole produced from *E. coli* ECO861, ECO883 and W3110, as an effect of altering the amount of tryptophan in MSSM from 0 to 253 mg/l is shown in Fig. 4. This is a plot of the

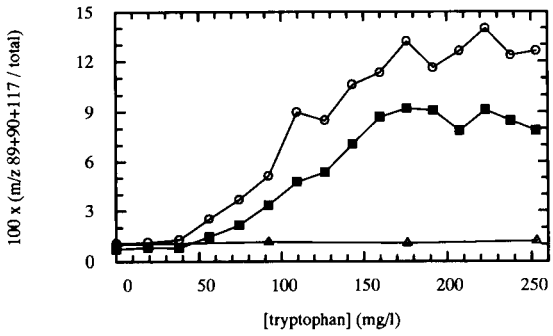

Fig. 4. Graph showing the percentage of the 3 major "indole peaks" (masses 117, 90 and 89) for *E. coli* ECO861, ECO883 and W3110 when grown on minimal media with increasing concentrations of tryptophan.

relative percentage of the indole peaks in the pyrolysis mass spectra, i.e., the ion counts at m/z 89 + 90 + 117 (63 was omitted because of its low intensity) over the total ion count against the true tryptophan concentration. It can be seen that increasing the amount of tryptophan in the medium has no effect on the indole-negative *E. coli* ECO883 strain, but in the stated representation (Fig. 4) gives an S-shaped curve with both *E. coli* ECO861 and W3110. In the region from 0 to 50 mg/l added tryptophan no indole was apparently produced, either because the tryptophanase gene had not yet been activated or (more likely) because the tryptophan was being used by the bacteria in biosynthetic processes. At greater values of added tryptophan the tryptophanase gene appears to be induced and indole was produced in an amount approximately linear with respect to the amount of tryptophan added, until at about 175 mg/l tryptophan the graph levelled off, showing that indole production had reached a maximum. This phenotypic change in *E. coli* ECO861 and W3110 can be attributed to the production of indole from tryptophan-containing medium, since these bacteria possess the tryptophanase gene. It is clear that alterations in the amount of tryptophan in the growth medium can cause measurable phenotypic changes in these bacteria.

As described above, the neural network was then trained with the various spectral inputs and the effectiveness of training determined in terms of the RMS error between the actual and the desired outputs; this "learning curve" is shown in Fig. 5. Training was effected five times; because the five curves were found to superimpose, despite the randomised starting connection weights, it is clear that training was executed in a rather reproducible manner. At various points during training, the network was interrogated both with spectra that were used to train the network (closed circles) and with "unknown" spectra (open circles) which were not in the training set; these are displayed in Fig. 6. Each plot consists of the five replicate trainings of Fig. 5 (although the initial random weightings on the connections in the network will have been different), shown as an average with standard error bars.

These experiments display some very interesting neurodynamics. It can be seen in the learning curve (Fig. 5) that the network very quickly reached a plateau after 100 epochs and between this time and some $2–3 \times 10^4$ epochs training appeared to have finished. When the network was interrogated in the middle of this plateau, a plot of the network's estimate vs. the true output (the initial concentrations of tryptophan) (Fig. 6A) gave a sigmoidal plot, and it was evident that although the network had made some sort of estimate of the tryptophan concentration, training was not yet finished, i.e. (Fig. 5), the net appeared to have found a very flat area in weight space. When the network was left to train a bit further the RMS error rather "suddenly" and reproducibly decreased (between 3×10^3 and $2 \times$

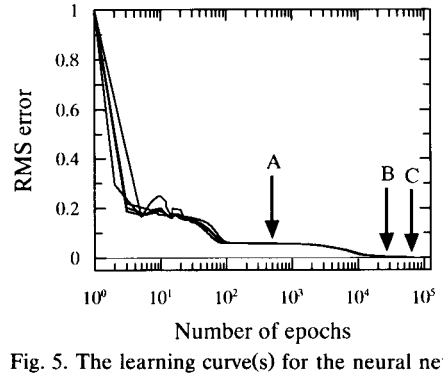

Fig. 5. The learning curve(s) for the neural network using the standard-back propagation algorithm with 1 hidden layer consisting of 8 nodes. For details see text.

10^4 epochs) to approximately 0.005 and there was an approximately flat area until the error slowly diminished to 0.001 (Fig. 5). At an RMS error of 0.005 (Figs. 5 and 6B) the network's estimate of initial tryptophan concentration was very similar to the true concentrations, both for spectra that were used as the training set and the "unknown" spectra. If training was allowed to proceed further to an RMS error of 0.001, however, a different trend was seen: the network's estimate of the

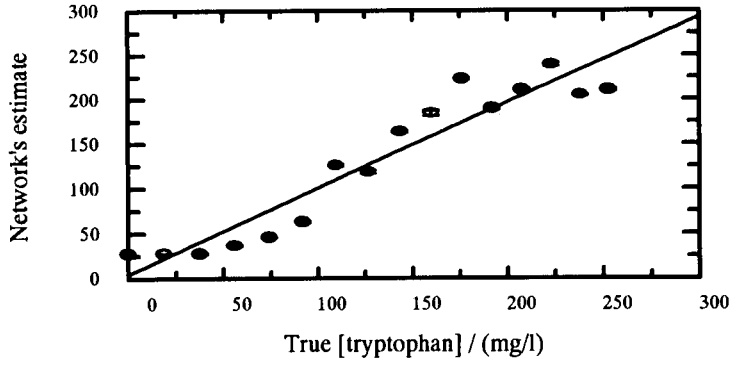

A

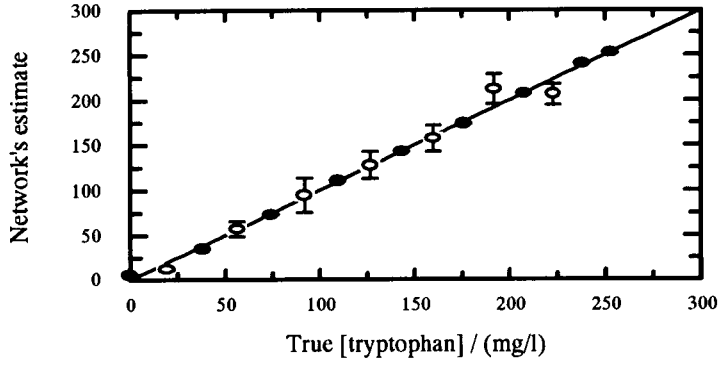

B

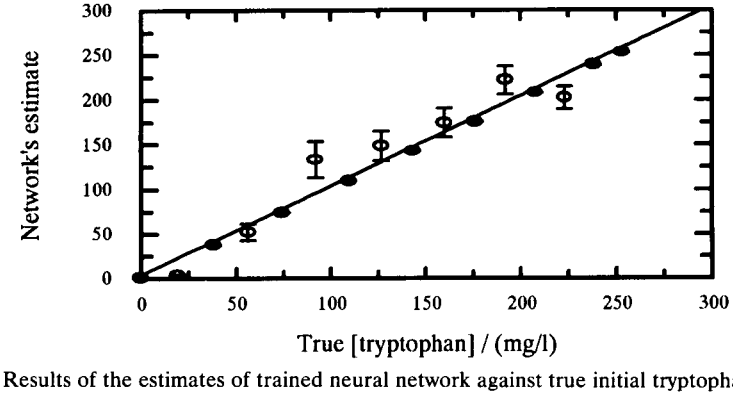

C

Fig. 6. Results of the estimates of trained neural network against true initial tryptophan concentration, at interrogation points A, B and C from Fig. 5; points are the average of five trainings. Closed circles represent spectra that were used to train the network and open circles indicate "unknown" spectra which were not in the training set. Error bars show standard deviation. The best linear fits were calculated using all data.

training set is very good, whilst the "unknown" spectra (test set) are not nearly as well estimated. This indicated that the network had now been over-trained.

That optimal training was achieved when an RMS error of 0.005 was reached is most important for studies of the present type. For ANNs accurately to learn the concentrations of determinands in biological systems the network must be trained to the correct point (and must be trained with the appropriate number of standards [38]. Therefore it is imperative that ANNs should be trained several (perhaps many) times to ascertain whether they reproducibly converge, in concert with appropriate multivariate statistical techniques such as "leave-one-out" [39].

In other studies ANNs were set up with the same architecture as the ones used above except that they contained fewer, including no, hidden layers. It was interesting to observe that the networks were still able to converge, i.e. they were successfully trained (data not shown), indicating in the boundary case that the differences due to indole in these pyrolysis mass spectra were linearly separable in 150-dimensional space.

In summary, we have shown that the combination of PyMS and ANNs was able quantitatively to detect the component indole, which in pure form gave a pattern of peaks at m/z 117, 90, 89 and a murmur at 63, and was important in the detection of a single genotypic difference, attributed to tryptophanase, between *E. coli* ECO861 and ECO883. It was also demonstrated that varying the amount of tryptophan in a minimal supplemented salts medium gave a measurable phenotypic change in indole-positive strains. It should be obvious that this approach might be exploited, inter alia, for the analysis of any fermentation or biotransformation of interest, and that the combination of PyMS and ANNs constitutes a novel, powerful and interesting technology for the analysis of the concentrations of appropriate substrates, metabolites and products in chemical processes generally.

We thank Roger Berkeley for his help with PyMS, Mark Bale for providing the ECO strains, and Andy Edmonds for constructive criticism of the manuscript. This work is supported under the terms of the UK SERC LINK scheme in Biochemical Engineering, in collaboration with Horizon Instruments, ICI Biological Products and Fine Chemicals, and Neural Computer Sciences.

Note added in proof

D. Lloyd et al. [40] have observed the tryptophan-enhanced production of indole by *Trichomonas vaginalis*, using membrane-inlet electron impact mass spectrometry and with a mass spectrum very similar to that shown in Fig. 1C.

REFERENCES

1 D.B. Drucker, Methods Microbiol., 9 (1976) 51.
2 W.J. Irwin, Analytical Pyrolysis: A Comprehensive Guide, Marcel Dekker, New York, 1982.
3 H.L.C. Meuzelaar, J. Haverkamp and F.D. Hileman, Pyrolysis Mass Spectrometry of Recent and Fossil Biomaterials, Elsevier, Amsterdam, 1982.
4 C.S. Gutteridge, Methods Microbiol., 19 (1987) 227.
5 R.C.W. Berkeley, R. Goodacre, R.J. Helyer and T. Kelley, Lab. Pract., 39 (1990) 81.
6 L.A. Shute, C.S. Gutteridge, J.R. Norris and R.C.W. Berkeley, J. Gen. Microbiol., 130 (1984) 343.
7 G. Wieten, H.L.C. Meuzelaar and K. Haverkamp, in G. Odham, L. Larsson and P.A. Mårdh (Eds.), Gas Chromatography/Mass Spectrometry: Applications in Microbiology, Plenum Press, New York, 1984, pp. 335–380.
8 R. Goodacre and R.C.W. Berkeley, FEMS Microbiol. Lett., 71 (1990) 133.
9 R. Kajioka and P.W. Tang, J. Anal. Appl. Pyrol., 6 (1984) 59.
10 H.L.C. Meuzelaar, P.G. Kistemaker, W. Eshuis and H.W.B. Engel, Rapid Methods and Automation in Microbiology, Learned Information, Oxford, 1976, pp. 225–230.
11 G. Wieten, K. Haverkamp, H.B.W. Engel and L.G. Berwald, Rev. Infect. Diseases, 3 (1981) 871.
12 G. Wieten, K. Haverkamp, H.L.C. Meuzelaar, H.B.W. Engel and L.G. Berwald, J. Gen. Microbiol., 122 (1981) 109.
13 R. Freeman, M. Goodfellow, F.K. Gould, S.J. Hudson and N.F. Lightfoot, J. Med. Microbiol., 32 (1990) 283.
14 J.T. Magee, J.M. Hindmarch, I.A. Burnett and A. Pease, J. Med. Microbiol., 30 (1989) 273.
15 S.M. Chantler and M.B. McIllmurray, Methods Microbiol., 19 (1987) 273.
16 A. Saano and K. Lindström, Symbiosis, 8 (1990) 61.
17 W. Windig and H.L.C. Meuzelaar, Anal. Chem., 56 (1984) 2297.

18 N.H. Nie, C.H.G. Hull, J.G. Jenkins, K. Steinbrenner and W.H. Brent, Statistical Package for the Social Sciences, McGraw-Hill, New York, 1975.
19 W. Windig, P.G. Kistemaker and J. Haverkamp, J. Anal. Appl. Pyrol., 3 (1981) 199.
20 D.L. Massart, B.G.M. Vandeginste, S.N. Deming, Y. Michotte and L. Kaufmann, Chemometrics: A Textbook, Elsevier, Amsterdam, 1988.
21 S.D. Brown, Anal. Chem., 64 (1992) 22R.
22 P.D. Wasserman and R.M. Oetzel, NeuralSource: the Bibliographic Guide to Artificial Neural Networks, Van Nostrand Reinhold, New York, 1989.
23 J.L. McClelland and D.E. Rumelhart, Explorations in Parallel Distributed Processing; A Handbook of Models, Programs and Exercises, MIT Press, Cambridge, MA, 1988.
24 P.D. Wasserman, Neural Computing: Theory and Practice, Van Nostrand Reinhold, New York, 1989.
25 R.C. Eberhart and R.W. Dobbins, Neural Network PC Tools, Academic Press, London, 1990.
26 P.K. Simpson, Artificial Neural Systems, Pergamon Press, Oxford, 1990.
27 J. Hertz, A. Krogh and R.G. Palmer, Introduction to the Theory of Neural Computation, Addison-Wesley, Redwood City, 1991.
28 D.E. Rumelhart, J.L. McClelland and the PDP Research Group, Parallel Distributed Processing, Experiments in the Microstructure of Cognition Vols. I & II. MIT Press, Cambridge, MA, 1986.
29 K. Hornik, M. Stinchcombe and H. White, Neural Networks, 2 (1989) 359.
30 K. Hornik, M. Stinchcombe and H. White, Neural Networks, 3 (1990) 551.
31 H. White, Neural Networks, 3 (1990) 535.
32 B. Curry and D.E. Rumelhart, MSnet: A Neural Network that Classifies Mass Spectra, Hewlett Packard Technical Report HPL-90–161, 1990.
33 B.J. Bachmann, Bacteriol. Rev., 36 (1972) 525.
34 M.J. Bale, P.M. Bennett, M. Hinton and J.E. Beringer, in J.C. Fry and M.J. Day (Eds.), Bacterial Genetics in Natural Environments, Chapman and Hall, London, 1990, pp. 231–239.
35 D. Ubben and R. Schmitt, Gene, 41 (1986) 145.
36 S.J. Bale, personal communication.
37 R.E. Aries, C.S. Gutteridge and T.W. Ottley, J. Anal. Appl. Pyrol., 9 (1986) 81.
38 R. Goodacre, A.N. Edmonds and D.B. Kell, J. Anal. Appl. Pyrol., (1993) in press.
39 E.R. Malinowski, Factor Analysis in Chemistry, Wiley, New York, 1991.
40 D. Lloyd, F.R. Lauritsen and H. Degn, J. Gen. Microbiol., 137 (1991) 1743.

Analytica Chimica Acta, 279 (1993) 27–37
Elsevier Science Publishers B.V., Amsterdam

Characterization of a sampling unit based on tangential flow filtration for on-line bioprocess monitoring

Torbjörn Buttler, Lo Gorton and György Marko-Varga
Department of Analytical Chemistry, University of Lund, P.O. Box 124, S-221 00 Lund (Sweden)

(Received 1st October 1992; revised manuscript received 17th December 1992)

Abstract

The performance of a sampling unit (Waters Filter/Acquisition Module) based on tangential flow filtration, in conjuction with column liquid chromatography, is described. Filtration characteristics of this module were investigated. Two membrane types and pore sizes and their influence on the sampling were determined. The influence of feed rate on the flow-rate of the filtrate for model solutions and real fermentation substrates and broths was investigated. Membrane recovery values for carbohydrates in solutions varying in complexity were determined. The contents of amino acids and organic acids in these substrates and broths and their recovery values are presented.

Keywords: Liquid chromatography; Process analysis; Amino acids; Carbohydrates; Fermentation; Filtration; Membrane filtration; Sampling

Progress in the analysis of biotechnological processes has developed rapidly during the last decade. Classical batch detection techniques based on chemical derivatization reactions and titrations, UV–visible spectrophotometry and, more selectively, enzyme assays are commonly used techniques. Many of these are still used today but transferred into various flow-techniques such as flow injection (FI) analysis, gas chromatography (GC) and column liquid chromatography (CLC), sometimes coupled with mass spectrometry (MS) [1]. Despite these developments, in most fermentation processes, e.g., in antibiotics production such as penicillin, manual sampling is still used in combination with steam sterilization.

There are two different ways to sample continuously from a bioreactor, not including manual sampling methods: either the sampling unit is mounted inside the fermenter or is placed outside it. Several systems of both kinds have been reported during the last 10 years. The major advantage of an in situ module is that it is possible to obtain a true picture of the conditions of the bioreactor. The drawbacks are a relatively high response time, no possibility of changing the membrane during a fermentation and calibration difficulties. This type of sampling unit often consists of a stainless-steel carrier serving as a support for a porous membrane. The filtrate is then withdrawn by means of a peristaltic pump and transported further to analysis. Such an in situ module was used by Christensen et al. [2] to sample fed-batch penicillin fermentations. It requires a well stirred position in the bioreactor to avoid or reduce membrane clogging. Its simple operation, however, makes it an interesting approach. In early work by Mandenius et al. [3], a dialysis probe for continuous sampling in complex media was presented, and Håkanson et al. [4]

Correspondence to: T. Buttler, Department of Analytical Chemistry, University of Lund, P.O. Box 124, S-221 00 Lund (Sweden).

described a general sampling system based on a coaxial catheter. The latter system has the advantage that the metabolic processes might be stopped by adding inhibitors at the tip of the catheter. A new promising in situ technique that currently is being tested is microdialysis [5].

In all systems where the sampling unit is placed outside the fermenter, the fermentation broth must be pumped out of the bioreactor to the sampling unit and, after filtration, back again. This increases the risk of contamination. Also, the circulation itself may affect the morphology of the microorganisms owing to the high linear velocities obtained in the tubings [2]. It is, possible, however, to change the membrane during a fermentation. This type of sampling unit exists in several different designs and a number of them are commercially available. The basic principle of the unit is that the liquid transport of sample across the membrane is to be enhanced. The Biopem module [2,6,7] contains a magnetic stirrer placed above the membrane. This unit has been used successfully for yeast fermentations but is not so well suited for fermentations using fungi as the in situ module [2]. This is explained by an insufficiency of the stirrer to prevent material build-up. Tangential flow filtration (see below) is used by the A-SEP filter module (Applikon, Schiedam, Netherlands). This unit has been used to monitor glucose and amino acids [8] and acetate and phosphate [9]. The same filtration technique is used in the Waters Filter/Acquisition Module (FAM) that has been used by several workers [1,10,11] and also in this work. Recently, a hollow-fibre ultrafiltration module was successfully used to determine carbohydrates in an *Escherichia coli* batch culture [12]. That paper included a study of the influence of some system parameters on the sampling process using hollow fibres.

So far, papers concerning the FAM unit have been devoted to larger scale bioprocesses. No results have been presented where the FAM has been used as a sampling system for small-scale (< 1 l) fermentations. Nevertheless, it is important to have a sampling system for low reactor volumes to run test fermentations where the amount of microorganisms is very limited. These small-scale fermentations obviously require special sampling conditions, e.g., very low feed rates, and it is therefore of interest to investigate thoroughly and optimize the properties of such a module. This paper deals with the performance of the FAM at these low feed rates. First, the influence of the feed rate on the flow-rate of the filtrate was determined. Second, the recovery of the membrane for carbohydrates in model solutions of increasing complexity was studied. Finally, membrane properties for some other compounds found in fermentation substrates and broths were investigated.

EXPERIMENTAL

Chemicals

All carbohydrates, L-(+)arabinose, D-(+)cellobiose, D-(+)galactose, D-(+)glucose, D-(+)-mannose and D-(+)xylose, were of Sigma grade (Sigma, St Louis, MO). Amino acids, L-aspartic acid, L-phenylalanine and L-serine, were of Sigma grade (Sigma), except glycine, which was of analytical-reagent grade (Merck, Darmstadt). Salts of organic acids were obtained from Sigma, pyruvate (99%) and malate (Sigma grade), except lactate (purity and origin unknown) and acetate (analytical-reagent grade, Merck). The following substances were used as possible interfering compounds: bovine serum albumin (BSA) (fraction V) (Sigma), phenol, *o*-cresol and mandelic acid (analytical-reagent grade, Merck), benzenesulphonic acid (puriss, Fluka, Buchs, Switzerland), furfural (99%, Aldrich, Steinheim), baker's yeast (*Saccharomyces cereviseae*) (Jästbolaget, Stockholm) and ethanol [spectrographic grade (99.5%), Kemetyl, Stockholm]. Nutritients added were yeast extract (Difco, Detroit, MI) and ammonium sulphate (analytical-reagent grade, Merck). The fermentation substrate, spent sulphite liquor (SSL), was obtained from Modo (the Swedish Ethanol Development Foundation, Örnsköldsvik, Sweden) and penicillin broth from Gist-Brocades (Strängnäs, Sweden).

All solutions were prepared by dissolving the substance(s) in water obtained from a Millipore (Bedford, MA) Milli-Q water-purification system. This water was also used as the mobile phase.

Equipment

The set-up used throughout all the experiments is shown in Fig. 1. The main component was the sampling unit, a Waters Filter/Acquisition Module (FAM) (Millipore), equipped with a Rheodyne (Cotati, CA) Model 7045 six-port injection valve with a 20-μl loop. Membranes from Millipore (MF and Durapor) were used. The LC system consisted of a high-pressure pump (Waters Model 590 programmable solvent-delivery module) and a refractive index detector (Model 2142, LKB, Bromma, Sweden). The analytical column (300 × 7.8 mm i.d.) was a ligand-exchange column in Ca^{2+} form (Aminex HPX-87C, Bio-Rad Labs., Richmond, CA) heated to 85°C in a chromatographic oven (Waters column heater module, controlled by a Waters temperature control module). The mobile phase was pumped at a flow-rate of 0.6 ml min^{-1}. The detector signal was sent to a chart recorder (LKB Model 2210) and to a data station (Baseline 810 Chromatography Workstation, Dynamic Solutions, Millipore). The bioreactor solution was circulated by a peristaltic pump (Minipulse 2, Gilson, Villiers-le-Bel, France). Viscosity measurements were made at room temperature with an Ostvald 7–24 glass viscosimeter. The amino acid samples were analysed on a Biotronic (Munich) Model 5001 amino acid analyser, column dimensions 385 × 3.2 mm i.d., resin type BTC 2710. The mobile phase, pumped at a flow-rate of 0.25 ml min^{-1}, consisted of lithium chloride and citrate buffer, programmed in four steps, as recommended by the manufacturer: step A (14 min), 0.15 M LiCl, 0.070 M citrate buffer (pH 2.86), 34°C; step B (21 min), 0.25 M LiCl, 0.067 M citrate buffer (pH 2.89), 34°C; step C (34 min), 0.35 M LiCl, 0.067 M citrate buffer (pH 3.20), 34°C; step D (16 min), 0.45 M LiCl, 0.067 M citrate buffer (pH 4.02), 61°C. The amino acids were determined spectrophotometrically at 570 nm using postcolumn derivatization with ninhydrin, pumped at 0.14 ml min^{-1}. α-Aminoadipic acid was used as an internal standard. Samples were evaporated and dissolved in 0.5 ml of step A buffer before injection (50 μl).

The content of organic acids was determined with a Dionex (Sunnyvale, CA) Model 4000i ion chromatograph equipped with an ion exclusion column (ICE-AS1, Dionex), an anion micro membrane suppressor (AMMS-ICE, Dionex) and a conductimetric detector. The mobile phase, 1 mM HCl, was pumped at a flow-rate of 0.8 ml min^{-1} and the suppressor regenerated by pumping a 5 mM *tert*-butylammonium hydroxide (TBA^+OH^-) solution at 2.0 ml min^{-1} through it. All crude samples taken from the bioreactor were manually

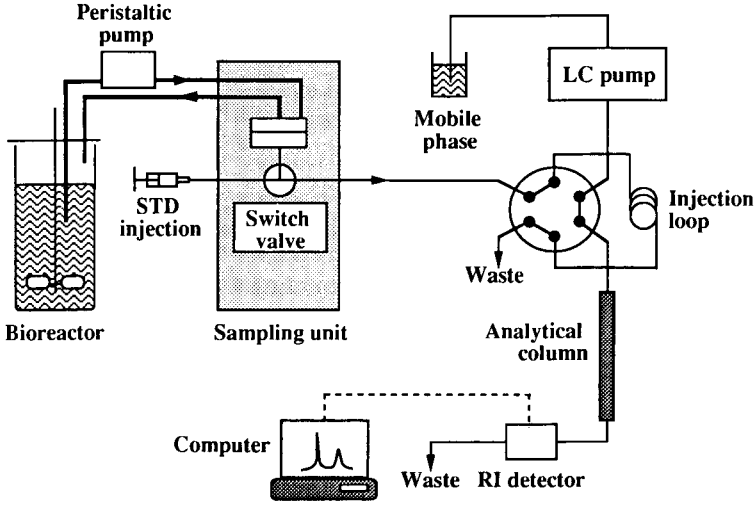

Fig. 1. Schematic diagram of the experimental set-up including the sampling unit coupled on-line to the CLC system.

filtered with a Millipore Millex HV or HA (0.45-μm pore size) membrane and diluted 50-fold prior to analysis. The injection volume was 50 μl.

RESULTS AND DISCUSSION

General description of the sampling unit

The sampling device used in this study is based on the Waters FAM filtration unit. It utilizes a tangential flow (or cross-flow) filtration (TFF) assembly (see Fig. 2), to divide the bioreactor solution into two streams, the particle-enriched retentate and the particle free filtrate. A normal filtration unit, where the plane of the filter is perpendicular to the direction of the flow, is not well suited owing to the large content of particles in broths. This causes a material build-up, giving a decreased filtration rate, and ends in total clogging of the membrane. In TFF, the solution is driven along a path that is parallel to the filter. This movement of fluid across the surface of the filter keeps it clean and prevents sedimentation of material. In this study, two different Millipore membranes were used, one made of acetate and nitrate esters of cellulose, denoted MF, and the other of poly(vinylidene difluoride), denoted Durapor. Two different pore sizes of each type, 0.22 and 0.45 μm, were used.

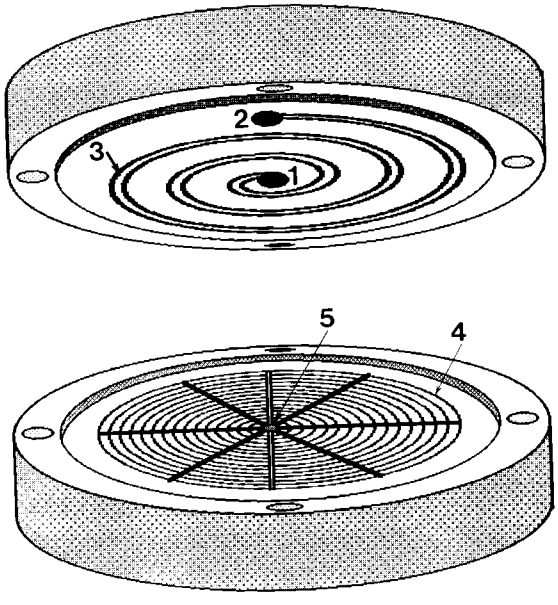

Fig. 2. Schematic illustration of the tangential flow filtration assembly. 1 = Feed inlet; 2 = retentate outlet; 3 = spiral grooves; 4 = filtrate collection; 5 = filtrate outlet.

After filtration, the retentate is returned to the stirred fermenter and the filtrate is transferred to a switching valve placed inside the FAM. This valve allows an alternate passage of either the filtrate or manually loaded standards to the sampling loop (see Fig. 1). The ability to analyse standards during a fermentation is important for accurate quantification. The dead volume between the filtration unit (or the standard injection inlet) and the sampling loop was estimated to be 200 μl. The sample (filtrate or standard) is then passed through the sampling loop placed on the injection valve and thereafter to waste. Next, the trapped sample is introduced into the CLC system, separated and evaluated.

Several model solutions of varying complexity together with complex biotechnological samples were used to characterize the sampling unit. The results of these experiments and investigations are reported below.

Viscosity measurements

Under controlled conditions, the model solutions and real broths were used to characterize the sampling unit. The first and simplest model solution was just a 50 mM phosphate buffer solution at pH 6.0 (A). To increase the complexity, baker's yeast (80 g l^{-1}) was added to the buffer solution (B). Further, spent sulphite liquor (SSL) containing yeast extract (0.25%, w/v), ammonium sulphate (0.025%, w/v) and baker's yeast (80 g l^{-1}) was used (C). The very complex composition of SSL has been discussed in detail previously [13]. It may be used as a model substrate in ethanol fermentations as it contains large amounts of soluble sugars. It is a dark-brown liquid which, except for sugars, contains lignin decomposition products, browning reaction compounds and phenolic derivatives. The fourth solution was a penicillin fermentation broth (PFB) (D). To describe these solutions further, their viscosities were measured. The relative viscosity, η_r, was calculated using the relationship

$$\eta_r = \eta/\eta_o \quad (1)$$

where η is the viscosity of the sample and η_0 the viscosity of a reference solution (water). Addition of 80 g l^{-1} of yeast increases the viscosity of the phosphate buffer solution by about 20% to a value of 1.20. Moreover, SSL with yeast is more than twice as viscous as water ($\eta_r = 2.36$) and is indeed a complex fermentation broth that places high demands on pumps and also on the sampling and filtration procedure. It was not possible to determine the viscosity of the penicillin broth. Although this solution in fact seems less viscous than SSL, it contains a high concentration of mycelium, resulting in a very inhomogeneous solution. This inhomogeneity made the mycelia clog the capillary of the viscosimeter.

Filtrate flow-rate measurement

The driving force for filtration is the average transmembrane pressure (ATP) [14], which is defined as

$$ATP = (P_i + P_r)/2 - P_f \quad (2)$$

where P_i is the inlet (feed) pressure, P_r is the retentate pressure and P_f is the filtrate pressure. The flow-rate of the filtrate is therefore dependent on ATP and the rate of the feed pump. No debubbler or degassing unit [10,11] is necessary as there is no filtrate pump, responsible for sustaining a small pressure drop over the membrane, which may lead to bubbles in the filtrate. In addition, the filtrate flow-rate can be controlled by a restrictor, situated inside the FAM. The restrictor performance is based on the feed rate of the circulating solution. However, it was found that the flow-rate of the filtrate does not vary linearly with the created back-pressure for all flow-rates of the feed pump.

Choosing sampling conditions is an important part of fermentation monitoring. The flow-rate of the filtrate must be high enough to rinse thoroughly and fill the sampling loop with fresh filtrate on each sampling occasion. If the pore size of the membrane is decreased, the cleaner the filtrate will be. However, a smaller pore size also reduces the flow-rate of the filtrate. Moreover, the mechanical strength of the membrane must be as high as possible so that the filtration performance is not deteriorated during long fermentations. In addition, the viscosity of the solution also affects the filtration process. Therefore, the influence of pumping feed rate, membrane type and pore size on the flow-rate of the filtrate was studied. Table 1 shows the flow-rate of the filtrate at different feed rates for the four model solutions described above. The values are averages of several ($n = 3$–5) measurements. The initial filtrate flow-rate is, however, higher in most instances than the values given in Table 1. In accordance with theory, the flow-rate of the filtrate increases with increae in feed rate (see Table 1). Further, as the two membrane types are equally hydrophilic, one could expect small differences between membrane types and large differences between pore sizes. Indeed, this is actually true for all four model solutions. For example, the flow-rates of the filtrate obtained with the SSL using MF and Durapor membranes (0.22 μm) are similar (0.32 and 0.30 ml min^{-1}), and

TABLE 1

Influence of feed rate on the flow-rate of the filtrate [a]

Feed rate (ml min^{-1})	Filtrate flow-rate (ml min^{-1})									
	Solution A		Solution B		Solution C				Solution D	
	GV	GS	GV	GS	GV	GS	HV	HA	HV	HA
1.0	0	0	0	0	0	0	0	0	– [b]	0.07
3.0	0	0	0	0	0	0	0.07	0.05	– [b]	0.17
6.0	0.16	0.15	0.19	0.18	0	0.05	0.22	0.20	0.32	0.30
9.0	0.33	0.33	0.36	0.36	0.08	0.10	0.37	0.32	0.35	0.40
12.0	0.54	0.54	0.60	0.56	0.32	0.30	0.67	0.58	0.40	0.50

[a] Abbrevations of membrane types: GV = Durapor (0.22 μm), GS = MF (0.22 μm), HV = Durapor (0.45 μm), HA = MF (0.45 μm). For solutions A, B, C and D, see text. [b] Clogging problems of the membrane.

also for the membranes with larger pores (0.45 μm) (0.67 and 0.58 ml min^{-1}). The absence of values at low feed rates for the PFB with the Durapor membrane is due to clogging problems of the membrane. These problems are probably caused by the high mycelium concentration giving inhomogeneous solutions, as found in the viscosity measurements. Similar tendencies could also be observed for higher feed rates (6–12 ml min^{-1}). The problems occurred, however, only after several hours of filtration. A pump feed rate of 12 ml min^{-1} was chosen, as Table 1 shows that it is favourable to have as high a flow-rate of the filtrate as possible. This means, naturally, that the restrictor mentioned above will be kept totally open.

Carbohydrate recovery in model solutions

It is, of course, of utmost importance that the analytes of interest will diffuse easily through the membrane, so that the filtrate will reflect the content of the bioreactor solution. This was investigated by circulating test solutions in the sampling system, collecting the filtrate and analysing both the filtrate and a crude sample from the fermenter by CLC. If the filtrate contains the same amount of a substance as is in the bioreactor solution, the recovery is said to be 100%. The recovery can thus be expressed as follows:

$$\text{Recovery}\,(\%) = 100(\text{peak area}_{\text{filtrate}}/\text{peak area}_{\text{reactor soln.}})$$

Peak height may be used instead of peak area, as distorted peaks have less effect on calculations based on peak height. The optimized membrane filtration procedure, using a feed rate of 12 ml min^{-1} and a 0.22-μm Durapor membrane, was investigated with pure reference sugar solutions containing 10 mM each of the sugars cellobiose, glucose, galactose and arabinose, and the filtrate and crude solutions were analysed as described above. The recoveries were found to be between 93 and 95%, collected at two different sampling times (see Table 2). The recovery values were calculated for both peak area and height. As shown in Table 2, the values for glucose, galactose and arabinose correlate well for both peak areas and heights. Only cellobiose gave a recovery of more than 100% in both area and height measurements, which is due to distorted chromatographic peaks, difficult to evaluate. The reason for this behaviour is not clear.

These experiments were followed by exchanging the pure sugar solution for well defined model

TABLE 2

Recovery of cellobiose, glucose, galactose and arabinose in model solutions

Solution type [a]	Recovery calculated from		Recovery (%)			
			Cellobiose	Glucose	Galactose	Arabinose
Pure standard solution	Area:	25 min	225	94	94	94
		50 min	224	94	94	94
	Height:	25 min	144	93	94	95
		50 min	144	93	94	95
A	Area:	45 min	101	96	98	96
		90 min	99	94	95	94
	Height:	45 min	96	92	90	91
		90 min	94	92	92	92
B	Area:	25 min	100	104	99	108
		50 min	109	102	84	157
	Height:	25 min	102	104	108	105
		50 min	104	104	99	133

[a] A and B represent the solutions containing interfering compounds. For details, see text.

solutions. Except for the sugars used above, these solutions contained compounds interfering with the CLC detection system and which are normally present or very similar to those present in industrial ethanol fermentation samples [15]. Solution A contained BSA (0.5%, w/v) and yeast extract (0.25%, w/v) (see Table 2), and solution B a mixture of phenol, *o*-cresol, mandelic acid, benzenesulphonic acid, furfural (2 mM each) and yeast extract. These model solutions were run in the set-up as described above.

After the analysis of solution A, the recovery values found were well in accordance with those obtained with the pure sugars (all above 90%). The separation of BSA and yeast extract does not directly interfere chromatographically as they elute earlier than the carbohydrates. However, the physical properties of the solution are changed, which might be the reason for the slightly different recoveries.

The level of interfering compounds was increased by the addition of the phenolic compounds (solution B), for which most recovery values were found to exceed 100%. This indicates that the phenolics, e.g., decomposition products of lignin, interfere by co-eluting with the carbohydrates and thereby disturb the CLC analysis. This effect is clearly seen in Fig. 3, where the separation of solution B and the phenols present in B is shown.

To investigate further the membrane properties, *Saccharomyces cereviseae* (80 g l^{-1}), ammonium sulphate (0.025%, w/v) and ethanol (10 mM) were added to model solution B. To maintain the idea of having no biological activity in the model solutions, the sugars (cellobiose, glucose, galactose and arabinose) previously used were exchanged for the pentoses xylose and arabinose, as they are not fermented by the microorganism. In Table 3, recovery values of xylose and arabinose are shown at three sampling occasions. They were all found to be around 100% even after almost 2 h using the Durapor membrane. The same experiment was performed with the MF cellulose-based membrane. There was no significant difference in the recovery values obtained with the Durapor compared with the MF membrane (both 0.22 μm), e.g., 111% for xylose and

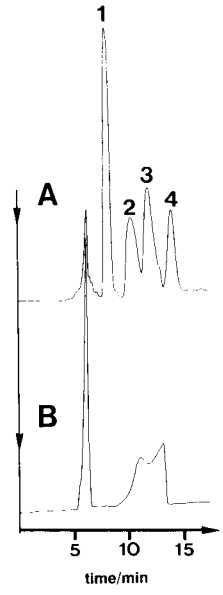

Fig. 3. Chromatograms obtained with the set-up in Fig. 1. (A) Separation of four carbohydrates and five phenolic compounds; (B) separation of the five phenolic substances. Peaks in (A): 1 = cellobiose; 2 = glucose, 3 = galactose; 4 = arabinose (10.0 mM each). The concentration of the phenolic compounds (phenol, *o*-cresol, mandelic acid, benzenesulphonic acid and furfural) were (A) 2.0 and (B) 6.0 mM. Detector, refractive index (attenuation 16); injection volume, 20 μl. For further details, see text.

115% for arabinose (samples taken after 25 min). As the cellulose-based membrane may not be so chemically inert as the polymer-based membrane, this type of membrane was immersed in a 10%

TABLE 3

Recovery of xylose and arabinose in a model solution [a]

Recovery calculated from		Recovery (%)	
		Xylose	Arabinose
Area:	25 min	168	99
	50 min	100	109
	100 min	110	118
Height:	25 min	115	122
	50 min	96	103
	100 min	106	112

[a] Solution C, representing a solution containing interfering compounds. For details, see text.

(v/v) ethanol solution for several days. However, no visual deteriorations or dissolution tendencies or similar could be observed. This indicates that one might use the cellulose membrane also for sampling purposes in the FAM. However, the polymer-based membranes are of greater mechanical strength and were therefore chosen.

Amino acid recovery in an ethanol fermentation substrate and a penicillin fermentation broth

The experiments described above provided valuable information on how well known interferences affect membrane transport using TFF for carbohydrates in defined model solutions. To obtain a more complete characterization of the sampling unit, one fermentation broth and one fermentation substrate (SSL) were chosen as test solutions for the FAM unit. The broth was obtained from a penicillin fermentation plant in Sweden. This sample was taken directly from the antibiotic production process after 150 h. At this step in the process, the mycelium concentration is ca. 10% (v/v), the pH is ca. 4.7 and the nitrogen content is ca. 1000 μg ml^{-1} (as ammonium ion). Almost all the sugar content is consumed and the penicillin content is ca. 3 mg ml^{-1}. The SSL sample used was a waste water from a pulp industry in Sweden having a pH of ca. 4 and sugar levels of ca. 0.15 M (based on calculations of the concentration of monosaccharides). These two samples were chosen as examples of a very well defined process for antibiotic production, in which all steps during the 1-week fermentation are thoroughly feedback controlled and documented, and of a technical substrate of industrial origin with an extremely complex composition. Owing to its great potential as a cheap fermentation substrate, it is at present receiving considerable international attention, in combination with yeasts, for ethanol production to be used as an alternative energy source [16].

Other compounds present in these fermentation solutions are proteins, peptides, amino acids (the nitrogen source) and organic acids. It is of interest to know the extent to which they may pass the membrane, both in a pure solution and in a complex matrix, here exemplified by SSL or the PFB.

Initially a solution containing 1 mM each of the amino acids glycine, aspartic acid, phenylalanine and serine was circulated (at 12 ml min^{-1}) using an MF membrane (0.45 μm) and a filtrate sample was taken after 20 min when the circulating fluid was in equilibrium with the membrane. Simultaneously, a crude sample was taken from the bioreactor. These two samples were run in the ion-exchange chromatographic set-up (see Experimental). The recovery values were found to be close to 100% (data not shown), i.e., almost all components freely pass the membrane. These results were expected and were similar to those obtained with the pure carbohydrate solution, as all components in the solution are of low molecular weight and no strong interaction forces with the membrane should prevail.

These experiments were followed by investigating the influence of a complex matrix on similar amino acid determinations to the above. To obtain information on the background level of the amino acid content of pure SSL, a solution of this type was circulated and samples were taken as above. The four amino acids were then added by standard addition to the bioreactor (1 mM each). Sampling was then made and the amino acid content determined, in both the crude solution and the filtrate (sampled after 20 min). A similar set of investigations were also performed using PFB instead of SSL. The recoveries of amino acids in PFB were calculated in the same way.

TABLE 4

Amino acid (AA) concentrations in a fermentation substrate (SSL) and a broth (PFB)

Sample	Concentration (mM)			
	L-Aspartic acid	L-Serine	Glycine	L-Phenylalanine
SSL crude	< 0.01 [a]	< 0.01	< 0.01	< 0.01
SSL filtrate	< 0.01	< 0.01	< 0.01	< 0.01
SSL + AA crude	1.4	1.1	1.1	1.2
SSL + AA filtrate	0.7	0.6	0.5	0.6
PFB crude	1.2	1.3	0.4	0.6
PFB filtrate	1.0	1.2	0.4	0.6
PFB + AA crude	1.2	1.8	1.2	1.6
PFB + AA filtrate	1.2	1.6	0.8	1.1

[a] Detection limit in this matrix.

Table 4 shows the results of these experiments, where the concentrations of the different amino acids in the SSL and penicillin broth are presented. Interestingly, different results were obtained when a matrix was present. Starting with SSL, several conclusions can be drawn. First, the amino acid content in pure, unspiked SSL is very low, less than the detection limit, which in this matrix was calculated to be 10 μM. Second, after the SSL had been spiked with the standard amino acid solution containing 1 mM of each, the contents of the crude samples correlate well to the expected values. Third, the filtrate taken 20 min after the addition contains approximately half the amount, reflecting that the recovery of the amino acids in this complex matrix is only about 50%. This very low value should be contrasted with the 100% recovery for the pure amino acid solution.

The results obtained with the penicillin broth are not so easy to interpret as with SSL. Pure, unspiked broth (PFB crude) contains more than 1 mM aspartic acid and serine, whereas the concentration of glycine and phenylalanine were found to be about half as much or less. The content of the filtered PFB crude gave recoveries between 80 and 100%. By comparing the results obtained after standard addition, the values for serine, glycine and phenylalanine were found to be as expected or lower (see Table 4), except for aspartic acid, which was not affected by the addition. The recovery of the filtrate for aspartic acid was found to be 100% and lower for serine, and the recoveries for glycine and phenylalanine were 70%. One explanation for the low values found after standard addition might be binding of these amino acids to macromolecules or solids present in the sample. This would mean that only the free amino acids in solution are able to penetrate the membrane. This effect is most pronounced for aspartic acid, indicating an equilibrium strongly favouring an adsorbed or chelated form of this amino acid. Similar results have been obtained in previous work, where the level of D-amino acids added to a penicillin broth was found to be lower compared with the same total concentration in a pure buffer solution [17]. Also in this case, partitioning of the solutes between the bound fraction and the free form is expected to occur.

Organic acid recovery in an ethanol fermentation substrate and a penicillin fermentation broth

Organic acids are compounds sharing some properties with amino acids, e.g., both have reactive carboxylic groups and both may contain hydrophilic and hydrophobic parts in the molecular structure. Some organic acids are known components of SSL and PFB. To investigate the performance of some of these acids in the FAM unit, a similar set of experiments were run as for the amino acids (see above), but exchanging them for 1 mM each of pyruvate, malate, lactate and acetate.

The background level of organic acids or compounds with the same retention time is high in this type of matrix. As a consequence, an interpretation of the results from the organic acid analysis in SSL was much too difficult to allow their respective identification and determination,

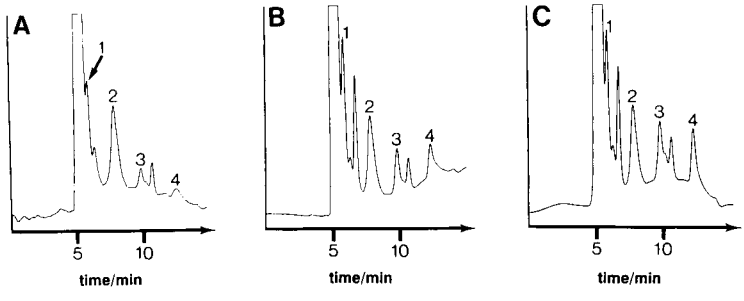

Fig. 4. Ion chromatographic separation of organic acids in PFB. Samples used: (A) crude PFB; (B) as in (A) but with the addition of 1.0 mM each of the organic acids; (C) a filtrate collected after 20 min. Peaks: 1 = pyruvate; 2 = malate; 3 = lactate; 4 = acetate. Detector conductimetric, range 10 μmho; injection volume, 50 μl. For further details, see text.

TABLE 5

Organic acid concentrations in a penicillin broth

Sample	Concentration (mM)			
	Pyruvate	Malate	Lactate	Acetate
PFB crude	2.7	1.1	0.8	0.3
PFB filtrate	2.8	0.9	0.3	2.1
PFB + OA crude	4.0	1.2	1.6	0.9
PFB + OA filtrate	3.8	1.1	2.1	1.5

as the chromatograms were very complex; although efforts were made using chromatographic software.

The chromatograms of the penicillin broth (Fig. 4) turned out to be easier to evaluate. The concentrations of the acids in the crude were found to be between 0.3 and 2.7 mM (Table 5). The recoveries were found to vary substantially, being both low and very high, e.g., lactate and acetate. A similar pattern was obtained for these organic acids as for the amino acids concerning the free acids found after standard addition. By examining the values for malate, lactate and acetate (Table 5), it can be stated that a major part seems to be bound in the solution. However, the filtrate values for pyruvate and malate are close to 100%, whereas higher recoveries were found for lactate and acetate.

In the characterization experiments of the tangential flow sampling unit, it is seen that the physico-chemical interaction between the acids and the compounds present in the two fermentation samples chosen is obvious. The ratio between bound and free acid in solution is probably determined by the structure of the analyte in question and is clearly seen for some of the acids in Tables 4 and 5.

There is also an effect by the membrane controlling the flow properties of these analytes through the sampling unit. This results in varying recovery values, depending on the analyte. As this is not observed in pure solution, it is believed that other factors may contribute to a combination of both membrane effects and physical properties of these complex fermentation substrates and broths.

Conclusions

It has been shown that Waters FAM sampling unit based on tangential flow filtration can be used for analyses of carbohydrates in complex media in small-scale fermentations, yielding recovery values close to 100% for some small sugars. Amino and other organic acids were, however, found to show a more complex membrane transport behaviour in complex matrices, the nature of which remains unclear. Many of the recovery values were found to be low, which might reflect some physico-chemical properties of these analytes in complex solutions. These acids are all charged in different ways and differ in that sense to the carbohydrates which are very weak acids (pK_a 11–14) lacking any strong, interactive side-chains in their structures. As far as the amino acids are concerned, glycine contains a hydrogen atom and serine a hydroxyl group as the side-chain, the latter therefore being somewhat polar. Aspartic acid has a carboxyl group that is ionized above pH 4.4 and phenylalanine is an aromatic amino acid with a phenyl ring. When acids are to be determined in these types of complex fermentation media, careful optimization of the matrix interactions is necessary prior to use. In other fermentations of less complex composition but still with important economic interest, this unit is believed to work well as no experimental problems were found when running for longer times with standard or simple solutions. Considering the use for carbohydrate analyses coupled on-line to CLC, the system works very well and can be claimed to make the separation easier as the presence of these acids (that are or can be a major separation problem) is smaller.

It was found that the experimental values obtained for sampling times less than 1 h correlated well with those found for longer operational times (more than 10 h). Operation of this sampling unit in combination with on-line CLC for 24-h fermentations is being studied and will be reported in a separate paper [18].

The authors thank Dr. George Vella, Waters Millipore, Milford, MA and Mr. Ingolf Elmhammar, Waters Division of Millipore (Sweden) support during this investigation. Thanks are also

due to Mrs. Marianne Stenberg and Ms. Lena Grönberg for the amino acid and organic acid analyses, Dr. Istvan Csiky, Gist Brocades, Strängnäs, Sweden, for the penicillium broth, and the Swedish Ethanol Development Foundation for the SSL, respectively. The skilful drawing of the filtration module was made by Mr. Ulf Wellmar. Financial support from the National Energy Administration (STEV) and the Swedish Natural Science Research Council (NFR) is gratefully acknowledged.

REFERENCES

1 M.J. Hayward, T. Kotiaho, A.K. Lister, R.G. Cooks, G.D. Austin, R. Narayan and G.T. Tsao, Anal. Chem., 62 (1990) 1798.
2 L.H. Christensen, J. Nielsen and J. Villadsen, Anal. Chim. Acta, 249 (1991) 123.
3 C.F. Mandenius, B. Danielsson and B. Mattiasson, Anal. Chim. Acta, 163 (1984) 135.
4 H. Håkanson, M. Nilsson and B. Mattiasson, Anal. Chim. Acta, 249 (1991) 61.
5 G. Marko-Varga, T. Buttler, L. Gorton and C. Grönsterwall, Chromatographia, 35 (1993) 285.
6 K.H. Kroner and M.R. Kula, Anal. Chim. Acta, 163 (1984) 3.
7 U. Nalbach, H. Schiemenz, W.W. Stamm,W. Hummel and M.R. Kula, Anal. Chim. Acta, 213 (1988) 55.
8 D.A. Dubois, M.A. Mouyart and A.O.A. Miller, in preparation.
9 L.W. Forman, B.D. Thomas and F.S. Jacobson, Anal. Chim. Acta, 249 (1991) 101.
10 A.K. Dincer, M. Kalyanpur, W. Skea, M. Ryan and T. Kierstead, in Developments in Industrial Microbiology, Vol. 25, Society for Industrial Microbiology, Arlington, VA, 1984, pp. 603–611.
11 M. Garn, M. Gisin, C. Thommen and P. Cevey, Biotechnol. Bioeng., 34 (1989) 423.
12 N.C. van de Merbel, I.M. Kool, H. Lingeman, U.A. Th. Brinkman, A. Kolhorn and L.C. de Rijke, Chromatographia, 33 (1992) 525.
13 G. Marko-Varga, E. Dominguez, B. Hahn-Hägerdahl, L. Gorton, H. Irth, G.J. De Jong, R.W. Frei and U.A. Th. Brinkman, J. Chromatogr., 523 (1990) 173.
14 Waters FAM Operators Manual, Millipore, Milford, MA, 1st edn., 1988.
15 T.A. Clark and K.L. Mackie, J. Chem. Tech. Biotechnol., 343 (1984) 101.
16 T. Lindén and B. Hahn-Hägerdahl, Enzyme Microb. Technol., 11 (1989) 583.
17 G. Marko-Varga, L. Gorton, E. Dominguez and D. Barceló, Chromatographia, in press.
18 T.A. Buttler, K.A.J. Johansson, L.G.O. Gorton and G.A. Marko-Varga, Anal. Chem., submitted for publication.

Analytica Chimica Acta, 279 (1993) 39–50
Elsevier Science Publishers B.V., Amsterdam

Automated monitoring of biotechnological processes using on-line ultrafiltration and column liquid chromatography

N.C. van de Merbel, H. Lingeman and U.A.Th. Brinkman

Department of Analytical Chemistry, Free University, De Boelelaan 1083, 1081 HV Amsterdam (Netherlands)

A. Kolhorn

Bio-Flo, 32 St Andrews Road, Glasgow G41 1ST (UK)

L.C. de Rijke

Pharmacia LKB Biotechnologie Nederland, Houttuinlaan 4, 3447 GM Woerden (Netherlands)

(Received 1st October 1992; revised manuscript received 15th January 1993)

Abstract

The efficient control of fermentation processes requires reliable monitoring systems. This paper describes a fully automated monitoring system based on the on-line combination of ultrafiltration and column liquid chromatography. An evaluation of the performance of a hollow-fibre ultrafiltration module is provided and a method for the determination of sugars, alcohols and organic acids during a gluconic acid and a beer fermentation is presented. The system can be used for at least 250 h with complex fermentation broths under both aerobic and anaerobic conditions without any detrimental effect on either the fermentation or the chromatographic part. Depending on the application 3–5 analyses can be performed every hour, using only 3.0 μl of sample per analysis. Using refractometric or direct UV detection the linear dynamic range is from 0.2 to 150 g l^{-1} for most of the compounds, while with a simple post-column derivatization procedure sugars can be determined in the low mg l^{-1} range.

Keywords: Liquid chromatography; Alcohols; Biotechnology; On-line fermentation monitoring; Organic acids; Sugars; Ultrafiltration

In order to optimize fermentation processes, i.e. to ensure maximum growth and productivity of a micro-organism population, the fermentation conditions should be controlled and maintained at their optimum values. So, for an effective control of such a process the relevant parameters should be monitored regularly. In this respect, three approaches can be distinguished: the application of (i) non-invasive techniques, (ii) sensors for in situ measurements and (iii) traditional analytical methods such as spectroscopy and chromatography [1].

As yet, the use of non-invasive techniques has been limited and reliable monitoring by in situ sensors is restricted to the measurement of physical parameters such as temperature, pH and dissolved oxygen tension. The most important chemical variables such as the concentration of the carbon source and the fermentation products are often followed off-line, by traditional analytical

Correspondence to: N.C. van de Merbel, Department of Analytical Chemistry, Free University, De Boelelaan 1083, 1081 HV Amsterdam (Netherlands).

techniques. These usually involve manual sampling, which may result in delayed, infrequent and less reliable data, substantial loss of fermentation fluid and increase the risk of infection [2]. In recent years, the fast developments in biotechnological research resulted in an increasing demand for monitoring systems that allow the unattended determination of the key components in fermentation broths. Therefore, there is a growing interest to use on-line methods which may be automated and fully integrated into the process.

On-line measurement usually requires the use of a filtration interface which allows direct sample introduction into an analytical system by removing interfering broth components. Flow-injection analysis (FIA) is the most frequently applied technique for the on-line monitoring of chemical variables and is normally performed in combination with a microfiltration interface for the removal of cells. Although FIA is a rather simple and fast technique, it is difficult to determine several compounds simultaneously and for accurate quantification selective enzymatic or chemical reactions are needed. As a result, only a limited number of compounds have been determined by this technique, e.g., glucose [3–8], acetate [9], lactate [3,5,7], phosphate [9] and amino acids [10]. In principle, chromatographic techniques, such as gas chromatography (GC) [11] and, in particular, column liquid chromatography (LC) [10,12–15] do not possess these limitations and can be successfully applied to determine multiple components in fermentation broths. Also in this case, a reliable interface, generally an ultrafiltration (UF) device, between the bioreactor and the analytical system is of major importance [16].

Ideally, the interface should have the following characteristics. Firstly, it should protect the LC column by efficiently removing both cellular and macromolecular broth constituents, which is achieved by proper selection of the nominal molecular weight cut-off (NMWCO) value of the membrane. Secondly, it should not disturb the fermentation process and, in particular, infections have to be avoided. This means that a fully closed sampling system should be used that can be readily sterilized. Furthermore, it has to provide fast and representative samples to guarantee that rapidly changing processes can be followed accurately. In addition, the performance of the filtration interface should not decrease during the fermentation process (typically days to weeks), meaning that the inherent problem of fouling of the membrane by broth constituents is to be kept to a minimum [17]. Finally, it should be possible to utilize a single type of interface with a variety of fermentation processes and analytical systems, for the determination of a wide range of analytes in all kinds of fermentation broths under both aerobic and anaerobic conditions.

In this paper the performance of a hollow-fibre UF device, placed in an external sampling loop, is studied with respect to the criteria mentioned above. The monitoring of different types of analytes, including nutrients, metabolites and products by the on-line combination of UF and LC during a gluconic acid and a beer fermentation is described.

EXPERIMENTAL

Chemicals

D-Glucose, maltose and maltotriose were obtained from Baker (Deventer), Sigma (St. Louis, MO) and Janssen Chimica (Geel), respectively. D-Gluconic acid (sodium salt) was purchased from Merck (Darmstadt) and 2-keto-D-gluconic acid (hemicalcium salt) and 5-keto-D-gluconic acid (hemicalcium salt) from Sigma. Yeast extract was obtained from Oxoid (London), *p*-aminobenzoic acid hydrazide from Janssen Chimica and Decon Neutracon from Decon Laboratories (Hove). All other chemicals and solvents came from Baker. HPLC-grade water was prepared by using a Milli-Q purification system (Millipore, Bedford, MA); for the preparation of fermentation media demineralized water was used.

Set-up

A schematic drawing of the monitoring system is shown in Fig. 1. The fermentations were run in a Multiferm (Quintus, Gouda) 5 l fermenter equipped with temperature, pH, dissolved oxygen tension and stirring control. Filtration was per-

formed with a Bio 2000 Mk II cross-flow filtration system (Bio-Flo, Glasgow) equipped with a peristaltic pump and a hollow-fibre UF module (polysulphone, NMWCO 54 kD, fibre diameter 500 μm, wall thickness 50 μm, area 90 cm^2), connected with 4 mm i.d. silicone rubber or viton tubings. A detailed drawing of the UF module is presented in Fig. 2. The total volume of the external filtration loop, including tubings, pump and filter was 20 ml. Filtration was performed by continuously pumping the fermentation broth through the UF module at a flow-rate of 100 ml/min and applying a pressure of 0.3–0.4 bar. The retentate was pumped back to the fermenter and the filtrate was transferred on-line to a 3.0-μl loop mounted on a six-port switching valve, which was connected to the LC system. The filtrate was returned to the fermenter; to prevent contamination of the fermentation broth it was passed through a sterile barrier, i.e. a 0.2 μm mixed cellulose ester microfilter, type Culture Gard (Microgon, Laguna Hills, CA).

The LC system (Pharmacia LKB, Uppsala) consisted of two Model 2248 high-pressure piston pumps, a Model 2155 column oven, a Model 2142 differential refractometer and a Model 2141 variable-wavelength UV–vis photometer. An Interaction Chemicals (Mountain View, CA) ION-300 column (300 mm × 7.8 mm i.d.) was used with 0.005 M sulphuric acid as the eluent (flow-rate 0.5 ml min^{-1}, temperature 90°C). Because of the high analyte concentrations, for monitoring of the gluconic acid fermentation the column effluent was on-line diluted with water (1.5 ml min^{-1}); the UV–vis detector (215 nm) and the refractometer were coupled in series. The beer fermentation was monitored using only refractometric detection without dilution of the column effluent.

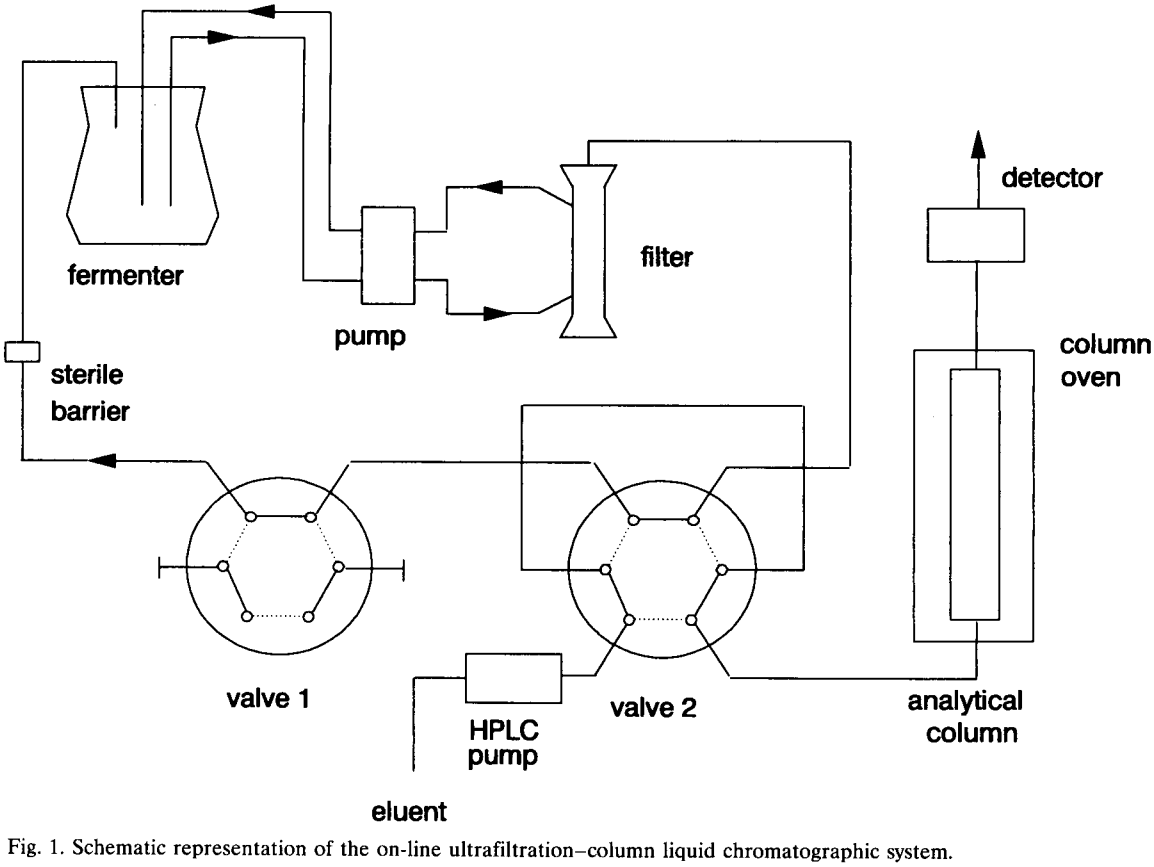

Fig. 1. Schematic representation of the on-line ultrafiltration–column liquid chromatographic system.

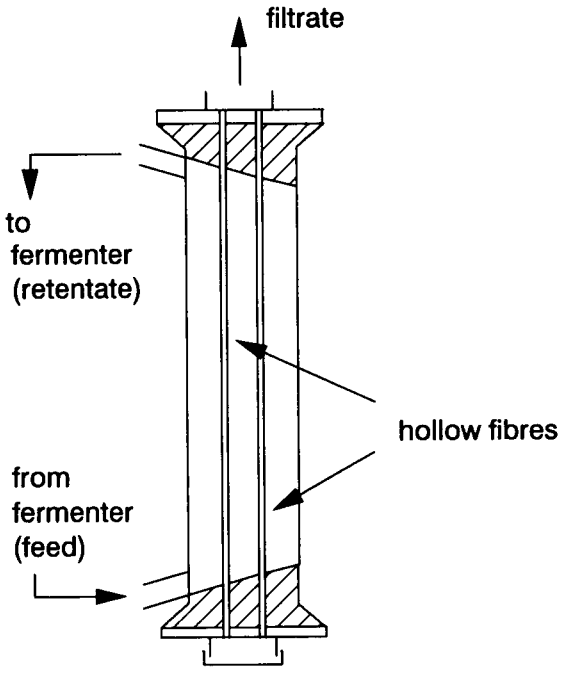

Fig. 2. Schematic drawing of the hollow-fibre ultrafiltration module. Only two hollow fibres are shown, the hatched areas indicate the potting material used to seal the fibre bundle in the housing. The sample is pumped through the dead volume of the module, the filtrate is collected within the fibres. During filtration one of the filtrate outlets is closed.

Post-column derivatization was performed by mixing the column effluent with a reagent solution, consisting of one part 0.5% *p*-aminobenzoic acid hydrazide in 0.5 M hydrochloric acid and two parts 2.4 M sodium hydroxide (flow-rate, 0.4 ml min^{-1}). The reaction took place for 45 s in a 3.0 m × 0.54 mm i.d. stainless-steel reaction coil at 90°C. The signal was recorded by a Model 2210 dual channel recorder (Pharmacia LKB) or a Hewlett-Packard (Waldbronn) Model 3396A integrator. Valve switching was controlled by a Prospekt 1.0 (Spark Holland, Emmen).

Procedures

The fermenter was sterilized by autoclaving for 30 min at 120°C. The filtration system was sterilized by flushing with 0.5 l of 96% ethanol and subsequently rinsed with 2 l of sterile water. Between two fermentation runs the UF module was cleaned by flushing with an aqueous 2.5% Decon Neutracon solution, followed by thorough rinsing with water. When not in use, the module was stored in a 0.05% sodium azide solution.

The gluconic acid fermentation was performed with *Gluconobacter suboxydans* (ATCC 621h) using 2 l medium consisting of 2.5 g l^{-1} magnesium sulphate 7-hydrate, 1.0 g l^{-1} potassium monohydrogen phosphate, 2.0 g l^{-1} ammonium sulphate, 3.5 g l^{-1} yeast extract and 62 g l^{-1} glucose. The temperature was maintained at 30.0 ± 0.3°C and the pH at 3.5 with 5 M sodium hydroxide. The dissolved oxygen tension was kept in the range 35–50% relative air saturation by stirring with a rate of 600–1200 rpm. After the initial glucose level had decreased below 5 g l^{-1}, 0.75 l of an aqueous 300 g l^{-1} glucose solution was added through a Culture Gard microfilter (Microgon) at a flow-rate of 6.5 ml min^{-1}.

The beer fermentation was carried out by cultivating a yeast strain (PRG-1) in an aqueous 150 g l^{-1} wort powder solution. The medium was added under sterile conditions to the fermenter by filtering through a Culture Gard microfilter

TABLE 1

Time schedule of the on-line analytical procedure using the system depicted in Fig. 1 [a]

Time (min)	Event	Valve positions		Recorder
		Valve 1	Valve 2	
0.00	Filtration	–	–	Off
10.00	Loop filling	–	...	
12.00	Sample injection, start analysis	–	–	On
12.10	Close filtrate outlet	...	–	
29.00	Stop analysis	...	–	Off
30.00	End of run			

[a] Sampling twice per hour.

(Microgon). The temperature was held constant at 10.0 ± 0.8°C and the stirring rate at 250 rpm. The pH was monitored but not adjusted; in the course of the fermentation it gradually decreased from 5.3 to 3.9. The fermentation broth was saturated with oxygen at $t = 0$, followed by headspace flushing with nitrogen. This caused the dissolved oxygen tension to decrease to zero in about 4 h; after this the broth was kept under anaerobic conditions.

As an example, the time schedule of the analytical procedure for monitoring a gluconic acid fermentation is given in Table 1. To obtain a representative sample, filtration of the fermentation broth takes place for 12 min. During the first 10 min the filtrate is directly returned to the fermenter, during the following 2 min, after switching of valve 2, it is passed through the injection loop. After this, valve 2 is switched again and the analysis starts. By switching valve 1 the filtrate outlet is closed and the filtration stops. The programme is repeated for the next analysis 18 min later, so two sampling steps are performed per hour.

RESULTS AND DISCUSSION

Filtration

For the appropriate monitoring of bioprocesses the delay time between sampling and presentation of the data should be short compared with the kinetics of the fermentation. To obtain a representative sample, i.e. to assure that the analyte concentration at the filtrate side of the membrane equals that at the sample side, filtration has to take place for a certain period of time, the sampling dead time. The value of this parameter mainly depends on the dead volume of the filtration module and the filtrate flux through the membrane. Therefore, to obtain a fast response, both parameters should be optimized.

The flux through a membrane is described by [17]:

$$J = \frac{\Delta P}{\eta} \cdot \frac{1}{R_{tot}} = \frac{\Delta P}{\eta} \cdot \frac{1}{R_m + R_{cp}} \quad (1)$$

where J is the flux ($m^3\ s^{-1}$), ΔP the pressure applied across the membrane (bar), η the filtrate viscosity (kg m s^{-1}) and R_{tot} the total hydraulic resistance of the filtration system (m^{-5}), which consists of R_m, the resistance of the membrane itself, and R_{cp}, the resistance of the concentration polarization layer, which is formed on the membrane as a result of the accumulation of retained solutes. R_m is given by:

$$R_m = \frac{8d}{n\pi A r^4} \quad (2)$$

where d is the membrane thickness (m), n the number of pores per unit area, A the membrane area (m^2) and r the pore radius (m).

Eqns. 1 and 2 demonstrate that to obtain a maximum flux a proper construction of the filtration module is essential. Firstly, the pore radius is of major influence and should be carefully optimized to find an acceptable compromise between a high filtrate flux and an efficient removal of macromolecular compounds. UF membranes with NMWCO values of 20–100 kD (2–10 nm) are normally used in combination with LC. It has been demonstrated that a 54 kD membrane can be used for the filtration of a complex fermentation broth for over 250 analyses without any significant effect on the performance of the LC system, while still giving a sufficient flux [15]. Therefore, this NMWCO value was also selected for the present work.

A second requirement for a high filtrate flux is a large membrane area or, rather, a high membrane-area-to-volume ratio, which favours the application of hollow-fibre membranes compared with the more commonly used flat sheet membranes. Since the dead volume of the hollow-fibre UF module used in this study was 3.2 ml outside the fibres and 0.8 ml at the inside (cf. Fig. 2), it is advantageous to collect the filtrate inside the fibres. In this case, the sampling dead time was found to be 5 min at a filtrate flux of 1.0 ml min^{-1}, as compared to 10 min when collecting the filtrate outside the fibres. In addition, the membrane thickness is an important parameter. In the case of hollow fibres its actual value is dictated by technical requirements: to ensure proper pressure resistance the membrane thick-

ness should be increased for larger fibre diameters. Typical values are 20–100 μm.

Apart from the membrane parameters mentioned, the composition of the sample exerts a major influence on the filtrate flux. On the one hand the filtrate viscosity is important (cf. Eqn. 1) and on the other hand, when sample components are retained, the concentration polarization layer contributes to the total resistance, thereby reducing the filtrate flux [17]. The concentration polarization resistance R_{cp} is proportional to the applied pressure:

$$R_{cp} = \phi \Delta P \quad (3)$$

ϕ being a proportionality constant ($kg^{-1}\ m^{-4}\ s^2$). Eqns. 1 and 3 show that at low pressures, when no accumulation of solutes on the membrane occurs ($R_{cp} \ll R_m$) the filtrate flux is a linear function of the applied pressure. At higher pressures, when a layer is formed on the membrane, the filtrate flux approaches a limiting value of $1/\eta\phi$ ($R_{cp} \gg R_m$). To ensure a maximum flux the formation of the concentration polarization layer has to be be minimized. This can be accomplished by choosing a sufficiently low pressure or enhancing the turbulence of the sample flow [15].

Figure 3a and b illustrates the influence of the parameters mentioned above. In this case, filtration of either water or one of the fermentation media was performed (at room temperature or the fermentation temperature) by pumping the sample through the volume outside the hollow fibres and collecting the filtrate within. The relative viscosities of the several filtrates, measured using an Ubbelohde capillary viscometer, are given in Table 2. The effect of viscosity is most clearly demonstrated in Fig. 3b. The highly viscous beer medium yields a much lower filtrate flux than pure water. The flux of the gluconic acid medium, which has a viscosity comparable to

TABLE 2

Relative viscosities of water and 54 kD filtrates of two fermentation media at different temperatures
(Values in parentheses are from literature [18])

Medium	Temperature (°C)	Relative viscosity
Water	22	1.00
	10	1.43 (1.37)
	30	0.87 (0.84)
Beer medium [a]	22	1.50
	10	2.33
Gluconic acid medium [a]	22	1.10
	30	0.95

[a] For composition, see Experimental section.

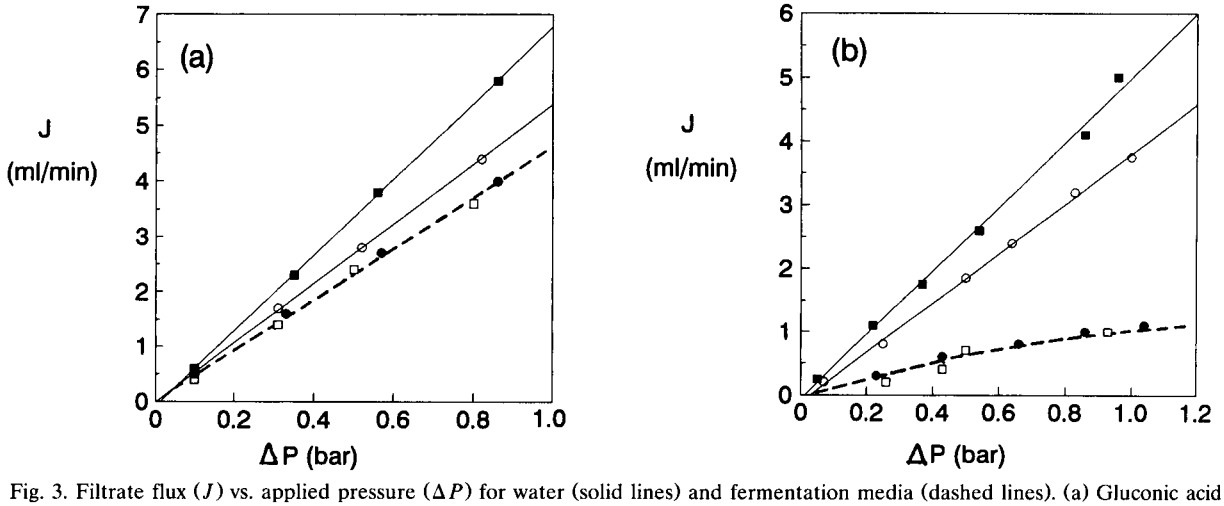

Fig. 3. Filtrate flux (J) vs. applied pressure (ΔP) for water (solid lines) and fermentation media (dashed lines). (a) Gluconic acid fermentation. Sample: water, flow-rate 75 ml min^{-1}, temperature 30°C (■), 22°C (○); sample: fermentation medium, temperature 30°C, flow-rate 16 ml min^{-1} (●), 75 ml min^{-1} (□). (b) Beer fermentation. Sample: water, flow-rate 75 ml min^{-1}, temperature 22°C (■), 10°C (○); sample: fermentation medium, temperature 10°C, flow-rate 75 ml min^{-1} (●), 150 ml min^{-1} (□).

water deviates much less from the pure water flux (Fig. 3a). An important consequence is that the sampling dead time and, thus, the sampling frequency significantly depends on the viscosity of the fermentation broth. For example, when applying a pressure of 0.3 bar, the filtrate flux for the gluconic acid medium was 1.5 ml min^{-1} while for the beer medium it was 0.3 ml min^{-1}. The respective sampling dead times were 5 min and 12 min. This means that the sampling frequencies were 12 and 5 samples per hour, respectively.

The effect of concentration polarization is somewhat less obvious in the present case. However, in Fig. 3b, with the beer medium the flux vs. pressure relationship slightly deviates from linearity, which indicates that some concentration polarization does occur in that instance. It was attempted to reduce the concentration polarization layer by increasing the sample flow-rate and, thus, the flow turbulence. In neither case was the filtrate flux seen to improve when the sample flow-rate was increased. Probably, when pumping the sample through the volume outside the fibres, a fully turbulent flow already takes place at relatively low flow rates.

Concentration polarization is a reversible phenomenon but even when its effect is minimized, a continuous flux decline is often observed with time. This is the result of membrane fouling, which is caused by the irreversible deposition of retained components. This phenomenon is very complex and strongly depends on the physical

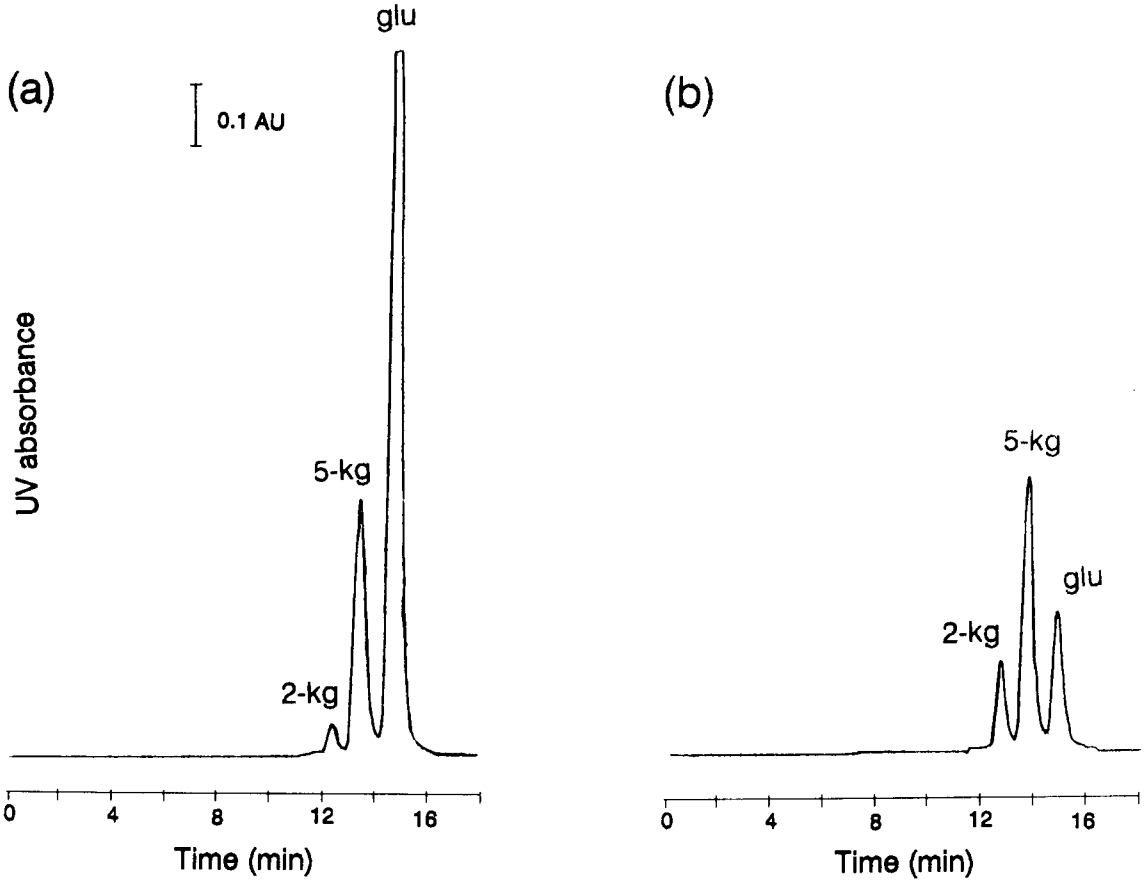

Fig. 4. LC–UV_{410} chromatograms obtained after derivatization with ABH of ultrafiltered gluconic acid fermentation medium; fermentation time (a) 38 h and (b) 44.5 h. 2-kg = 2-ketogluconic acid, 5-kg = 5-ketogluconic acid, glu = glucose. For LC details, see text.

and chemical properties of both the membrane and the solution to be filtered [17]. A general way to minimize the effect of membrane fouling and, thus, to optimize the sampling dead time is removing the pressure difference over the membrane as frequently as possible. This was tested with the beer fermentation broth. The filtrate flux decreased from 0.4 to 0.2 ml min^{-1} in about 1 h when the broth was continuously filtered using a pressure of 0.3–0.4 bar. Subsequently the flux was stable at 0.2 ml min^{-1} for at least 120 h. Continuous filtration is, however, not always necessary. With the beer fermentation, samples were taken every 6 h, while the sampling dead time was only 12 min. By closing the filtrate outlet and, thus, removing the pressure difference between two sampling periods a smaller flux decline was found, viz. from 0.4 to 0.3 ml min^{-1}.

Chromatography and detection

Although with the LC column used for the monitoring of the gluconic acid fermentation, the main fermentation product gluconic acid and two minor metabolites 2-ketogluconic acid and 5-ketogluconic acid could be separated, no separation could be achieved between glucose and gluconic acid. To overcome this problem, a double detection system was used consisting of a refractive index (RI) detector and a variable-wavelength UV–vis detector set at 215 nm, coupled in series. Since glucose hardly shows UV absorbance at 215 nm, gluconic acid can be selectively determined with the latter detector. The RI detector monitors both glucose and gluconic acid; that is, by combining both signals the concentration of glucose can be calculated. However, for the accurate determination of low concentrations of glucose in the presence of relatively high concentrations of gluconic acid (i.e. at the end of the fermentation process) a more selective detection mode for glucose will be needed.

Post-column derivatization with *p*-aminobenzoic acid hydrazide (ABH) was tested since this reagent has successfully been applied for the determination of low mg l^{-1} concentrations of reducing sugars in a complex fermentation broth [15]. The column effluent was on-line mixed with a reagent consisting of one part 5% ABH in 0.5 M hydrochloric acid and two parts 2.4 M sodium hydroxide at 90°C. It was found that under these conditions glucose as well as 2-keto- and 5-ketogluconic acid react with ABH to a derivative with an optimum absorbance at 410 nm. ABH was also found to react with gluconic acid but to a much lesser extent, the response being about 300-fold lower than for glucose. By using UV detection at 215 nm followed by derivatization with ABH and UV detection at 410 nm both gluconic acid and glucose can be accurately determined. As an illustration, Fig. 4 shows two chromatograms obtained at the end of the fermentation by using this derivatization procedure. Analytical data on

TABLE 3

Analytical data on the determination of glucose and gluconic acids during a gluconic acid fermentation

Compound	Detection [a]	Linearity ($n = 6$)				Detection limit (g l^{-1})	Precision (%) ($n = 8$)
		Intercept (±S.D.)	Slope (±S.D.)	R^2	Range (g l^{-1})		
Glucose	RI	−0.2 ± 0.6	1.03 ± 0.01	0.9997	0.5 –120	0.5	2.3
	UV_{410}	−1.6 ± 1.6	21.1 ± 0.1	0.9999	0.005– 20	0.005	2.4
Gluconic acid	UV_{215}	−0.5 ± 0.5	0.33 ± 0.01	0.9991	0.2 –160	0.2	0.8
	RI	1.0 ± 1.5	0.91 ± 0.02	0.9987	0.5 –160	0.5	3.0
2-ketogluconic acid	UV_{215}	−0.1 ± 0.1	0.69 ± 0.01	0.9993	0.2 – 15	0.2	3.3
	RI	−0.5 ± 0.5	6.25 ± 0.07	0.9996	0.5 – 15	0.5	3.7
	UV_{410}	−2.6 ± 3.1	10.1 ± 0.3	0.9955	0.01 – 15	0.01	1.4
5-ketogluconic acid	UV_{215}	0.0 ± 0.1	0.41 ± 0.01	0.9989	0.2 – 15	0.2	2.3
	RI	0.1 ± 0.3	1.72 ± 0.03	0.9984	0.5 – 15	0.5	3.6
	UV_{410}	−0.8 ± 2.3	11.4 ± 0.3	0.9977	0.01 – 15	0.01	2.4

[a] Detection modes: UV_{215}, direct UV detection (215 nm); RI, refractive index detection; UV_{410}, post-column derivatization with ABH, UV detection (410 nm).

all three detection modes are presented in Table 3.

On-line monitoring

Based on the above results, an automated monitoring system was set up for the determination of the key components in a gluconic acid and a beer fermentation. In both cases the broth was pumped through the dead volume of the UF module at a flow-rate of 100 ml min^{-1}. Since the total volume in the external sampling loop was 20 ml, the residence time outside the fermenter was only 12 s.

During the gluconic acid fermentation, two analyses were performed every hour according to the schedule presented in Table 1, using a pressure difference of 0.3–0.4 bar. To make sure that the samples taken were really representative, the actual sampling time was 12 min, i.e. longer than the sampling dead time of 5 min. Figure 5 shows that the sampling frequency of 2 per hour is amply sufficient to follow the concentrations profiles of glucose and the fermentation products. Gluconic acid and 2-keto- and 5-ketogluconic acid were determined by UV detection, glucose by RI detection.

G. suboxydans converts glucose into gluconic acid by means of glucose dehydrogenase. Between 17 and 19 h, 750 ml of a 300 g l^{-1} aqueous glucose solution were added to the fermenter. In this period the glucose concentration therefore sharply increased, whereas the gluconic acid concentration slightly decreased because of dilution of the fermentation broth. By the action of gluconate dehydrogenase gluconic acid can be further transformed into 2-keto- and 5-ketogluconic acid [19]. Figure 5 shows that small amounts were present in the broth at the end of the fermentation, as can also be seen from Fig. 4.

During the anaerobic beer fermentation introduction of oxygen has to be prevented. The highly oxygen-permeable silicone rubber tubings (polydimethylsiloxane, permeability constant 115×10^{-8} cm^3 s^{-1} atm^{-1}) connecting the different parts of the system were, therefore, replaced by viton tubings (vinylidene fluoride/hexafluoropropylene copolymers, permeability constant 0.5×10^{-8} cm^3 s^{-1} atm^{-1}) [20]. In this way anaerobicity could be maintained in the whole system. Also in this application the applied pressure was 0.3–0.4 bar; the actual sampling time was 20 min. which is somewhat longer than the sampling dead time (12

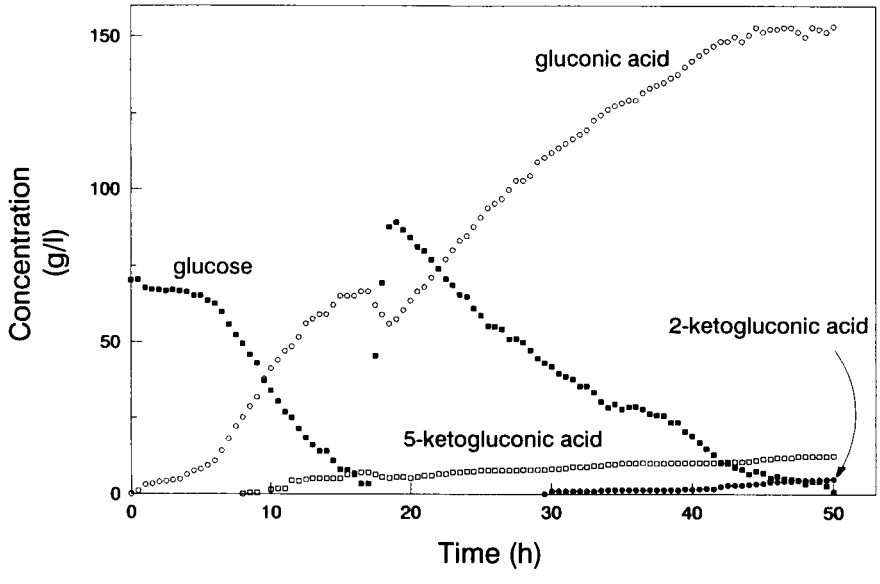

Fig. 5. Concentration profiles of gluconic acid (○), glucose (■), 5-ketogluconic acid (□) and 2-ketogluconic acid (●) during a fermentation of *Gluconobacter suboxydans*.

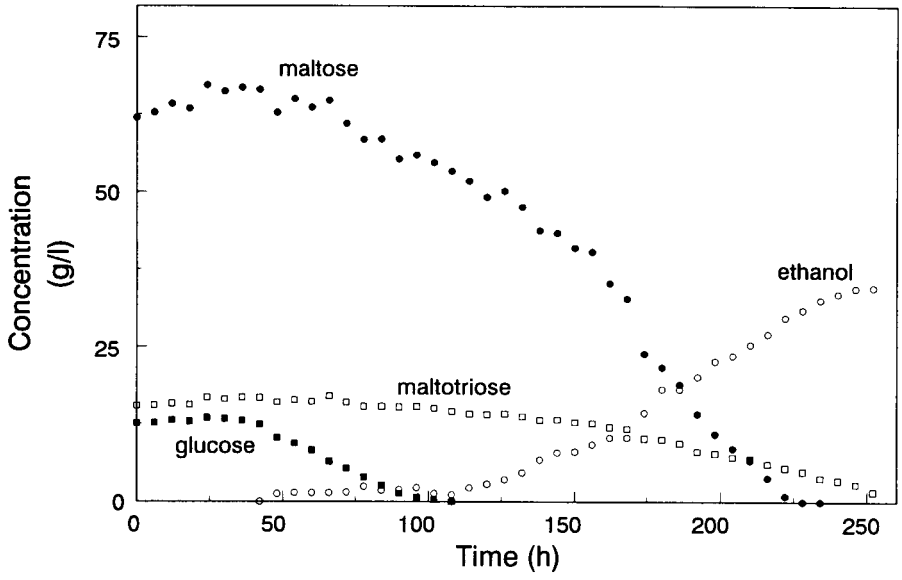

Fig. 6. Concentration profiles of maltose (●), maltotriose (□), glucose (■) and ethanol (○) during an anaerobic beer fermentation.

min). Figure 6 shows the concentration profiles of the most important analytes in the fermentation medium, the sugars maltotriose, maltose and glucose and the major product, ethanol. As can be concluded from the figure, a frequency of one analysis per six hours is sufficient to monitor the fermentation process. Of the three sugars present in the broth, glucose is the first to be consumed; consumption of maltose and maltotriose takes place only after almost all glucose has been used up. This may be due to the deactivating effect of glucose on the transport system which is responsible for the uptake of maltose and maltotriose into the yeast cell [21]. Figure 7 shows typical chromatograms obtained in the course of the fermentation process. The analytical data are summarized in Table 4.

A distinct difference was found between the decrease in flux during the gluconic acid and during the beer fermentation. During the 250-h beer fermentation the decrease was from 0.35 to 0.3 ml min^{-1}, whereas during the 50-h gluconic acid fermentation the decrease was from 1.5 to 0.8 ml min^{-1}. This illustrates the large influence of the composition of the fermentation broth on the membrane fouling, which in its turn affects the long-term stability of the filtrate flux. In the course of the present study, more than 300 analyses were performed without any deterioration of the separation efficiency of the analytical column

TABLE 4

Analytical data on the determination of four analytes during an anaerobic beer fermentation [a]

Compound	Linearity ($n = 6$)				Detection limit (g l^{-1})	Precision (%) ($n = 8$)
	Intercept (±S.D.)	Slope (±S.D.)	R^2	Range (g l^{-1})		
Maltotriose	0.4 ± 0.3	2.02 ± 0.03	0.9989	0.2–15	0.2	3.8
Maltose	2.2 ± 1.8	1.66 ± 0.05	0.9965	0.2–70	0.2	3.2
Glucose	0.3 ± 0.4	2.06 ± 0.05	0.9979	0.2–15	0.2	2.9
Ethanol	0.2 ± 0.3	0.38 ± 0.01	0.9983	0.6–50	0.6	3.6

[a] For details, see text.

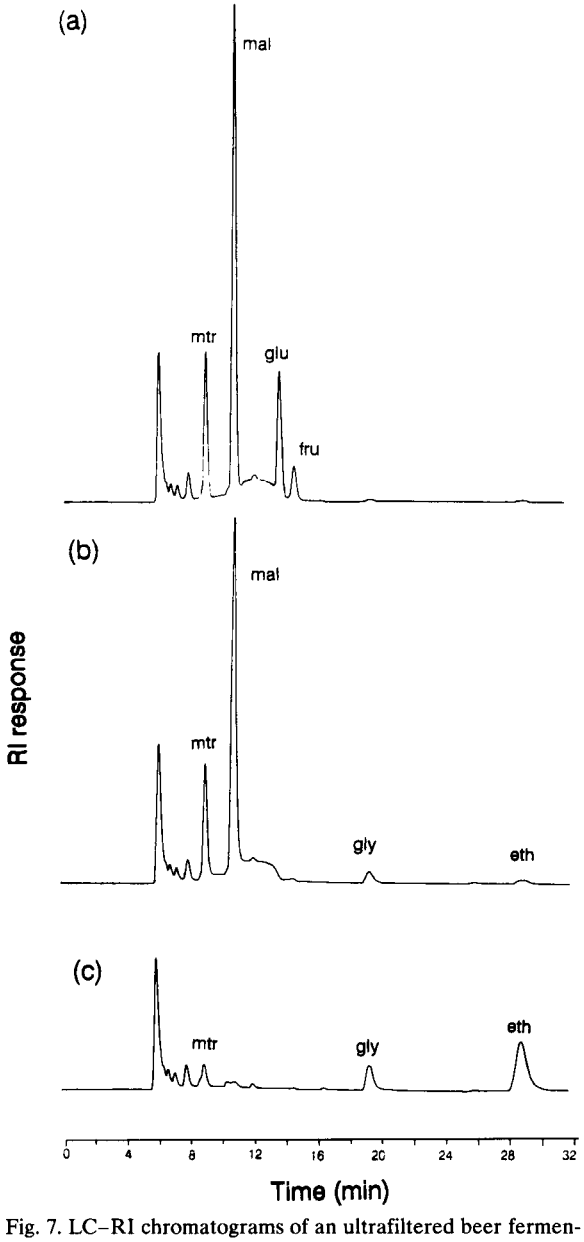

Fig. 7. LC–RI chromatograms of an ultrafiltered beer fermentation medium; fermentation time (a) 24 h, (b) 150 h and (c) 246 h. Mtr = Maltotriose, mal = maltose, glu = glucose, fru = fructose, gly = glycerol, eth = ethanol. For LC details, see text.

or a significant increase in back-pressure. The fermentation broths were regularly inspected under a microscope, but no contamination with external micro-organisms was ever observed.

As a further check of the validity of our aproach, the on-line data obtained for maltose during the beer fermentation were compared to those of an off-line method to test the accuracy of the on-line sampling procedure. Off-line sample pretreatment was performed by adding 1 ml of an aqueous 10% (w/v) trichloroacetic acid solution to 5 ml of the fermentation broth, followed by vortex mixing for 1 min and centrifugation (1500 *g*) for 15 min. The supernatant was analysed with the same chromatographic and detection system as the on-line samples. For maltose the following regression equation was found ($n = 8$):

$$y = 2.8(\pm 2.0) + 0.97(\pm 0.03)x$$

where y refers to the off-line and x to the on-line data. The R^2 value found was 0.9965, indicating the good correlation of both methods.

Conclusions

A monitoring system which can be generally applied in fermentation studies and control is presented. Several aspects of the on-line combination of ultrafiltration and column liquid chromatography for the monitoring of fermentation processes have been studied. An ultrafiltration membrane with a nominal molecular weight cut-off value of 54 kD was found to offer sufficient protection of the chromatographic system by removing all interfering fermentation broth components. Since a closed sampling system was used and the filtrate was led back into the fermenter via a sterile barrier, contamination by external micro-organisms could be prevented. A drawback of the present system is that the fermenter and the filtration unit are sterilized separately and have to be connected afterwards. Recently, a total-containment system has become commercially available which allows the fermenter and filtration system to be steam-sterilized together. However, this system was not available as yet during the present study.

The sample volume required per analysis was only 3.0 μl, which means that the total sample loss during a fermentation is negligible. The time delay between sampling and presentation of the

data is influenced by membrane parameters as well as by the composition of the fermentation broth. By using a hollow-fibre module a relatively high membrane-area-to-dead-volume ratio is obtained, which leads to a quick response. When the broth is pumped through the dead volume of the UF module outside the fibres, a turbulent flow pattern exists, which reduces the influence of concentration polarization. Membrane fouling causes the filtrate flux to decrease with time, but it can be reduced to an acceptable level if the pressure across the membrane is removed as frequently as possible by closing the filtrate outlet. The composition of the fermentation broth has a major influence on the membrane fouling and, thus, on the decrease of the flux.

The filtration system was successfully used for monitoring of two rather different fermentations which involved both aerobic and anaerobic conditions and bacterial as well as yeast cultures. Depending on the filtrate viscosity, the sampling dead time is about 5 min (gluconic acid fermentation) or about 12 min (beer fermentation). To make sure that the samples taken are really representative, the actual sampling times were chosen to be 12 min and 20 min, respectively. The corresponding maximum sampling frequencies are 5 and 3 samples per hour, which is amply sufficient for these kinds of applications. Compared with off-line monitoring, the system has several advantages: it allows unattended operation, a higher sampling frequency and a better precision. Furthermore, the sample losses and the risk of contamination are smaller. The extension of the method to filamentous fungi fermentations and the determination of higher-molecular-weight compounds is currently under investigation.

The cooperation and valuable suggestions of Dr. D.R. Kremer (AVEBE, Foxhol, the Netherlands) are gratefully acknowledged. This work was supported by the Dutch Foundation for Technical Science, Grant No. 349-2119.

REFERENCES

1 J.A.C. Claessens and H.J. Noorman, Biotechnol. Ned., 6 (1989) 119.
2 G.A. Montague, A.J. Morris and A.C. Ward, Biotechnol. Genet. Engin. Rev., 7 (1989) 147.
3 J. Nielsen, K. Nikolajsen and J. Villadsen, Biotechnol. Bioeng., 3 (1989) 1127.
4 R. Appelqvist and E.H. Hansen, Anal. Chim. Acta, 235 (1990) 265.
5 J. Nielsen, K. Nikolajsen, S. Benthin and J. Villadsen, Anal. Chim. Acta, 237 (1990) 165.
6 F. Valero, J. Lafuente, M. Poch, C. Solã, A.N. Auraja and J.L.F.C. Lima, Biotechnol. Bioeng., 36 (1990) 647.
7 S. Benthin, J. Nielsen and J. Villadsen, Anal. Chim. Acta, 247 (1991) 45.
8 S. Chung, X. Wen, K. Vilholm, M. De Bang, G. Christian and J. Ruzicka, Anal. Chim. Acta, 249 (1991) 77.
9 L.W. Forman, B.D. Thomas and F.S. Jacobson, Anal. Chim. Acta, 249 (1991) 101.
10 K. Schügerl, L. Brandes, T. Dullau, K. Holzhauer-Rieger, S. Hotop, U. Hübner, X. Wu and W. Zhou, Anal. Chim. Acta, 249 (1991) 87.
11 C. Filippini, J.U. Moser, B. Sonnleitner and A. Fiechter, Anal. Chim. Acta, 255 (1991) 91.
12 R.C. Dinwoodie and D.W. Mehnert, Biotechnol. Bioeng., 27 (1985) 1060.
13 X. Monseur and J.C. Motte, Anal. Chim. Acta, 204 (1988) 127.
14 K. Holzhauer-Rieger, W. Zhou and K. Schügerl, J. Chromatogr., 499 (1990) 609.
15 N.C. van de Merbel, I.M. Kool, H. Lingeman, U.A.Th. Brinkman, A. Kolhorn and L.C. de Rijke, Chromatographia, 33 (1992) 525.
16 B.J. Compton, Bioprocess Technol., 6 (1990) 39.
17 M.H.V. Mulder, Basic Principles of Membrane Technology, Kluwer, Dordrecht, 1991.
18 Handbook of Chemistry and Physics, Chemical Rubber Co., Cleveland, 69th edn., 1988.
19 P.R. Levering, G. Weenk, W. Olijve, L. Dijkhuizen and W. Harder, Arch. Microbiol., 149 (1988) 534.
20 Polymer catalogue, Eriks, Alkmaar, 1969.
21 C.P. Cartwright, A.H. Rose, J. Calderbank and M.H.J. Keenan in A.H. Rose and J.S. Harrison (Eds), The Yeasts, Vol. 3, Academic Press, London, 1989, p. 5.

Analytica Chimica Acta, 279 (1993) 51–58
Elsevier Science Publishers B.V., Amsterdam

On-line monitoring of penicillin V during penicillin fermentations: a comparison of two different methods based on flow-injection analysis

Morten Carlsen, Claus Johansen, Rong Wei Min and Jens Nielsen
Department of Biotechnology, Technical University of Denmark, DK-2800 Lyngby (Denmark)

Helmut Meier and Francois Lantreibecq
Laboratoire de Biotechnologie, École des Mines de Saint-Etienne, F-42023 Saint-Etienne Cedex 02 (France)

(Received 1st October 1992; revised manuscript received 19th January 1993)

Abstract

Two different flow-injection analysis (FIA) methods used for on-line monitoring of penicillin V during fed-batch penicillin fermentations are compared. The fermentations are carried out using a high yielding strain of *Penicillium chrysogenum* and both analyzers are used continuously for on-line monitoring during 200 h. Both methods are based on a reaction catalyzed by β-lactamase, which converts penicillin V to penicilloic acid. In analyzer 1 the sample is injected into a buffer stream and carried to a stirred measurement cell containing an enzyme electrode. The enzyme electrode consists of β-lactamase immobilized onto a sensitive pH glass electrode with a very low response time. No predilution of the sample is required in this analyzer. In analyzer 2 the sample is injected into an enzyme reactor containing immobilized β-lactamase. The formed penicilloic acid is detected by decolorization of an iodine–starch complex. By means of a second injection valve it is possible to have the sample by-pass the enzyme reactor and instead pass a dummy reactor in which no β-lactamase is immobilized. Thereby both the concentration of penicillin and penicilloic acid can be measured. On-line dilution of the sample is ensured by a gradient technique. Experimental results from on-line monitoring of penicillin V using the two methods are presented. The large amount of precise measurements enables a very good resolution of the penicillin production; something of extreme value for verification of mathematical models describing the fermentation kinetics.

Keywords: Biosensors; Flow injection; Fermentation; Penicillin; On-line measurements

The application of flow-injection analysis (FIA) for on-line monitoring of many different medium components during fermentation processes has been illustrated in several publications [1–3], and the experimental data obtained hereby have been valuable for characterization of the fermentation kinetics [4]. Despite the industrial importance of the penicillin fermentation and the description of several different FIA systems for measuring penicillin (see e.g. [5,6]) there are, however, no reports on the application of these analyzers for on-line monitoring of penicillin fermentations. Applications of other analysis techniques, e.g. liquid chromatography (LC) [7], have been described, but due to the lower price, high speed and reliability of FIA this technique is to be preferred over LC for on-line monitoring. In this paper two different FIA systems are applied for on-line monitoring of the penicillin fermentation and their performance is compared. The many

Correspondence to: J. Nielsen, Department of Biotechnology, Technical University of Denmark, DK-2800 Lyngby (Denmark).

precise measurements of the penicillin concentration enable an in-depth analysis of the product formation kinetics.

EXPERIMENTAL

Analyzer 1

This analyzer is based on immobilization of β-lactamase in a very thin film on a conventional combined pH glass electrode [8]. Thus, the principle of this analyzer is measurement of the change in the H^+-ion concentration resulting from the enzymatic hydrolysis of penicillin by β-lactamase. The incorporation of the enzyme electrode in a FIA system is described elsewhere [5].

The manifold is shown in Fig. 1 (analyzer 1). The flow-rate of the carrier stream is 1.1 ml min^{-1}. The volume of the detection cell is 2 ml and the injection volume is 100 μl. The analyzer is controlled by a Macintosh Plus computer. The software is written in QuickBasic and it contains subroutines for control of the injection valve and pumps, data acquisition, calibration and data analysis.

The calibration curve is established by adding known amounts of penicillin V to a filtered fermentation medium obtained 5 h after inoculation. The following concentrations are used to obtain the calibration curve: 2.5, 10.0, 17.5 and 25.0 g l^{-1} K-pen-V. Before each calibration the detection cell and the active surface of the enzyme electrode are cleaned with the buffer solution. The samples withdrawn from the bioreactor are injected directly into the carrier stream and are diluted in the detection cell by mixing with the buffer solution. This dilution is necessary for measuring penicillin concentration up to 30 g l^{-1} K-pen-V. However, it also reduces the interference from components in the sample matrix. A smaller carrier flow-rate gives an increasing response time of the biosensor but also a higher sensitivity. Furthermore, the linear range is expanded when a low flow-rate is used. When a

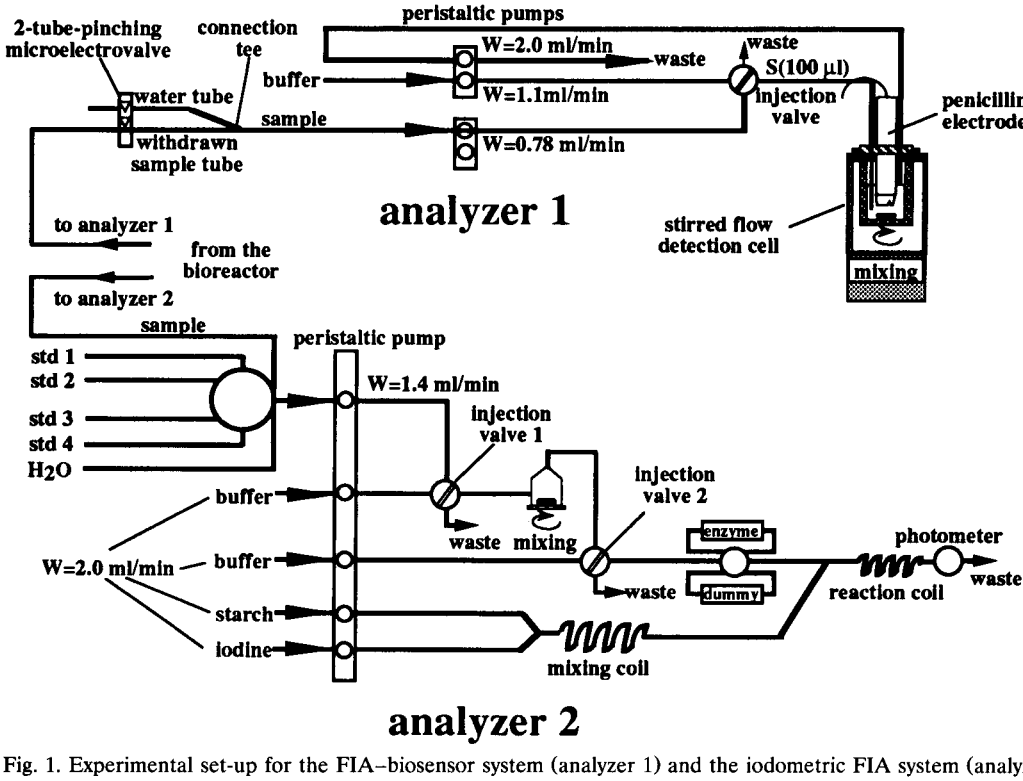

Fig. 1. Experimental set-up for the FIA–biosensor system (analyzer 1) and the iodometric FIA system (analyzer 2).

flow-rate of 1.1 ml min^{-1} is used, the linear range of the electrode is 0–35 g l^{-1} K-pen-V which enables measurement of penicillin during the whole fermentation for the applied strain of *P. chrysogenum*. In order to ensure a complete return of the potential to the baseline an analysis time of 12 min has been chosen.

Analyzer 2

Analyzer 2 is based on enzymatic hydrolysis of penicillin to the corresponding penicilloic acid using immobilized β-lactamase, followed by an oxidation of penicilloic acid by I_2 (the classic iodometric method). The iodine consumption is colorimetrically detected by measuring the decrease in the absorbance of an iodine–starch complex.

The FIA system used for on-line measurement during penicillin fermentations is a modification of a FIA system described in [6]. Two kinds of reactors have been tested concerning on-line measurements: (1) a packed-bed (PBR) with the enzyme immobilized on controlled pore glass (CPG) beads and (2) a wall-coated tubular reactor (WCTR) with the enzyme immobilized on the inside of a nylon tube. Experiments have showed that the long-term stability is poor for the PBR because of an increasing pressure drop across the reactor. This kind of reactor is therefore unsuitable for on-line measurements of penicillin fermentation lasting more than 200 h. The long-term stability for the WCTR is good [9] and it is therefore preferred.

Probably due to the mass-transfer effects in the WCTR it is not possible to have a 100% conversion of penicillin to penicilloic acid in the reactor. This requires careful calibration of the system since a sample from a penicillin fermentation also contains penicilloic acid. The FIA system is therefore designed such that it is possible to measure the concentrations of both penicillin and penicilloic acid. This is done by introducing an extra injection valve (see Fig. 1, analyzer 2) which makes it possible to pump the sample through either the enzyme reactor or a dummy reactor. By means of the dummy reactor, the concentration of penicilloic acid can be measured. Since penicillin can not reduce iodine to iodide [10] it will not interfere with the measurement of penicilloic acid.

For estimation of the penicillin concentration three different standard curves are used:

Standard curve 1: penicillin standard through the enzyme reactor
Standard curve 2: penicilloic acid standard through the enzyme reactor
Standard curve 3: penicilloic acid standard through the dummy reactor

From Eqs. 1 and 2 the concentrations of penicillin (pen) and penicilloic acid (cille) in a sample solution can be calculated:

$$C_{\text{sample, cille}} = \frac{1}{\text{slope 3}}\left[\text{peak height}^{\text{D}}_{\text{sample}}\right] \quad (1)$$

$$C_{\text{sample, pen}} = \frac{1}{\text{slope 1}}\left\{\left[\text{peak height}^{\text{E}}_{\text{sample}}\right] - \frac{\text{slope 2}}{\text{slope 3}}\left[\text{peak height}^{\text{D}}_{\text{sample}}\right]\right\} \quad (2)$$

Slope 1, slope 2 and slope 3 are the slopes of the three standard curves (1, 2 and 3). Peak $\text{height}^{\text{E}}_{\text{sample}}$ and peak $\text{height}^{\text{D}}_{\text{sample}}$ are the peak heights of the sample injected through respectively the enzyme reactor and the dummy reactor.

The calibration graph for the penicillin standards in the enzyme reactor is linear in the range from 5.0 to 250.0 mg l^{-1} K-pen-V. To ensure linearity of the signal in the range 0–30 g l^{-1} K-pen-V the analyzer is equipped with a gradient dilution system. The gradient dilution system [2,11] consisting of an injection valve and a stirred chamber upstream of the injection valve in the analyzer, i.e. the outlet from the stirred chamber passes the loop of the injection valve in the analyzer (see Fig. 1).

The injection volume is 10 μl and the reaction coil is 1 m tube (0.8 mm i.d.). The enzyme reactor is a 1 m nylon tube (1.0 mm i.d) while the dummy reactor is 0.5 m tube (0.8 mm) both coiled in figure eight shape. All reactors (the enzyme and the dummy reactor together with the mixing and reaction coil) are thermostated at 28°C. All flow-rates are 2.0 ml min^{-1}. Data acquisition and control of the valves of the FIA system are performed by a microcomputer with a Motorola

68000 processor. The software is written in PEARL (Process Experimental Automation Real Time Language) using the operating system RTOS (Real Time Operating System), which permits multi tasking [12].

Procedure

The fed-batch penicillin fermentations are carried out in a 41-l Chemap bioreactor and in a 15-l MBR bioreactor with an industrial, high yielding strain of *P. chrysogenum* obtained from Novo Nordisk (Bagsværd, Denmark). The medium contains initially 100 or 200 g l^{-1} corn steep liquor (CSL), 3 g l^{-1} sucrose, 6.0 g l^{-1} phenoxyacetic acid and inorganic salts [$(NH_4)_2SO_4$, KH_2PO_4 and $CaCl_2$] and the size of the inoculum is 15–20% (w/w). The feed is a mixture of 450 g l^{-1} glucose, 46.0 g l^{-1} $(NH_4)_2SO_4$ and 33.3 g l^{-1} phenoxyacetic acid. The gas flow-rate to the bioreactor is 1 volume air/volume fermentation medium/min and the temperature and pH are kept constant at 25°C and 6.5, respectively. For further details on the fermentation conditions there is referred to [13]. The cell free sample from the bioreactor is delivered to the FIA systems by an in situ membrane (ABC module, Advanced Biotechnology Co., Munich) with a 0.22-μm nominal pore diameter [14].

Analyzer 1. β-Lactamase is immobilized over a combined pH-glass electrode: (type LoT 403-M8-S7, Ingold, Paris) as described previously [5,8]. The potentiometric measurements are obtained using a pH-meter (Radiometer pHM-64 research pH meter, Copenhagen) connected to a recorder (Sefram-Servotrace, Paris) which is linked to a Macintosh Plus computer. A laboratory-developed stirred flow detection cell is used as the detection chamber (Fig. 1). PVC and PTFE are used to construct the detection cell. The sample, water, waste and buffer solution are pumped by two peristaltic pumps (Ismatec Sa, Zürich) using tygon tubes (Bioblock, Illkirch, France). A two-tube-pinching micro electrovalve (Bioblock) controls the sample and water flow. Automatic sample injection is carried out by use of a timing control pneumatic actuator connected with a four-way teflon injection valve (Rheodyne, Cotati, USA). Reagents used were 0.01 M sodium phosphate buffer, pH 6.5 (NaH_2PO_4 and $Na_2HPO_4 \cdot 2H_2O$ from Riedel-de Häen) containing 0.1 M NaCl as the working buffer and for the preparation of the penicillinase solution. Commercial penicillin-V (Sigma) is used in order to carry out the calibration procedure. The enzyme is β-lactamase from *Bacillus cereus* (Sigma No. 0389). 25% aqueous solution of glutaraldehyde (Sigma) was used as the cross-linking agent.

Analyzer 2. The FIA system consist of a peristaltic pump (Watson-Marlow, Falmouth) and pneumatically driven injection and multi position valves (Rheodyne, Cotati). The spectrophotometer is an in-house design containing a light emitting diode (660 nm) and a photodiode as detector which is linked to a RTOS computer. The mixing chamber is an in-house design made of PVC with a volume of 1.0 ml. Tubes are made of PTFE (0.5 mm and 0.8 mm i.d.). The β-lactamase (from *Bacillus cereus*, Leo Pharmaceutical Products, Ballerup) is immobilized on 1 m of nylon tubing (1.0 mm i.d.) as described previously [9] but with an enzyme loading of 5 mg enzyme per meter nylon tubing. The reagents used were starch solution containing 0.69 g l^{-1} soluble starch and 0.72 g l^{-1} KI prepared as described in [6]. A 100 μM I_2 solution is prepared from a stock of 0.1 M I_2. The buffer solution is a 25 mM Tris buffer at pH 6.0 [3.03 g Tris(hydroxymethyl)aminomethane], 2.9 g of malic acid and 65 ml of 0.2 M NaOH in 1 l of distilled water. All solutions are freshly prepared every day and degassed before they are used in the FIA system to avoid air bubbles in the detector.

RESULTS AND DISCUSSION

Analyzer 1

An analysis frequency of 2 injections per hour is used during the fermentation. The on-line monitoring is started from the 7th hour directly after calibration and calculation of the calibration slope. Since the sensitivity of the electrode is stable for more than a month [5] frequent calibrations during the fermentation procedure are unnecessary. However, to test the stability during the on-line monitoring two calibrations were con-

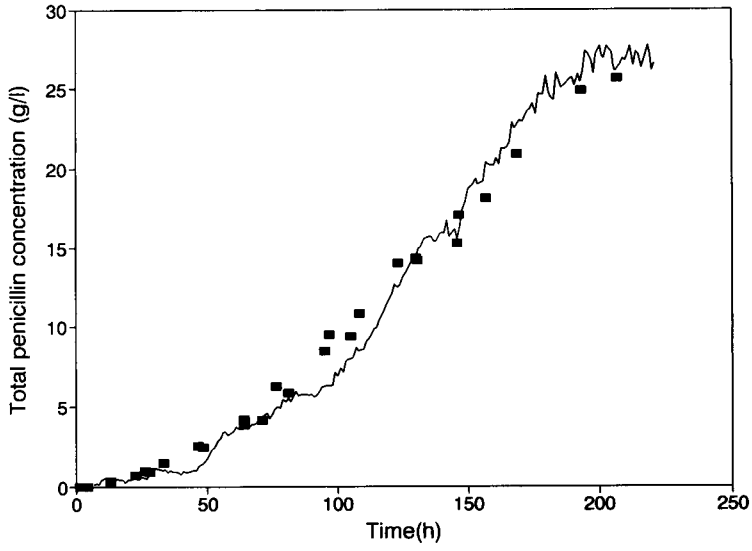

Fig. 2. Comparison of the on-line measurements of the fed-batch penicillin fermentation FB023 using analyzer 1 (———) with off-line LC measurements (■).

ducted (after 129 and 171 h) using the same fermentation medium as the first calibration run and a relative slope difference of less than 5% was observed. The baseline drift during the fermentation was less than 2 mV.

Results using the penicillin electrode are compared with off-line measurements using LC [15]. Figure 2 shows the results of the monitoring of the total penicillin V concentration (including the concentrations of penicillin V and p-OH-penicil-

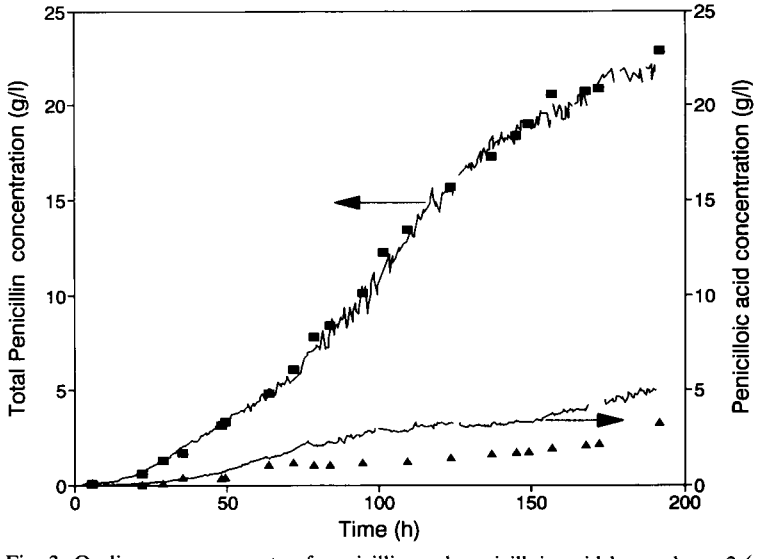

Fig. 3. On-line measurements of penicillin and penicilloic acid by analyzer 2 (———) for the fed-batch penicillin fermentation FB024 compared with off-line LC measurements (■ is penicillin and ▲ is penicilloic acid).

lin V, which also is formed during the fermentation) during a fed-batch penicillin fermentation using analyzer 1. The figure shows a good agreement between the on-line biosensor measurements and the LC measurements results. After approximately 200 h the penicillin production levels off. In three periods (after approximately 40, 90 and 140 h) the penicillin concentration does not seem to increase and this is probably due to changes in the sample matrix, e.g. small changes in the pH-value of the fermentation medium will interfere with the measurements [5].

Analyzer 2

In order to increase the accuracy of the on-line measurements, three different dilution levels are used (the linear range is respectively: 0–7 g l^{-1}, 7–15 g l^{-1} and 15–25 g l^{-1} K-pen-V) and the relative standard deviation at each dilution level is approximately 1%. Calibration is carried out as one-point calibration using the average of two standards of the same standard solution. The analysis cycle used in this analyzer is summarized in Table 1 and its lasts 55 min. Each standard and sample are injected two times. It is moreover necessary to calibrate the system once by a mixed standard containing both penicillin and penicilloic acid.

TABLE 1

Analysis cycle for the analyzer 2

Penicillin standard through the enzyme reactor
Penicilloic acid through the enzyme reactor
Sample through the enzyme reactor
Penicilloic acid through the dummy reactor
Sample through the dummy reactor

Results from application of analyzer 2 for on-line monitoring during a fed-batch penicillin fermentation are shown in Fig. 3 compared with off-line measurements using LC. As for analyzer 1 the sum of penicillin V and pOH-penicillin V is detected. A good agreement between the on-line penicillin measurements and the off-line LC measurements is observed. The on-line measurements of penicilloic acid shows the same trend as the measurements of penicilloic acid by the LC method, but there is some deviation. Experiments of hydrolysis of penicillin have shown that when penicillin is degraded to penicilloic acid, an intermediate with reducing power is formed [15]. It has not yet been possible to quantify this intermediate. Formation of this "unknown" may explain some of the deviation between the on-line measurements and LC measurements of penicilloic acid. Furthermore, it is likely that *P. chryso-*

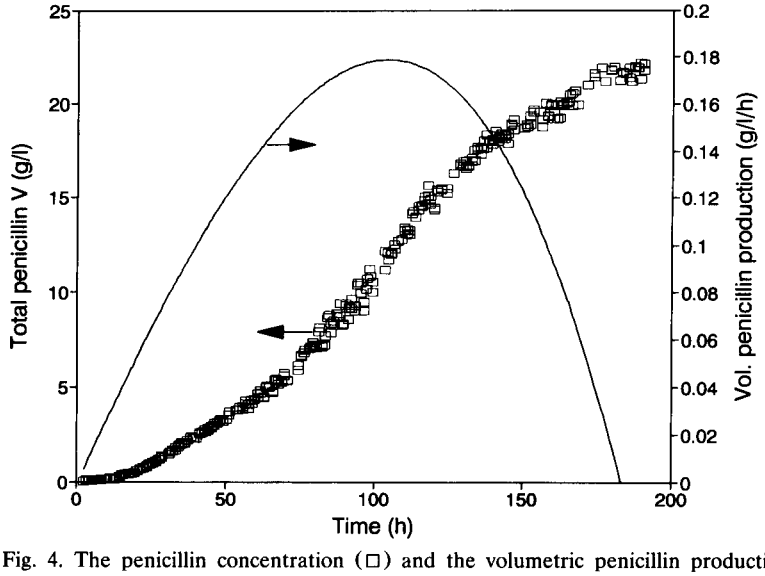

Fig. 4. The penicillin concentration (□) and the volumetric penicillin production rate (———) are shown for the fed-batch fermentation FB024.

genum produce one or more compounds which have reducing power, and this will give a too high signal in the FIA measurements compared with the LC method.

The penicillin curve shows that the penicillin production starts to level off after approximately 150 h which is about 50 h earlier than the penicillin fermentation shown in Fig. 2. The medium only contained 100 g l^{-1} CSL and this may result in a depletion in the end of the fermentation of one or more components which are essential for the penicillin production. In the other fermentation (Fig. 2) a medium containing 200 g l^{-1} CSL was used and the richer medium may explain the prolonged penicillin production.

From the on-line measurements it is possible to calculate the volumetric penicillin production rate throughout the fermentation. Figure 4 shows that the penicillin production starts almost immediately after the inoculation and the volumetric penicillin production rate reach a maximum after 110 h, whereafter it rapidly declines. It is obvious that the many precise on-line measurements permit a detailed study of the fermentation kinetics.

Comparison of the two systems

As illustrated above both of the on-line analyzers work very well during fed-batch penicillin fermentations lasting about 200 h. However, when one wants to develop an on-line analyzer it is important to pay attention to many aspects, e.g. the calibration of the FIA systems, the complexity of the analyzer and the sensitivity. The two method are compared in Table 2, where advantages and disadvantages are discussed.

Analyzer 1 is a simple system including only

TABLE 2

Comparison of the two on-line FIA systems

	Analyzer 1 (biosensor)	Analyzer 2 (iodometric method)
Calibration	The system is calibrated once at the beginning of the fermentation	The system is calibrated every hour
Interference	The analyzer is sensitive to small variations in the sample matrix, especially pH changes	For the penicillin measurements the analyzer is very robust. For the penicilloic acid measurements other reducing compounds interfere with the measurements
Measurement range	With the applied flow-rate: 0.5–30.0 g l^{-1} K-pen-V	With the three dilution levels: 0.1–30.0 g l^{-1} K-pen-V
Complexity	A very simple system, consisting of only one injection valve	A complicated system, due to the dummy reactor and the dilution step. The system consist of 3 injection valves and 1 multi-position valve
Analysis frequency	The maximum analysis frequency is 3 samples per hour for a flow-rate at 1.1 ml min^{-1}	The maximum analysis frequency is 6 samples per hour without calibration. With the accurate calibration procedure only 2 samples are analyzed per hour
Maintenance	The enzyme electrode is rinsed every 3th day	Rinsing, fresh reagents and fresh standards once a day
Number of components	Penicillin	Penicillin Penicilloic acid
Substrate consumption	1.5 l day^{-1} of the buffer solution	3.5 l day^{-1} of iodine and starch solutions 7.0 l day^{-1} of the buffer solution
Price for 200 h of on-line measurement	about US$40	about US$50

one valve and because of the very stable signal from the biosensor it is sufficient to calibrate the analyzer very few times during the whole fermentation. Furthermore, the reagent consumption for analyzer 1 is small compared with analyzer 2. However, a drawback of this analyzer is that small changes in the sample matrix and especially changes in the pH value of the sample interfere with the sample measurements.

Analyzer 2 is obviously more complicated than the analyzer 1, but both the concentration of penicillin and penicilloic acid can be measured. The penicillin measurements are insensitive to changes in the sample matrix, because a sample is taken through both the enzyme reactor and the dummy reactor. However, reducing components in the medium will interfere with the measurement of the penicilloic acid concentration. The FIA system has three dilution levels, which make it possible to have a good accuracy for both low and high penicillin concentration. Analyzer 2 has to be calibrated very often (every hour) and fresh standards and reagents should be made every day in order to ensure reliable measurements.

Conclusion

Two different on-line systems for measuring penicillin are described. Both on-line analyzers work very well during penicillin fermentation lasting about 200 h, but for routine on-line measurements during fed-batch penicillin fermentations analyzer 1 is to be preferred, because of its simplicity and easy handling. This means that the system needs very little maintenance; an important factor for fermentations lasting more than 200 h.

REFERENCES

1 J. Nielsen, Process Control Qual., 2 (1992) 371.
2 M. Garn, M. Gisin, C. Thommen and P. Cevey, Biotechnol. Bioeng., 34 (1989) 423.
3 K. Schügerl, Anal. Chim. Acta, 213 (1988) 1.
4 J. Nielsen, K. Nikolajsen and J. Villadsen, Biotechnol. Bioeng., 37 (1991) 11.
5 H. Meier and C. Tran-Minh, Anal. Chim. Acta, 264 (1992) 13.
6 M. Carlsen, L.H. Christensen and J. Nielsen, Anal. Chim. Acta, 274 (1993) 117.
7 J. Möller, R. Hiddessen, J. Niehoff and K. Schügerl, Anal. Chim. Acta, 190 (1986) 195.
8 H. Meier, S. Kumaran, A.-M. Danna and C. Tran-Minh, Anal. Chim. Acta, 249 (1991) 405.
9 J. Nielsen, K. Nikolajsen, S. Benthin and J. Villadsen, Anal. Chim. Acta, 237 (1990) 165.
10 H.T. Clarke, J.R. Johnson and R. Robinson, The Chemistry of Penicillin, Princeton University Press, Princeton, 1949.
11 S. Benthin, J. Nielsen and J. Villadsen, Anal. Chim. Acta, 247 (1991) 45.
12 C.L. Johansen, L.H. Christensen, J. Nielsen and J. Villadsen, Comp. Chem. Eng., 16 S297.
13 L.H. Christensen, J. Nielsen and J. Villadsen, Anal. Chim. Acta, 249 (1991) 123.
14 L.H. Christensen, J. Nielsen and J. Villadsen, Chem. Eng. Sci., 46 (1991) 3304.
15 L.H. Christensen, Ph.D Thesis, Technical University of Denmark, Lyngby 1992.

Analytica Chimica Acta, 279 (1993) 59–66
Elsevier Science Publishers B.V., Amsterdam

Development of an on-line method for the monitoring of vicinal diketones and their precursors in beer fermentation

C. Mathis [1], M.N. Pons and J.M. Engasser

Laboratoire des Sciences du Génie Chimique, CNRS-ENSIC-ENSAIA-INPL, Nancy (France)

M. Lenoel

Tepral Centre de Recherches BSN, Branche Bière, Strasbourg (France)

(Received 1st October 1992; revised manuscript received 19th January 1993)

Abstract

Methods for on-line monitoring of vicinal diketones and their precursors during beer fermentation have been developed. Vicinal diketones can be directly monitored using a gas membrane device connected to a GC-ECD system. Liquid phase heat conversion of their precursors into diketones, after automatic liquid sampling, proved to be the most satisfactory technique for the monitoring of α-acetolactate and acetohydroxybutyrate. The methods were successfully tested on beer fermentation.

Keywords: Gas chromatography; Beer fermentation; Diketones; Gas membrane device; On-line measurements

Vicinal diketones (i.e. diacetyl and 2,3-pentanedione) have been a research topic for many years because they contribute to the bad taste of beer by giving a characteristic and very unpleasant buttery taste [1]. The human taste threshold is very low (0.05–0.1 ppm for a lager beer), which explains the research undertaken to understand the formation and reduction of diacetyl by yeast, for quality control purpose. The precursors of diacetyl and 2,3-pentanedione, α-acetolactate and acetohydroxybutyrate respectively, are intermediaries in the synthesis routes of valine, leucine and isoleucine. These precursors are produced inside the cell, then excreted into the broth where they are converted into diketones [2]. This non-enzymatic conversion is an oxidative decarboxylation. Later the yeast reduces enzymatically the diketones.

As the diketones can be considered as secondary metabolites in the synthesis of isoleucine and valine, the regulation of amino acid synthesis has an effect on diketone synthesis. Moreover the diketone precursors are highly instable compounds, sensitive to temperature and redox potential (rH = 10 is the limit for α-acetolactate according to Inoue et al. [2]). Oxygen or any other electron acceptors such as Cu^{2+}, Fe^{3+} and Al^{3+} favor the decarboxylation, the rate of which is increased by temperature.

The production of high quality beer requires an adequate process control, which is impeded by the lack of on-line sensors for the key elements of the flavour profile such as ethanol and other

Correspondence to: M.N. Pons, Laboratoire des Sciences du Génie Chimique, CNRS-ENSIC-ENSAIA-INPL, BP 451, F-54001 Nancy Cedex (France).

[1] Also at Tepral.

volatile compounds. The formation of beer flavour requires the production of desirable amounts of esters and higher alcohols (ethyl acetate, isoamyl acetate, isoamyl alcohol) and the resorption of undesirable compounds such as vicinal diketones.

It has already been demonstrated that gas membrane interfaces based on microporous hydrophobic membranes, coupled to a gas chromatograph, can be used successfully to monitor alcohols, aldehydes and esters in alcoholic fermentations. The purpose of this paper is to describe the use of such techniques to monitor the concentrations of free vicinal diketones and their precursors in beer fermentations.

Free vicinal diketones are volatile compounds easily transferred through the gas membrane and their concentration in the carrier gas is monitored by means of gas chromatography equipped with electron capture detection (GC-ECD). Only the undissociated part of acetohydroxy acids can be transferred through the membrane. A transformation into the corresponding diketones is then required for analysis.

MATERIALS AND METHODS

Fermentation

The fermentation is run on a fully-instrumented 20-l reactor (LSL-Biolafitte, Saint-Germain-en Laye). A condenser (−0.5°C) prevents the volatile stripping at the gas outlet. An industrial lager-type strain, *Saccharomyces carlsbergensis*, provided by Tepral-BSN (Strasbourg) is used. The must is inoculated with 6.7 g pressed yeast l^{-1}, which corresponds to 20×10^6 cell ml^{-1}. The culture medium is an industrial wort transferred to the fermentor under sterile conditions. The standard temperature is 12°C and the stirring speed is 50 rpm. The pressure is controlled at 0.5 bar. Before inoculation the wort is aerated with pure oxygen and the initial dissolved oxygen concentration is 8 mg O_2 l^{-1}.

Gas membrane

Two types of gas membrane were used: a flat membrane with a surface available to transfer of 2.5 cm^2, made out microporous PTFE (Sartorius, Palaiseau). The pore diameter is 0.2 μm with a porosity of 70%; a tubular membrane (12 cm × 4 mm o.d. × 3 mm i.d., equivalent pore diameter 1 μm, porosity 70%) made out microporous PTFE (Goretex from Gore & Ass). Except when specified the flat membrane device is used for fermentation monitoring.

Off-line analyses

All chromatographic analyses are made on filtrated samples (0.8 μm). Diacetyl and 2,3-pentanedione are determined on a gas chromatograph (Carlo Erba 4200) equipped with an electron capture detector and an automated headspace injector (Carlo Erba HS250). The separation is taking place in a glass column (4 m × $\frac{1}{4}$ in.) packed with Chromosorb W, 80/100 mesh (AW-DMCS), impregnated with Carbowax 1540 (10%) with the following temperature settings: oven 80°C, injector 180°C, detector 150°C. Carrier gas is nitrogen quality U. Due to the precursors the yeast-free sample is neutralized with sodium hydroxide and immediately analyzed. Internal standard is 1,3-dichloropropane.

Precursors are determined after their thermal conversion (60°C during 1 h) into the corresponding diketones. The result is the sum of free vicinal diketones contained in the sample plus the diketones resulting from the precursors conversion. The gas chromatograph (Hewlett Packard 5710) is equipped with an electron capture detector and an automatic injector (DANI HSS 3950). Internal standard is 1,3-dichloropropane. The separation is taking place in a stainless steel column (4 m × $\frac{1}{8}$ in.), packed with Chromosorb P-AW, 80/100 mesh impregnated with Carbowax 20M. Carrier gas is a mixture of argon and methane (90 : 10). The following temperature settings are used: oven 90°C, injector 150°C, detector 150°C.

The calibration curves for the diketones are not linear and a logarithmic correction is applied

$$\ln C = a \ln\left(\frac{A}{IS}\right) + b$$

where C is the vicinal diketone concentration, A the peak area and IS the internal standard peak area.

On-line analyses

A 121FL Delsi Instruments (Perkin-Elmer, Saint-Quentin-en-Yvelines) gas chromatograph equipped with an automatic injection valve (volume, 0.3 ml), a flame ionisation detector and an electron capture detector is used. The separation is taking place in a stainless steel column (4 m × $\frac{1}{8}$ in.) packed with Chromosorb W, 80/100 mesh (AW-DMCS), impregnated with Carbowax (10%) with the following temperature settings: oven 80°C, injector 120°C, flame ionisation detector 120°C, electron capture detector 140°C. Carrier gas is nitrogen quality U.

Synthesis of α-acetolactate

In order to perform the preliminary tests synthetic α-acetolactate was obtained by reaction of ethyl-2-acetoxy-2-methylacetoacetate (Aldrich, ref 22 039–6) with sodium hydroxide under strict anaerobic conditions to avoid the immediate transformation into diacetyl.

The reaction produces ethanol as a by-product, which was monitored by a gas membrane sensor connected to the gas chromatograph. From this measurement, the reaction yield was calculated to be 80 ± 2% of the theoretical yield, in agreement with De Man's observations [3]. The precursor is then transferred to a reactor containing degassed beer for the subsequent experiments. The beer is made anaerobic by addition of yeast 12 h before the experiment, in order to consume the residual oxygen. The synthetic precursor was not found to be stable in anaerobic water or buffer solutions.

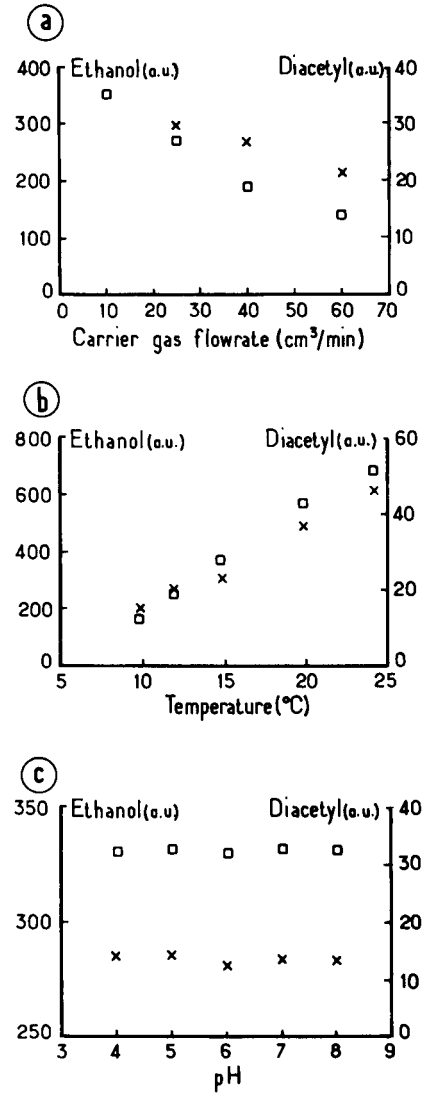

Fig. 1. Effect of operation condition on detection of ethanol (×) and diacetyl (□) by the flat membrane device: (a) effect of carrier gas flow-rate; (b) effect of temperature; (c) effect of pH.

RESULTS

Diacetyl and 2,3-pentanedione

The vicinal diketones are sufficiently volatile to be easily detected on-line with the flat membrane device. As for other volatiles such as alcohols, esters, the detection signal decreases when the carrier gas flow-rate increases in the gas membrane device (Fig. 1a), and it increases when the broth temperature increases (Fig. 1b). No effect of pH or pressure in the normal range of beer fermentation has been noticed (Fig. 1c). The repeatability of the on-line method is better than the one obtained on off-line analyses of the same beer sample. The detection limit is 10 ppb for both diketones. The response curve is logarithmic as for the off-line analysis due to the ECD characteristics. Figure 2 presents the typical results of on-line and off-line monitoring of both diketones. High levels are measured off-line, when diacetyl is detected on-line at the beginning of the fer-

mentation only, when the dissolved oxygen is still high enough to have a conversion of the precursors in the corresponding diketones. These results can be compared to those of Wainwright [4], who suggested that the analysis method was very important. Two hypotheses can be suggested

(1) Diketones are bound in the broth to some other compound, which limits their volatility and therefore their transfer through the gas membrane. This binding can be destroyed during the sample preparation for off-line analysis.

(2) In spite of very careful handling of liquid samples, a small amount of oxygen can be introduced in off-line sample, which causes a conversion of the precursors into diketones.

The second hypothesis seems the most likely as diketones are effectively measured on-line at the beginning of the fermentation and also when a fermentation perturbation is deliberately induced (Fig. 3).

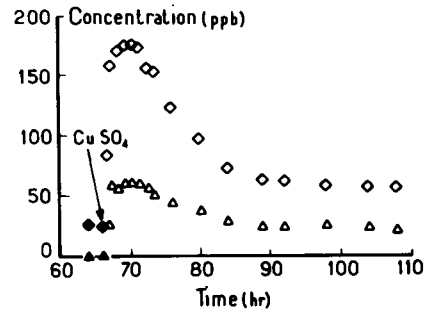

Fig. 3. Effect of addition of $CuSO_4$ during a normal beer fermentation; (◇) diacetyl; (△) 2,3-pentanedione.

Precursors

Gas-phase conversion. The simplest way to transform the precursors into their corresponding diketones is to operate a gas phase conversion (Fig. 4a), once the undissociated part of the acetohydroxyacids has been transferred across the membrane. However, their volatility coefficient and their pK_a are unknown, especially in beer. No estimation of the part available for gas phase transfer can be reasonably made. In order to increase the quantity of precursor in the gas phase, the flat membrane device was replaced by the tubular gas membrane. The conversion is taking place in a reactor containing KMnO4 crys-

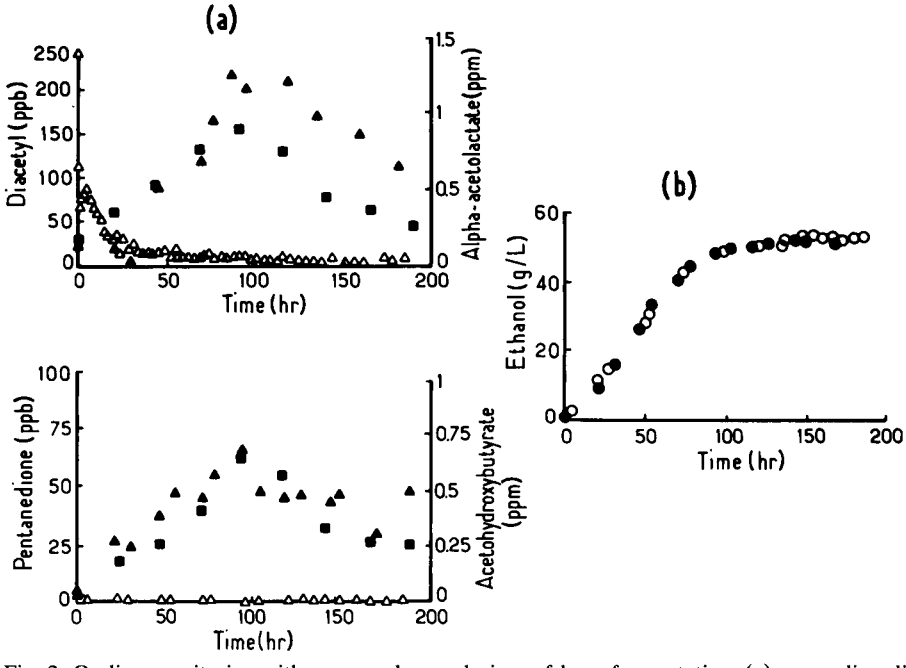

Fig. 2. On-line monitoring with gas membrane devices of beer fermentation. (a) △, on-line diketone; ▲, off-line diketone; ■, on-line precursor. (b) ○, on-line ethanol; ●, off-line ethanol.

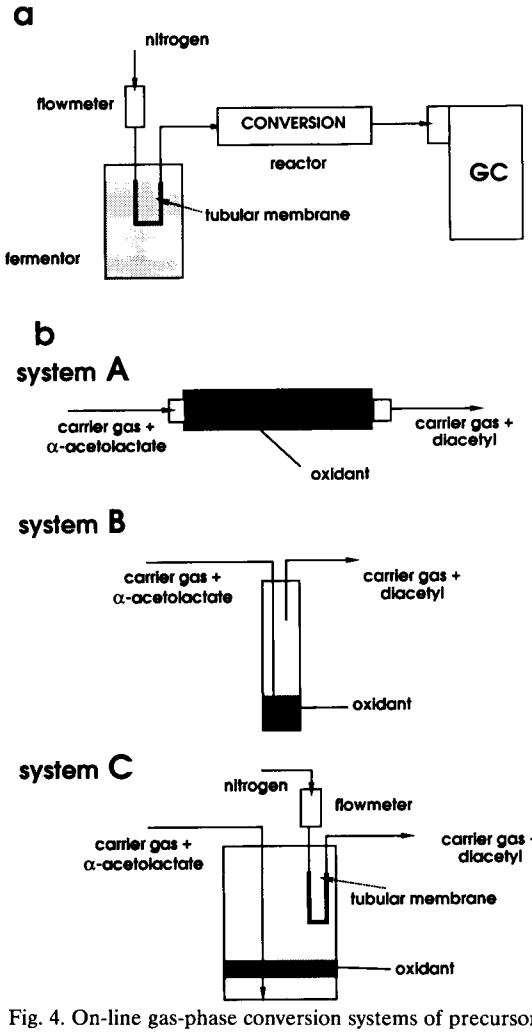

Fig. 4. On-line gas-phase conversion systems of precursors: (a) general set-up; (b) tested systems.

tals in order to oxidate the precursors [3,4]. Three systems were tested (Fig. 4b) but only the settup C produces some interesting results (Fig. 5). However the repeatability was poor and the detection limit (1 ppm) was too high for beer fermentation monitoring.

Liquid-phase conversion; conversion by oxidant. The addition of an oxidative compound such as $CuSO_4$ during the fermentation produces the immediate formation of vicinal diketones (Fig. 3): the liquid phase conversion of the precursors by addition of $CuSO_4$ is therefore possible, even under anaerobic conditions.

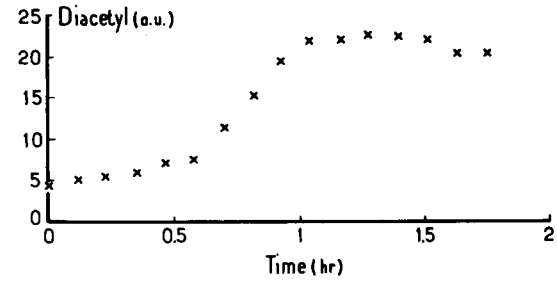

Fig. 5. Monitoring of diacetyl with system C (see Fig. 4), in response to the transfer of synthetic α-acetolactate from the fermentor and its conversion in the reactor.

The liquid phase conversion requires an on-line liquid sampling system (Fig. 6). After transfer into the conversion reactor, 2.5 ml of a 10 g $CuSO_4$ l^{-1} solution is added to start the conversion which is monitored by diacetyl formation (Fig. 7). There is a correlation between the rate of production of diacetyl and the initial content in α-acetolactate (Fig. 8). In spite of the oxidant the conversion is slow, and to have to wait for its completion would severely limit the use of the technique. Furthermore, when yeast cells are pre-

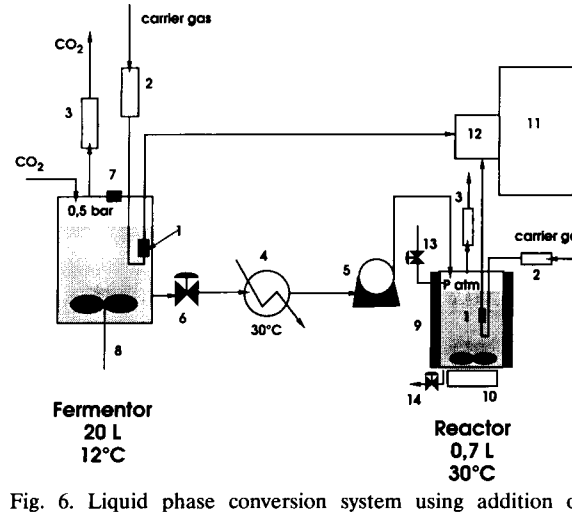

Fig. 6. Liquid phase conversion system using addition of $CuSO_4$ solution. (1) Gas membrane device; (2) mass flowmeter; (3) condenser; (4) heat exchanger; (5) peristaltic pump; (6) liquid sampling valve; (7) septum; (8) mechanical agitation; (9) jacketed reactor; (10) magnetic agitation; (11) GC with FID and ECD; (12) gas phase sampling valve; (13) liquid inlet for rinsing; (14) liquid outlet.

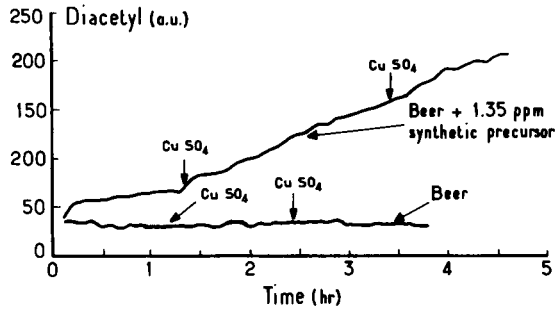

Fig. 7. Monitoring of diacetyl, in response of the conversion of synthetic α-acetolactate after addition of $CuSO_4$.

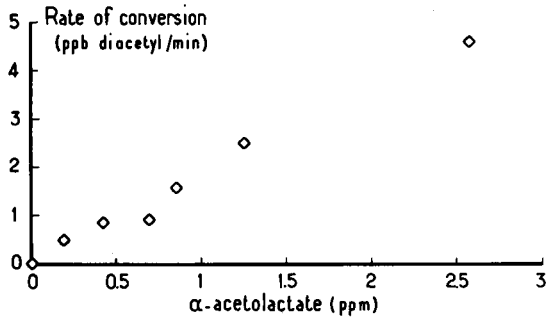

Fig. 8. Correlation between the rate of formation of diacetyl and the concentration of synthetic α-acetolactate.

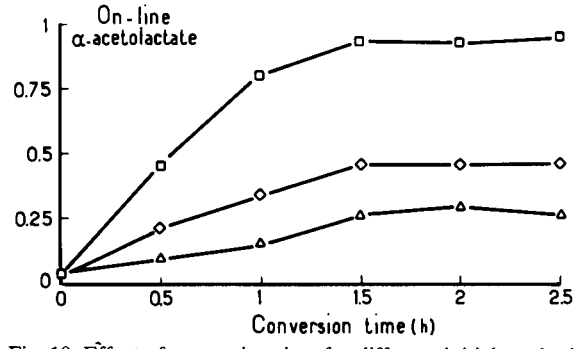

Fig. 10. Effect of conversion time for different initial synthetic precursor concentrations: □, 1.3 ppm; ◇, 0.6 ppm; △, 0.3 ppm.

sent, they are able to convert the diketones in the conversion reactor.

Liquid phase conversion; heat conversion. Finally, liquid phase conversion by heat has been tested by similarity with the off-line analysis method. After its transfer into a 1.2-l stirred reactor, the beer sample was maintained at 65°C during 90 min (Fig. 9). Different reaction temperatures have been suggested in literature. Postel and Beier [5] heated a sample at 80°C for 60 min.

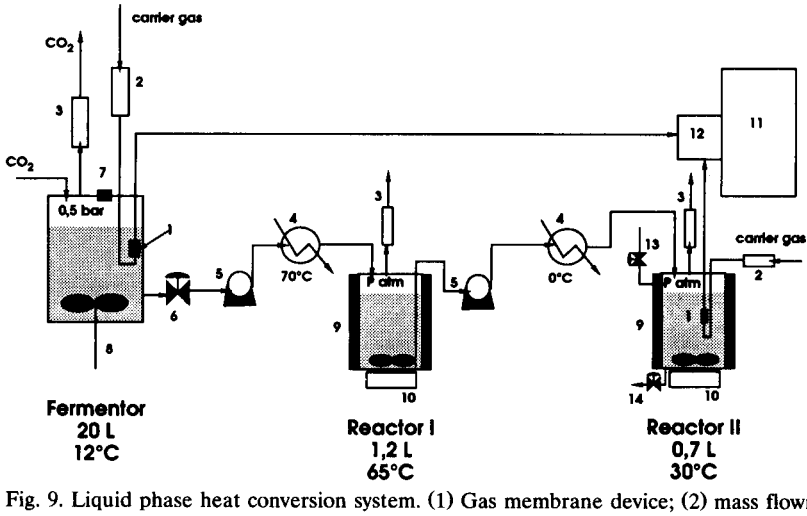

Fig. 9. Liquid phase heat conversion system. (1) Gas membrane device; (2) mass flowmeter; (3) condenser; (4) heat exchanger; (5) peristaltic pump; (6) liquid sampling valve; (7) septum; (8) mechanical agitation; (9) jacketed reactor; (10) magnetic agitation; (11) GC with FID and ECD; (12) gas phase sampling valve; (13) liquid inlet for rinsing; (14) liquid outlet.

Inoue [6] proposed 90°C for 10 min. Pajunen et al. [7] obtained best results at 60–70°C for 45 min. According to Fig. 10, the reaction is nearly complete after 90 min.

Figure 11 shows the linear relationship obtained between the on-line and off-line analyses with the synthetic precursor. However the off-line value is always the double of the on-line one. The off-line validity limit is 1 ppm. The off-line values would correspond to an unrealistic production yield of synthetic α-acetolactate sligthly higher than 1.

These results show the good behavior of the on-line system in spite of the differences with the off-line method. As indicated in literature, the operation conditions have a great importance and it is not sure that the synthetic precursor added to beer can fully represent the natural substance produced during the fermentation.

The concentrations in natural α-acetolactate and acetohydroxybutyrate have been monitored on-line and off-line during fifteen fermentations. Figure 12 presents the correlation between the on-line and off-line data for two special instants: when the precursor concentration reaches its maximal value (Fig. 2) and at the end of the fermentation, when 94% of the fermentescible sugars have been consumed. The gas membrane sensor placed in the fermentor indicates that no vicinal diketones are accumulated in the broth. It is therefore unnecessary to correct the precursor concentrations.

For α-acetolactate a linear relationship is obtained in the range 0–1.5 ppm between off-line and on-line concentrations. The slope (0.75) is lower than for the tests with synthetic precursor. It is however doubtful that α-acetolactate can reach 3 ppm in beer fermentation [8,9]. For acetohydroxybutyrate, a linear relationship is also found with a slope of 0.68, in the range 0–1.5 ppm.

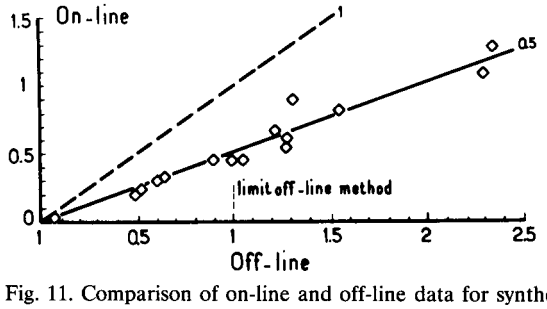

Fig. 11. Comparison of on-line and off-line data for synthetic α-acetolactate.

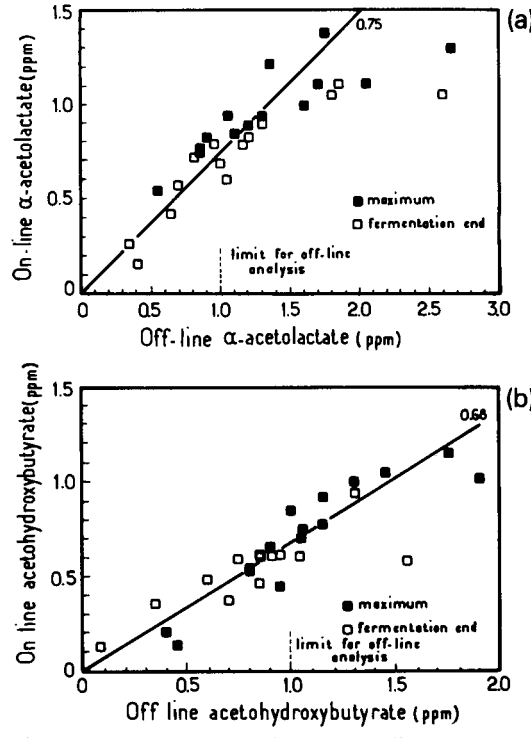

Fig. 12. Comparison of on-line and off-line data for natural α-acetolactate produced during 15 fermentation runs.

Fermentation monitoring

Figure 2 presents global fermentation results obtained for a classical run. For classical volatiles such as ethanol, there is an excellent agreement between off-line and on-line data. As already mentioned, diketones are not detected on-line except at the beginning of the fermentation. Both precursor curves exhibit a maximal value. Although there is a difference in terms of absolute values, it should be noticed that the on-line precursor curves are quite similar to the off-line diketones curves, making stronger the hypothesis of pollution by oxygen of the liquid sample in the off-line method.

Conclusions

Gas membrane based methods have been developed for the monitoring of vicinal diketones and of their precursors during beer fermentation. The monitoring of vicinal diketones is not more difficult than the monitoring of other volatile components such as alcohols, esters, etc. Only the use of an electron capture detector on the gas chromatograph can induce larger maintenance problems of the global systems. The use of a gas membrane device eliminates any artefact like oxygen pollution of the sample.

Vicinal diketone precursors could not be satisfactorily monitored by means of an on-line gas phase conversion, at least in the case of beer fermentation. A liquid phase system had to be used which is certainly a less elegant solution but it worked correctly in the laboratory and later on a pilot plant.

REFERENCES

1 D.B. West, A.L. Lautenbach and K. Becker, Am. Soc. Brew. Proc., (1952) 81.
2 T. Inoue, K. Masuyama, Y. Yamamoto, K. Okada and Y. Kuroiwa, J. Ferment. Technol., 46 (1968) 342.
3 J.C. De Man, Recueil Trav. Chim., 78 (1959) 480.
4 T. Wainwright, J. Inst. Brew., 79 (1973) 451.
5 W. Postel and B. Meier, Z. Lebensm. Unters. Forsch., 173 (1981) 85.
6 T. Inoue, Rep. Res. Lab. Kirin Brew. Co., 25 (1982) 13.
7 E. Pajunen, V. Makinen and R. Gisler, Eur. Brew. Conv. Proc. 1987, (1987) 441.
8 A.D. Haukeli and S. Lie, J. Inst. Brew., 78 (1972) 229.
9 G. Lipus, Diplôme d'ingénieur CNAM, Nancy, 1988.

Analytica Chimica Acta, 279 (1993) 67–72
Elsevier Science Publishers B.V., Amsterdam

Monitoring of fermentation by infrared spectrometry

Alcoholic and lactic fermentations

D. Picque
INRA, LGPBA, 78850 Thiverval-Grignon (France)

D. Lefier and R. Grappin
INRA, SRTAL, 39800 Poligny (France)

G. Corrieu
INRA, LGPBA, 78850 Thiverval-Grignon (France)

(Received 1st October 1992; revised manuscript received 9th February 1993)

Abstract

Infrared spectrometry offers a great potential for quantitative analysis of substrates and products in fermentation media. Like this, a rapid measurement of lactose, galactose and lactic acid during lactic fermentation and sugars (glucose and fructose), glycerol and ethanol during alcoholic fermentation will constitute a major progress for the monitoring and the control of these processes. The samples, taken manually during the fermentations, permitted the determination of the interesting spectral ranges for the measurement of these compounds. These ranges, characterized by significant evolutions of absorbance, are situated in the middle infrared zone: between 1100 and 1040 cm^{-1} for lactose and galactose, between 1593 and 1515 cm^{-1} for lactate, between 1206 and 1026 cm^{-1} for molecules of the alcoholic fermentation and between 3000 and 1026 cm^{-1} for ethanol. Calibration is realized by the partial least-squares method from representative samples of the studied concentrations. The regression coefficients of the correlation between the concentrations measured by infrared spectrometry and liquid chromatography are better than 0.99. The maximum standard errors are 0.46, 0.57 and 0.95 g l^{-1}, respectively for lactose, galactose and lactic acid; 2.5, 0.09 and 0.98 g l^{-1}, respectively for the sugars, glycerol and ethanol.

Keywords: Infrared spectrometry; Liquid chromatography; Alcohols; Calibration; Fermentation; Sugars

Fermentation processes can be improved by controlling the physicochemical parameters of the cultures. Although many parameters, essentially physical, are measurable on-line, others such as the concentrations of substrates and residual products are difficult, if not impossible, to determine. An approach to resolving these problems, extensively studied for the past several years, involves the use of classical analysis methods [liquid chromatography (LC), gas chromatography (GC), flow-injection analysis (FIA), biosensors, etc.] coupled to bioreactors [1–4]. In this case, sampling loops must be used, increasing analysis time and contamination risks. In addition, on-line filtration systems are required, which remain open to clogging.

Direct measurement in the bioreactor, or in samples without prior treatment, is the ideal solution. An interesting potential for realizing this is

Correspondence to: D. Picque, INRA, LGPBA, 78850 Thiverval-Grignon (France).

offered by infrared spectrometry (IR), already used in a number of near-IR applications in food and agriculture industries [5]. Theoretically, it enables a number of compounds to be quantified, as a result of the relationship between the spectra and the structure of the substances. This method is also rapid and non-destructive, analysis times being on the order of several seconds. Prior work has shown the value of these measurements in the field of fermentations [6–8]. Furthermore, considerable developments in the field of optical fibres and their coupling to spectrometers has led to multipoint on-line measurements, either directly in reactors [9,10] or in sampling cells [11].

One aim of the present study was to determine the interesting spectral zones in the domains of near (800–3000 nm, 12500 to 3330 cm^{-1}) and middle IR (3000–12500 nm, 3330–800 cm^{-1}) for following changes in lactic and alcoholic fermentations. After calibration, we then determined the concentrations of the principal molecules involved in these processes and compared the results obtained with those supplied by LC assays.

MATERIALS AND METHODS

Fermentation conditions

A 15-l automated bioreactor (LSL Biolafitte) was used. Ten liters of medium were prepared for each fermentation.

The initial sugar concentration of the must was 200 g l^{-1} and it was thermostatted at 20°C without aeration and agitation. The inoculum was prepared from a active commercial dry yeast (*Saccharomyces cerevisiae*, Fermivin, Gist Brocades, Delft).

The medium for lactic acid bacteria (*Lactobacillus* and *Streptococcus*) contained 60 g l^{-1} whey and 5 g l^{-1} yeast extract. It was sterilized at 110°C for 10 min. Growth conditions were: temperature 30°C, agitation speed 200 rpm, pH 6.5.

Analytical methods

Glucose, fructose, glycerol, ethanol, lactose, galactose and lactic acid concentrations were determined by liquid chromatography. The analyser was composed of a Model 510 pump, a WISP automatic injector, a Model 410 refractometer detector and a Model 440 integrator (Waters, Millipore). The column was an Aminex HPX87H (Biorad) with a mobile phase of 0.005 M H_2SO_4 at a flow-rate of 0.6 ml min^{-1}. The internal standard was 1% propionic acid.

Spectrometry

FT-IR spectra were recorded on a Nicolet Model 740 spectrometer. For the near infrared (NIR), the spectrometer was equipped with a quartz–halogene source and PbSe detector. For the mid infrared (MIR), we used a globar source and a DTGS detector. The spectrometer was operated at a resolution of 4 cm^{-1} and 32 scans were accumulated for each spectrum.

Two cells were studied: transmission cells with 0.02 mm path length (Window ZnSe for NIR, Cafe for MIR) and attenuated total reflectance cell (ATR) with a 60° horizontal ZnSe crystal.

The water spectrum presents two regions with high absorbance, viz. 5400–4760 cm^{-1} and 7400–6250 cm^{-1}. All sample spectra were obtained by subtracting the water background spectrum from the measured spectra.

The spectral data obtained were analysed with the PLS software of Nicolet using the partial least-squares treatment. Concentrations and absorbances of standard samples are used for calibration. Then, the model is used to predict the concentration of components of other fermentation samples.

Calibration

The calibration was done with samples of alcoholic and lactic fermentation. The concentrations of these samples were: sugars (glucose + fructose) 0–200 g l^{-1}, glycerol 0–8 g l^{-1}, ethanol 0–100 g l^{-1}, lactose 0–90 g l^{-1}, galactose 0–50 g l^{-1} and lactic acid 0–50 g l^{-1}.

RESULTS

Studies of spectra

The NIR spectra obtained from alcoholic or lactic fermentation samples contained no peaks or zones whose absorbance varied significantly

during fermentation. Spectral differences between samples at the beginning and end of fermentation were too low to be useful for on-line NIR measurements, especially with multiplex optical fibre systems. No calibration test was attempted on these data.

The MIR spectra obtained in the transmission mode with several lactic fermentation samples are shown in Fig. 1. S0 and S10 are samples obtained at the beginning and end (10 h) of fermentation, and S1–S9 are samples obtained during the process with increasing time. There were significant absorbance changes in three frequency zones: between 1593 and 1515 cm^{-1}, at the peak at 1575 cm^{-1} characteristic of the lactate ion, and between 1298 and 1470 cm^{-1} and 1100 and 1040 cm^{-1}, corresponding to the disappearance of lactose and the appearance of galactose and lactic acid. The absorption differences between the samples at the beginning (high lactose concentration) and the end of fermentation (high galactose and lactic acid concentrations) were high: about 0.22 unit at 1076 cm^{-1} and 0.69 unit at 1575 cm^{-1}. Spectra obtained in ATR were

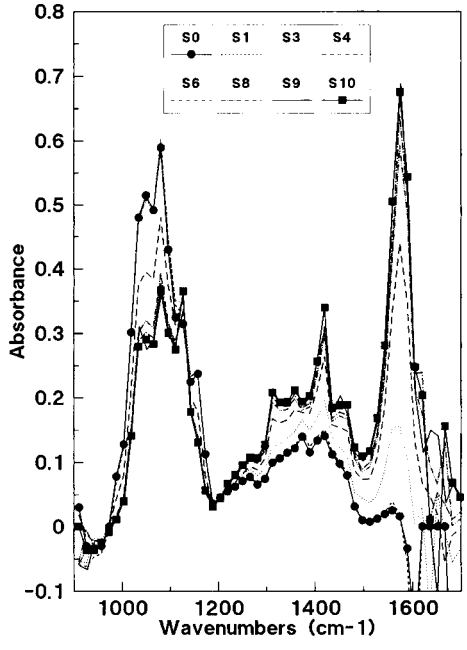

Fig. 1. Mid-IR absorbance spectra of lactic fermentation samples measured by transmission. S = sample; 0–10 = fermentation time (h).

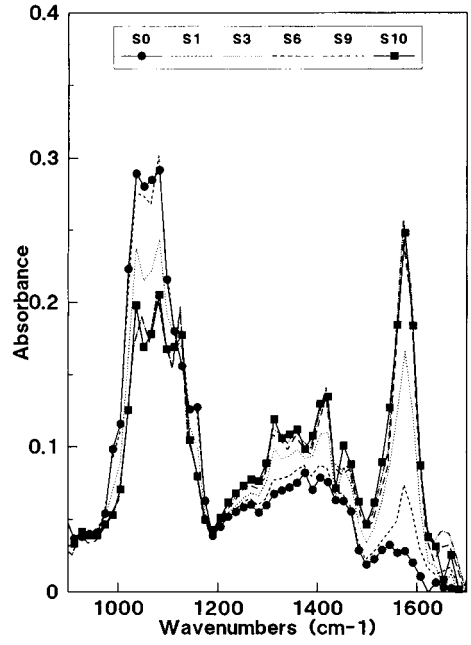

Fig. 2. Mid-IR absorbance spectra of lactic fermentation samples measured by ATR. S = sample; 0–10 = fermentation time (h).

practically identical and contained the same characteristic zones (Fig. 2). Nevertheless, absorbances were about 50% lower and the differences between the beginning and end of fermentation were also lower: 0.09 unit at 1076 cm^{-1} and 0.22 unit at 1575 cm^{-1}. These three spectral zones were chosen for calibration of lactic fermentation and to determine the concentrations of unknown samples.

The transmission MIR spectra of representative samples of alcoholic fermentation enabled two interesting frequency zones to be identified. The zone between 3000 and 2965 cm^{-1} exhibited an increase in absorbance concomitant with the increase in the ethanol concentration in the samples. Changes in the zone between 1206 and 1026 cm^{-1} are characteristic of the decrease in sugar concentrations and the increase in the glycerol and ethanol concentrations (Fig. 3). The profiles of the spectra obtained in ATR were similar (Fig. 4). These two zones were thus adopted for calibration of alcoholic fermentation. The absorbance changes between samples at the beginning and the end of fermentation were considerable.

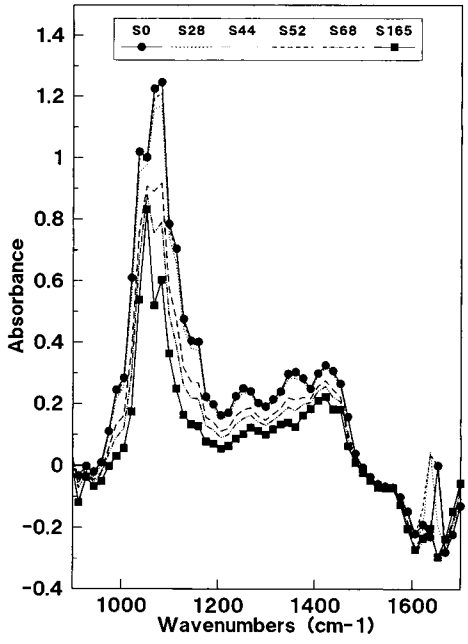

Fig. 3. Mid-IR absorbance spectra of alcoholic fermentation samples measured by transmission. S = sample; 0–165 = fermentation time (h).

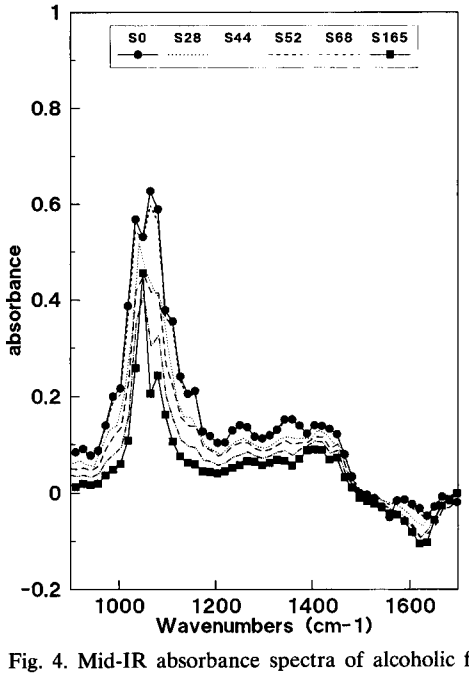

Fig. 4. Mid-IR absorbance spectra of alcoholic fermentation samples measured by ATR. S = sample; 0–165 = fermentation time (h).

There was a decrease of 0.6 unit at 1062 cm^{-1} and an increase of 0.2 unit at 2978 cm^{-1} in transmission MIR. These changes were about 50% lower in ATR.

Following fermentations

Lactic fermentation. Changes in the concentrations of lactose, galactose and lactic acid (Fig. 5) were measured by (A) LC, (B) transmission MIR and (C) ATR MIR. Table 1 lists the linear correlations established between the LC and infrared measurements for each of the three compounds. The regression coefficients were systematically higher than 0.99, showing the consistency between the different types of measurement. The maximum standard errors between LC and IR were 0.46 g l^{-1} for lactose, 0.57 g l^{-1} for galactose and 0.95 g l^{-1} for lactic acid.

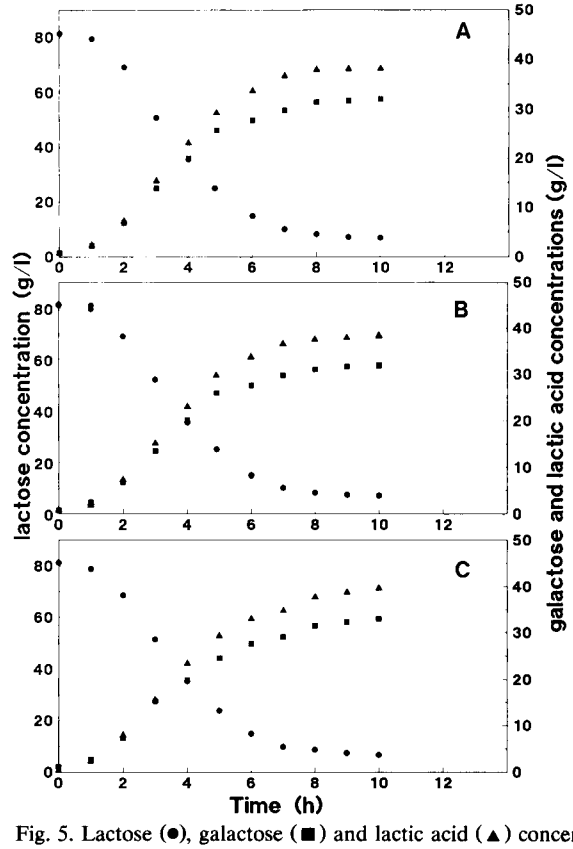

Fig. 5. Lactose (●), galactose (■) and lactic acid (▲) concentrations measured by (A) LC, (B) mid-IR transmission and (C) Mid-IR ATR during lactic fermentation.

TABLE 1

Correlations between the lactose (L), galactose (G), lactic acid (AL), sugars (S), glycerol (GL) and ethanol (E) concentrations measured by LC (C) and by infrared (T for transmission, A for attenuated total reflectance)

No.	Compound	Correlation	Regression coefficient	Standard deviation		Standard error
				slope	intercept	
1	Lactose	L(T) = 1.01 L(C) − 0.01	0.999	0.004	0.18	0.36
2		L(A) = 0.99 L(C) + 0.09	0.999	0.004	0.17	0.46
3	Galactose	G(T) = 0.99 G(C) + 0.02	0.999	0.003	0.07	0.14
4		G(A) = 0.99 G(C) + 0.45	0.997	0.015	0.34	0.57
5	Lactic acid	AL(T) = 1.01 AL(C) − 0.13	0.999	0.003	0.09	0.21
6		AL(A) = 0.99 AL(C) + 0.04	0.996	0.020	0.54	0.95
7	Sugars	S(T) = 0.99 S(C) + 0.27	0.998	0.006	0.78	1.81
8		S(A) = 0.99 S(C) + 0.48	0.995	0.006	1.04	2.48
9	Glycerol	GL(T) = 1.01 GL(C) − 0.05	0.998	0.006	0.03	0.07
10		GL(A) = 1.01 GL(C) − 0.05	0.998	0.008	0.04	0.09
11	Ethanol	E(T) = 0.99 E(C) + 0.30	0.999	0.004	0.27	0.57
12		E(A) = 0.99 E(C) + 0.49	0.998	0.007	0.36	0.98

Alcoholic fermentation. The concentration changes of sugars (glucose + fructose), glycerol and ethanol measured by (A) LC, (B) transmission MIR and (C) ATR MIR are shown in Fig. 6. The regression coefficients of the correlations between the different types of measurements were higher than 0.99 (Table 1). The maximum standard errors between the concentrations measured by LC and IR (transmission or ATR) were 2.48 g l^{-1} for sugars, 0.98 g l^{-1} for ethanol and 0.09 g l^{-1} for glycerol.

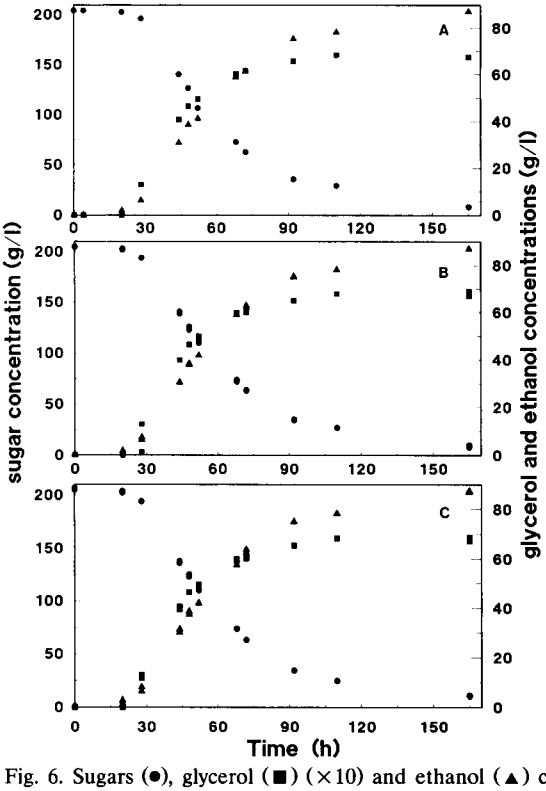

Fig. 6. Sugars (●), glycerol (■) (×10) and ethanol (▲) concentrations measured by (A) LC, (B) Mid-IR transmission and (C) Mid-IR ATR during alcoholic fermentation.

DISCUSSION AND PERSPECTIVES

In spite of the considerable concentration variations of the compounds analysed, the results obtained show the limits of measuring in the near infrared, as a result of insufficient absorbance changes, and confirm prior results [7,8]. These low variations are a major disadvantage for carrying out on-line measurements with multiplex optical fibres.

Several spectral zones in the MIR underwent considerable changes. They were generally situated in the frequency range of 1600–1000 cm^{-1}. The valence vibration zone of alcohol functions is located between 1000 and 1200 cm^{-1}, and that of the deformation vibrations of carboxylic functions between 1550 and 1610 cm^{-1}. The principal absorption wavelengths of the compounds of interest here are 1041 cm^{-1} and 1074 cm^{-1} for lactose, 1078 cm^{-1} for galactose, 1575 cm^{-1} for

lactic acid, 1033 cm^{-1} and 1078 cm^{-1} for glucose, 1062 cm^{-1} for fructose, 1040 cm^{-1} and 1018 cm^{-1} for glycerol and 1045 cm^{-1} and 887 cm^{-1} for ethanol. In addition, measurement by MIR offers a number of advantages:

– analysis time, which depends on the number of spectra recorded and on the resolution chosen, is about 1 min;

– the measurement is non-destructive and very precise, providing calibration was correct. To this end, calibration should be done with samples representative of the medium to be studied and containing all the compounds which may modify the absorption spectrum. It is thus specific to the process to be controlled;

– it requires little or no sample preparation.

The major disadvantage of this type of measurement is the high cost of equipment and the problems posed by its use in an industrial environment. In order to protect the spectrometer and lower instrumental analysis costs, multipoint remote measurements can be envisioned, using multiplex optical fibres. The spectra can be recorded by direct measurement in the reactor or in a sampling loop, without prior treatment.

Today, optical fibres capable of carrying signals over large distances without excessive attenuation are limited to frequencies of about 5000 cm^{-1} for silica and 2000 cm^{-1} for zircon fluoride. They do not cover the most interesting spectral zones for the analysis of biological compounds. Recent developments [9–12] have shown that chalcogenide fibres can be used in the frequency zone of 3200–900 cm^{-1}, but they are usable only over distances not exceeding 5 m. Research in this field is thus necessary before seeing MIR techniques adopted for fermentation processes control.

REFERENCES

1 G. Chotani and A. Constantinides, Biotechnol. Bioeng., 24 (1982) 2743.
2 J.K. Mclaughlin, C.L. Meyer and E.T. Papoutsakis, Biotechnol. Bioeng., 27 (1985) 1246.
3 X. Monseur and C.L. Motte, Anal. Chim. Acta, 204 (1988) 127.
4 D. Picque and G. Corrieu, Biotechnol. Bioeng., 40 (1992) 919.
5 A. Polesello and R. Giangiocomo, CRC Crit. Rev. Food Sci. Nutr., 18(3) (1983) 203.
6 P. Fairbrother, W.O. George and J.M. Williams, Appl. Microbiol. Biotechnol., 35 (1991) 301.
7 A. Davenel, P. Grenier, B. Foch, J.C. Bouvier, P. Verlaque and J. Pourcin, J. Food Sci., 56 (1991) 1635.
8 J.C. Bouvier, Sci. Aliment., 8 (1988) 227.
9 P.J. Melling, W.L. Truett and G.D. Propster, Am. Lab., December (1991) 32C.
10 N. Graber, H. Lüdi and H.M. Widmer, Sensors Actuators, B1 (1991) 239.
11 E.K. Kemsley, R.H. Wilson and P.S. Belton, J. Agric. Food Chem., 40 (1992) 435.
12 W.R. Bradburg and A. Afram, Int. Lab. News, February (1992) 12.

Analytica Chimica Acta, 279 (1993) 73–88
Elsevier Science Publishers B.V., Amsterdam

Chromatographic analysis of biopolymers distribution in "poly-hemoglobin", an intermolecularly crosslinked hemoglobin solution

Jan Simoni, Grace Simoni and Mario Feola

Department of Surgery, Texas Tech University Health Sciences Center, Lubbock, TX 79430 (USA)

(Received 1st October 1992; revised manuscript received 22nd December 1992)

Abstract

In order to eliminate the toxic effect introduced by the presence of large hemoglobin (Hb) polymers formed during intermolecular crosslinking, quality control of therapeutic-grade solution must include analysis of its molecular masses. Molecular mass distribution in glutaraldehyde polymerized Hb ("poly-Hb") was evaluated using direct size exclusion chromatography (SEC). SEC separation revealed that type of packing materials, particle and pore sizes, column length and mobile phase composition are important factors for the precise analysis of poly-Hb molecular mass distribution. Computer analysis of the elution pattern showed that Asahipak® GFA-50F and Protein Pak™ 300SW columns were effective only in the isolation of polymers with masses up to 204 kDa, without ability for complete separation of larger polymers. Using Asahipak® GFA-7M, poly-Hb was separated only into two fractions. Coupling in series three SEC columns (Asahipak GFA-7M, Protein Pak 300SW and Asahipak GFA-50F) significantly increased the separative resolution. It was found that glutaraldehyde, a nonspecific crosslinking agent, produces polymers with large molecular masses. About 42% of polymers have masses of 340–952 kDa and 5% have masses above 1020 kDa. Mobile phase containing 300 mM NaCl improved the separation of polymers with molecular masses 340–952 kDa. Reaction of poly-Hb with 300 mM NaCl revealed the presence of electrostatic interactions between oppositely charged Hb polymers and formation of ca. 7% "pseudo-polymers".

Keywords: Chromatography; Blood substitutes; Biopolymers; Glutaraldehyde; Hemoglobin

Pure bovine hemoglobin solution free of viral contamination (HIV in particular) can be considered an effective blood substitute, capable of reversibly binding oxygen and providing oncotic activity [1]. Chemical modification of bovine Hb is not required to reduce oxygen affinity, since this Hb has a higher P_{50} value than human Hb (28 vs. 13 Torr) [2]. However, intermolecular crosslinking is necessary to increase vascular retention and to reduce nephrotoxicity [3,4]. The most popular crosslinking agent, introduced in early 1970s and still in extensive use today, is glutaraldehyde [5–11]. This is a nonspecific crosslinker, that may polymerize 68 kDa basic Hb tetramers into "particulate aggregates" [12]. Consequently, several non-ionic poly-aldehyde cross-linkers, including *o*-raffinose, have been introduced [13]. These intermolecular modifications may change the surface and mass of Hb molecule and enhance the antigenic property of bovine Hb, which is naturally nonimmunogenic [14,15]. It was found that Hb polymers with large molecular mass can behave like impurities and activate the alternative pathway of the complement system [16,17]. It was also found that polymers with molecular mass above 400 kDa can stimulate human mononu-

Correspondence to: J. Simoni, Department of Surgery, Texas Tech University Health Sciences Center, Lubbock, TX 79430 (USA).

clear cells to produce toxic level of cytokines TNF-alfa, IL-1 and PAF [18].

Previous descriptions, both in the scientific and patent literature, of the biophysical characteristics of poly-Hb, including direct determination of molecular mass distribution on the base of size exclusion chromatography (SEC), presented inconsistent interpretation of similar chromatographic patterns [8,13,19–22]. Interpretation problems were related to improper classification of basic Hb molecule as 32 kDa dimers in equilibrium with 64 kDa tetramers [23]. Also, the peak that separated at the earliest retention time was variously classified, as representing 750, 600, 400, or 256 kDa molecule [19,20,21,24,25].

Molecular weight distribution in poly-Hb obtained by SDS-PAGE gel electrophoresis is inaccurate due to the changes in Hb polymeric structure introduced by the processing of samples and separation procedure [20,26]. Experimental methods of differential viscometry or multi-angle light scattering on line with SEC are not yet in common use, due to high cost and lack of scientific validation. At present, direct SEC appears to be still the most useful method of analysis, being of low cost, quick, and effective in separating Hb polymers in the "native" condition. However, this method must be perfected, and a correct interpretation of obtained results must take place.

Aim of this study was to develop the most effective direct method of size exclusion chromatography for precise separation of polymeric forms of hemoglobin and to identify the real composition of therapeutic-grade glutaraldehyde-crosslinked poly-Hb.

EXPERIMENTAL

Poly-hemoglobin solution

The hemoglobin (genotype AA from Hereford cattle) was prepared from washed red blood cells using the method of hyposmotic dialysis-ultrafiltration according to Sheffield et al. [27]. Stromal lipids including amino-phospholipids, non-hemoglobin proteins, vasoactive peptides and bacterial endotoxin were removed by methods previously described [1,16,17,21,28,29]. In order to minimize proteolysis and autoxidation during hemoglobin isolation and purification, all procedure was done at 4°C. Pure bovine Hb was intermolecularly crosslinked with glutaraldehyde according to previously described procedures [1,4–7,11,21]. In brief, deoxy-Hb in concentration 1.5 mM (pH 7.4) was reacted with glutaraldehyde [$HCO(CH_2)_3CHO$], Grade I (Sigma, St. Louis, MO) in a molar ratio of 7:1 (glutaraldehyde–Hb) at 4°C for approximately 12 h. The polymerization reaction was stopped by adding the aqueous solution of L-lysine (Sigma, St. Louis, MO) (pH 7.4) in tenfold molar excess compared to glutaraldehyde. To stabilize the polymerization by reduction of Schiff bases, sodium borohydride ($NaBH_4$) (Aldrich, Milwaukee, WI) was added in a 2:1 molar ratio to glutaraldehyde. Poly-Hb was dialyzed against Normosol®-R pH 7.4 (Abbott Labs., North Chicago, IL) using 6 kDa cut-off dialysis unit (CD Medical, Miami Lakes, FL) and filtered through 0.20-μm pore size rating filtration module (Microgon, Laguna Hills, CA). Modified Hb at final concentration of 10.2 g/100 ml was stored in sterile transfer packs (Fenwal, Deerfield, IL) at 4°C.

Total hemoglobin was determinated by transforming Hb into CO-Hb and measuring its absorbance in 421 nm, with molar absorptivity $\epsilon = 195\,000\ l\ mol^{-1}\ cm^2$ [30]. The concentration of met-Hb was measured by the spectrophotometric method of Evelyn and Malloy [31]. Purity of hemoglobin in regard to endotoxin, non-Hb proteins, peptides, lipids and phospholipids was characterized by earlier developed quality control methods [32]. Oxygen affinity (P_{50} values) was obtained by use of Hem-O-Scan (SLM-Aminco, American Instrument Co., Silver Spring, MD). Oncotic pressure was determined by use of Weil oncometer Model 186 (Instrumentation Laboratory, Inc., Lexington, MA). Viscosity was assessed at 37°C, at the shear rate of 100 s^{-1} by use of Brookfield digital viscometer (Brookfield Engineering Labs., Stoughton, MA). Electrolyte concentration: sodium/potassium were measured with a Flame photometer Model 343 (Instrumentation Laboratory, Inc.) and chloride with Digital Chloridometer Model 4–2500 (Buchler Instruments, Port Lee, NJ). Osmolarity was read on

Vapor Pressure Osmometer Model 5500 (Vescor, Logan, UT).

Molecular weight markers

In order to establish a size exclusion chromatography (SEC) calibration curve, different commercial MW standards were used: (1) Blue Dextran: 2000 kDa, (2) IgM: 900 kDa, (3) thyroglobulin: 669 kDa, (4) apoferritin: 440 kDa, (5) catalase: 232 kDa, (6) lactate dehydrogenase: 140 kDa, (7) bovine serum albumin (BSA): 67 kDa and (8) carbonic anhydrase: 29 kDa (Sigma).

Chromatographic procedure and LC columns

LC separation was performed with a Waters liquid chromatography system (Waters Chromatography Division, Millipore Co., Milford, MA), which consists of a Waters 600E system controller, a refrigerated 712 WISP autoinjector and a Waters 990 UV/VIS photodiode array detector connected with a 40-MB Power Mate 2 computer.

Reagents used in the preparation of mobile phases were analytical grade from Aldrich (Milwaukee, WI). Pyrogen free, HPLC-grade water (Technics Water System, Seattle, WN) was daily tested by conductimeter, the mean conductivity value being 1.8×10^{-6} Ω^{-1} cm^{-1}. All mobile phases were prepared under sterile, pyrogen free conditions, filtered through 0.22-μm filters (Becton Dickinson, Lincoln Park, NJ) and sonicated under vacuum. The pH was adjusted with sterile 1 M HCl or 1 M NaOH and pH measurement were performed with a Model 815 MP (Fisher Scientific, Lexington, MA). The LC were run at ambient temperature.

The following LC columns and methods were used.

Protein Pak™ 300SW. A 300 × 7.5 mm i.d. column was packed with irregularly shaped porous silica base with diol coating ($Si\text{-}CH_2\text{-}CH_2\text{-}CH_2\text{-}O\text{-}CH_2\text{-}CHOH\text{-}CH_2OH$), particle size 10 μm, pore size 300 Å, > 5000 plates per column, and exclusive MW 400000 (Waters–Millipore). Following purging of the autoinjector and an equilibration run with 0.1 M KH_2PO_4 (pH 7.0) as mobile phase, 0.5 mg of "poly-Hb" or unmodified-Hb in 25 μl volume was injected and separated in 20 min at a flow-rate of 1.0 ml min^{-1} and pressure 53.0 kg^{-1} cm^2.

Asahipak® GFA-50F. A 300 × 7.6 mm i.d. column packed with spherical shaped vinyl alcohol copolymer-based hard gel totally hydroxylated without bonded phase, particle size 5 μm, pore size 500 Å, > 15000 plates per column, and exclusive MW 300000 (Asahi, Kawasaki). Modified or unmodified Hb (0.5 mg in 25 μl volume) was injected and a chromatogram developed in 20 min, using 0.1 M NaH_2PO_4 (pH 7.0) as mobile phase, at a flow-rate of 0.75 ml min^{-1} and a pressure of 49.5 kg^{-1} cm^2.

Asahipak® GFA-7M. A 300 × 7.6 mm i.d. column packed with synthesized polyvinyl alcohol high molecular weight spherical shaped hard gel with not bonded phase, particle size 7 μm, pore size 700 Å, > 11000 plates per column and exclusive MW 10000000 (Asahi). Polymerized or unmodified Hb (0.5 mg in 25 μl volume) was injected and separated with eluent 0.1 M NaH_2PO_4 (pH 7.0). Separation was completed in 20 min with a flow-rate of 0.65 ml min^{-1} and a pressure 45.2 kg^{-1} cm^2.

Two SEC column in series: Asahipak GFA-7M and Asahipak GFA-50F. In order to increase resolution, two columns were coupled in series and separation of poly-Hb polymers was performed. Chemistry of SEC was similar like for Asahipak GFA-50F separation, with three exemptions: flow-rate was 0.55 ml min^{-1}, separation time 50 min and pressure 72.2 kg^{-1} cm^2.

Three SEC column in series: Asahipak GFA-7M with Protein Pak 300SW and Asahipak GFA-50F. Separation of "poly-Hb" polymers was performed with three columns coupled in series. Basic LC method was similar as described for two columns in series, however some modifications were applied. Two types of mobile phases were introduced. First, 0.1 M NaH_2PO_4 (pH 7.0) and the second, 0.1 M NaH_2PO_4 with 300 mM NaCl (pH 7.0). In this two types of separation, flow-rate was the same: 0.60 ml min^{-1}, and pressure 90.3 kg^{-1} cm^2 and 91.1 kg^{-1} cm^2 respectively. Separation was completed in 50 min.

Anion-exchange LC of unmodified and poly-Hb by Protein Pak DEAE-5PW. A 75 × 7.5 mm i.d. column was packed with porous polymer contain-

ing diethylaminoethyl groups on a hydrophilic rigid resin, pore size 1000 Å and particle size 10 μm (Waters–Millipore). Polymerized or unmodified Hb (5 mg in 100 μl volume) was injected and a chromatogram developed using a linear gradient with solvent A (20 mM Tris, pH 8.0) and solvent B (solvent A + 300 mM NaCl, pH 8.0), from 0 to 40% B in 35 min and from 40 to 100% B in 40 min. Separation was completed in 60 min at a flow-rate 1.0 ml min^{-1}, and a pressure 19.6 kg^{-1} cm^2.

Isoelectric focusing (IEF)

Analysis by IEF was carried out using the Pharmacia Phast Gel System, p*I* 3–9, and the Phast Gel Silver Stain Kit (Pharmacia, Piscataway, NJ). A sample consisting of 0.5 μl of unmodified Hb and poly-Hb, concentration 10 mg ml^{-1}, was applied by use of the Phast Gel sample applicator and the separation was run at 600 V h at 15°C. The gel was developed using Pharmacia's Phast Gel Silver Stain Kit. Details of the method have been reported previously [32].

Calibration and data evaluation

Calibration of the SEC columns, in order to correlate retention time with molecular mass, was performed with various protein MW standards (2000 to 29 kDa) listed above, using the methods described for each single LC column or columns in series.

The data from the Waters 990 UV/VIS photodiode array detector of each LC separation were stored in D-drive of the computer hard disk and analyzed using various softwares: Waters 990 Integrator at 214, 230, 285 and 415 nm and slope 1E-10 A.U. min^{-1}, Waters 990 Spectrum Index with Max Mode 200–650 nm, Waters 990 Peak Calculation with Max Mode 200–650 nm, Waters 990 Spectrum Analysis/Spectrum Calculation and Waters 990 Chromatogram Analysis/Chromatogram Calculation (Copyright Phoenix Technologies, Phoenix, AZ). Each sample was injected in triplicate and the average value taken in each case. The "goodness of the fit" of the standard curves and the molecular weight determination was evaluated by using a linear regression statistical method with power curve fit.

RESULTS

Characteristics of hemoglobin solutions

The unmodified hemoglobin and poly-Hb used in these experiments had the characteristics shown in Table 1. Examination by isoelectric focusing IEF-PAGE and thin-layer chromatography (TLC) methods [32] demonstrated the elimination of all non-Hb proteins, peptides and phospholipids from the unmodified Hb solution. The viscosity of unmodified Hb at concentration 10.2 g/100 ml was 0.83 cP and the oncotic activity was 49.3 mmHg. Intermolecular crosslinking with glutaraldehyde resulted in higher viscosity (2.25 cP) and lower oncotic pressure (21.8 mmHg). Polymerization of bovine Hb resulted in higher oxygen affinity (P_{50}; 20 vs. 26 mmHg) and higher autoxidation rate (met-Hb level 7.5% vs. 1.5%). During storage at 4°C, the monthly autoxidation rate of poly-Hb was higher than that of unmodified Hb (2.5 and 0.3%, respectively). Crosslinking procedure and final dialysis did not significantly increased the endotoxin level. The concentration of endotoxin in final product was 0.12 E.U. ml^{-1}.

Size exclusion chromatography

SEC is now the generally accepted terminology to describe gel permeation chromatography (GPC) for polymer analyses in organic solvent, or gel filtration chromatography (GFC) for biopoly-

TABLE 1

Characteristics of hemoglobin solutions

	Unmodified Hb	Poly-Hb
Hemoglobin, g/100 ml	10.2	10.2
Met-Hb, % of total Hb	1.5	7.5
pH	7.38	7.41
Osmolarity, mOsm/l	295	298
Oncotic pressure, mmHg	49.3	21.8
Viscosity, cP	0.83	2.25
P_{50}, mmHg	26	20
Sodium, mEq/l	139	140
Potassium, mEq/l	3.5	5.0
Chloride, mEq/l	90	98
Endotoxin, E.U./ml	0.08	0.12
Phospholipids (TLC)	Absent	Absent
Non-Hb proteins/ peptides (IEF)	Absent	Absent

mers in aqueous medium [33]. In the present study the general term SEC was related to the GFC type of separation. The transformation of SEC elution curve to polymer molecular weight distribution was made possible by the calibration relationship between sample molecular weight and SEC retention time/volume.

In general, the three LC columns and five SEC methods used in these experiments varied in their ability to separate biopolymers of intermolecularly crosslinked Hb solution.

The calibration curve and separation of poly-Hb and unmodified-Hb with the Protein Pak 300SW column are presented in Fig. 1. The calibration curve obtained with molecular weight markers showed the same elution time (5.05 min) for Blue Dextran 2000 kDa, IgM 900 kDa, thyroglobulin 669 kDa and apoferritin 440 kDa. The

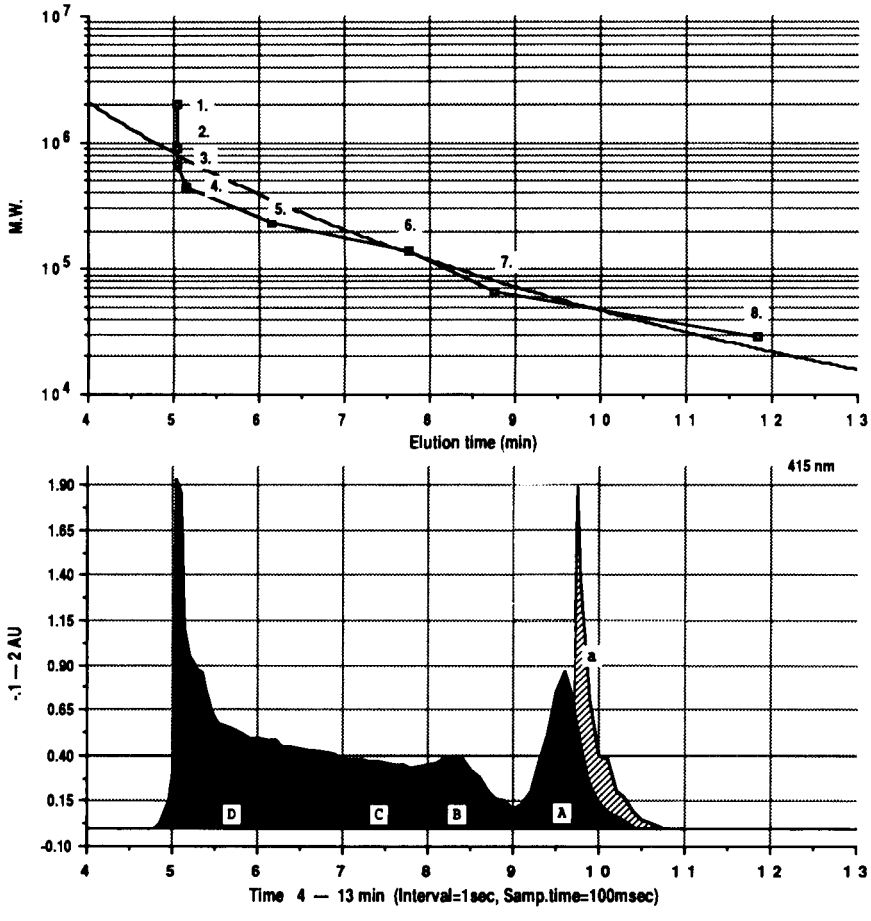

Fig. 1. Calibration curve and separation of poly-Hb and unmodified Hb using Protein Pak 300SW size exclusion chromatography (SEC) column. Samples: (1) Dextran Blue (2000 kDa), (2) IgM (900 kDa), (3) thyroglobulin (669 kDa), (4) apoferritin (440 kDa), (5) catalase (232 kDa), (6) lactate dehydrogenase (140 kDa), (7) BSA (67 kDa), (8) carbonic anhydrase (29 kDa), Poly-Hb intermolecularly crosslinked bovine Hb (solid black), and unmodified Hb purified bovine Hb (lines). Least squares results: (1) least squares best fit (power curve fits with equation $y = aX^b$, where $a = \exp[1/n\Sigma \ln y - b/n\Sigma \ln X]$ and $b = [\Sigma \ln X \ln y - 1/n\Sigma \ln X \Sigma \ln y]/[\Sigma(\ln X)^2 - 1/2(\Sigma \ln X)^2]$, $y = 6.3590 \times 10^8\ X^{-4.1291}$, (2) Goodness of fit of the curve measured by coefficient of determination $r^2 = 0.896$. Integrator results: poly-Hb, peak A (molecular weight 68 kDa), retention time (t_R), 9.54 min; integrated peak area (PA), 16%. Peak B (136 kDa), $t_R = 8.25$ min; PA = 12%. Peak C (204 kDa), $t_R = 7.42$ min; PA = 9%. Peak D (272 kDa and above), $t_R = 7.05$–4.55 min, PA = 63%. Unmodified Hb, peak a (68 kDa), $t_R = 9.74$ min, PA = 100%.

elution time for catalase 232 kDa, lactate dehydrogenase 140 kDa, BSA 67 kDa and carbonic anhydrase 29 kDa was 6.22, 7.76, 8.80 and 11.87 min, respectively.

Tetramers of unmodified Hb (68 kDa) were eluted at 9.74 min. Polymerized hemoglobin was separated into the 68 kDa tetrameric form at 9.54 min (16%), 136 kDa octameric form at 8.25 min (12%), and 204 kDa decameric form at 7.42 min (9%), and 63% of polymers above 272 kDa were separated with 4.55 min left time (LT) and 7.05 min right time (RT).

Using the Asahipak GFA-50F column, standard proteins with masses from 669 to 2000 kDa were separated at the same 6.45 min retention time. Molecular weight markers with masses 440, 232, 140, 67 and 29 kDa were eluted at 7.16, 8.31, 9.12, 9.85 and 12.42 min, respectively (Fig. 2). The chromatogram shows 10.84 min retention time for 68 kDa tetramers of unmodified Hb. The elution pattern of poly-Hb revealed that 16% of hemoglobin remained in unmodified 68 kDa form with retention time 10.42 min and 11% represented 136 kDa octamers. About 42% of hemoglobin molecules formed polymers with masses 500–204 kDa, and 31% large polymers with masses above 500 kDa which were eluted between 6.05 min LT and 7.15 min RT.

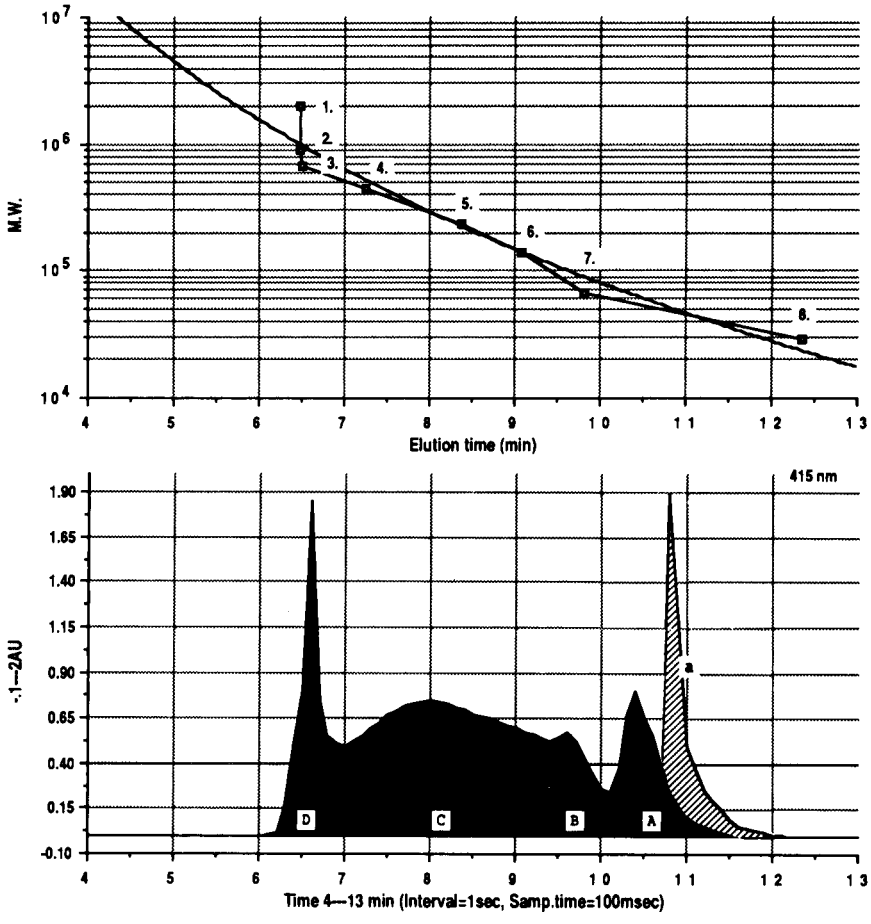

Fig. 2. Calibration curve and separation of poly-Hb and unmodified Hb using Asahipak GFA-50F SEC column (samples as Fig. 1). Least squares results: (1) $y = 3.9334 \times 10^{10}\ X^{-5.6761}$. (2) $r^2 = 0.942$. Integrator results: poly-Hb, peak A (68 kDa), $t_R = 10.42$ min; PA = 16%. Peak B (136 kDa), $t_R = 9.58$ min, PA = 11%. Peak C (204 kDa–ca. 500 kDa), $t_R = 9.35$–7.16 min; PA = 42%. Peak D (> 500 kDa), $t_R = 7.15$–6.05 min; PA = 31%. Unmodified Hb, peak a (68 kDa), $t_R = 10.84$ min; PA = 100%.

Lack of selectivity was observed during separation of standard proteins by Asahipak GFA-7M column (Fig. 3). Eight various molecular weight markers (2000–29 kDa) were separated during the 1.22 min elution period. The proteins with masses 29, 67 and 140 kDa were eluted together at retention time 10.00 min. With relatively better precision 2000 kDa Blue Dextran (8.78 min) was separated from 900 kDa IgM (9.22 min). Using the GFA-7M column, polymerized Hb was separated into two fractions with retention time 9.17 min (74%) and 10.2 min (26%). Separation of unmodified Hb appeared at 10.51 min retention time.

Increased resolution was accomplished by using two SEC columns in series, Asahipak GFA-7M and Asahipak GFA-50F (Fig. 4). Protein standards were eluted between 21.15 min (Blue Dextran) and 33.55 min (carbonic anhydrase).

Unmodified Hb was separated with 31.42 min retention time, but modified poly-Hb was eluted as the native 68 kDa tetramer at 31.00 min (17%), 136 kDa octamer at 28.99 min (12%), and 204 kDa and more polymer complex between 21.30

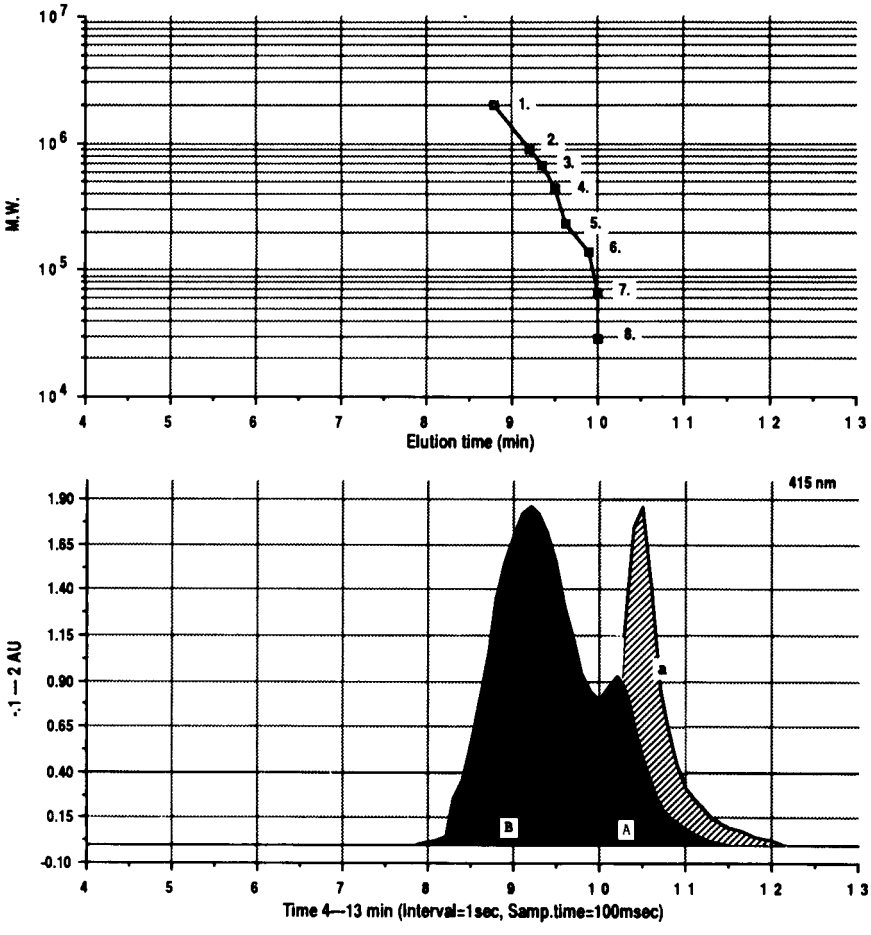

Fig. 3. Calibration curve and separation of poly-Hb and unmodified Hb using Asahipak GFA-7M SEC column (sample as Fig. 1). Least squares results: (1) $y = 9.6996 \times 10^{34}\ X^{-30.175}$. (2) $r^2 = 0.912$. Integrator results: poly-Hb, peak A (68–136 kDa), $t_R = 10.20$ min; PA = 26%. Peak B (> 204 kDa), $t_R = 9.97$–8.85 min; PA = 74%. Unmodified Hb, peak a (68 kDa), $t_R = 10.51$ min; PA = 100%.

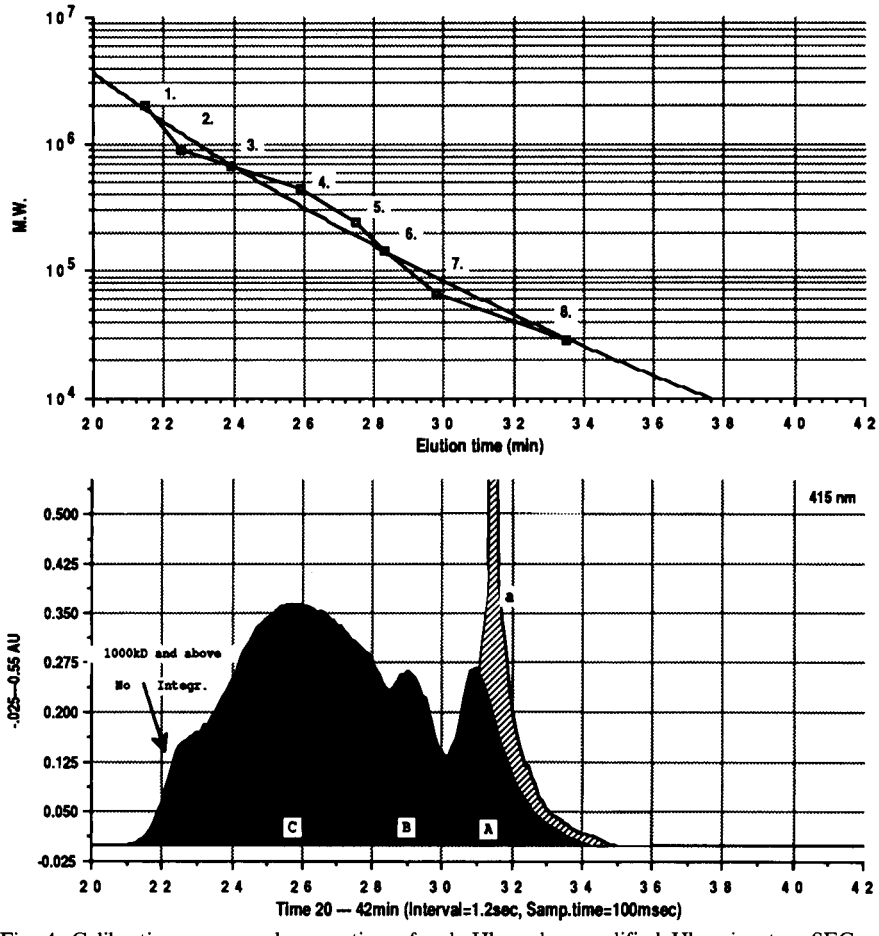

Fig. 4. Calibration curve and separation of poly-Hb and unmodified Hb using two SEC columns coupled in series, Asahipak GFA-7M and Asahipak GFA-50F (samples as Fig. 1). Least squares results: (1) $y = 3.6878 \times 10^{18}\ X^{-9.2317}$. (2) $r^2 = 0.975$. Integrator results: poly-Hb, peak A (68 kDa), $t_R = 31.00$ min; PA = 17%. Peak B (136 kDa), $t_R = 28.99$ min; PA = 12%. Peak C (> 204 kDa), $t_R = 27.89$–21.30 min; PA = 71%. Unmodified Hb, peak a (68 kDa), $t_R = 31.42$ min; PA = 100%.

min (LT) and 27.89 (RT) (71%). First fraction of this large polymer contained Hb molecules with masses 1000 kDa and above, however computer integration was unsuccessful due to the low selectivity.

The quality of SEC separation was greatly improved by introducing the three LC column system. Coupling in series Asahipak GFA-7M with Protein Pak 300SW and Asahipak GFA-50F resulted in higher resolution and selectivity of separation of the various protein standards and the two different forms of hemoglobin.

Using a 0.1 M NaH_2PO_4 (pH 7.0) as mobile phase (Fig. 5), poly-Hb was separated into 15% of 68 kDa tetramers (37.95 min), 13% of 136 kDa octamers (34.25 min), 10% of 204 kDa decamers, 8% of 272 kDa dodecamers, 53% of 340–952 kDa polymer complexes (25.60 min LT, 30.65 min RT) and 7% of polymers above 1020 kDa (25.15 min). Tetramers of unmodified Hb were eluted at 38.82 min. The standard proteins were separated during the period of 17.62 min (Blue Dextran was eluted at 24.31 min and carbonic anhydrase at 41.93 min).

Significantly increased selectivity was observed when 300 mM of NaCl was added to the 0.1 M NaH_2PO_4 mobile phase (Fig. 6). Separation of polymerized hemoglobin revealed, that 19% of

Hb molecules were 68 kDa tetramers, 15% 136 kDa octamers, 11% 204 kDa decamers, 8% 272 dodecamers, 6% 340 kDa polymeric forms, 6% 408 kDa polymers, 17% 680–476 kDa polymers, 13% 952–748 kDa polymers and 5% polymer with mass 1020 kDa and above. Unmodified Hb was separated at 38.20 min.

Salt in 300 mM concentration as part of mobile phase introduced changes in the composition of Hb biopolymers. Generally, the level of tetramers and low molecular weight polymers was increased, when at the same time the amount of large polymer complexes was decreased. The elution times of various standard proteins were similar (Fig. 6).

Anion exchange LC

Separation of unmodified and modified Hb by anion-exchange LC revealed that intermolecular crosslinking with glutaraldehyde may introduce changes in distribution of surface ionic groups in the Hb molecule (Fig. 7). The chromatographic behavior and electrophoretic mobility of unmodified and poly-Hb were different. Unmodified

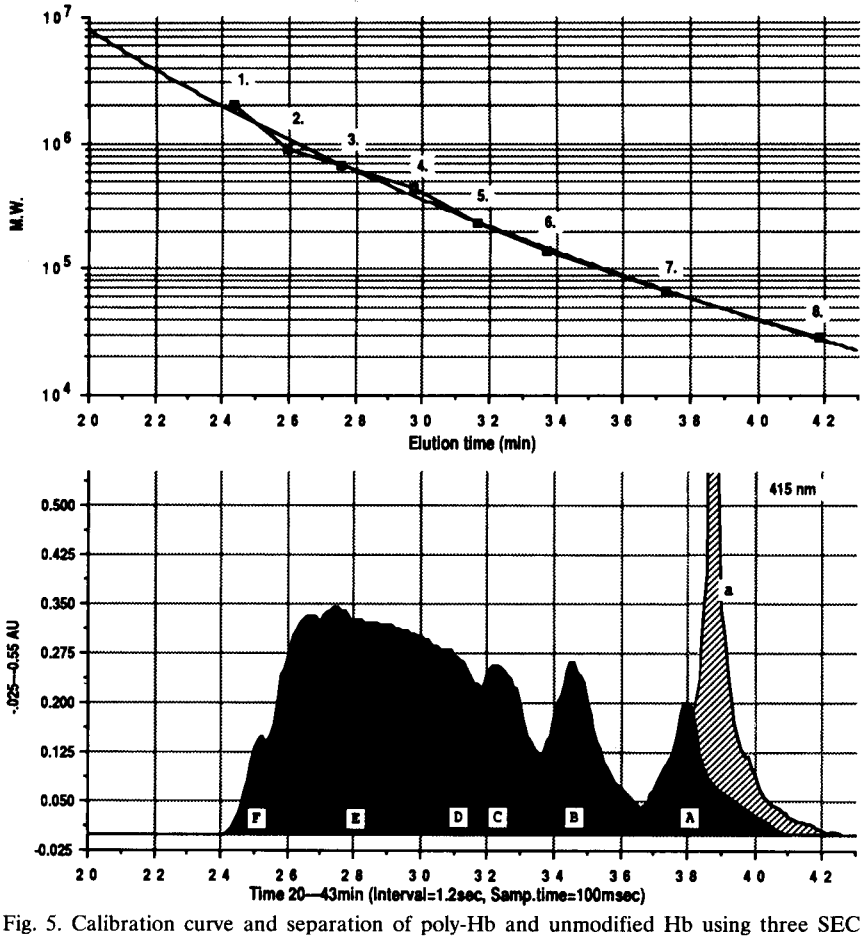

Fig. 5. Calibration curve and separation of poly-Hb and unmodified Hb using three SEC columns coupled in series, Asahipak GFA-7M, Protein Pak 300SW and Asahipak GFA-50F (samples as Fig. 1). Least squares results: (1) $y = 7.4258 \times 10^{16}\ X^{-7.6570}$. (2) $r^2 = 0.993$. Integrator results: poly-Hb, peak a (68 kDa); $t_R = 37.95$ min; PA = 15%. Peak B (136 kDa), $t_R = 34.25$ min; PA = 13%. Peak C (204 kDa), $t_R = 32.28$ min, PA = 10%. Peak D (272 kDa), $t_R = 30.98$ min; PA = 8%. Peak E (340–952 kDa), $t_R = 30.65$–25.60 min; PA = 53%. Peak F (> 1020 kDa), $t_R = 25.15$ min; PA = 7%. Unmodified Hb, peak a (68 kDa), $t_R = 38.82$ min; PA = 100%.

bovine hemoglobin (type AA) was separated into the basic component HbAo (75%) at 24.5 min and 25% of different hemoglobin variants at 17.71, 21.54, 23.76, 32.09, 32.90, 34.95 and 51.22 min.

The same LC method used in poly-Hb analysis showed that 65% of Hb polymers eluted at 49.01 min retention time represent electronegative surface charge. The remaining 35% of polymers (including tetramer, octamer and decamer) separated between 17.20 and 42.99 min, representing positive or moderate net charges.

Isoelectric focusing (IEF)

IEF with the silver staining method revealed that poly-Hb electrophoretic behavior was different from that of unmodified Hb (Fig. 8). Unmodified Hb was separated into various fractions, which represented different types and derivatives present in the native Hb molecule. Polymeriza-

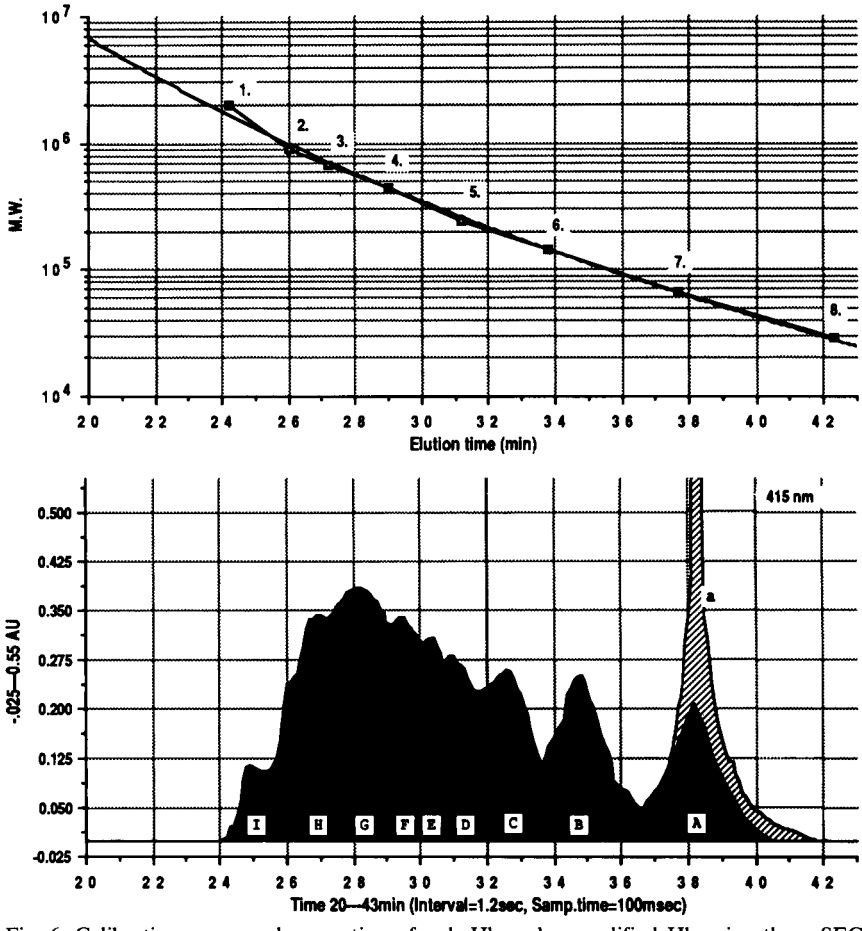

Fig. 6. Calibration curve and separation of poly-Hb and unmodified Hb using three SEC columns coupled in series, Asahipak GFA-7M, protein Pak 300SW and Asahipak GFA-50F. In order to increase the selectivity, mobile phase was supplemented with 300 mM NaCl (samples as Fig. 1). Least squares results: (1) $y = 2.01 \times 1016\ X^{-7.2907}$. (2) $r^2 = 0.995$. Integrator results: poly-Hb, peak A (68 kDa), $t_R = 38.10$ min; PA = 19%. Peak B (136 kDa), $t_R = 34.75$ min; PA = 15%. Peak C (204 kDa), $t_R = 32.61$ min; PA = 11%. Peak D (272 kDa), $t_R = 31.01$ min; PA = 8%. Peak E (340 kDa), $t_R = 30.54$ min; PA = 6%. Peak F (408 kDa), $t_R = 29.46$ min; PA = 6%. Peak G (476–680 kDa), $t_R = 29.01$–27.20 min; PA = 17%. Peak H (748–952 kDa), $t_R = 27.20$–25.20 min; PA = 13%. Peak I (> 1020 kDa), $t_R = 24.90$ min; PA = 5%. Unmodified Hb, peak a (68 kDa), $t_R = 38.20$ min; PA = 100%.

tion with glutaraldehyde introduced the changes in the surface charge. The isoelectric point of poly-Hb changed from p*I* 7.05–6.90 to p*I* 7.05–6.75.

DISCUSSION

SEC operates by excluding large molecules from small pores. The exclusion becomes selective when molecules predominantly differ from each other in size or shape. Separation and column exclusion limit are affected by the particle size, pore size, shape and homogeneity of stationary phase. With larger particles, the efficiency of SEC separation is reduced. Theory predicts an optimum particle size (3 μm) and spherical shape [33]. Small biomolecules exhibit greater pore penetration, while the largest molecules, above column exclusion limit, are excluded and eluted from the column, passing around the stationary phase [33]. Another important feature affecting the separation is the type of bonded phase used, especially for highly polar silica gel (eg. Protein Pak 300SW column). To minimize the adsorption interaction between the stationary phase and solutes, surface SiOH groups are chemically bonded (e.g., with diol). However, this partition type stationary phase of the silica gel becomes less stabile with time.

In recent years, it was found that polyvinyl alcohol copolymer can form 5–7 μm spherical particles, which not need to be bonded (e.g., Asahipak GFA series). This porous hard gel with

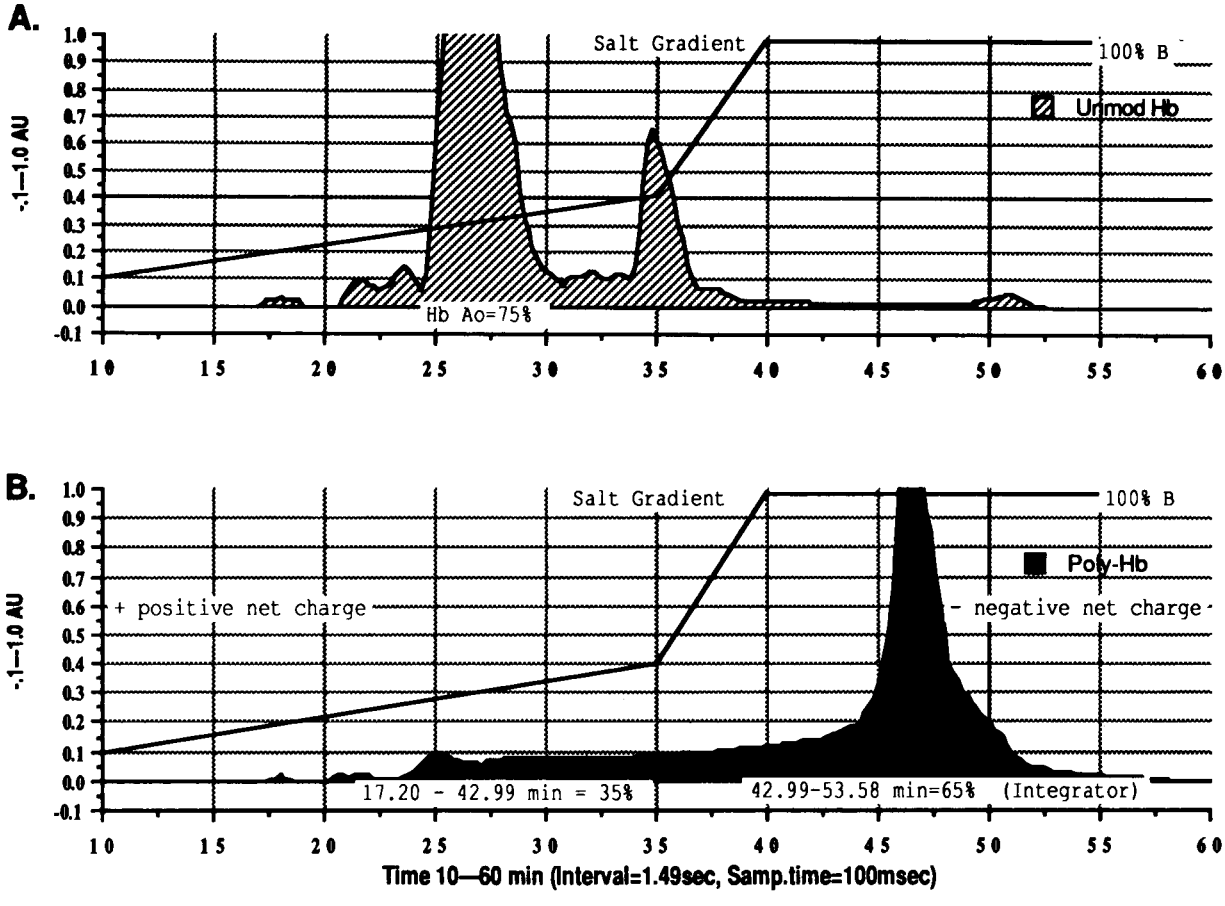

Fig. 7. Chromatograms of unmodified Hb (A) and poly-Hb (B) obtained by use the Protein Pak DEAE 5PW anion-exchange LC column, illustrating the different electrophoretic mobilities of unmodified and intramolecularly crosslinked Hb.

totally hydroxylated surface, now commercially available and use exclusively for aqueous SEC, prevents solute–surface interaction [34].

In present experimental work, these two types of stationary phase, bonded silica and polyvinyl alcohol copolymer, were used. The obtained results showed differences in selectivity and resolution of separation for biopolymers of Hb.

We observed a low resolution of separation when using a single SEC column for the analysis of poly-Hb. This was not due to interaction between the stationary phase (bonded silica gel or polyvinyl alcohol copolymer) and solute, because Hb polymers below the columns' exclusion limit were selectively eluted (Figs. 1 and 2). In order to eliminate the possibility of such interaction, the pH of mobile phases used in these experiments was correlated with isoelectric point (p*I*) of bovine hemoglobin. Additionally, in order to protect the stability of native 68 kDa Hb tetramer during separation, SEC was performed under non-dissociating conditions.

Protein Pak 300SW and Asahipak GFA-50F were both effective in isolation of polymers with masses varying from 68 to 204 kDa, but without ability for complete separation of larger polymers (Figs. 1 and 2). The similarity of performance by these two columns was probably due to the fact

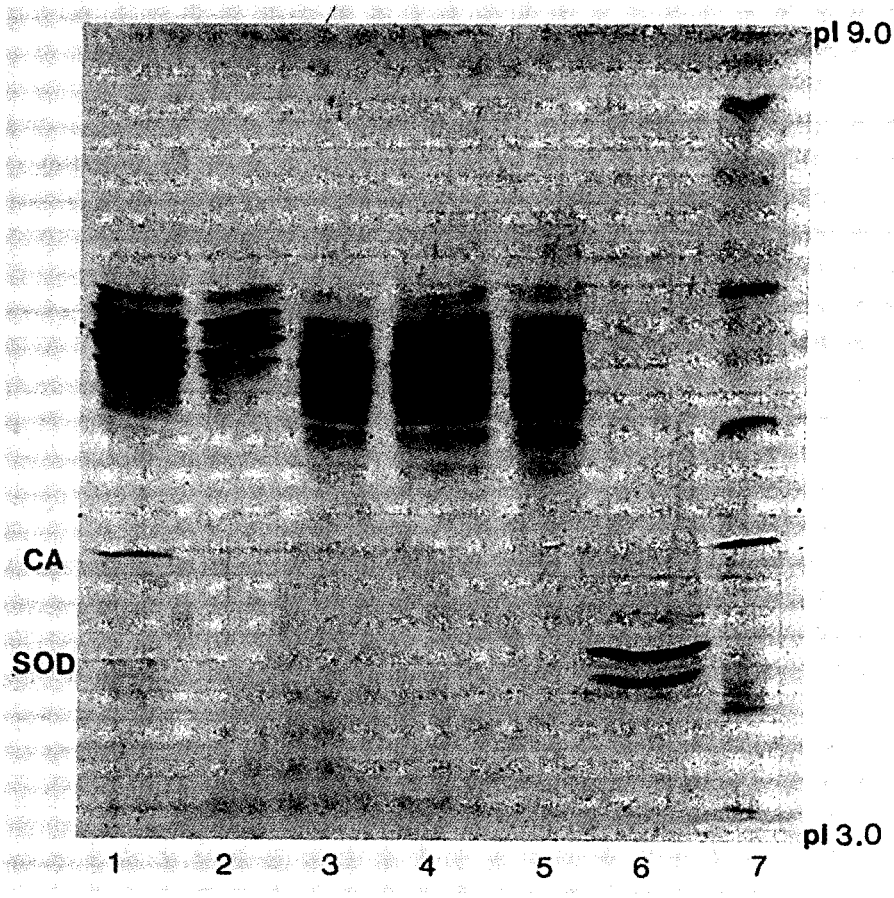

Fig. 8. Isoelectric focusing (IEF) of various bovine Hb solutions. Lane 1: unmodified Hb before purification from non-Hb proteins and peptides (CA, carbonic anhydrase; SOD, superoxide dismutase). Lane 2: unmodified Hb after purification. Lanes 3, 4 and 5: poly-Hb (intermolecularly crosslinked with glurataldehyde). Lane 6: SOD from bovine erythrocytes. Lane 7: Pharmacia Broad p*I* Calibration Kit (pH 3–9).

that the Protein Pak 300SW column had large (10 μm) silica particles with relatively small (300 Å) pore size, while the Asahipak GFA-50F column had particles of almost ideal size (5 μm) but larger (500 Å) porosity. Calibration of the column revealed that the exclusion limit for Protein Pak 300SW was below 440 kDa, while most for the Asahipak GFA-50F was between 440 and 669 kDa. Proteins with masses above this exclusion limit were separated at the same retention time (see Figs. 1 and 2). SEC of poly-Hb by use of these columns revealed poor selectivity in the separation of biopolymers with molecular masses above 204 kDa. The Asahipak GFA-50F was able to separate clearly polymers with masses above 500 kDa, suggesting that 500 Å pore size is an important factor in the isolation of large polymers. Instead, separation of large polymers was less effective with the Protein Pak 300SW column, whose silica gel has 300 Å pore size. The data obtained by us with this column are similar to those reported by other authors.

Many poly-Hbs crosslinked with glutaraldehyde have been described in the literature. While these solutions had essentially the same composition (ca. 85% polymerized and 15% tetrameric Hb) and presented similar chromatographic profiles, different interpretations of the chromatograms were offered by the various investigators. We believe this to result from the fact that the exclusion limit of various SEC columns used in these experiments was lower than the molecular mass of the large Hb polymers. Thus, Kothe et al. [22], using Waters Protein Pak 125 (Native Globular MW range 2000–80 000 Da) for analysis of their poly-Hb, found that 15% of the total Hb molecules remained non-crosslinked, and the mean molecular weight of the poly-Hb was 200 kDa. However, the molecular weight distribution was not described. Sehgal et al. [20] found that the molecular weight range of their poly-Hb, obtained by SEC was 128–400 kDa. However, this estimate did not correspond to the average molecular weight obtained by ultracentrifugation (120 kDa) or to the value obtained by measurement of oncotic pressure (150 kDa). The SDS-PAGE method used by the same authors failed in the proper analysis of polymeric species' and, typically, 4–6 new polypeptide bands were seen, ranging in molecular weight from 16 to 96 kDa. Chang et al. [24], in an analysis of in vitro properties of their poly-Hb, found that its molecular weight was between 130 and 600 kDa. Berbers et al. [21] showed that their poly-Hb analyzed by Superose-12 gel filtration method was composed of 15% 68 kDa, 10% 136 kDa, 30% 204–272 kDa, and 45% 300–600 kDa molecules. Keipert and Chang [19], using Sephadex G-200 gel chromatography with higher exclusion limit, found that 33% of polymers were in the 470–750 kDa range, 60% had a 470 kDa mass and approximately 10% of total hemoglobin molecules were unmodified. The full distribution of Hb polymers was not however, described.

The poly-Hb used in this study was similar in composition to the ones previously reported, in that it consisted of 85% polymerized and 15% unpolimerized Hb.

In the present study, use of a single SEC column with exclusion limit 10 000 kDa (Asahipak GFA-7M) resulted in the least effective separation of our poly-Hb (Fig. 3). Hemoglobin polymers were separated only into 2 fractions; the first fraction contained 74% of the total Hb in the form of polymers above 207 kDa, and the second contained the remaining 26% as tetramers and octamers together. Lack of selectivity was observed for standard proteins from 29 to 140 kDa, poor separation was obtained for proteins from 440 to 669 kDa. Only 2000 kDa Blue Dextran was clearly isolated form 900 kDa IgM. This low resolution was related to the fact that stationary phase of this column was made of 7 μm spherical particles with 700 Å pore size. This type of SEC separation cannot, therefore, be applied to the analysis of Hb biopolymers, below masses ca. 600 kDa.

Coupling in series two LC columns, Asahipak GFA-7M and Asahipak GFA-50F, resulted in the separation of 3 fractions: large polymers with molecular mass above 204 kDa, 136 kDa octamers and 68 kDa tetramers (Fig. 4). However, this column system failed to yield a satisfactory analysis of Hb polymer distribution. A similar effect by use of a column system for the analysis of "poly-Hb" was described by Moore et al. [25].

These authors used TSK-Gel G3000SW and G 2000SW columns, coupled in series for the molecular weight determination of a human Hb, intermolecularly crosslinked with nonspecific, nonionic polyaldehyde, *o*-raffinose. Polymers were separated into 4 fractions: 64, 128, 192 and 256 kDa. However, the chromatographic pattern of *o*-raffinose–Hb elsewhere described [13] was identical to the one described by us using the Protein Pak 300SW column (Fig. 1).

The use of three column in series, Asahipak GFA-7M, Protein Pak 300SW and Asahipak GFA-50F, significantly improved resolution and resulted in the separation of 6 fractions (Fig. 5). This techniques was unable to produce satisfactory separation of polymers between 340 and 952 kDa, however it separated polymers between 952 and 1020 kDa.

The analysis of chromatographic behavior of native 68 kDa tetramers in unmodified Hb and nonpolymerized tetramers of poly-Hb revealed that these molecules, which represented identical molecular mass, were eluted at different retention times. Thus, unpolymerized tetramers of poly-Hb (ca. 16%) were eluted 0.44 ± 0.26 min earlier than native tetramers of unmodified Hb. Excluding the possibility of solute stationary phase interaction, we interpret the shorter elution time of tetramers in poly-Hb as due to an interaction between them and polymers with high molecular mass, or an attraction of the tetramers by the high molecular mass polymers. A similar phenomenon is represented by the shorter retention time of bovine serum albumin as compared to bovine hemoglobin in tetrameric form, despite their identical molecular weight (67 and 68 kDa, respectively). In this case, the difference in retention time is due to the fact that albumin has a different molecular shape as compared to Hb tetrameric form, with different rotary diameters: $22 \times 50 \times 145$ Å for albumin versus $50 \times 55 \times 60$ Å for hemoglobin [35]. This difference was not taken into consideration in some earlier published papers, where native Hb tetramers were classified as 32 kDa dimers, probably due to the fact that they eluted later with respect to albumin [23]. More recently, however, Moore et al. [25] described that the apparent MW of various poly-Hb components was shifted with respect to commercial MW standards.

In order to establish the existence of polymer–polymer–tetramer interactions, the chromatographic behavior of unmodified and of poly-Hb were analyzed by anion-exchange chromatography. This study revealed that polymerization with glutaraldehyde caused changes in the electrophoretic mobilities of poly-Hb. In fact, 65% of polymers presented electronegative net charges,

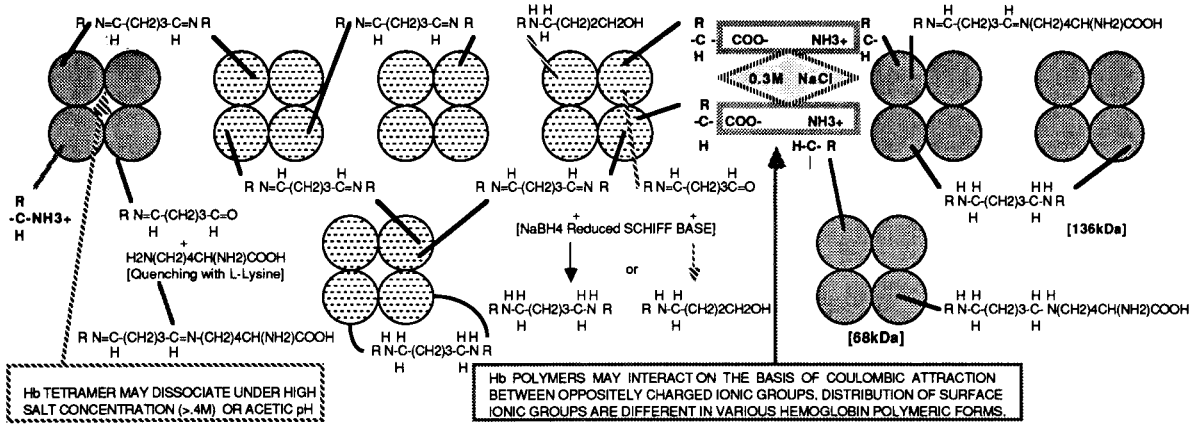

Fig. 9. Theoretical model of electrostatic interaction between polymers in poly-Hb solution with formation of pseudo-polymers. The pseudo-polymer with molecular mass ca. 544 kDa contains: 68 kDa tetramer, 136 kDa octamer and 340 kDa solid polymers complex. Polymerization with non-specific crosslinker glutaraldehyde introduces changes in distribution of surface ionic groups (NH_2 and COOH). Differently charged Hb polymers may interact on the basis of coulombic attraction. Mobile phase with 300 mM NaCl may protect against formation of pseudo-polymers, but cannot dissociate the native 68 kDa tetramer.

while 35% of Hb molecules remained with moderately and electropositive net charges (Fig. 7). SEC analysis of the electropositive and moderately-charged poly-Hb fraction revealed that its majority contained only tetramers and octamers, while the electronegative-charged fraction was made up of high molecular mass Hb polymers. As they possess different isoelectric points, different polymeric forms may interact on the basis of coulombic attraction between oppositely-charged ionic groups and form "pseudopolymers" (Fig. 9). Isoelectric focusing of "poly-Hb" may support this finding. Isoelectric point of polymerized Hb was much wider and contained more electronegative Hb fractions than that of the unmodified Hb (Fig. 8). A similar electrostatic interaction has been previously described for native 68 kDa Hb tetramers and electronegative non-Hb proteins and peptides [28].

The existence of polymer–polymer–tetramer electrostatic interactions with formation of "pseudopolymers" was also suggested by our study using SEC separation by the three column system with the mobile phase supplemented with 300 mM NaCl. Poly-Hb was separated by this technique into 9 fractions: 68, 136, 204, 340, 408, 476–680, 746–952 kDa and > 1020 kDa molecules. Computer analysis revealed that the fractions consisting of 68, 136 and 204 kDa were larger by approximately 7% than those obtained by "non salt" separation. At the same time, the fraction containing the above 1020 kDa polymeric forms was reduced by about 2%. It was found, that salt in 300 concentration mM did not dissociate the tetrameric structure of Hb molecule [33].

Glutaraldehyde is a nonspecific crosslinking agent, that reacts preferentially with Lys residues of Hb, but also with Arg and His residues [5,11,35,37]. By reacting on the basis of the Schiff reaction with large number of Lys residues of Hb molecule, glutaraldehyde introduces changes in the distribution of surface ionic groups (Fig. 9). Quenching of the reaction with additional lysine may eliminate this effect, however this is only possible when one aldehyde group of glutaraldehyde reacts with a Lys residue and the other is quenched by lysine (see Fig. 9). When glutaraldehyde reacts with two Lys residues on the same Hb molecule it crosslinks the Hb tetramer intramolecularly, while by reacting with Lys residues of different Hb molecules it forms Hb polymers. These types of reaction cannot be quenched with additional lysine. Therefore, these molecules will have a higher number of COOH groups in relation to NH_2 groups. Also, in order to stabilize the Schiff base formed by the aldehyde group of glutaraldehyde and the amino group of the Lys residue, a reductive reaction with sodium borohydride is generally carried out. This reduction introduces the hydroxylation of free aldehyde groups not quenched by the additional lysine and produces further changes in the surface ionic distribution.

The polymerization reaction induced by glutaraldehyde is very quick and almost impossible to control. This reaction leads to the formation of "particulate aggregates" [12]. Berbers et al. [21] showed that, when the polymerization reaction involves more than 60% of the Hb tetramers, very large aggregates are formed, bypassing the formation of octamers and decamers. This suggests that electropositively-charged 68 kDa tetramers are incorporated much easier into the larger polymers with the highest electronegative net charge than into the smaller ones. Thus, control of the polymerization process by glutaraldehyde is only possible with yields lower than 60%. Increases in yield cost the formation of large, even "particulate" aggregates. Our study showed that polymerization with 81% yield led to the formation of polymers, 41% of which had a mass above 400 kDa and 5% of which had a mass above 1020 kDa.

Glutaraldehyde–Hb is potentially toxic. The presence in a "therapeutic grade poly-Hb" of 41% polymers with molecular mass above 400 kDa activates the alternative pathway of the complement [16,17], stimulates the monocyte–macrophage system to produce toxic level of cytokines and "platelet activating factor" (PAF) [18], and amplifies the antigenicity of hemoglobin [14]. The improper use of SEC analytic methods and the incorrect interpretation of obtained chromatograms can obfuscate the toxicity of poly-Hb solutions. It is noteworthy in this regard that Phase I clinical trials with glutaraldehyde-polymerized

hemoglobin have thus far been unsuccessful [38,39]. On the other hand, the intermolecular crosslinking of bovine hemoglobin with agents other than glutaraldehyde has allowed the preparation of nontoxic solutions. One of these has, for the first time ever, been found not only non toxic but beneficial in a human clinical trial [29].

REFERENCES

1 M. Feola, J. Simoni, P.C. Canizaro, R. Tran, G. Raschbaum and F.J. Behal, Surg. Gynecol. Obstet., 166 (1988) 211.
2 H.F. Bunn, Science, 172 (1971) 1049.
3 P.E. Keipert and T.M.S. Chang, Trans. Am. Soc. Artif. Intern. Organs, 29 (1983) 329.
4 W. Mok, D. Chen and A. Mazur, Fed. Proc., 34 (1975) 1458.
5 P. Bonsen, M.B. Laver and K.C. Morris, U.S. Pat., 4 001 401 (1977).
6 F. DeVenuto and A. Zegna, J. Surg. Res., 34 (1983) 205.
7 L.R. Sehgal, A. Rosen, S. Gould and G.S. Moss, Fed. Proc., 39 (1980) 2383.
8 D. Nelson, A. Ton Hai, A. Srnak, A. Ebeling, G. Kunas, J. Catarello and K. Burhop, Biomater. Artif. Cell Artif. Organs, 20 (1992) 253.
9 J.C. Bakker, G.A.M. Berbers, W.K. Bleeker, P.J. den Boer and P.T.M. Biessels, Biomater. Artif. Cells Immob. Biotech., 20 (1992) 233.
10 G.T. Hodakowski, R.D. Page, W. Harringer, E.E. Jacobs, Jr., P.J. LaRaia, T. Svizzero, J.L. Guerrero, G. Austen and G.J. Vlahakes, Biomater. Artif. Cells Immob. Biotech., 20 (1992) 669.
11 K. Bonhard, U.S. Pat., 4 136 093 (1979).
12 A.G. Greenburg, Biomater. Artif. Cells Artif. Organs, 16 (1988) 71.
13 J.C. Hsia, U.S. Pat., 4 857 636 (1989).
14 T.M.S. Chang and R. Varma, Biomater. Artif. Cells Artif. Organs, 16 (1988) 205.
15 M. Feola, J. Simoni and P.C. Canizaro, Trasfus. Sangue, 3 (1988) 121.
16 M. Feola, J. Simoni, M. Dobke and P.C. Canizaro, Circ. Shock, 25 (1988) 275.
17 M. Feola, J. Simoni, R. Tran and P.C. Canizaro, Biomater. Artif. Cells Artif. Organs, 16 (1988) 217.
18 J. Simoni, G. Simoni, C.D. Lox, J. Rubin and M. Feola, Biomater. Artif. Cells Immob. Biotech., 19 (1991) 487.
19 P.E. Keipert and T.M.S. Chang, Biomater. Artif. Cells Artif. Organs, 16 (1988) 185.
20 L.R. Sehgal, H.L. Sehgal, A.L. Rosen, S.A. Gould, R. DeWoskin and G.S. Moss, Biomater. Artif. Cells Artif. Organs, 16 (1988) 173.
21 G.A.M. Berbers, W.K. Bleeker, P. Stekkinger, J. Agteberg, G. Rigter and J.C. Bakker, J. Lab. Clin. Med., 117 (1991) 175.
22 M. Kothe, B. Eichentopf and K. Bonhard, Surg. Gynecol. Obstet., 161 (1985) 563.
23 W.M. Vogel, J.C. Hsia, L.L. Briggs, S.S. Er, G. Cassidy, C.S. Apstein and C.R. Valeri, Life Sciences, 41 (1987) 89.
24 T.M.S. Chang, Biomater. Artif. Cells Artif. Organs, 16 (1988) 1.
25 G.L. Moore, R.M. Fishman, M.E. Ledford, J.C. Hsia, D.L. Song, L.T.L. Wong and S.S. Er, Biomater. Artif. Cells Immob. Biotech., 19 (1991) 443.
26 V.K. Laemmli, Nature, 277 (1970) 680.
27 C.L. Shefield, G.E. Spates and J.R. DeLoach, Biomater. Artif. Cells Artif. Organs, 16 (1988) 887.
28 J. Simoni, G. Simoni, M. Feola and P.C. Canizaro, Anal. Chim. Acta, 249 (1991) 169.
29 M. Feola, J. Simoni, R. Angelillo, Z. Luhruma, M. Kabakele, M. Manzombi and M. Kaluila, Surg. Gynecol. Obstet., 174 (1992) 379.
30 E. Bucci, C. Fronticelli, C. Orth, M.C. Maratorana, L. Aebischer and P. Angeloni, Biomater. Artif. Cells Artif. Organs, 16 (1988) 197.
31 K.A. Evelyn and H.T. Malloy, J. Biol. Chem., 126 (1938) 655.
32 M. Feola, J. Simoni and P.C. Canizaro, Artif. Organs, 15 (1991) 243.
33 W.W. Yan, J.J. Kirkland and D.D. Bly, Modern Size Exclusion Liquid Chromatography, Wiley, New York, 1979.
34 Y. Mukoyama and S. Mori, J. Liq. Chromatogr., 12 (1989) 1417.
35 G. Lenz, H. Jungar, M. Schneider, N. Kothe, R. Lissner and A.M. Prince, Biomater. Artif. Cells Immob. Biotech., 19 (1991) 669.
36 I. Ramasamy and P.J. Butterworth, Biochem. Biophys. Acta, 370 (1974) 477.
37 L.R. Manning and J.M. Manning, Biochemistry, 27 (1988) 6640.
38 L.R. Sehgal, A.L. Rosen, S.A. Gould and G.S. Moss, Anasthesiol. Rev., 17 (1990) 38.
39 G.S. Hughes and E. Jacobs, Fifth International Symposium on Blood Substitutes, San Diego, CA, March 17–20, 1993, Program and Abstracts, H-15.

Analytica Chimica Acta, 279 (1993) 89–94
Elsevier Science Publishers B.V., Amsterdam

Applications of HY-APATITE in liquid chromatography

G.W. Boers, J.J. Kettenes-van den Bosch and A. Bult

Department of Pharmaceutical Analysis, Faculty of Pharmacy, Utrecht University, P.O. Box 80082, 3508 TB Utrecht (Netherlands)

(Received 9th October 1992)

Abstract

HY-APATITE [1] is a high-purity calcium hydroxyapatite with primary application in the medical field, for bone implants. Its suitability as a liquid chromatographic (LC) column packing material for the analysis of sugars, alkaloids, enzymes and proteins was investigated. Experiments with sintered HY-APATITE were promising. The regular material was found to be mechanically unstable and, therefore, not suitable for LC. Results are presented for both regular and sintered HY-APATITE columns.

Keywords: Liquid chromatography; Alkaloids; Enzymes; Hydroxyapatite; Proteins; Sugars

HY-APATITE [1] is a high-purity calcium hydroxyapatite, which is a natural component of bone. HY-APATITE consists of spherical agglomerates of needle-shaped crystals; the agglomerates vary in size. So far, its primary use has been in the medical field, as such or as a coating material for bone implants. In this work, its behaviour as a column packing material in liquid chromatography (LC) was investigated.

Calcium hydroxyapatite has been used in LC before, mainly for the separation of biomolecules. It was first mentioned in 1956 [1], but its use declined because the results were not sufficiently reproducible, columns had a limited lifetime and in LC applications the material was not sufficiently pressure resistant. Interest has revived in recent years, particularly for the analysis and purification of biotechnologically manufactured products. To overcome the unfavourable properties, calcium hydroxyapatite has been modified in several ways, e.g., by high-temperature treatment [2–6] and chemical modification [7–9]. At present, several hydroxyapatite columns are commercially available. However, from the specifications provided by the suppliers, it is not clear which variety of hydroxyapatite is used.

Columns were packed with both regular and sintered HY-APATITE and tested with various classes of compounds (sugars, alkaloids, enzymes and proteins) and with various solvent systems.

Correspondence to: J.J. Kettenes-van den Bosch, Department of Pharmaceutical Analysis, Faculty of Pharmacy, Utrecht University, P.O. Box 80082, 3508 TB Utrecht (Netherlands).

[1] HY-APATITE is the trademark of a hydroxyapatite manufactured by Euro Crystals, Landgraaf (Netherlands).

EXPERIMENTAL

Instrumentation

Columns were packed with a Shandon 628x51 (pneumatic) column packer or with a Waters Model 510 LC pump.

LC experiments were carried out with a system consisting of a Waters Model 510 pump, a Waters Model 680 automated gradient controller and a Waters U6K injector. For detection of non-UV-absorbing samples (e.g., sugars) a Waters R401 differential refractometer was used; for UV detection a Kratos Analytical Spectroflow 757 absorbance detector and for fluorescent samples

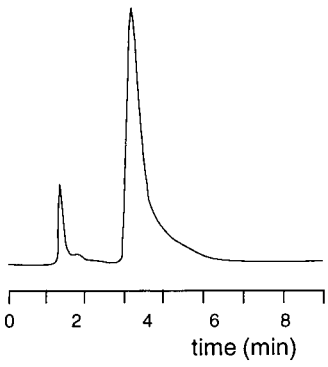

Fig. 1. Chromatogram of fructose. Column, regular HY-APATITE, fines removed only; eluent, acetonitrile–water (60 +20); refractometric detection.

(indole alkaloids) a Hitachi F-1000 fluorescence detector were employed.

For experiments with HY-APATITE, Valco 100 × 4.6 mm i.d. and Merck 125 × 4 mm i.d. LC columns were used. The commercial column was a Pentax SH-0410F hydroxyapatite column (Pentax New Ceramics, Hamburg).

Particle size distributions were measured with a Malvern 3600D particle sizer (Malvern Instruments, Malvern, UK).

Diffuse reflection infrared spectra were recorded with a Perkin-Elmer Model 1800 double-beam Fourier transform IR spectrometer at a resolution of 4 cm^{-1} and a concentration of ca. 5 mg in 300 mg of KBr.

Column packing

Columns were slurry-packed in methanol, either with an LC pump (regular HY-APATITE), increasing the flow-rate from 0.5 to 3.0 ml min^{-1} over a 2-h period, or with a pneumatic column packer at 300–500 atm (for sintered material).

Chemicals

Arabinose, fructose, galactose, glucose, lactose, maltose, mannose, rhamnose and saccharose were obtained from Merck, and xylose from Janssen Chimica. Serotonin was obtained from Sigma and the psilocybin reference sample from

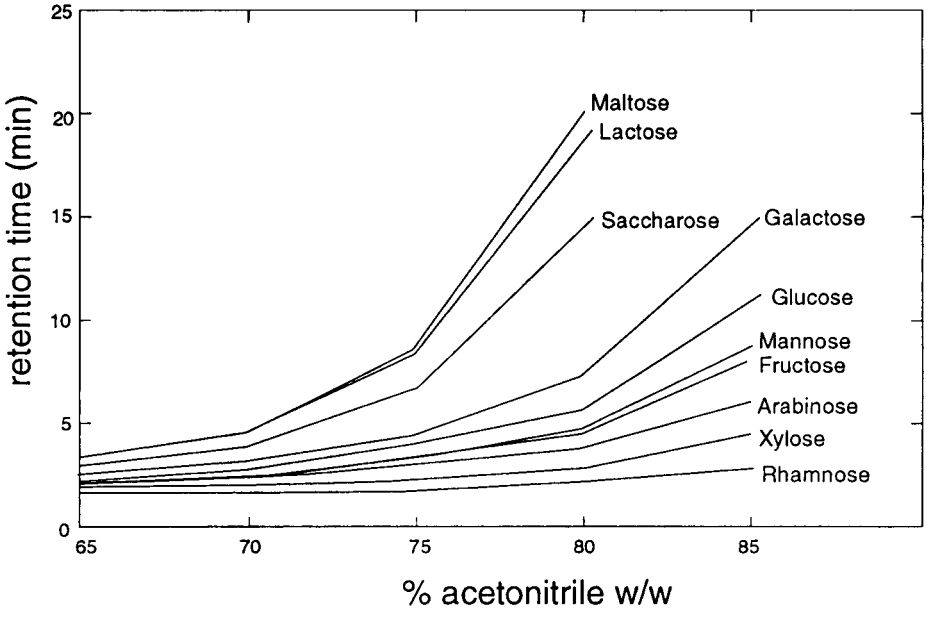

Fig. 2. Retention times of sugars as a function of acetonitrile concentration. Column, regular HY-APATITE; eluent, acetonitrile–water.

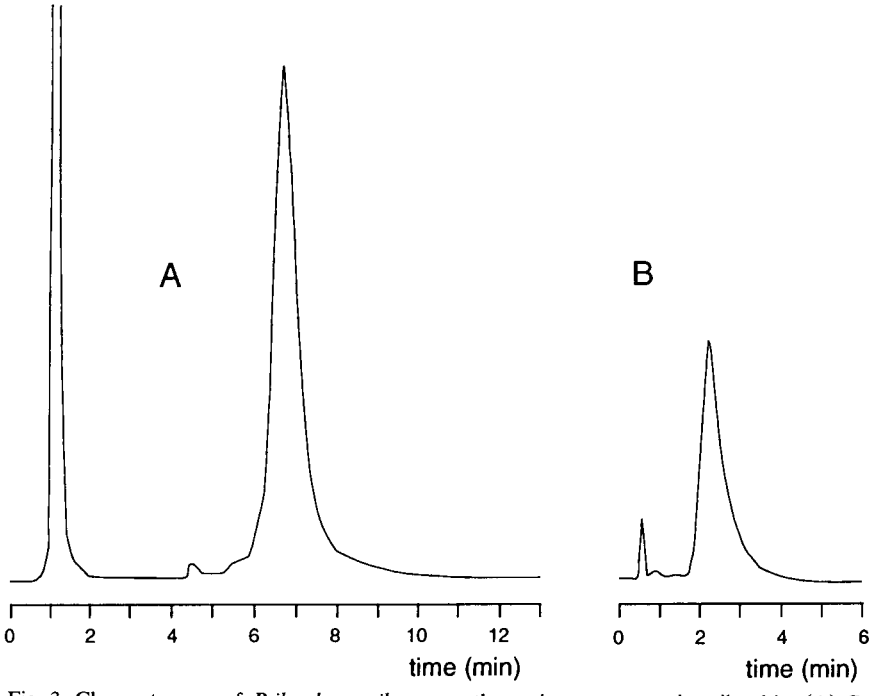

Fig. 3. Chromatogram of *Psilocybe semilanceata*; the main component is psilocybin. (A) Column, regular HY-APATITE; eluent, acetonitrile–water (65 + 35); (B) column, silica (10 μm); eluent, methanol–water–1 M ammonium nitrate (220 + 70 + 10); fluorescence detection.

the Forensic Laboratory, Rijswijk, Netherlands. Bovine serum albumin, lysozyme and cytochrome *c* were obtained from Sigma.

Samples of *Psilocybe semilanceata* and *Panaeolus sphinctrinus* were collected in Drenthe, Netherlands (October 1990), and were identified

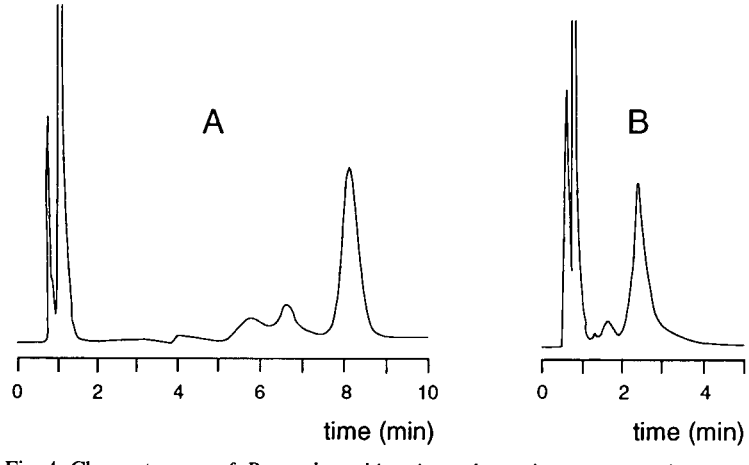

Fig. 4. Chromatogram of *Panaeolus sphinctrinus*; the main component is serotonin. Column, (A) sintered HY-APATITE (particle size 11 μm); (B) Pentax SH-0410F; eluent, acetonitrile–water (65 + 35); fluorescence detection.

by PSL (Mushroom Study Group, Limburg, Netherlands).

Methanol and acetonitrile (Merck) were of analytical-reagent grade.

RESULTS

Regular HY-APATITE columns

Figure 1 presents a typical chromatogram of a sugar, obtained with a regular HY-APATITE column, with acetonitrile–water (60 + 20) as the eluent and refractive index detection. Fines were removed from the HY-APATITE after sonication (to destroy the larger agglomerates) by sedimentation in methanol, but the material was not separated according to particle size.

Figure 2 shows the retention times on this column for a number of sugars as a function of the acetonitrile concentration. All sugars tested show severe tailing. As a result, baseline separation could not be achieved.

Figure 3A presents the chromatogram of a *Psilocybe semilanceata* extract with psilocybin as the main component, on a similar column. Acetonitrile–water (65 + 35) was used as the eluent and fluorescence detection was applied. For comparison, Fig. 3B shows the chromatogram of the same extract obtained with a silica column and methanol–water–1 M ammonium nitrate (220 + 70 + 10) as the eluent [10]. Apart from the column and eluent, the same equipment was used for both chromatograms. The HY-APATITE column gave a better peak shape and higher plate number (235 vs. 56) and has the advantage that no inorganic salts are present in the eluent.

Sintered HY-APATITE columns

Because of lack of pressure resistance of regular HY-APATITE, additonal experiments were done with sintered HY-APATITE. Figure 4A shows the chromatogram of a *Panaeolus sphinctrinus* extract (main component serotonin). The column was packed with sintered HY-APATITE, with an average particle size of 11 μm but a wide size distribution (fraction obtained with dynamic sedimentation in methanol at a flow-rate of 2.0 ml min^{-1}). The eluent was acetonitrile–water

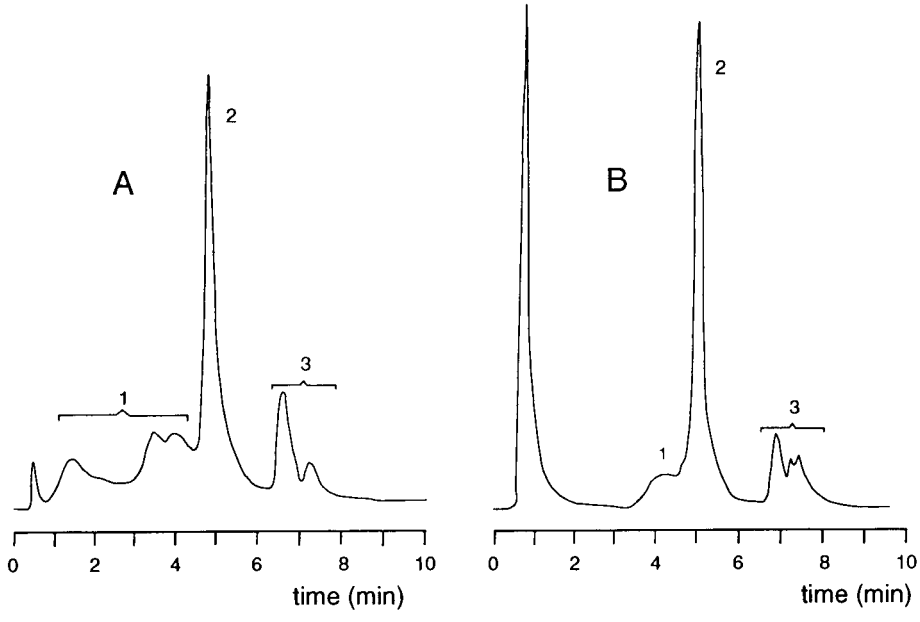

Fig. 5. Chromatogram of (1) bovine serum albumin, (2) lysozyme and (3) cytochrome *c*. Column, (A) sintered HY-APATITE (particle size 9 μm); (B) Pentax SH-0410F; eluent, linear gradient of phosphate buffer (pH 6.8) from 10 to 300 mM in 20 min; UV detection.

(65 + 35), with fluorescence detection. The chromatogram in Fig. 4B is for the same extract, obtained under identical conditions but with a commercial hydroxyapatite column (Pentax SH-0410F). The HY-APATITE column gave a higher plate number (1500 vs. 300) and better resolution than the commercial column. However, the retention times were longer.

Figure 5 shows examples of chromatograms of a mixture of (1) bovine serum albumin, (2) lysozyme and (3) cytochrome *c*, obtained with (A) a HY-APATITE and (B) the Pentax column. The HY-APATITE column was packed with material with an average particle size of 9 μm. Phosphate buffer (pH 6.8) was used as the eluent, with a linear gradient from 10 to 300 mM in 20 min and UV detection. Oxidized and reduced cytochrome *c* are clearly resolved.

Particle size distribution

Both regular and sintered HY-APATITE show a wide distribution in particle size. Therefore, the material was separated into fractions by dynamic sedimentation in methanol [11]. The flow-rates varied from 0.5 to 8.0 ml min^{-1}. The particle size distribution of sintered HY-APATITE fractions was determined with a laser particle sizer. The average particle size was 11 μm (52% between 8.2 and 33.7 μm), 14 μm (65% between 8.2 and 23.7 μm) and 19 μm (71% between 13.6 and 33.7 μm) for flow-rates of 0.5, 2.0 and 4.0 ml min^{-1}, respectively. (The Pentax material had an average particle size of 5 μm; 73% between 3.0 and 10.5 μm.) A second experiment, with flow-rates of 0.34, 0.68, 1.36 and 2.72 ml min^{-1}, yielded fractions with an average particle size of 5 μm (82% between 3.9 and 10.5 μm), 7 μm (84% between 5.0 and 13.6 μm), 9 μm (85% between 6.4 and 17.7 μm) and 12 μm (87% between 8.2 and 23.7 μm), respectively. The residue had an average particle size of 20 μm (82% between 10.5 and 33.7 μm).

Infrared spectrometry

The main difference between the reflection spectra of regular and sintered HY-APATITE is in the OH band region. The spectrum of sintered material shows a sharp band at 3580 cm^{-1} (non-hydrogen-bonded hydroxyl), whereas the regular material shows a broad OH band between 3600 and 2300 cm^{-1} in addition to the monomer band at 3580 cm^{-1}. There are small differences in intensities in the 1100–950 and the 650–550 cm^{-1} regions. Sintered HY-APATITE shows an additional absorption band at 560 cm^{-1}. In the fingerprint region, the spectrum of the Pentax material resembles that of regular HY-APATITE. However, it shows little bonded OH, although more than the sintered HY-APATITE.

DISCUSSION

Calcium hydroxyapatite has been used for the separation of biomolecules for several decades. The separation of proteins is assumed to be based on interactions of positively charged calcium groups of hydroxyapatite and negatively charged carboxylate groups in the proteins on the one hand, and interaction of negatively charged hydroxyl and phosphate groups of hydroxyapatite and positively charged quaternary ammonium groups in proteins on the other. The proposal for this mechanism was based on the effect of ions with varying positive and/or negative charges in the eluent [12,13]. The retention mechanism for other classes of compounds has been investigated less extensively, but a normal phase mechanism seems likely [14].

Regular HY-APATITE, after removal of the fines, gives good separations for the compounds tested. As this column packing is not sufficiently pressure resistant, its use is limited to low-pressure LC. Sintered material is superior in mechanical strength and gives good separations for tryptophan alkaloids and for several enzymes and proteins. The preliminary results encourage further work.

The authors are grateful to Ms. J.J.M. Reith, Department of Sedimentology, Utrecht University, for the particle size distribution measurements and to Mr. E.T.H.G. Lutz, Department of Analytical Molecular Spectrometry, Utrecht University, for running the infrared spectra.

REFERENCES

1 A. Tiselius, S. Hjerten, and Ö. Lenin, Arch. Biochem. Biophys., 65 (1956) 132.
2 Toa Nenryo Kogyo, Eur. Pat., 216.621, 1986; C.A., 106 (1987) 198694c.
3 Toa Nenryo Kogyo and Asahi Chemical Industry, Eur. Pat., 217.614, 1986; C.A., 107 (1987) 150767x.
4 Asahi Optical, DE 3.831.557, 1989; Ger. Offen., 6-4-1989; C.A., 111 (1989) 70018w.
5 Asahi Optical, Eur. Pat., 313.090, 1988; C.A., 111 (1989) 44259f.
6 Toa Nenryo Kogyo, Eur. Pat., 261.458, 1987; C.A., 109 (1988) 1125453a.
7 Mitsui Toatsu Chemicals, Eur. Pat., 342.932, 1989; C.A., 112 (1989) 229171k.
8 Asahi Optical, DE 3.831.260, 1989; Ger. Offen., 23-3-1989; C.A., 111 (1989) 140569c.
9 K. Majumder and N. Ramesh, Chromatographia, 24 (1987) 400.
10 A.L. Christiansen, K.F. Rasmussen and K. Hoiland, Planta Med., 51 (1984) 341.
11 K. Tesariuk and M. Necasova, J. Chromatogr., 75 (1973) 1.
12 T. Kawasaki, J. Chromatogr., 544 (1991) 147.
13 M.J. Gorbunoff, Anal. Biochem., 136 (1984) 425 and 432.
14 T. Okuyama, M. Takata, K. Takahashi, T. Ishikawa, K. Miyasaka and N. Kaneyama, J. Chromatogr., 466 (1989) 390.

Analytica Chimica Acta, 279 (1993) 95–106
Elsevier Science Publishers B.V., Amsterdam

In situ thermal monitoring of adsorption column performance

Y. Meng-Yang, R.R. Rathbone, J. Hubble and A.D. Lockett

School of Chemical Engineering, University of Bath, Claverton Down, Bath BA2 7AY (UK)

(Received 1st October 1992; revised manuscript received 28th December 1992)

Abstract

A detection technique for monitoring adsorption chromatography has been developed which is based on following temperature changes resulting from heats of adsorption. Although a similar approach has previously been described for use with pressure swing adsorption systems, the smaller magnitude of the thermal changes encountered in liquid-based separations generate significantly greater technical problems which have inhibited similar developments in this area. The current report presents results for the ion-exchange-based adsorption of aspartic acid which show that these problems can be overcome and that thermal monitoring offers a practical alternative to existing methods of column monitoring.

Keywords: Ion exchange; Chromatography; Thermometric methods; Aspartic acid; Column performance

Adsorption chromatography is of considerable importance in the downstream processing of biological materials, bcause it offers the potential for both selective recovery and significant concentration in a single process step. Given the high value of many of the new generation of biochemical products, optimisation of adsorption chromatography in terms of fractional product recovery becomes extremely important. In practice, one of the major problems is predicting when column adsorption capacity will be reached, so that excess adsorbate is not lost during loading and washing stages. This problem has been discussed by Chase [1] who concludes that, although modelling of column performance can form the basis for a prediction of adsorbate breakthrough, experimental variations and decline of adsorbent capacity with repeated use limit the accuracy of this approach. While ultraviolet absorbtion (UV) offers a valuable method for following breakthrough in model systems using single component feeds, in practical applications its use is severely limited by the high background optical adsorption arising from contaminating materials which are not retained by the column. In cases for which the adsorbate is only a small fraction of the protein in the process stream the detection of breakthrough by optical methods will not be possible. As a practical alternative Chase reports the use of continuous enzyme assays and automated sampling of column eluants followed by rapid chromatographic analysis as two methods which can be used to monitor adsorbate breakthrough. Although these methods were of use for specific applications, their lack of general applicability was highlighted and the potential for biosensors in the area of chromatography control was cited.

Despite recent advances in biosensor development, the very specificity which makes them attractive limits the application of any individual

Correspondence to: R.R. Rathbone, School of Chemical Engineering, University of Bath, Claverton Down, Bath BA2 7AY (UK).

sensor to a limited range of compounds. Ideally, what is needed is a more generally applicable technique which is robust, cheap, and which can follow the extent of adsorption at positions within the bed. The significance of detection methods which allow the position of the adsorption front to be followed within the column is highlighted by the work of Dantigny et al. [2] which uses model predictions to determine the potential productivity benefits of an optimised loading strategy. With adsorbents showing low capacity and/or high dissociation constants for adsorption this productivity increase might be as high as 75%.

This report considers the use of a thermal monitoring system similar in concept to the enzyme thermistor which has been described for biospecific measurement and control [3]. These units use simple semiconductor devices (thermistors) whose electrical resistance varies strongly with temperature. When placed in a packed bed of immobilised enzyme these can be used to follow temperature changes resulting from heats of reaction. In this case the method of detection is generic and the specificity arises from the choice of catalyst. A comparison between the heats of reaction quoted for enzyme thermistor applications and the reported heats of adsorption for ion-exchange processes, suggest that thermal monitoring should be experimentally feasible. In practice the temperature changes observed are likely to be higher for the adsorption systems given that significantly more mass will be involved. The use of thermal monitoring for the control of adsorption processes has recently been demonstrated in the case of pressure swing adsorption. In this instance the temperature changes observed were reported to be 5–45°C making detection relatively easy [4]. However, given the higher value of biotechnological products, the greater detector sophistication required to follow the smaller temperature changes is not unreasonable.

Literature reports [5,6] suggest that the heats of adsorption for low molecular weight compounds on ion-exchange resins are of the order of ΔH 5–10 kJ mol^{-1}, while interaction of antibodies and enzymes with their corresponding ligands show values of the order of 40 kJ mol^{-1} (ΔH hydrolysis of urea used in an enzyme thermistor 6.6 kJ mol^{-1}). In each case temperature changes within the range which can be detected in enzyme thermistor devices might be expected. These devices are usually based on highly sophisticated thermostatted units and have been reported to be sensitive to changes of the order of 1×10^{-4} K [7]. However, in an assessment of the effects of operating conditions on the performance of a differential enzyme thermistor it was found that temperature changes of less than 0.01 K could be detected in a unit submerged in a non-thermostatted water bath [8]. This suggests that the appropriate use of a reference sensor can elimi-

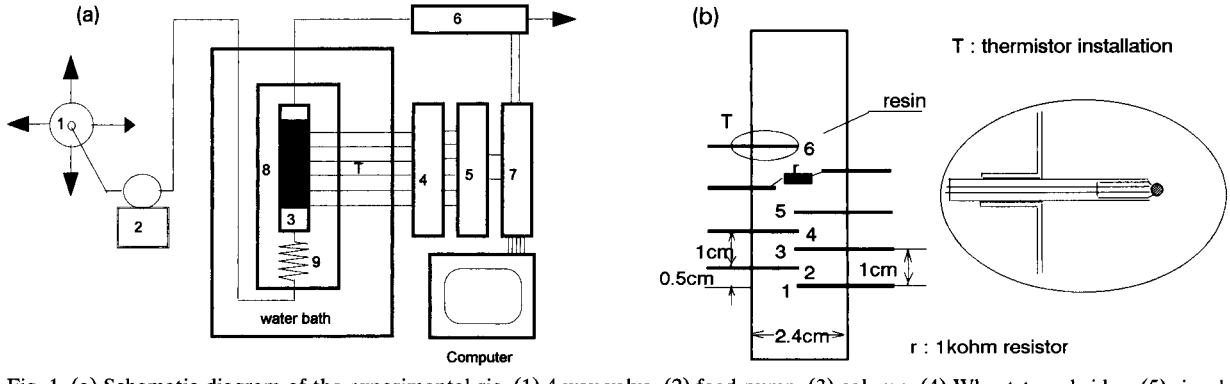

Fig. 1. (a) Schematic diagram of the experimental rig. (1) 4 way valve, (2) feed pump, (3) column, (4) Wheatstone bridge, (5) signal amplifier, (6) UV detector, (7) AD card, (8) column jacket, (9) heat exchanger. T denotes sensing thermistors. (b) Enlargement showing position and mounting of thermistors.

nate a significant proportion of the background noise, while still retaining sufficient sensitivity. The work reported here has aimed to develop a thermal monitoring system using ion-exchange based separations to take advantage of the larger thermal changes arising from their higher binding capacity.

EXPERIMENTAL RIG

The thermal monitoring liquid chromatography system (Fig. 1a) described in this work consists a borosilicate Pyrex glass column (150 × 25 mm o.d. length adjustable; Omnifit, modified in house by the addition of 8 side ports) placed in a plexiglass jacket (200 × 85 mm i.d.) filled with water. The column together with its jacket is vertically placed in a water bath (400 × 300 mm). The jacket design has been proved to be an effective means of reducing short period thermal disturbances resulting from water turbulence. In the thermostatted water bath temperature within the jacket can be maintained at a given set point with a fluctuation less than 1 mK.

The column with 6 thermistors mounted in is shown in Fig. 1b. The thermistors (miniature bead type, RS 151–158, 47 kΩ) were sealed with epoxy in glass tubes of 3 mm o.d. and 40 mm length. The sealed thermistors then were aged in water for at least 4 days, whilst the insulation resistance was monitored. Only thermistors whose insulation resistance were greater than 100 MΩ were chosen to be mounted into the column. A 1-kΩ resistor was also mounted as a point heat source in the column for calibration experiments. All the reference thermistors were mounted in an aluminium ring fixed around the column end.

Wheatstone bridges similar to those described previously [8] were used to output signals from thermistors to the computer data collection system. The bridges were driven by a laboratory power supply at a potential of 3.5 V. Based on the quoted characteristics of the thermistor used, theoretical analysis suggested a response of 31.5 mV K^{-1} should be obtained.

The data logging and analysis system consists of an OPUS PCXS microcomputer, a high-performance data acquisition card, pcl-818 whuch provides 16 analog input channels [9], used as an analog/digital converter, and a pre-amplifier board, pcl-889 [10] (gain range 1–1000, programable setting) for amplifying the signals output by the bridges in order to fit the input range (say ±1 V) of pcl-818 card. A BASIC program was written to perform data collection, averaging and storage.

The baseline electronic stability of the above system is in the range of ±0.04 mV per 4 h (a typical running period for breakthrough in this work) with a thermostatted water bath, or ±0.25 mV per 4 h if unthermostatted. This allows a temperature change of as little as 0.004 K in the column to be routinely measured.

A UV detector, LKB2238 (LKB, Sweden), set at 205 nm is used to monitor the aspartic acid concentration at the column outlet. A pulse free peristaltic pump (Minipulse 2, Gilson, France) is used to drive the liquid flow through the column.

MATERIALS

DEAE based resin was produced by Waitaki (New Zealand). The particle size of the resin is in the range of 250–425 μm. 14 g of the resin (wet) was used as column packing materials, which gave a bed height of 4.0 cm, and a diameter of 2.4 cm the water content of the resin settled in the column is 89% .

Aspartic acid, minimum assay 99%, purchased from BDH, was dissolved in 2.5 mM Tris–HCl buffer of pH 7.1. All other reagents were of AnalaR grade and were purchased from BDH.

METHODS

Point heat source tests

To investigate the sensitivity and response time of the thermistor system, as well as to estimate some thermal properties of the column packing material, point heat source tests were carried out. Heat was input either in the form of a pulse or continuously by passing a known current through a 1-kΩ resistor implanted in the column.

Determination of adsorption parameters

Batch experiment was carried out in order to obtain adsorption equilibrium and kinetic parameters which are necessary for modelling of the overall thermal process in the column. The rig and procedure used for batch experiment were similar to those described by Cowan et al. [11], however in this case the UV detector signal was fed into the computer instead of a chart recorder.

Breakthrough experiments

The column was recycled with 2.5 mM Tris–HCl buffer, until both thermal and UV detector base lines stabilised (approximately 4 h), then the loading stage was started by turning the 4 way valve onto the aspartic acid solution reservoir, meanwhile the data logging system was started to log thermal and UV responses. For the conditions used the amplifier gain range was set to 200, and pcl-818 analog input range was set to ± 1 V. After total breakthrough had occurred, the bed was washed with distilled water, then regenerated with 0.5 M NaOH. Finally it was washed with distilled water until the pH value returned to 7 prior to the next experiment. It was expected that thermal signals would depend on flow rate and temperature as well as feed concentration. To study these relationships, a series of breakthrough runs under different condition were undertaken.

While the majority of breakthrough experiments were conducted at 20–25°C a few were carried out at lower temperatures to assess the influence of temperature on sensitivity, while a number of runs were conducted in an unthermostatted bath to assess the effects of thermal "noise".

THEORY

Heat transfer in a packed bed

A two-dimension heat transfer model has been developed to describe thermal waves in the adsorption column. The model is based on main assumptions detailed below.

(i) The packing material together with the liquid is considered as a homogeneous system, in which the medium and the surrounding liquid are in local thermal equilibrium. This allows the rate of thermal diffusion to be expressed in terms of the overall heat conductivity and the temperature gradient in the medium. The validity of this assumption can be assessed by point source experiments, and will be discussed later.

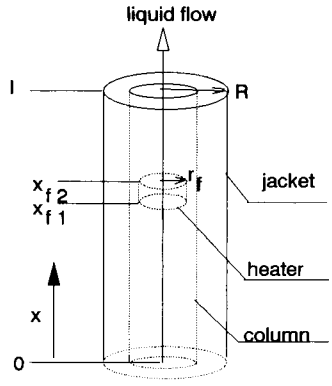

Fig. 2. Reference points used in the derivation of the heat transfer model.

(ii) Heat transfer due to radiation is negligible.

(iii) Heat generated by adsorption is uniformly distributed at any cross-section of the bed, and temperature profiles in the bed show axial-symmetry. Fluid transport is in dispersed-plug flow.

(iv) The column wall thickness is negligible. The heat balance then gives (Fig. 2)

$$\frac{\partial T}{\partial t} = \frac{k}{c\rho}\frac{\partial^2 T}{\partial x^2} - v\frac{\partial T}{\partial x} + \frac{k}{c\rho}\left(\frac{\partial^2 T}{\partial r^2} + \frac{1}{r}\frac{\partial T}{\partial r}\right) + \frac{\Delta H}{c}\frac{\partial q}{\partial t} \quad (1)$$

with boundary conditions

$$\pm k\frac{\partial T}{\partial x} = h_c(T_0 - T) \text{ at } x = 0 \text{ or } x = 1 \quad (2)$$

$$k\frac{\partial T}{\partial r} = h_w(T - T_0) \text{ at } r = R \quad (3)$$

and natural boundary condition at $r = 0$

$$\frac{\partial T}{\partial r} = 0 \quad (4)$$

where the adsorption rate, in the last term of Eq. 1, may be calculated from the adsorption kinetic

models which are described in the following section. (For explanation of symbols, see List of Symbols.) In the case of a point heat source (in fact a heat source lies in a small region) the expression for the heat emission rate takes the following form:

where $x_{f1} < x < x_{f2}$ and $r < r_f$

$$\frac{\partial H}{\partial t} = p_f / \left[(x_{f2} - x_{f1}) \pi r_f^2 \right] \quad (5)$$

and anywhere else

$$\frac{\partial H}{\partial t} = 0 \quad (6)$$

where p_f = power of the fixed point source, and x_{f1}, x_{f2}, and r_f are the boundary of the source.

Mathematical descriptions of the adsorption process

Stage model. A simple stage model to predict column performance [12] was used in conjunction with the above heat transfer model, allowing temperature profiles at any point in the bed, as well as the breakthrough curve to be numerically predicted. The model takes an empirical approach to adsorption and assumes that all the rate limiting processes can be represented by kinetic rate constants. In the model the bed is considered as a series of discrete stages. Each stage can be described as a well-mixed tank with adsorption proceeding for the residence time of a given fluid element in the stage. Thus the empirical rate equation

$$\frac{dq}{dt} = k_1 C (q_{max} - q) - k_2 q \quad (7)$$

can be integrated with respect to time over the residence time in each stage, subsequently the average adsorption rate within this residence time may be calculated.

The empirical parameters k_1, k_2 and q_{max} can be estimated from the adsorption isotherm and rate data obtained in batch experiments, under an assumption that the adsorption equilibrium behaviour can be represented by the Langmuir equation.

A program based on the finite difference method has been written to solve the overall heat transfer model. In the program the step size in column length is set to equal the stage height.

Film and pore diffusion model. In the stage model the overall adsorption process is specified by the empirical, lumped parameters: k_1, k_2 and q_{max}. Considering the different steps that occur in a packed bed may lead to a more rigorous approach for modelling the adsorption process. A number of more detailed models [13–15] have also been employed. The basic principles of these are discussed below:

The mechanism of adsorbate uptake consists of transport through the liquid film surrounding the adsorbent particles, diffusion within the pores of the particles and the adsorption itself. For the sake of simplification some assumptions are usually made, these are:

(i) that pore diffusion is expressed in terms of effective diffusivity and the gradient of adsorbate concentration in pores;

(ii) the adsorbent particles are spherical, and with uniform size, adsorption sites are evenly distributed throughout the interior of the particles;

(iii) mass transfer to the particle surface is described in terms of film diffusion coefficient and the concentration difference; and

(iv) surface adsorption rate is described by equation (7); the axial mass diffusion is negligible.

The mass balance then gives

$$\epsilon \frac{\partial C_i}{\partial t} = \epsilon D \left(\frac{\partial^2 C_i}{\partial r_p^2} + \frac{2}{r_p} \frac{\partial C_i}{\partial r_p} \right) - (1 - \epsilon) \frac{\partial q_i}{\partial t} \quad (8)$$

where the last term is the surface adsorption rate which can be described in the same form as Eq. 7, however the parameters k_1, k_2 and q_{max} in this model are intrinsic and are not lumped in the same manner as in the stage model. The boundary condition at $r_p = R_p$

$$k_f (C - C_i) = \epsilon D \frac{\partial C_i}{\partial r_p} \quad (9)$$

and natural boundary condition at $r_p = 0$

$$\frac{\partial C_i}{\partial r_p} = 0 \quad (10)$$

Also the mass balance in the mobile phase gives (note the axial diffusion is neglected)

$$\frac{\partial C}{\partial t} = -v\frac{\partial C}{\partial x} - R_i \quad (11)$$

where the last term, the rate of mass transfer through the liquid film to the particle surface (i.e., at $r_p = R_p$), may be described by:

$$R_i = k_f D \frac{3}{R}\frac{(1-\epsilon_b)}{\epsilon_b \epsilon}(C - C_i) \quad (12)$$

To solve these Eqns. 7 parameters have to be estimated, they are k_1, k_2, q_{max}, D, k_f, ϵ, and ϵ_b. For the first three Cowan et al. [11] have taken the values determined from isotherm and batch uptake experiments as their initial estimates and have then adjusted them to get the best fit for the earlier part of the breakthrough curve. A semi-empirical method [16] may be used to estimate k_f; however, determination of the effective pore diffusivity D might be more difficult. Horstmann and Chase [14] treated D as an unknown parameter which was determined by fitting the predicted to the experimental results.

A simple program based on this model solved using a finite difference method has been written to solve the heat transfer model and to predict the breakthrough curve.

Overall heat conductivity and heat transfer coefficient

In view of the high water content (89% approximately) of the packed bed, a reasonable estimation of k is between 89% and 100% of the heat conductivity (0.6 W m^{-1} K^{-1}) of water, hence k is given as 0.55 W m^{-1} K^{-1}. In this work the column with its jacket is placed in a water bath, which is in forced convection, and for such a case the method to determine heat transfer coefficient has been well established [17]. The following relations may be applied

$$Nu = 0.174 Re^{0.618} Pr^{0.33} \quad (13)$$

$$h_c = \frac{k}{d} Nu \quad (14)$$

The velocity of the water along the jacket wall due to water circulation in the water bath was measured as 0.07 m s^{-1}, which leads to a heat transfer coefficient of 190 W m^{-2} K^{-1}.

Estimating the heat of adsorption

To solve the heat transfer model values for the adsorption heat are required, however the data of adsorption heat for liquid–solid systems are rarely available. The good agreement between the calculated and observed temperature profiles in point heat source experiments (described in the results section) allows the estimation of the adsorption heat given the following assumptions.

(i) A heat source caused by an adsorption front moving along the column may be approximated by a moving point source, hence the power of the point source can be an approximation of that caused by the adsorption.

(ii) At a certain point the temperature increase caused by a point source nearby is in proportion to its power at steady state. This has been supported by the results of the point source experiments reported later.

Considering a moving point source s_m of unknown power p_m which moves from position x_1 to position x_2 in a time interval t, resulting in a temperature increase T_m at a subsequent point x_3. This can be bounded in terms of two separate changes: a fixed point source at x_1 with a power of p_f causing a temperature increase T_1 at x_3 and a second fixed point source at x_2 with the same power resulting in a temperature increase T_2 at x_3. Under these conditions the following relation may be applied:

$$\frac{p_f}{T_1} < \frac{p_m}{T_m} < \frac{p_f}{T_2} \quad (15)$$

hence p_m can be estimated, as T_1 and T_2 may be calculated from the model. If x_1, x_2, and the time interval, t, are chosen in such a way that the speed of the moving point source equals that of the adsorption front, the adsorption heat may be estimated.

RESULTS

Temperature profiles in point heat source experiments

A typical temperature profile in the fixed point source experiments is given in Fig. 3a, which also shows the model prediction. The good agreement

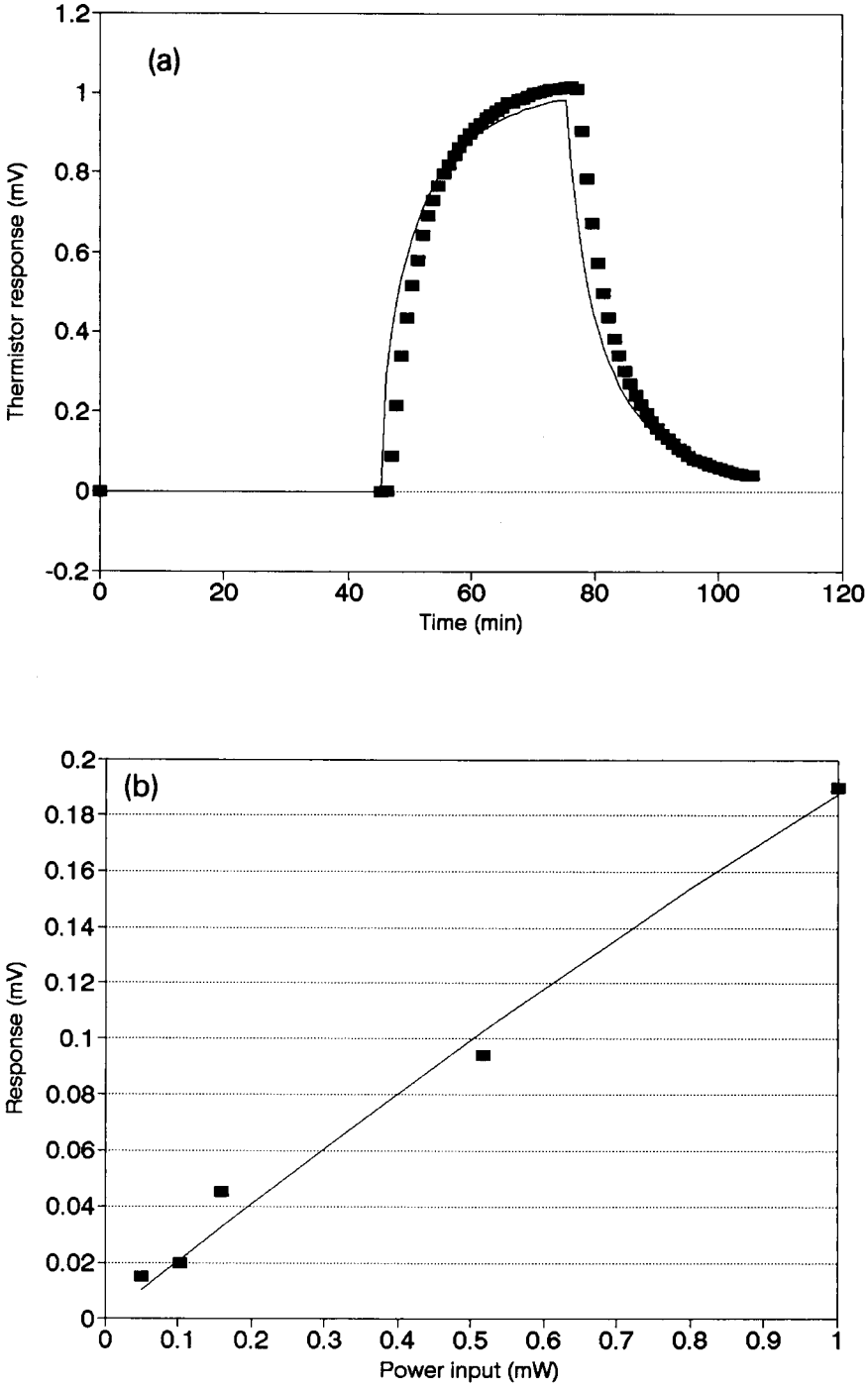

Fig. 3. (a) Thermistor response to a step power input. Position of source 2.75 cm from inlet. Position of thermistor 3.5 cm from inlet. Power input 4 J min^{-1}. Temperature 20°C, flow-rate 1.6 ml min^{-1}. (b) Thermistor response to a constant power input. Source and sensor position as for (a), temperature 20°C, flow-rate 1 ml min^{-1}.

TABLE 1

Adsorption parameters

T (°C)	Q_m (10^{-2} g g^{-1})	K_d (10^{-5} g ml^{-1})	k_1 (g ml^{-1} min^{-1})	K_2 (10^{-3} min^{-1})
10	1.86	5.8	107	6.2
20	1.75	4.4	135	6.2

implies that the assumptions of the model and estimates of the thermal parameters are reasonable. Figure 3b shows proportionality between the thermal response and continuous power input.

Adsorption parameters

Adsorption isotherms were measured in batch experiments and the results fitted to the Langmuir equation. Adsorption rate coefficients were calculated from data of adsorbate concentration varying with the time assuming the rate process can be described by Eqn. 7. At steady state this gives:

$$q = \frac{q_{max}C}{K_d + C} \tag{16}$$

where $K_d = k_2/k_1$. The best estimates of the adsorption parameters obtained are given in Table 1.

Temperature profiles in breakthrough experiments

Throughout all the breakthrough experimental runs thermal waves in the column were clearly observed. Typical thermal response curves obtained during the loading stages for three breakthrough experiments conducted using an unthermostatted water bath are shown in Fig. 4, similar results being obtained in a thermostatted bath with little evidence of an improvement in signal quality. The time at which the maximum temperature is measured by a particular thermistor was found to be linearly related to its position. This relationship was found in all experimental runs, a typical result is shown in Fig. 5 which also shows

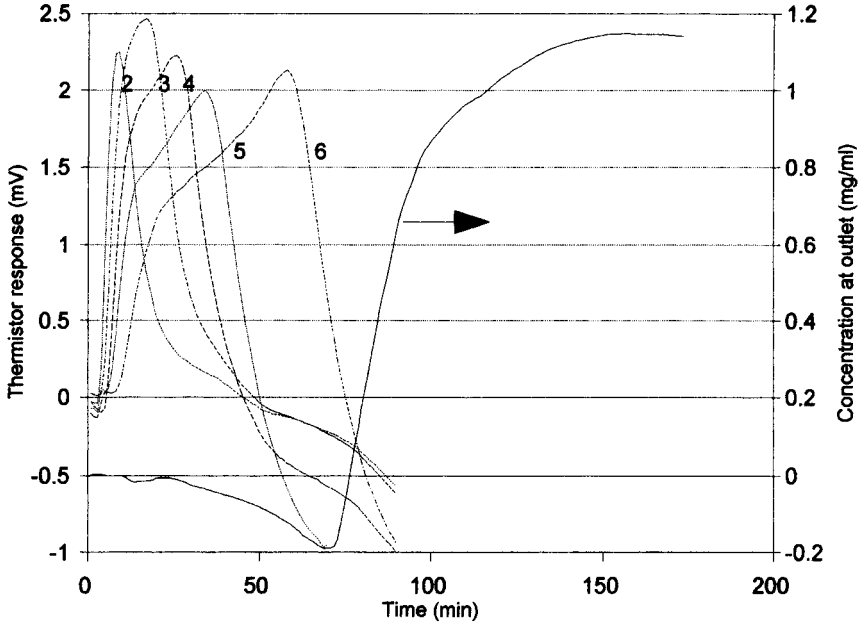

Fig. 4. Thermal responses obtained during column loading. 2–6 indicate thermistors in positions shown in Fig. 1b. Feed concentration 0.0012 g ml^{-1}, flow-rate, 2.341 ml min^{-1}, ambient temperature 21°C (unthermostatted).

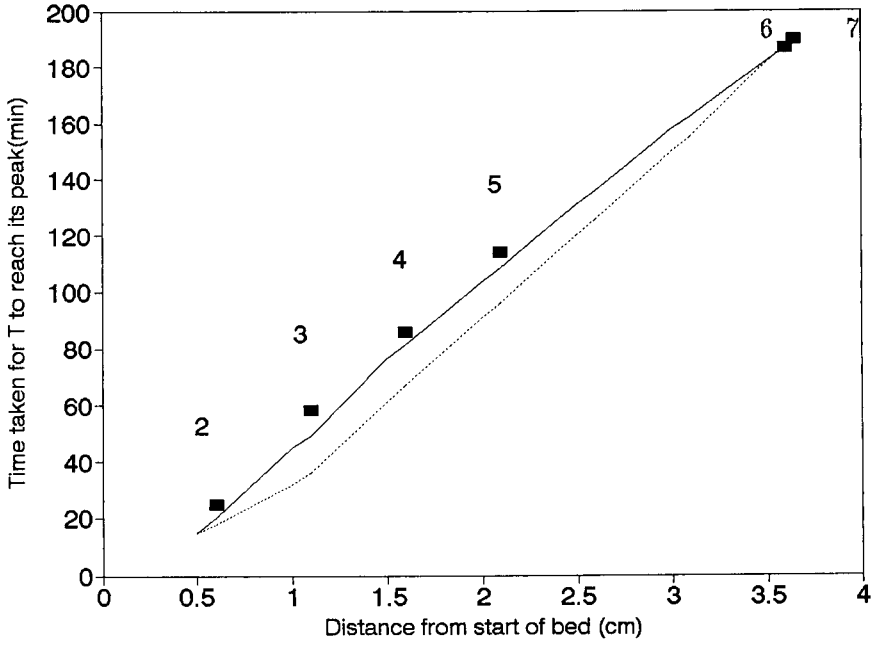

Fig. 5. Relationship between time to peak response and thermistor position. Symbols represent experimental values, dashed line diffusion model prediction, solid line stage model prediction. Temperature 20°C (thermostatted), flow-rate 1.66 ml min^{-1}.

the predictions obtained using the stage and diffusion models. The breakthrough curves were examined, and it was found that an extrapolation of this relationship to a point equal to the column length gave a consistent prediction of the time to reach 20% breakthrough. This suggests there is coincidence of the maximum thermal response and the adsorption front, which makes it possible to predict the position of the adsorption front from the thermal measurements.

Thermal responses, as expected, were a function of the feed concentration as well as the flow rate used, these relationships are shown in Fig. 6a and b. The overall dependence of thermal response on the feed rate gives an approximately linear relationship. If 0.1 mV is taken as a limit for the resolution of the temperature profiles this implies a minimum practical feed concentration of 1×10^{-4} g ml^{-1} for the experimental system in its current form. However, over the range studied, higher feed rates allow more precise resolution of the temperature profiles.

Adsorption heat

Taking point sources at $x_1 = 0$ and $x_2 = 0.5$ cm the predicted temperature profiles at $x_3 = 1.0$ cm can be calculated. Equation 15 applies until the adsorption front (moving source) passes position x_2. After 18.5 min the adsorption front reached x_2, and the signal from the thermistor at x_3 was 1.32 mV. Using this data the adsorption heat is estimated to be 18 kJ mol^{-1}.

Comparison of results and theory

To apply the stage model q_{max} is translated from that obtained in batch isotherm into the term of g ml^{-1} of settled volume, i.e., $q_{max} = 0.0126$ g ml^{-1}. For pore and film diffusion model q_{max} is translated into 0.166 g ml^{-1} (pure resin), $\epsilon = 0.89$ is estimated from the water content, $\epsilon_b = 0.35$ estimated by consideration of the settled volume and the weight of the resin (wet) added, $k_f = 0.2$ cm min^{-1} by the approach proposed by Geankoplis [16], and finally the value of D is taken to be that give the best fit to the observed

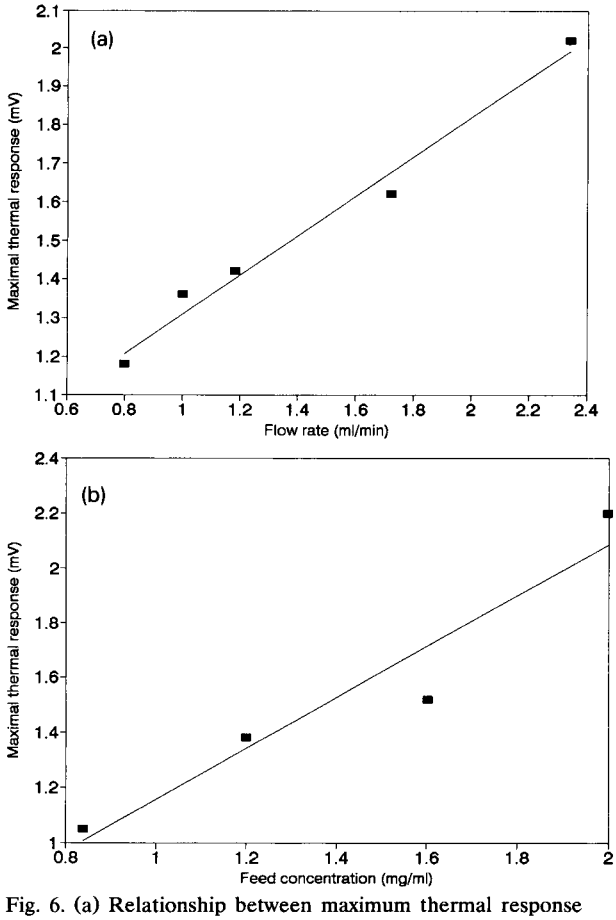

Fig. 6. (a) Relationship between maximum thermal response and column feed rate. Thermistor number 6, temperature 20°C, feed concentration 0.0012 g ml^{-1}. (b) Relationship between maximum thermal response and column feed concentration. Conditions as in (a), flow-rate 1.0 ml min^{-1}.

curve. An example of the predicted response is shown in Fig. 7, for the stage model, similar results are obtained for the diffusion model. For the studied system no significant difference is found in using stage and diffusion models provided the feed concentration is above 0.001 g ml^{-1}, but with lower feed concentration, the predicted fit was better with diffusion model. The reasonable agreement in temperature profiles between the predicted and the observed results makes the overall heat transfer model acceptable. For the breakthrough curve, a good agreement to the initial region stage is observed, however a deviation in the later part of the curve is significant with both stage and diffusion models. A similar problem has also described by Graham et al. [13] and a possible explanation proposed was the wide range of the particle distribution in the resin preparation used.

Figure 5 shows comparisons of the predicted and observed trajectories of thermal waves together with the extrapolations to the time of 20% of the breakthrough and again the diffusion model gives a little closer fit than the stage model at lower feed concentrations. In the early stages of the column the observed thermal waves are a little slower than the predicted. A possible explanation for this apparent slow movement of thermal waves in the early stages of the column is that the liquid flow may be disturbed by channeling effects resulting from uneven packing. Once a fraction of the liquid flow bypasses parts of the adsorbent, saturation in the early stages of the bed would be delayed, and in turn thermal waves in the same region would be slowed.

DISCUSSION

The approach described in this paper is based on the fact that a measurable thermal process occurs during the adsorbate uptake in a packed column. According to Eqn. 1 the shape and magnitude of thermal waves will strongly depend on the rate of adsorption heat, the heat conductivity, and the specific heat capacity of the resin. In practice packed columns for biochemical separation have a high water content, so that the thermal conductivity and specific heat capacity of the bed are close to those of water. The most important factor is the rate at which the heat of adsorption is evolved. This will be a function of the adsorption heat (ΔH), and the overall adsorption rate which under most practical conditions will be limited by the column feed rate. For the studied system, taking the estimation of the adsorption heat, and the feed rate used, the rate of heat evolution can be calculated to be with in the range of 0.11 to 0.62 J min^{-1}. This corresponds to thermal waves in the range of 0.62 to 2.8 mV. If 0.001 g min^{-1} is taken as a typical column feed rate, and 0.1 mV as the limit for thermal wave

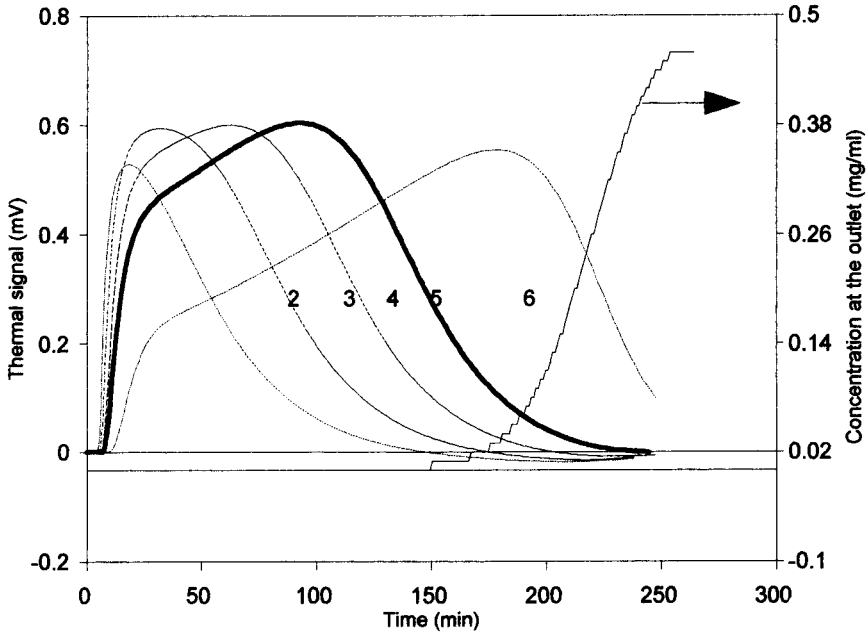

Fig. 7. Results from simulations of loading performed using the stage model. Conditions specified: feed concentration 0.0005 g ml^{-1}, flow-rate 1.66 ml min^{-1}, constant values obtained at 20°C.

resolution, this suggests that the minimum heat of adsorption necessary for viable detection as approximately 18 J g^{-1}. It is interesting to make a comparison with the similar approach used in pressure swing adsorption [4], where the adsorption heat is about 150 J g^{-1}, and the rate evolution of adsorption heat 5 kJ min^{-1}.

The prediction of breakthrough is based on the coincidence of the trajectories of thermal waves and the adsorption front and the simplest procedure is to extrapolate the linear relation of the thermal wave trajectories to the column outlet such that the time when the breakthrough reaches a preset point (e.g., 20%) can be directly obtained. This method of prediction, although simple, is subject to significant errors. A more precise prediction could be achieved by using model based estimation techniques such as the Kalman filter, or by utilising a neural network to descibe a more complete relationship between thermal signals and adsorption front position.

The use of a series of thermistors may premit precise tracking of the adsorption front at the expense of greater complexity. In practice simple extrapolation of a line plotted from zero at the column entrance to the time taken for thermistor No. 6 to reach its maximum output can be extrapolated to give the time taken for 20% breakthrough at the column exit, as shown in Fig. 6. This relationship was found in all experimental runs. The above figures also show that the heat transfer model gives the better prediction for the thermal trajectories at the rear region of the column. This implies that the best site for the thermistor installation is in the lower region of the column which also allows real time model simulation and prediction. The optimum position for the thermistor was found to be at a point equivalent to 60% of the bed length, i.e., the position of thermistor No. 6 in this work.

Conclusions

A generic and simple device using thermistors can be used to follow temperature changes in an adsorption column provided the heat of adsorption is not too low (not less than 18 J g^{-1} in this work). Experiments conducted over a range of external temperatures ranging from 10–25°C indicate little temperature sensitivity, and effective monitoring could be obtained without sensitive

control of the water bath temperature. The coincidence of thermal wave trajectories and the adsorption front has been established by the experiments and the heat transfer model proposed, so that the movement of the adsorption front can be described by temperature profiles or thermal waves. This allows the breakthrough to be predicted in real time.

The financial support of the SERC is gratefully acknowledged, as is the gift of ion-exchange resins provided by Dr. M. Fang.

LIST OF SYMBOLS

C Liquid phase concentration (g ml^{-1})
C_i Point concentration of liquid inside particles (g ml^{-1})
c Specific heat
D Effective diffusivity (cm min^{-1})
h_c Heat transfer coefficient (J cm^{-2})
ΔH Adsorption heat (J g^{-1})
k Effective conductivity (J cm^{-1} K^{-1})
k_1 Forward rate constant for surface adsorption (ml g^{-1} min^{-1})
k_2 Reverse rate constant for surface adsorption (min^{-1})
k_f Liquid film mass transfer coefficient (cm min^{-1})
K_d Dissociation constant (g ml^{-1})
Nu Nusselt number
q Concentration of adsorbate in adsorbent (g ml^{-1})
q_i Point concentration of adsorbate inside particles (g ml^{-1})
q_{max} Langmuir isotherm constant (g g^{-1} or g ml^{-1})
R Jacket radius (cm)
R_i Rate of interface mass transfer (g ml^{-1} min^{-1})
R_p Particle radius (cm)
r Radial coordinate (cm)
r_p Radial coordinate inside particles (cm)
t Time (min)
T Temperature (K)
T_0 Temperature of water bath (K)
v Superficial velocity of liquid (cm min^{-1})
x Axial coordinate in the bed (cm)
ϵ, ϵ_b Particle and bed porosity
μ Viscosity (kg m^{-1} s^{-1})
ρ Density of the bed (g/ml)

REFERENCES

1 H.A. Chase, J. Chem. Tech. Biotechnol., 36 (1986) 351.
2 P. Dantigny, Y. Wang, J. Hubble and J.A. Howell, J. Chromatogr., 545 (1991) 27.
3 K. Mosbach and B. Danielsson, Anal. Chem., 53 (1981) 83A.
4 M.J. Matz and K.S. Knaebel, Ind. Eng. Chem. Res., 26 (1987) 1638.
5 F. Helfferich, Ion-exchange, McGraw Hill, New York, London, 1962.
6 G. Rialdi and R.L. Biltonen, in H.A. Skinner (Ed.), International Review of Science, Physical Chemistry, Series 2, Butterworths, London, Boston, 10 (1973) 147.
7 B. Danielsson and K. Mosbach, Methods Enzymol., 137 (1988) 181.
8 J. Hubble, J. Chem. Tech. Biotechnol., 36 (1986) 487.
9 PCL-818 User's Manual, Part No. 2003818000 Rev.A1, Intercole Systems.
10 PCL-889 User's Manual, Part No. 2003889000 Rev. A2, Intercole Systems.
11 G.H. Cowan, I.S. Gosling, J.F. Laws and W.P. Sweetenham, J. Chromatogr., 363 (1986) 37.
12 J. Hubble, Biotech. Tech., 3 (1989) 113.
13 E.E. Graham, L. Skidmore, B.J. Horstmann and H.A. Chase, J. Chromatogr., 498 (1990) 113.
14 B.J. Horstmann and H.A. Chase, Chem. Eng. Res. Des., 67 (1989) 243.
15 E.E. Graham, A. Pucciani and H.G. Pinto, Biotech. Prog., 3 (1987) 141.
16 C.J. Geankoplis, Transport Processes and Unit Operations, Allyn and Bacon, Boston, MA, 2nd edn., 1983.
17 K. Cornwell, The Flow of Heat, Van Nostrand Reinhold, New York, 1977, p. 160.

Analytica Chimica Acta, 279 (1993) 107–113
Elsevier Science Publishers B.V., Amsterdam

Retention characteristics of a β-cyclodextrin polymer-coated liquid chromatographic column

Tibor Cserháti and Esther Forgács

Central Research Institute for Chemistry, Hungarian Academy of Sciences, P.O. Box 17, H-1525 Budapest (Hungary)

András Ujházy

CYCLOLAB Research and Development Laboratory, Budapest (Hungary)

(Received 1st October 1992; revised manuscript received 14th December 1993)

Abstract

A silica based, β-cyclodextrin polymer-coated liquid chromatographic column was prepared and its retention characteristics were determined using 28 ring-substituted phenol derivatives as solutes and methanol–water mixtures as eluents. The column showed a good separation power; the log k' value decreased linearly with increasing methanol concentration. Stepwise regression analysis demonstrated that the lipophilicity does not determine the retention on the β-cyclodextrin polymer. Accordingly, the retention mechanism deviates from that of traditional reversed-phase columns. The steric characteristics and to a lesser extent the electronic parameters of the solutes have the greatest impact on the retention, which means that the inclusion complex formation also prevails after polymerization, resulting in a modified retention behaviour of the complexed solutes.

Keywords: Liquid chromatography; Cyclodextrin polymer-coated column; Phenols; Retention behaviour

Cyclodextrins (CDs) can form inclusion complexes with a wide variety of compounds [1,2]. As the complex formation modifies the apparent lipophilicity and polarity of the guest molecule, CDs have found growing acceptance and application in many fields of chromatography [3]. Reversed-phase thin-layer chromatography has been used to determine the inclusion complex stability of several chlorophenol derivatives with two hydroxypropyl-β-CDs [4]. The effective mobilities of various inorganic ions such as iodide, periodate and tetrahionate decreased with increasing concentration of α-, β- and γ-CD in the isotacophoretic determination of these ions [5]. The application of α- and β-CD in the capillary electrophoretic separation of peptides enhanced the separation [6]. Polar [7] and non-polar [8] CD derivatives have been been equally used in capillary gas chromatography for enantiomer separations. The Gibbs–Helmholtz parameters of enantiomer discrimination on a permethylated β-CD gas capillary column have recently been determined [9]. CDs have been used extensively in liquid chromatography (LC) either as eluent additives or covalently bonded to a silica surface. CDs added to the eluent modify the retention of aliphatic alcohols [10], steroids [11] and derivatized steroids [12]. The stability of inclusion complexes can be calculated from the dependence of retention on the concentration of CD, as was demonstrated for NADH and NADP [13] and also for several nucleotides, nucleosides and nu-

Correspondence to: T. Cserháti, Central Research Institute for Chemistry, Hungarian Academy of Sciences, P.O Box 17, H-1525 Budapest (Hungary).

cleic acid bases [14]. LC columns with covalently bonded CDs have been applied for direct injection analysis for drug enantiomers in serum [15], for enantiomeric separations of dansylated amino acids [16] and for the separation of di- and tripeptides [17]. The application of a covalently bonded β-CD column for semi-preparative separations has also been reported [18]. CD columns are generally applied in aqueous eluents, but CD derivatives for the direct phase separation of enantiomers have also been synthesized [19].

Reversed-phase (RP) LC has been extensively used to determine the hydrophobicity (lipophilicity) of various compounds [20,21]. To increase the accuracy of the lipophilicity determination, linear correlations were calculated between the log k' value and the concentration of organic modifier in the eluent. The intercept of the correlation was considered as the best estimate of lipophilicity [22] and the slope was considered to be related to the specific hydrophobic surface area [23]. The good correlation between the intercept and slope values indicates the structural homogeneity of solutes [24].

The objectives of this work were to prepare a CD column without covalently binding the CD to the silica surface, to test the separation power of the column using polar solutes, to prove that its retention characteristics deviate from those of common RP columns and to establish the molecular parameters of solutes that influence their retention behaviour.

TABLE 1

Structures of ring-substituted phenol derivatives

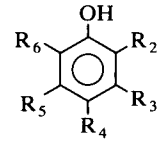

General structure

No.	R_2	R_3	R_4	R_5	R_6
1	H	H	H	H	H
2	CH_3	H	H	H	H
3	H	H	CH_2CH_3	H	H
4	H	OCH_3	OCH_3	H	H
5	$C(CH_3)_3$	H	H	H	$C(CH_3)_3$
6	$C(CH_3)_3$	H	$C(CH_3)_3$	H	H
7	H	$N(CH_3)_2$	H	H	H
8	H	OH	CH_2CN	H	H
9	H	OCH_3	H	H	OCH_3
10	CH_3	H	$CH(CH_3)_2$	H	H
11	NH_2	H	H	H	H
12	H	H	NH_2	H	H
13	Cl	H	H	H	H
14	H	H	Cl	H	H
15	Cl	H	H	H	Cl
16	H	Cl	H	Cl	H
17	Cl	H	NO_2	H	Cl
18	H	Br	H	H	H
19	H	H	Br	H	H
20	Br	H	Br	H	H
21	Br	H	Br	H	Br
22	H	H	F	H	H
23	H	H	CN	H	H
24	NO_2	H	H	H	H
25	H	H	NO_2	H	H
26	NO_2	H	NO_2	H	H
27	H	OH	H	H	H
28	H	OC_6H_5	H	H	H

EXPERIMENTAL

Monomer β-CD was polymerized on the surface of silica particles without binding the polymer covalently to the silanol groups. A 250 × 4 mm i.d. column was filled with the β-CD polymer-coated silica. The LC system consisted of a Liquopump Model 312 pump (LaborMIM, Budapest), a CE-212 variable-wavelength UV detector (Cecil Instruments, Cambridge), a Valco (Houston, TX) injector with a 20-μl sample loop and a Model 740 integrator (Waters–Millipore, Milford, MA). The flow-rate was 1 ml min^{-1} and the detection wavelength was set to 254 nm. Mixtures of methanol–water were used as eluents, with methanol contents varying between 65 and 80% (v/v) in steps of 5%.

The structures of the ring-substituted phenol derivatives are shown in Table 1. The phenols were dissolved in the eluent at a concentration of 0.05 mg ml^{-1}. The dead volume of the column was determined by injecting $NaNO_3$. Each determination was run in quadruplicate. As the correlation between the log k' value and the organic phase concentration is generally linear in LC, linear equations were also applied to describe the

dependence of log k' on the organic mobile phase concentration:

$$\log k' = \log k'_0 + bC \quad (1)$$

where k' is the capacity factor, k'_0 is the capacity factor extrapolated to zero organic mobile phase concentration (intercept), b is the change in log k' caused by unit a change (1%, v/v) of organic mobile phase concentration (slope) and C is the organic mobile phase concentration (%, v/v). To check the chromatographic homogeneity of the phenol derivatives, the linear correlation was calculated between the parameters of Eqn. 1.

To find the molecular parameters that significantly influence the retention, the intercept and slope values were separately correlated with several physico-chemical characteristics of phenol derivatives. The physico-chemical parameters included in the calculation were the following: π = Hansch–Fujita substituent constant characterizing hydrophobicity; *H-Ac* and *H-Do* = indicator variables for proton acceptor and proton donor properties, respectively; *M-RE* = molar refractivity; F and R = Swain–Lupton electronic parameters characterizing the inductive and resonance effect, respectively; σ = Hammett constant, characterizing the electron-withdrawing power of the substituent; E_s = Taft constant, characterizing steric effects of the substituent; and B_1 and B_4 = sterimol width parameters.

The calculation was done by stepwise regression analysis [25]. The number of accepted variables was not limited; their acceptance limit was set to the 95% significance level. As the type of correlation (linear or quadratic) between the dependent and independent variables was not previously elucidated, the calculation was done separately on the data matrices consisting of the linear and of the linear + quadratic forms of physico-chemical parameters.

A modified Free–Wilson analysis [26] was applied to select the substituents of phenol derivatives having the greatest impact on the retention behaviour of these compounds. In the traditional Free–Wilson analysis, the presence of independent variables exerting no significant influence on the dependent variable lessens the significance level of the independent variables significantly influencing the dependent variable. To overcome this difficulty, the modified Free–Wilson analysis automatically eliminates from the selected equation the insignificant independent variables, increasing in this manner the information power of the calculation. The intercept and slope values of Eqn. 1 were included in the modified Free–Wilson analysis as separate dependent variables. The independent indicator variables were the various substituents at different positions. The acceptance level for the individual independent variables was set to the 95% significance level.

RESULTS AND DISCUSSION

All the phenol derivatives showed symmetrical peaks in each eluent system (Figs. 1–3) but their retention times differed considerably. Accordingly, the β-CD polymer-coated column can be successfully used for the separation of ring-substituted phenol derivatives without buffering the eluent. Phenol derivatives with more bulky substituents are more strongly retained (Fig. 1), indi-

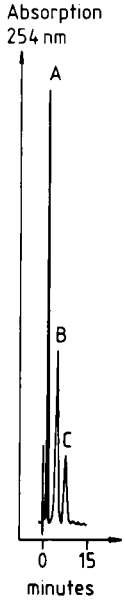

Fig. 1. Separation of some ring-substituted phenol derivatives on a β-cyclodextrin polymer-coated column. Eluent, methanol–water (65 + 35, v/v); flow-rate, 1 ml min^{-1}; detection wavelength, 254 nm. Peaks: A = 2-methylphenol; B = 2,4-di-*tert*-butylphenol; C = 2,6-di-*tert*-butylphenol.

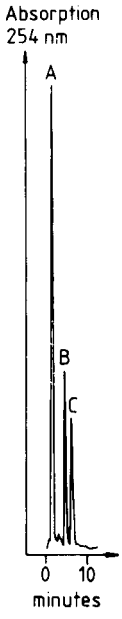

Fig. 2. Separation of some ring-substituted phenol derivatives on a β-cyclodextrin polymer-coated column. Eluent, methanol– water (65+35, v/); flow-rate, 1 ml min^{-1}; detection wavelength, 254 nm. Peaks: A = 4-chlorophenol; B = 3,5-dichlorophenol; C = 2,6-dichloro-4-nitrophenol.

cating that the steric parameters play a considerable role in the retention. However, the more bulky substituents are also more lipophilic, indicating that Fig. 1 does not prove unambiguously

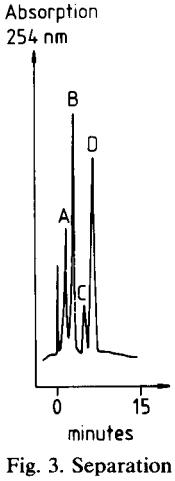

Fig. 3. Separation of some ring-substituted phenol derivatives on a β-cyclodextrin polymer-coated column. Eluent, methanol–water (65+35, v/v); flow-rate, 1 ml min^{-1}; detection wavelength, 254 nm. Peaks: A = 4-fluorophenol; B = 4-chlorophenol; C = 4-bromophenol; D = 4-aminophenol.

TABLE 2

Parameters of linear correlations between the log k' values of some ring-substituted phenol derivatives and the methanol concentration in the eluent (C): log $k' = \log k'_0 + bc$

Compound	Log k'_0	$s_{\log k'_0}$ $\times 10^{-1}$	$-b$ $\times 10^{-2}$	s_b $\times 10^{-3}$	r
1	1.70	1.64	2.51	1.61	0.9858
2	1.96	1.76	2.88	1.91	0.9868
3	2.23	1.93	3.08	1.50	0.9929
4	1.72	1.48	2.26	1.03	0.9939
5	3.96	3.07	4.96	1.14	0.9984
6	7.68	4.31	9.47	6.89	0.9896
7	1.64	1.42	2.26	1.68	0.9838
8	1.47	1.73	2.76	4.51	0.9167
9	0.87	1.15	1.81	0.99	0.9912
10	2.69	2.19	3.55	1.09	0.9972
11	1.75	1.18	2.08	0.71	0.9965
12	0.82	1.04	1.56	1.63	0.9688
13	2.01	1.62	2.63	0.43	0.9992
14	2.04	1.68	2.65	0.52	0.9989
15	2.04	1.65	2.74	0.51	0.9990
16	2.65	2.00	3.31	0.48	0.9994
17	5.24	7.38	8.83	34.2	0.7259
18	2.38	1.79	3.01	0.77	0.9977
19	2.56	1.98	3.21	8.05	0.9978
20	3.06	2.17	3.65	0.52	0.9994
21	1.86	1.63	2.72	1.41	0.9920
22	1.86	1.71	2.71	1.20	0.9932
23	1.68	1.58	2.53	0.95	0.9951
24	2.07	1.57	2.63	0.75	0.9975
25	2.06	1.69	2.60	0.81	0.9971
27	1.25	1.24	1.93	0.84	0.9934
28	2.80	2.12	3.43	0.72	0.9987

the preponderant role of steric parameters. The good separation of positional isomers which are inadequately separated on reversed-phase columns supports the hypothesis about the importance of steric parameters. The retention order of the solutes does not follow the retention order expected according to their lipophilicity. The hydrophilic nitro group enhances the retention (Fig. 2) and the less hydrophobic aminophenol elutes after the more hydrophobic fluoro, chloro and iodo derivatives (Fig. 3). These findings indicate that the retention behaviour of the β-CD polymer column differs from that of the common RP columns.

The parameters of Eqn. 1. are compiled in Table 2. As compound **26** eluted in the dead volume in each eluent, it was omitted from the

calculations. The relationship between the logarithm of the capacity factor and the concentration of organic phase in the eluent was significantly linear in each instance, that is, the retention of phenol derivatives decreases linearly with increasing concentration of the organic component in the eluent. The value of the correlation coefficient in most instances was over 0.9900, proving the applicability of Eqn. 1. This finding further indicates that the phenol derivatives follow the general rule also on the β-CD polymer column, no anomalous retention behaviour being observed. The slope and intercept values differ considerably from each other. This means that the ring-substituted phenol derivatives can be easily separated on the β-CD polymer column with methanol–water eluents.

The parameters in Table 2 make possible the calculation of retention time differences for each pair of phenol derivative at each eluent composition:

$$t_1 - t_2 = t_0(10^{a_1+b_1C} - 10^{a_2+b_2C}) \quad (2)$$

where a_1, a_2 and b_1, b_2 are the intercept and slope values for compounds 1 and 2 at organic phase concentration C. The eluent composition corresponding to the maximum difference in retention times can also be calculated: the first derivative of Eqn. 2 has to be equal to zero and the organic phase concentration has to be expressed accordingly:

$$C = (a_1 - a_2 + \log b_1/b_2)/(b_2 - b_1) \quad (3)$$

A good linear correlation was found between the slope and intercept values of Eqn. 1 (Fig. 4). This result indicates that from chromatographic point of view, the ring-substituted phenol derivatives can be considered as a homogeneous series of compounds.

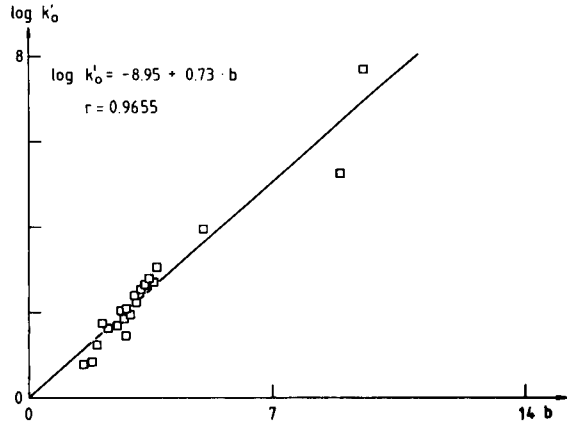

Fig. 4. Relationship between the retention parameters (slope and intercept of Eqn. 1) of some ring-substituted phenol derivatives on a β-CD polymer column.

TABLE 3

Dependence of the retention characteristics of some ring-substituted phenol derivatives on their physico-chemical parameters: results of stepwise regression analysis ($n = 27$)

Parameter	Equation [a]			
	I	II	III	IV
a	1.08	1.59	1.98	2.12
$b_1 \times 10^{-1}$	−7.21	−9.29	1.13	1.67
s_{b_1}	1.30×10^{-1}	1.83×10^{-1}	2.38×10^{-2}	3.24×10^{-2}
Path coefficient (%)	–	–	72.85	71.67
b_2	–	–	−1.37	9.53×10^{-1}
$s_{b_2} \times 10^{-1}$	–	–	5.82	4.35
Path coefficient (%)	–	–	27.15	28.33
r^2	0.5526	0.5280	0.6819	0.6304
F	30.88	27.97	25.72	20.47

[a] (I) $\log k'_0 = a + b_1E_s$, (II) $b = a + b_1E_s$, (III) $\log k_0 = a + b_1E_s^2 + b_2R^2$, (IV) $b = a + b_1E_s^2 + b_2F^2$ where E_s = Taft constant, characterizing steric effects of the substituent, and F and R = Swain–Lupton electronic parameters, characterizing the inductive and resonance effect, respectively.

The parameters of the correlations describing the dependence of the retention characteristics of phenol derivatives on their physico-chemical parameters are given in Table 3. Each equation fits the experimental data well; the significance level was over 99.9% (see F values). Only two physico-chemical parameters explain 53–68% of the total variance (see r^2 values). The lipophilicity value of the substituents did not influence significantly the retention characteristics, as would be expected in an RP separation mode, that is, the separation capacity of the β-CD polymer column differs considerably from that of hydrocarbon-coated columns.

The calculations demonstrated that the steric effects (Taft E_s value) of the substituents have the greatest impact on the retention and the role of electronic parameters is of secondary importance (see path coefficient values). The quadratic functions have a higher information content than the linear functions. This is in good agreement with the fact that the inclusion complex formation requires well defined dimensions of the guest molecules to reach optimum complex stability. When the guest molecules are larger or smaller, the complex stability decreases. This process can be described with the quadratic function. The role of electronic parameters in the retention can be explained by the supposition that the polar substructures of phenol derivatives pointing out of the hydrophobic cyclodextrin cavity may interact with the free hydroxyl group on the surface of the β-CD polymer. These results led to the conclusion that the complex-forming capacity of β-CD prevails even after the polymerization process and significantly modifies the retention behaviour of solutes in common RP eluents.

The results of the modified Free–Wilson analysis are summarized in Table 4. Both equations fit the experimental data well; the significance levels are over 99.9% (see F values). Only a few substituents from those included explain 70–75% of the change of the dependent variables (see r^2 values). The fact that the bulky substituents have the greatest impact on the retention, supports the previous conclusions that the steric parameters have the greatest influence on the retention of phenol derivatives on a β-CD polymer column.

TABLE 4

Influence of various substituents on the retention characteristics of some ring-substituted phenol derivatives: results of modified Free–Wilson analysis ($n = 27$)

Parameters	Equation [a]	
	V	VI
a	1.96	2.69
b_1	5.72	6.78
s_{b_1}	7.44×10^{-1}	1.09
Path coefficient (%)	56.85	51.20
b_2	2.00	2.27
s_{b_2}	7.39×10^{-1}	1.03
Path coefficient (%)	19.87	17.13
b_3	1.69	3.02
$s_{b_3} \times 10^{-1}$	5.41	7.76
Path coefficient (%)	23.28	31.67
r^2	0.7559	0.7009
F	23.74	17.97

[a] (V) $\log k'_0 = a + b[4\text{-}(C(CH_3)_3)] + b_2[6\text{-}C(CH_3)_3] + b_3(4\text{-}NO_2)$, (VI) $b = a + b_1[4\text{-}C(CH_3)_2] + b_2[6\text{-}C(CH_3)_3] + b_3(4\text{-}NO_2)$.

This work was supported by a grant (OTKA 2670) from the Hungarian Academy of Sciences.

REFERENCES

1 J. Szejtli, in J.L. Atwood, J.E. Davis and D.D. McNicol (Eds.), Inclusion Compounds, Vol. III, Academic, London, 1984, pp. 331–390.
2 J. Szejtli, Cyclodextrins and Their Inclusion Complexes, Akadémiai Kiadó, Budapest, 1982.
3 J. Szejtli, B. Zsadon and T. Cserháti, in W.L. Hinze and D.W. Armstrong (Eds.), Ordered Media in Chemical Separation (American Chemical Society Symposium Series, No. 342), American Chemical Society, Washington, DC, 1987, pp. 200–217.
4 T. Cserháti, J. Szejtli and M. Szögyi, J. Chromatogr., 509 (1990) 255.
5 K. Fukushi and K. Hiiro, J. Chromatogr., 518 (1990) 189.
6 J. Liu, K.A. Cobb and M. Novotny, J. Chromatogr., 519 (1990) 189.
7 D.W. Armstrong, W. Li, C.-D. Chang and J. Pitha, Anal. Chem., 62 (1990) 914.
8 D.W. Armstrong, W. Li and J. Pitha, Anal. Chem., 62 (1990) 215.
9 M. Jung, D. Schmalzing and V. Schurig, J. Chromatogr., 552 (1991) 43.
10 M. Gosselet and B. Sebille, J. Chromatogr., 552 (1991) 563.
11 B. Agnus, B. Sebille and M. Gosselet, J. Chromatogr., 552 (1991) 583.

12 K. Shimada, T. Oe and M. Suzuki, J. Chromatogr., 558 (1991) 1306.
13 M. Seno, M. Lin and K. Iwamoto, J. Chromatogr., 508 (1990) 127.
14 M. Seno, M. Lin and K. Iwamoto, J. Chromatogr., 523 (1990) 293.
15 J. Haginaka and J. Wakai, Anal. Chem., 62 (1990) 997.
16 K. Fujimura, S. Suzuki, K. Hayashi and S. Masuda, Anal. Chem., 62 (1990) 2198.
17 C.A. Chang, H. Ji and G. Lin, J. Chromator., 522 (1990) 143.
18 R.R. West and J.H. Cardellina, II, J. Chromatogr., 539 (1991) 15.
19 D.W. Armstrong, A.M. Stalcup, M.L. Hilton, J.D. Duncan, J.R. Faulkner, Jr., and S.-C. Chang, Anal. Chem., 62 (1990) 1610.
20 W.J. Haggerty and E.A. Murrill, Res. Dev., 25 (1974) 30.
21 J.M. McCall, J. Med. Chem., 18 (1975) 549.
22 K. Valkó, S. Olajos and T. Cserháti, J. Chromatogr., 499 (1990) 361.
23 C. Horvath, W. Melander and I. Molnar, J. Chromatogr., 125 (1976) 129.
24 K. Valkó, J. Liq. Chromatogr., 7 (1984) 1405.
25 H. Mager, Moderne Regressionsanalyse, Salle, Sauerlander, Frankfurt am Main, 1982, pp. 135–157.
26 S.M. Free and J.W. Wilson, J. Med. Chem., 7 (1964) 395.

Analytica Chimica Acta, 279 (1993) 115–122
Elsevier Science Publishers B.V., Amsterdam

Application of multivariate mathematical–statistical methods for the comparison of the retention behaviour of porous graphitized carbon and octadecylsilica columns

Esther Forgács and Tibor Cserháti

Central Research Institute for Chemistry, Hungarian Academy of Sciences, P.O Box 17, H-1525 Budapest (Hungary)

Barna Bordás

Plant Protection Institute, Hungarian Academy of Sciences, Budapest (Hungary)

(Received 1st October 1992; revised manuscript received 28th December 1992)

Abstract

The retention of sixteen ring-substituted aniline derivatives on porous graphitized carbon (PGC) column (eluents: acetonitrile–water and methanol–water mixtures) and on octadecylsilica (ODS) column (eluents: methanol–0.025 M K_2HPO_4 mixtures) was determined, and the relationship between retention characteristics and physico-chemical parameters were evaluated by principal component analysis followed by two-dimensional non-linear mapping and by cluster analysis and also by canonical correlation analysis. Calculations proved that marked differences can be detected between the retention characteristics of PGC and ODS columns, and the electronic and steric parameters of aniline derivatives have a great impact on their retention. The comparison of various multivariate mathematical–statistical methods indicated that principal component analysis followed by two-dimensional non-linear mapping is the most appropriate method for evaluation of large data matrices in reversed-phase liquid chromatography.

Keywords: Liquid chromatography; Principal component analysis; Anilines; Canonical correlation analysis; Cluster analysis; Multivariate analysis; Non-linear mapping; Retention behaviour

Application of silica or silica-based supports in liquid chromatography (LC) is limited by the low stability of silica at alkaline pH [1], and the undesirable electrostatic interactions between the polar substructures of solutes and the free silanol groups not covered by the hydrophobic ligand [2,3] limit the use of silica in reversed-phase separations. To decrease or eliminate the effect of residual acidic silanol groups, the eluent has to be buffered or various additives have to be added to the eluent to mask the effect of silanol groups.

Correspondence to: E. Forgács, Central Research Institute for Chemistry, Hungarian Academy of Sciences, P.O. Box 17, H-1525 Budapest (Hungary).

To increase the pH range of application, many other supports have been developed, such as alumina [5], octadecyl-coated alumina [6], zirconia [7,8] and various polymer-based supports. Many efforts have been devoted to the development of graphitized carbon supports [9–21]. Porous graphitized carbon columns (PGC) have been successfully used for the separation of diastereomers [22], geometric isomers [23] and various alkaline compounds [24] such as tioconazole derivatives. The influence of physico-chemical parameters of some ring-substituted phenol derivatives on their retention on PGC columns has also been studied. It has been established that the retention on PGC columns of ring-substituted

phenol derivatives is mainly governed by steric parameters of the substituents [25,26].

Multivariate mathematical–statistical methods such as canonical correlation [27], principal component analysis (PCA) [28] and cluster analysis [29] have been developed to extract maximum information from large data matrices. PCA and cluster analysis have also been successfully used for the evaluation of data structure in LC [30,31]. Canonical correlation analysis (a multivariate method for selecting one group of variables that significantly influence another group of variables) is also suitable for similar objectives, but it appears that it has never been applied to the evaluation of retention data in LC.

The objectives of this investigation were to compare the retention behaviours of some ring-substituted aniline derivatives on PGC and octadecylsilica (ODS) columns, to evaluate the retention data by means of multivariate mathematical–statistical methods and to elucidate the similarities and dissimilarities in the information content of the various methods applied.

EXPERIMENTAL

The LC system consisted of a Liquopump Model 312 pump (Labor MIM, Budapest, Hungary), a CE-212 variable-wavelength UV detector (Cecil Instruments, Cambridge), a Valco (Houston, TX) injector with a 20-μl sample loop and a Model 740 integrator (Waters–Millipore, Milford, MA). The reversed-phase column was Hypersil ODS (150 × 4 mm i.d., particle diameter 5 μm). The flow-rate was 1 ml min^{-1} and the detection wavelength was set to 254 nm. Mixtures of 0.025 M K_2HPO_4–methanol were used as eluents, with methanol contents ranging from 60 to 80% (v/v) (in 5% steps; pH adjusted in each instance to 7.90 with orthophosphoric acid).

The structures of the ring-substituted aniline derivatives are shown in Table 1. The aniline derivatives were dissolved in methanol at a concentration of 0.05 mg ml^{-1}. The retention time of each compound in each eluent was determined with three consecutive measurements. Chromatographic conditions for the determination of the retention of aniline derivatives on the PGC column have been described elsewhere [32].

TABLE 1

Structures of ring-substituted aniline derivatives

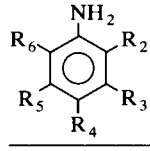

No.	R_2	R_3	R_4	R_5	R_6
1	I	H	H	H	H
2	Cl	H	H	H	H
3	CH_3	H	H	H	H
4	CH_2CH_3	H	H	H	CH_3
5	H	H	Br	H	H
6	H	Br	H	H	H
7	H	H	CH_3	H	H
8	H	H	I	H	H
9	H	H	Cl	H	H
10	H	H	NO_2	H	H
11	Br	H	Br	H	H
12	NO_2	H	NO_2	H	H
13	Cl	H	Cl	H	H
14	H	Cl	H	Cl	H
15	H	CH_3	H	CH_3	H
16	CH_3	H	CH_3	H	CH_3

As the correlation between the log k' value and the organic phase concentration is generally linear in LC, linear equations were also applied to describe the dependence of log k' on the organic mobile phase concentration:

$$\log k' = \log k'_0 + bc \quad (1)$$

Where k' is the capacity factor, k'_0 is the capacity factor extrapolated to zero concentration of organic component in the mobile phase (intercept, related to molecular lipophilicity), b is the change in log k' caused by unit change (1%, v/v) of organic mobile phase concentration (slope, related to the specific adsorption surface in contact with support) and C is the organic mobile phase concentration (%, v/v).

To compare the retention behaviours of aniline derivatives on the PGC and ODS columns the data matrix (parameters of Eqn. 1: slope and intercept values for methanol and acetonitrile on the PGC column and for methanol on the ODS column, total six parameters) were evaluated by multivariate mathematical–statistical methods as follows.

Principal component analysis combined with cluster analysis and with non-linear mapping

The parameters of Eqn. 1 {slope and intercept values, for methanol and acetonitrile on the PGC column (taken from [33]) and for methanol on the ODS column (total six parameters)} were considered as variables and the aniline derivatives were the observations. The limit of the variance explained was set to 99.9%. Both two-dimensional non-linear mapping [34] and cluster analysis were carried out on the principal component loadings. To elucidate the influence of PCA on the data evaluation the cluster analysis was also applied to the original data matrix.

Cluster analysis and non-linear mapping techniques are theoretically similar: both methods calculate and visualize the relative distances between the members of the data matrix (here the solutes and chromatographic parameters). To compare their information content, linear correlations were calculated between the distances determined by non-linear mapping and cluster analysis techniques:

$$y_{1-3} = a + bX_{1-3} \quad (2)$$

where $Y_{1,2}$ = relative distances between LC systems on the non-linear map, Y_3 = relative distances between LC systems on the cluster dendogram (original data matrix), $X_{1,2}$ = relative distances between LC systems on the cluster dendogram after PCA and X_3 = relative distances between LC systems on the cluster dendogram (original data matrix).

To facilitate the calculations only the distances between the nearest neighbours on the maps were included in the equations. The comparison of distances was hampered by the fact that their absolut value depends on the dimensions of the plots. This difficulty was overcome by data normalization: the greatest distances on each map were considered to be 100% and the other distances were calculated accordingly.

Canonical correlation analysis.

To find the molecular characteristics of aniline derivatives that significantly influence their retention on both the PGC and ODS columns, each parameter of Eqn. 1 (dependent variables) was simultaneously correlated with the physico-chemical characteristics of aniline derivatives (independent variables). The physico-chemical parameters included in the calculation were the following: π = Hansch–Fujita substituent constant characterizing hydrophobicity; *H-Ac* and *H-Do* = indicator variables for proton acceptor and proton donor properties, respectively; *M-RE* = molar refractivity; F and R = Swain–Lupton electronic parameters characterizing the inductive and resonance effect, respectively; σ = Hammett constant, characterizing the electron-withdrawing power of the substituent; E_s = Taft constant, characterizing steric effects of the substituent; and B_1 and B_4 = sterimol width parameters determined by the distance of substituents at their maximum perpendicular to attachment.

Calculations were carried out three times, slope + intercept values (calculation I, six dependent variables), slope only (calculation II, three dependent variables) and intercept values only (calculation III, three dependent variables) being the dependent variables. The independent variables were in each instance the molecular characteristics of anilines listed above.

RESULTS AND DISCUSSION

The retention order of solutes is different on the PGC and ODS columns (Fig. 1), demonstrating the differences between the retention mechanisms of the columns. The retention order of solutes on the PGC column does not follow their order of lipophilicity (the more hydrophilic nitro derivatives elute after the more hydrophobic methyl and chloro derivatives).

The parameters of Eqn. 1 are compiled in Table 2. The relationship between the logarithm of capacity factor and the concentration of organic phase in the eluent was linear. In most instances the value of correlation coefficient was over 0.99, proving the applicability of Eqn. 1.

Principal component analysis combined with cluster analysis and with non-linear mapping

The results of PCA are summarized in Table 3. Five principal components explain 95.06% of

the total variance. This result indicates that the six chromatographic systems can be substituted by five background variables. Unfortunately, PCA does not prove the existence of such background variables as concrete physico-chemical entities but only indicates its mathematical possibility. Most of the chromatographic parameters have considerable loadings in the first principal component. This indicates that the chromatographic systems have some common characteristics independently of the different supports and eluents. The slope and intercept values determined on the PGC column with acetonitrile–water and methanol–water eluents have the greatest loadings in the first and second principal components, respectively, that is, acetonitrile and methanol as organic modifiers are different.

The two-dimensional non-linear map of PCA loadings (LC systems) is shown in Fig. 2. The eluent systems for two distinct clusters containing separately the slope and intercept values. This result suggests that the adsorption capacity (related to the intercept value) and specific adsorption surface (related to the slope value) of the columns show some similarity.

The dendograms of cluster analysis calculated from the original data matrix and from the PC

TABLE 2

Parameters of linear correlations between the logarithm of capacity factor and the methanol concentration (C) in the eluent: $\log k' = \log k'_0 + bC$

Compounds	Log k'_0	$-b \times 10^{-2}$	$s_b \times 10^{-3}$	r
1	0.79	0.30	1.8	0.9928
2	0.63	0.33	1.2	0.9973
3	0.53	0.40	2.2	0.9937
4	0.74	0.18	3.3	0.9984
5	0.66	0.27	2.5	0.9946
6	0.66	0.25	2.4	0.9915
7	0.55	0.46	2.3	0.9948
8	0.78	0.50	1.6	0.9980
9	0.60	0.37	2.1	0.9933
10	0.41	0.46	2.8	0.9925
11	0.79	0.28	1.1	0.9967
12	0.63	0.37	3.3	0.9941
13	0.83	0.39	1.2	0.9905
14	0.75	0.27	0.6	0.9998
15	0.74	0.32	1.6	0.9947
16	0.64	0.43	1.1	0.9917

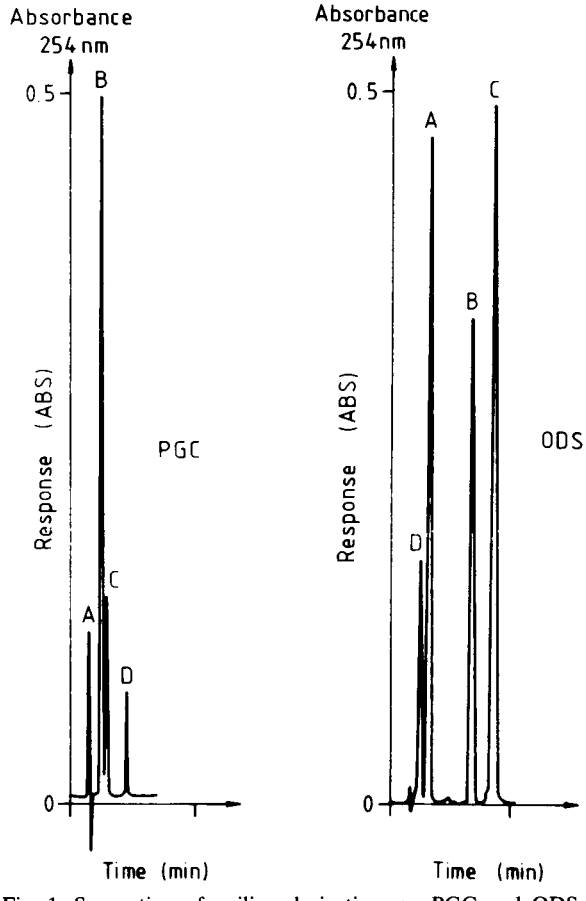

Fig. 1. Separation of aniline derivatives on PGC and ODS column. Eluent for PGC column, methanol–water (90+10, v/v); eluent for ODS column, methanol–0.025 M K_2HPO_4 (80+20, v/v); flow-rate, 1 ml min^{-1}; detection, 254 nm. Peaks: A = aniline; B = 2-methylaniline; C = 2-chloroaniline; D = 2-nitroaniline

loadings are shown in Figs. 3 and 4, respectively. The clusterings of chromatographic parameters are strikingly different, emphasizing the considerable impact of PCA on the clustering of chromatographic systems.

The comparison of the information content of cluster analysis and PCA followed by two-dimensional non-linear mapping resulted in only one significant linear correlation (between the relative distances of the two-dimensional non-linear map and the cluster analysis carried out after PCA):

$$Y_1 = 1.94 - 1.44X_1 \quad (3)$$

$n = 6$; $r = 0.9743$; $S_b = 0.23$; $r_{99\%} = 0.9740$

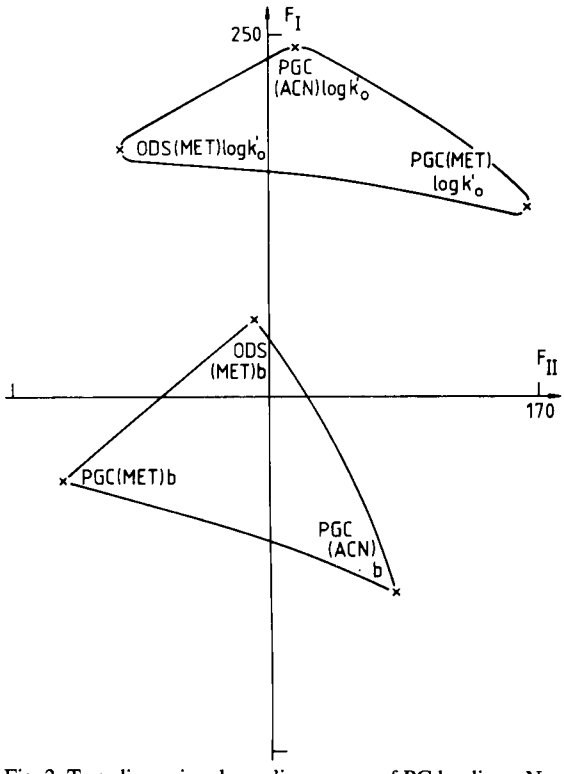

Fig. 2. Two-dimensional non-linear map of PC loadings. Number of iterations, 60; maximum error, 2.7×10^{-3}. PGC = porous graphitized carbon column; ODS = octadecylsilica column; ACN = acetonitrile–water eluent systems; MET = methanol–water eluent systems; $\log k'_0$ = intercept value in Eqn. 1; b = slope values in Eqn. 1.

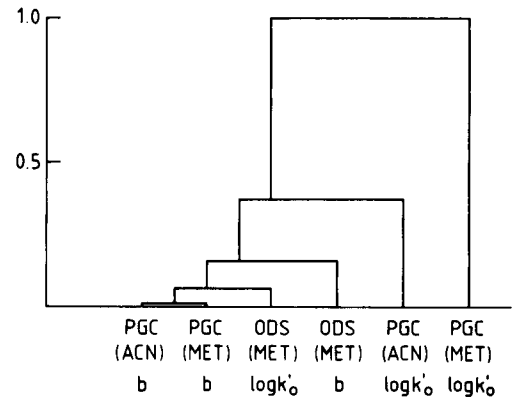

Fig. 3. Dendogram calculated from original data matrix. Symbols as in Fig. 2.

This finding indicates that the information contents of a non-linear map and a cluster dendogram may be similar. However, the application of the two-dimensional non-linear mapping technique instead of cluster analysis is strongly advocated. It is assumed that the two-dimensional non-linear map may contain more information than the one-dimensional structure of clusters.

Canonical correlation analysis

Canonical correlation analysis found three significant correlations. The parameters of significant correlations are compiled in Tables 4–6.

TABLE 3

Comparison of the retention characteristics of PGC and ODS columns: results of principal component analysis [a]

	Eigenvalue		Total variance explained (%)		
(1)	2.35		39		
(2)	1.91		71		
(3)	0.95		87		
(4)	0.46		95		
Column	Parameter	Organic modifier	Principal component loadings		
			1	2	3
PGC	Log k'_0	ACN	0.84	0.27	0.24
PGC	b	ACN	0.73	−0.33	0.43
PGC	Log k'_0	MET	0.63	−0.72	0.22
PGC	b	MET	0.59	0.75	−0.20
ODS	Log k'_0	MET	0.56	0.59	0.21
ODS	b	MET	0.17	0.53	0.75

[a] PGC = porous graphitized carbon column; ODS = octadecylsilica column; ACN = acetonitrile–water eluent systems; MET = methanol–water eluent systems; log k'_0 = intercept values in Eqn. 1; b = slope values in Eqn. 1.

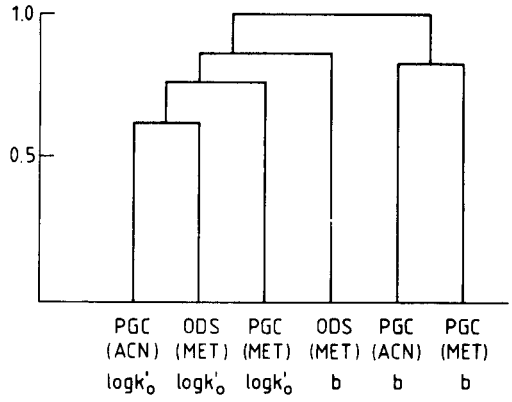

Fig. 4. Dendogram calculated from PCA loadings. Symbols as in Fig. 2.

When both the slope and intercept values were taken into consideration (Table 4), the relative weight of the slope value determined on the PGC column with acetonitrile–water eluent systems contains most of the information. This indicates again that the dependence of the retention of aniline derivatives on the physico-chemical parameters is different on PGC and ODS columns.

TABLE 4

Relationship between the physico-chemical parameters and retention characteristics of some aniline derivatives: results of canonical correlation analysis II ($r^2 = 0.9998$; $\chi^2 = 110.26$; $\chi^2_{99.9\%} = 73.40$)

Variables	Canonical coefficients	
	Standard	Weighted (%)
Chromatographic parameters		
(PGC) log k'_0 (ACN)	7.56×10^{-1}	1.28
(PGC) b (ACN)	5.88×10^{-1}	94.1
(PGC) log k'_0 (MET)	1.52×10^{-1}	1.24×10^{-1}
(PGC) b (MET)	3.49×10^{-1}	3.36×10^{-1}
(ODS) log k'_0	2.11×10^{-1}	2.51
(ODS) b	1.10×10^{-1}	1.62
Physico-chemical parameters		
π	5.37×10^{-2}	1.81
H-Ac	5.39×10^{-1}	30.8
M-RE	1.70×10^{-3}	9.00×10^{-3}
F	-4.20×10^{-2}	1.76
R	2.66×10^{-1}	29.1
σ	-8.95×10^{-1}	3.41
E_s	2.16×10^{-2}	2.83×10^{-1}
B_1	8.97×10^{-1}	21.1
B_4	6.93×10^{-1}	11.7

TABLE 5

Relationship between the physico-chemical parameters and retention characteristics of some aniline derivatives: results of canonical correlation analysis II ($r^2 = 0.9885$; $\chi^2 = 54.43$; $\chi^2_{99.9\%} = 50.90$)

Variables	Canonical coefficients	
	Standard	Weighted (%)
Chromatographic parameters		
(PGC) b (ACN)	1.85×10^{-1}	13.9
(PGC) b (MET)	-6.18×10^{-1}	46.2
(ODS) b	5.34×10^{-1}	39.9
Physico-chemical parameters		
π	-7.60×10^{-2}	66.9
H-Ac	5.98×10^{-2}	3.56
M-RE	1.48×10^{-1}	12.1
F	-4.18×10^{-1}	4.40
R	1.58×10^{-1}	2.83
σ	1.64×10^{-1}	3.00×10^{-1}
E_s	5.63×10^{-1}	7.37
B_1	-6.67×10^{-1}	2.29
B_4	-1.38×10^{-1}	1.62×10^{-1}

The data suggest that the electronic (*H-Ac*, *R*) and steric parameters (B_1 and B_4) have the greatest impact on the retention of aniline derivatives on the PGC column using acetonitrile–water mixtures as eluents.

TABLE 6

Relationship between the physico-chemical parameters and retention characteristics of some aniline derivatives: results of canonical correlation analysis III ($r^2 = 0.9505$; $\chi^2 = 43.97$; $\chi^2_{95\%} = 43.80$)

Variables	Canonical coefficients	
	Standard	Weighted%
Chromatographic parameters		
(PGC) log k'_0 (ACN)	-8.57×10^{-2}	1.23
(PGC) log k'_0 (MET)	-2.38×10^{-1}	1.64
(ODS) log k'_0	9.64×10^{-1}	97.1
Physico-chemical parameters		
π	-1.47×10^{-1}	3.35
H-Ac	-7.31×10^{-1}	28.2
M-RE	5.83×10^{-1}	2.22
F	-2.47×10^{-1}	7.00
R	-5.18×10^{-1}	38.5
σ	-4.13×10^{-1}	10.6
E_s	-3.85×10^{-1}	3.40
B_1	-3.04×10^{-1}	4.82
B_4	-1.49×10^{-1}	1.71

The results of canonical correlation II (only slope values included) are shown in Table 5. In contrast to canonical correlation analysis I, each slope value has a considerable weight in the correlation, indicating that the specific contact surface (slope value) of aniline derivatives depends on the same physico-chemical parameters on both PGC and ODS columns. Lipophilicity (π values) and molar refractivity (*M-RE* values) have the greatest influence on the specific adsorption surface.

The results of canonical correlation III (only intercept values included) are given in Table 6. The adsorption capacity (intercept values) of chromatographic systems depends on different physico-chemical parameters of aniline derivatives. The electronic parameters (*H-Ac*, *R* and σ values) have the greatest impact on the adsorption capacity of the ODS column. This surprising result can be explained by the supposition that the polar substructures of aniline derivatives interact with the free silanol groups on the surface of the ODS support, modifying in this manner the adsorption capacity of the support.

The individual contributions of aniline derivatives to the correlations are shown in Table 7. Their contribution differs according to the type of correlation. The bulky substituents exert the greatest influence in canonical correlation I, supporting the conclusions drawn from the data in Table 4 that the steric parameters have a considerable impact on the retention of aniline derivatives on the PGC column. The highly hydrophilic nitro and highly lipophilic bromo substituents have a considerable impact on the slope values determined on both the PGC and ODS columns in canonical correlation II, emphasizing again the importance of molecular lipophilicity in the correlation.

It can be concluded that the use of principal component analysis followed by two-dimensional non-linear mapping is superior to cluster analysis in the evaluation of reversed-phase retention data. Canonical correlation analysis proved to be a valuable tool for evaluating the simultaneous influence of the physico-chemical parameters of solutes on the retention capacity of PGC an ODS columns.

This work was supported by a grant (OTKA 2670) from the Hungarian Academy of Sciences.

TABLE 7

Contributions (arbitrary units) of individual phenol derivatives to the relationship between retention characteristics and physico-chemical parameters (results of canonical correlation analysis)

Compound	Canonical correlation analysis		
	I	II	III
1	−0.01	0.63	−0.11
2	−0.24	−0.51	−0.25
3	−0.29	−1.12	0.81
4	−0.68	1.08	0.47
5	−0.15	−0.07	−0.17
6	−0.26	0.04	−0.06
7	−0.52	−0.48	0.09
8	−0.11	0.63	−0.22
9	−0.24	−0.51	−0.17
10	0.88	−2.19	0.21
11	0.28	1.28	−0.67
12	1.19	−1.15	0.10
13	0.25	0.83	−0.87
14	0.21	1.03	−0.66
15	−0.04	0.61	1.37
16	−0.16	−0.09	0.13

REFERENCES

1 A. Berthod, J. Chromatogr., 549 (1991) 11.
2 A. Nahum and Cs. Horváth, J. Chromatogr., 203 (1981) 53.
3 K.E. Bij, Cs. Horváth, W.R. Melander and A. Nahum, J. Chromatogr., 203 (1981) 65.
4 H. Tayer, H. Waterbeend and B. Testa, J. Chromatogr., 320 (1985) 305.
5 C.J. Laurent, H.A.H. Billiet and L. de Galan, J. Chromatogr., 285 (1984) 161.
6 J.J. Sun and J.S. Fritz., J. Chromatogr., 522 (1990) 95.
7 J.A. Blackwell and P.W. Carr, J. Chromatogr., 549 (1991) 43.
8 J.A. Blackwell and P.W. Carr, J. Chromatogr., 549 (1991) 59.
9 H. Colin, C. Eon and G. Guichon, J. Chromatogr., 119 (1976) 41.
10 H. Colin, C. Eon and G. Guichon, J. Chromatogr., 122 (1976) 233.
11 H. Colin and G. Guichon, J. Chromatogr., 126 (1976) 43.
12 Z. Plzak, F.P. Dousek and J. Janska, J. Chromatogr., 147 (1978) 137.
13 V. Patzelova, J. Jansta and F.P. Dousek., J. Chromatogr., 148 (1978) 53.

14 T.H. Zwier and M.F. Burke, Anal. Chem., 53 (1981) 812.
15 P. Ciccioli, R. Tappa, A. di Corcia and A. Liberti, J. Chromatogr., 206 (1981) 35.
16 K. Unger, P. Roumeliotis, H. Müller and H. Goetz, J. Chromatogr., 202 (1980) 3.
17 M.T. Gilbert, J.H. Knox and B. Kaur, Chromatographia, 16 (1982) 138.
18 J.H. Knox, K. Unger and H. Müller, J. Liq. Chromatogr., 6 (1983) 1.
19 J.H. Knox, B. Kaur and G.R. Millward, J. Chromatogr., 352 (1986) 3.
20 O. Chiantore, I. Novak and D. Derek, Anal. Chem., 60 (1988) 638.
21 J.H. Knox and B. Kaur, in P.R. Brown and R.A. Hartwick (Eds.), High Performance Liquid Chromatography, Wiley, New York, 1989 pp. 189–222.
22 B. Kaur, LC·GC, 3 (1990) 41.
23 D. Derek and J. Novak, Chromatographia, 30 (1990) 582.
24 J.C. Berridge, J. Chromatogr., 449 (1988) 317.
25 E. Forgács, T. Cserháti and K. Valko, J. Chromatogr., 592 (1992) 75.
26 E. Forgács, K. Valkó and T. Cserháti, J. Liq. Chromatogr., 14 (1991) 3457.
27 L. Orloci, C.R. Rao and W.M. Stiteler, Multivariate Methods in Ecological Work, International Co-operative Publishing House, Fairland, MD, 1979.
28 K.V. Mardia, J.T. Kent and J.M. Bibby, Multivariate Analysis, Academic, London, New York, 1979.
29 P. Willett, Similarity and Clustering in Chemical Information Systems, Research Studies Press, New York, 1987.
30 M.G. Ford and D.J. Livingstone, Quant. Struct.–Act. Relat., 9 (1990) 107.
31 V.S. Rose, I.F. Croall and J.H. MacFie, Quant. Struct.–Act. Relat., 10 (1991) 350.
32 E. Forgács and T. Cserháti, J. Chromatogr., 600 (1992) 43.
33 E. Forgács and T. Cserháti, Chromatographia, 33 (1992) 357.
34 T. Cserháti, B. Bordás, L. Ekiert and J. Bojarski, J. Chromatogr., 287 (1984) 386.

Analytica Chimica Acta, 279 (1993) 123–127
Elsevier Science Publishers B.V., Amsterdam

High-performance size-exclusion chromatography of proteoglycans extracted from bovine articular cartilage

P.M. Dekeyser, S. De Smedt, K. Vercruysse, J. Demeester and A. Lauwers

Laboratory of General Biochemistry and Physical Pharmacy, University of Ghent, Wolterslaan 16, Ghent (Belgium)

(Received 1st October 1992; revised manuscript received 10th March 1993)

Abstract

The applicability of high-performance size-exclusion chromatography for determining the relative molecular weight of proteoglycans was tested with a new type of column. The method is extremely reproducible, precise and rapid and allows molecular weight determinations up to 3 millions, even done in the presence of considerable impurities of low molecular weight. This technique offers important advantages over the traditional techniques, such as light scattering, sedementation velocity and equilibrium ultracentrifugation and viscosity. The peak position method was used to calibrate our system using pullulan standards. For the pullulan standards in the molecular weight range between 1.0×10^4 and 8.5×10^5, an almost linear relationship between log M_p and the ratio between the retention time of the standard and that of the excluded salt was found. For the lower molecular weight standards, even at the lowest measured concentration, the curve deviated sharply for ratios above 0.80. The influence of the flow-rate on this ratio was negligible. We were able to separate the proteoglycan aggregates from the proteoglycan monomers in the KCl extracts. In the $CaCl_2$ extract however, we could not separate the monomers from the aggregates, since these were present in a much higher concentration than in the KCl extract. After the addition of hyaluronidase from bovine testes, the proteoglycan aggregates were broken down by lysis of the hyaluronic acid molecules, who are essential for the formation of these aggregates.

Keywords: Chromatography; Bovine articular cartilage; Proteoglycans

The extracellular matrix of articular cartilage contains several types of proteoglycans, which consist of a protein core to which glycosaminoglycans are covalently bound. Large proteoglycan monomers, with a molecular weight ranging from 1 to 4 millions, are composed of a core protein, with many chondroitin sulphate and keratan sulphate chains attached to it [1].

Only a small portion of the molecule (5–20%) is accounted for by the protein. Although this portion may appear to be very small, it contains both structural and functional domains which are essential for the biological function of the molecule. The domains, found in hyaline cartilage, are the hyaluronate binding region, a keratan sulphate-rich region and a chondroitin sulphate-rich region. Most monomers can interact with hyaluronate through a globular portion of the core protein to form large aggregates. This interaction is non-covalent and requires a strand of hyaluronate of at least ten monosaccharides length for binding. The stability of this interaction is highly increased by link proteins, which can bind to both the proteoglycan monomer and the hyaluronate chain. Aggregates containing up to 50 monomers can be formed.

Another domain of the proteoglycan core protein is the keratan sulphate-rich region. It contains about 60% of the keratan sulphate and

Correspondence to: P.M. Dekeyser, Laboratory of General Biochemistry and Physical Pharmacy, University of Ghent, Wolterslaan 16, Ghent (Belgium).

about 10% of the chondroitin sulphate. The largest domain, is the chondroitin sulphate-rich region, which represents approximately 60% of the chondroitin sulphate and 40% of the keratan sulphate.

In total 3 types of large proteoglycan monomers are encountered in bovine articular cartilage.

Additionally, two types of small non-aggregating proteoglycans have been characterized in bovine articular cartilage [2]. These species of proteoglycans, containing dermatan sulphate differ in core protein and contain one or two dermatan sulphate chains. In total, several types of large aggregating proteoglycans, together with at least two species of small non-aggregating proteoglycans have been found in bovine articular cartilage by several authors [3].

We present here an attempt to separate the different species of proteoglycans, from cartilage extract by high-performance size-exclusion chromatography (HP-SEC) on the basis of their differences in hydrodynamic volume.

MATERIALS AND METHODS

All chemicals used were of p.a. grade.

Specimens

Slices of bovine articular cartilage were collected immediately after killing a three years old cow. Those specimens were chilled in ice during transport and were stored at −20°C until extraction.

Extraction

Approximately 6 g of frozen cartilage was hydrated at −4°C with 30 ml of 2 M $CaCl_2$ or 0.15 M KCl. After 2 h the cartilage was cut into fine slices of maximum 1 mm thick and then extracted during 24 h at −4°C. After removal of the extraction solution by centrifugation (for 10 min at 900 *g*), the extraction was continued for another 24 h with 30 ml fresh extraction solution. The combined supernatants were thoroughly dialysed against distilled water until they were free of chloride ions (no precipitation with $AgNO_3$).

HP-SEC

Size exclusion chromatography was performed on a Waters LC instrument with a R410 differential refractometer detector. The retention times of the peaks and all calculations were done by the Baseline 810 software module of the instrument. The system contained one 510 LC pump and the injection was carried out with an U6K injector. All flow connections were made as short as possible.

HP-SEC was performed on a series of Ultrahydrogel columns of Waters (300 × 7.8 mm i.d.). A combination of a Ultrahydrogel 1000, 2000 and DNA column was used. Ultrahydrogel consists of a hydroxylated polymethacrylate packing with residual carboxyl groups. The columns are stable over a pH range from 2 to 12. The LC elution solvent was 0.5 M NaCl.

Precise determination of the exclusion volume was not possible because of the inavailability of well-characterized water-soluble high-molecular weight standards. According to the manufacturer, the exclusion limit corresponds for the Ultrahydrogel 1000 to a molecular weight of 1×10^6 and for the Ultrahydrogel 2000 and DNA to a molecular weight of 7×10^6 using polyethylene glycols. The limit of the included volume is identified on all chromatograms by the solvent peak.

Molecular weight standards

Pullulan standards were obtained from Showa Denko (Shodex Standard P-82). These standards have been characterized by a ultracentrifugal sedimentation equilibrium method. The standards were dissolved in the 0.5 M NaCl solution at 0.3 mg ml^{-1} (total polymer weight per sample). Pullulan, a neutral polysaccharide, was chosen to avoid ionic interactions problems.

Bovine cartilage extracts

Aliquots (100 μl) of each extract were injected on the columns.

Proteolytic degradation of proteoglycans in cartilage extracts

Trypsin (E.C. 3.4.21.4), 42.9 Eur. Pharm. U mg^{-1}, was obtained from the Centre for Standards of the International Commission on Phar-

maceutical Enzymes of the FIP (Ghent). An aliquot (200 μl) of an enzyme solution (0.1 mg ml^{-1} in 50 mM Tris–HCl buffer, pH 7.5) was mixed with 300 μl cartilage extract and 500 μl buffer solution. The mixture was incubated 90 min at 37°C.

Degradation of the hyaluronic acid by hyaluronidase

Hyaluronidase (E.C. 3.2.1.35), 110 FIP U mg^{-1}, was obtained from the Centre for Standards, FIP. 900 μl of the $CaCl_2$ extract was incubated with 100 μl of a 0.01 and a 0.1 mg ml^{-1} solution of hyaluronidase for 24 h at 37°C. 200 μl aliquots of the extract were then injected on the LC columns.

RESULTS AND DISCUSSION

All standards and aliquots of the extracts eluted within the inclusion volume of the columns. The calibration curve was made using the peak position method [4]. We used monodisperse pullulan standards and the ratio between the retention time of the standard and the retention time of the excluded salt (K) of the peaks (ordinate) was plotted against log M_p (abscissa) (M_p = molecular weight of the peak). A linear relationship was found for pullulan standards with M_p values ranging from 1.0×10^5 to 8.5×10^5. It was however impossible to determine the upper limit of the linear area because there were no pullulan standards available with a weight average molecular weight (MW) $> 8.5 \times 10^5$. Figure 1 shows the linear relationship between K and log M_p which sharply deviates from the linear curve for ratios above 0.80.

The reproducibility of our measurements was very good. Mean and standard deviation for each standard at 1 mg ml^{-1} are given in Table 1. The largest relative standard deviation among replicate determinations was less than 0.5%.

As shown in Table 1, the reproducibility was even better when the K values were used instead of the retention times. The largest relative standard deviation among replicate determinations was less than 0.15%.

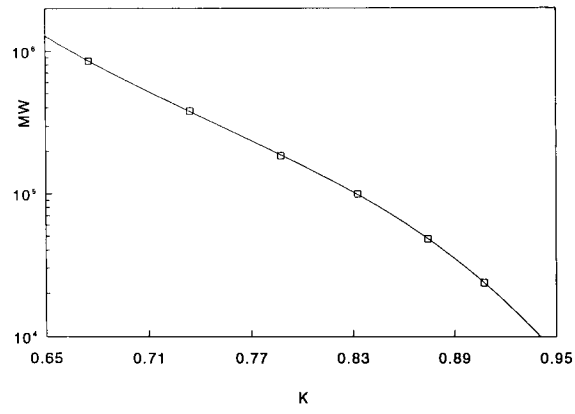

Fig. 1. HP-SEC standard curve for pullulan. Pullulan standards with varying mean molecular weights from 2.37×10^4 to 8.53×10^5 were chromatographed as described under Materials and methods. Each point represents the mean value of K, calculated from four different chromatograms. The column flow-rate was 0.6 ml min^{-1}. The ordinate is in log units and the line drawn is a cubic least squares fit showing the linearity of the procedure in the range between 1.0×10^5 and 8.53×10^5. The equation of this fitted line was used to obtain the relative molecular weights of unknowns from their K values. Log $M_p = A_3 \times K^3 + A_2 \times K^2 + A_1 \times K + A_0$; $A_0 = 32.86 \pm 0.02$, $A_1 = -99.12 \pm 0.09$, $A_2 = 125.7 \pm 0.1$, $A_3 = -56.29 \pm 0.05$, coefficient of correlation = −0.996.

Large errors can be introduced when the columns are overloaded. The increase of the peak width and the retention time with increasing concentration is called the concentration effect [5]. It can be seen from Fig. 2 that the retention times are independent from the concentration for concentrations less than 0.8 mg ml^{-1}. For lower molecular weight samples, no peak distortion was

TABLE 1

Results for pullulan standards

Pullulan standards		Retention times (min)		K	
Type	M_p ($\times 10^4$)	Mean [a]	S.D.	Mean [a]	S.D.
P-800	85.3	39.2	0.1	0.6748	0.0009
P-400	38.0	42.65	0.06	0.7347	0.0008
P-200	18.6	45.8	0.1	0.7883	0.0006
P-100	10.0	48.39	0.02	0.8335	0.0003
P-50	4.80	50.8	0.1	0.8739	0.0004
P-20	2.37	52.71	0.02	0.9080	0.0002

[a] $n = 4$.

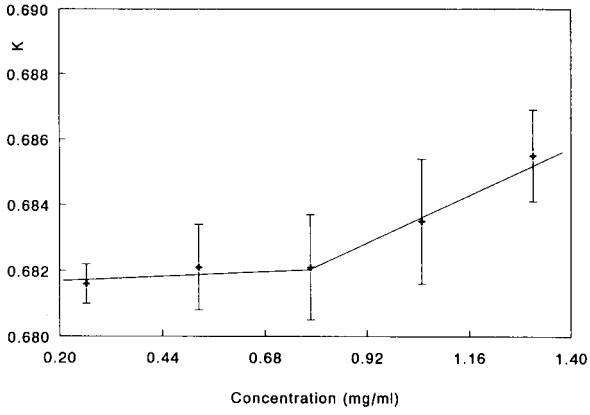

Fig. 2. Effect of concentration on the K value of pullulan. Samples of the pullulan standard 8.53×10^5 were prepared at various concentrations and chromatographed as described under Materials and methods. Each point represents a mean of K values $\pm$ S.D., calculated from three separate chromatograms.

observed in the concentration range used. For HP-SEC it was pointed out that the concentration dependency is also determined by the flow-rate [4].

Contrary to the well defined pullulan standards, natural polymers, such as proteoglycans, have broad molecular weight distributions. Moreover, proteoglycans are complex mixtures of monomers and aggregates, rendering their analysis even more difficult. We have analysed proteoglycans from cartilage extracts, extracted with salt solutions of different ionic strength. Our first extract was made using 0.15 M KCl and consisted mostly of proteoglycan monomers, since the elution pattern remained the same after incubation of the extract with hyaluronidase. In sharp contrast with the 0.15 M KCl extract, the $CaCl_2$ extract contained much more aggregates with very high molecular weight components. Figure 3a and b shows the substantial difference between these two extracts.

Treatment of the $CaCl_2$ extract with hyaluronidase increased as expected the retention times, resulting from enzymatic breakdown of the hyaluronate molecules, who are essential for the stability of the proteoglycan aggregates. Figure 3c illustrates the effects of hyaluronidase digestion on the chromatographic behaviour of the $CaCl_2$ extract. Prior to enzymatic digestion three peaks are observed (cf. Fig. 3b). The broad peak at 47 min corresponds to the proteoglycans; the small peak at 53 min corresponds to proteins and the large negative peak is due to the difference in the refractive index between the sample buffer and

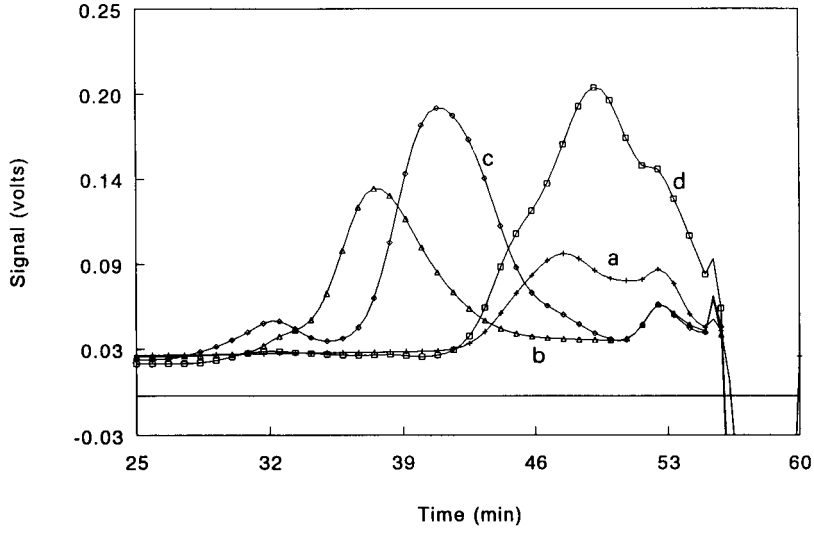

Fig. 3. HP-SEC on Ultrahydrogel 1000/2000/DNA of (a) the KCl extract of bovine hyaline cartilage, (b) $CaCl_2$ extract, (c) $CaCl_2$ extract after treatment with trypsin and (d) hyaluronidase.

the elution buffer. The latter peak also presents the lower limit of migration for molecular sieving. After prolonged incubation with hyaluronidase (24 h) the high molecular weight proteoglycan peak is shifted to the right. The $CaCl_2$ extract was also incubated with trypsin to investigate the impact of proteolytic enzymes on the proteoglycan aggregates and monomers. We found that both aggregates and monomers are easily degradated by trypsin (Fig. 3d). We observed that the area under the curve changes during the enzymatic degradation of the proteoglycans. This can probably be explained by the fact that proteoglycans are heterogeneous polymers and that by consequence heterogeneous products are formed during the degradation. The spectral characteristics (e.g., dn/dc value) of these degradation products are different from those of the original polymer.

Using HP-SEC combined with an enzymatic breakdown study, allows thus the determination of the nature of the proteoglycans and their relative molecular weights. To determine the absolute molecular weight of proteoglycan monomers, the separation of the different fractions and the determination of their intrinsic viscosities are in progress. The Mark–Houwink constants and the universal calibration method will be used to determine the absolute molecular weights. An alternative procedure to characterize these polymers is the use of gel permeation chromatography with low angle light scattering (GPC-LALLS) [6], a combination of the classical HP-SEC with a low angle light-scattering detector and a refractive index detector.

Conclusions

The most important advantage of HP-SEC over traditional techniques, such as light scattering, sedimentation velocity and equilibrium centrifugation and rheology is the fact that this technique allows the study of the distribution of the molecules present in the sample. It is a simple, rapid and precise technique, which does not require a sophisticated and expensive instrumentation. HP-SEC is a technique indicated for the rapid analysis of natural polymers, used in food as well as in pharmaceutical industries.

REFERENCES

1 S.L. Carney, in M.F. Chaplin and J.F. Kennedy (Eds.), Carbohydrate Analysis, IRL Press, Oxford, Washington, DC, 1986, pp. 97–141.
2 V. Vilim and J. Krajickova, Biochem. J., 273 (1991) 579.
3 D. Heinegard, A. Björne-Persson, L. Cöster, A. Franzen, S. Gardell, A. Malmström, M. Paulsson, R. Sandfalk and K. Vogel, Biochem. J., 230 (1985) 181.
4 T. Malfait, D. Slootmaekers and F. Van Cauwelaert, J. Appl. Polym. Sci., 39 (1990) 571.
5 J. Janca, J. Chromatogr., 134 (1977) 263.
6 K. Konishi, in P.L. Dubin (Ed.), Aqueous Size-Exclusion Chromatography (J. Chromatogr. Library, Vol. 40), Elsevier, Amsterdam, 1988, pp. 327–342.

Analytica Chimica Acta, 279 (1993) 129–134
Elsevier Science Publishers B.V., Amsterdam

Catalytic antibodies: new developments

R. Hilhorst

Department of Biochemistry, Agricultural University, Dreijenlaan 3, 6703 HA Wageningen (Netherlands)

(Received 1st October 1992; revised manuscript received 29th December 1992)

Abstract

Both antibodies and enzymes can specifically recognize and bind other molecules. In the case of enzymes and of antibodies ellicited against a transition state analogue of a reaction, binding is followed by catalysis. The first catalytic antibodies were generated against phosphonate-containing transition-state analogues, and catalysed hydrolytic reactions. Since those reports, antibody catalysis was shown to be feasible for many different types of reactions. Evidence has been presented that factors other than stabilization of the transition state can contribute to catalysis. These insights can be employed in the design of haptens. An alternative and complementary approach to the generation of catalytic antibodies is modification of antibodies, either by chemical introduction of catalytic groups or by site-directed mutagenesis. Potential applications of catalytic antibodies can be envisaged in the fields of analytical chemistry and medicine and as catalysts in the chemical industry. The limited availability of antibodies still hampers their application, but rapid progress is being made in the cloning of antibody fragments in a variety of host systems, e.g., *Escherichia coli*, yeast, hybridomas and plants. The expression of a combinatorial library of antibody heavy- and light-chain fragments in phage λ permits the screening of large numbers of antibodies that possess the desired binding or catalytic properties, and might eventually make immunization of animals redundant.

Keywords: Antibodies; Catalytic antibodies

Until recently it was assumed that only enzymes were able to catalyse reactions. In the mid-1980s, two new classes of biological catalysts were reported: RNA and antibodies [1–3]. Whereas the catalytic activity of RNA came as a surprise, catalysis by antibodies had already been envisaged by Jencks [4], who wrote in 1969, "If complementarity between the active site and the transition state contributes significantly to enzyme catalysis, it should be possible to synthesize an enzyme by constructing such an active site. One way to do this is to prepare an antibody to a haptenic group which resembles the transition state of a given reaction. The combining sites of such antibodies should be complementary to the transition state and should cause an acceleration by forcing bound substrates to resemble the transition state."

Attempts to verify this hypothesis by demonstrating catalytic activity with polyclonal antibodies were not succesful until much later [5]. The development of hybridoma technology for the production of monoclonal antibodies by Köhler and Milstein [6] provided the means for detecting catalytic activity in antibodies.

Correspondence to: R. Hilhorst, Department of Biochemistry, Agricultural University, Dreijenlaan 3, 6703 HA Wageningen (Netherlands).

STRUCTURE OF ANTIBODIES

Most catalytic antibodies belong to the IgG class. These antibodies consist of two heavy chains and two light chains, containing 450 and 212 amino acids, respectively. Covalent disulphide linkages exist between the two heavy chains and

between the heavy and light chains (Fig 1). In Fig. 1 the four different domains of an immunoglobulin are indicated. The amino acid sequence of three domains is relatively constant for different antibodies. The constant regions of the heavy chain are named C_{H1}, C_{H2} and C_{H3} and the constant region of the light chain C_L. The heavy chain constant regions are responsible for effector functions, such as complement fixation and binding to receptors. Antibodies are bivalent, i.e., they contain two binding sites. These binding sites are located at the *N*-terminal end of the heavy and light chain. Loops from both chains are involved in antigen binding. The amino acid sequence at the *N*-terminal end of the heavy and light chain depends on the antibody. In the variable regions, three hypervariable stretches are present, approximately at residues 24–34, 50–56 and 89–97 for the light chain and at 31–35, 50–65 and 95–102 for the heavy chain. These are termed the complementarity-determining regions (CDRs). Whereas the more conserved regions (the framework regions FR1, FR2, FR3 and FR4) of the variable regions form β-sheets, the hypervariable regions are loops (Fig. 2). The spatial structure of the variable region of the heavy and light chain is very similar. The three loops of the heavy and those of the light chain form the combining site of the antibody. The antigen binding sites are located at the tip of the arms of the Y-shaped antibody. The arms (Fab fragment) are

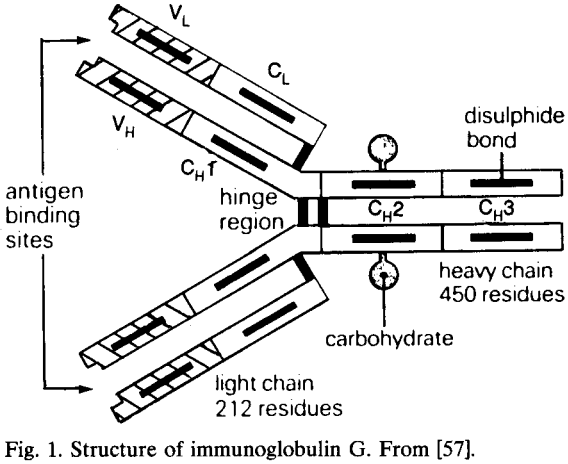

Fig. 1. Structure of immunoglobulin G. From [57].

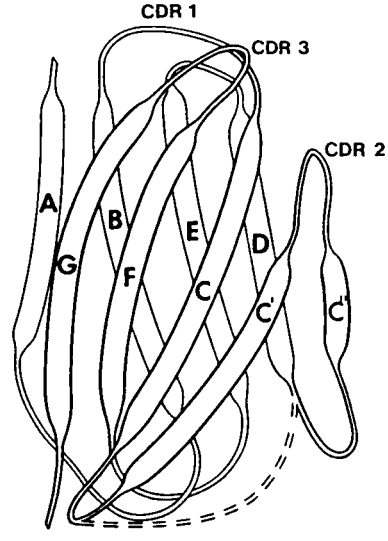

Fig. 2. Structure of the V domains of immunoglobulins. From [58].

flexibly attached to the stem of the Y (the Fc fragment). Fab fragments are easily prepared by treatment of antibodies with pepsin.

The binding of an antigen is generally very tight (dissociation constants are of the order 10^{-6}–10^{-12} M). Binding energy is provided by hydrophobic and electrostatic interactions and by the large contact area. The surface area of the binding pocket is in the order of 600 A^2, allowing interaction with about seven amino acid residues of the antigen.

CATALYSIS BY ANTIBODIES

Two groups reported independently hydrolytic activity with antibodies [2, 3]. In the first case, antibodies were raised against a mechanistically designed hapten, the transition state analogue of a carboxylic ester. Hydrolysis of a related ester by two of the obtained antibodies was observed. In the second case, existing antibodies against *p*-nitrophenylphosphorylcholine were shown to hydrolyse structurally related carbonates. This proved that antibodies raised against a transition state analogue can catalyse a reaction by stabilization of the transition state.

Since then, not only other esterolytic reactions have been reported [7–10], but also hydrolysis of amide bonds [11] and β-elimination [12]. More recently, C–C bond formation [13,14], cyclization reactions [15] and amide synthesis [16,17] have been described, in addition to redox reactions [18,19] and decarboxylation [20]. Recently, protease activity has been shown to be present in a naturally occurring antibody [21]. For a more complete overview of all types of reactions catalysed by antibodies (also named abzymes or catmabs), see [22].

The first studies on catalysis by antibodies revealed that the catalytic activity resides on the Fab fragment, that multiple turnovers take place, that saturation kinetics occurs and that the hapten is a strong competitive inhibitor. Substrate specificity was found to be narrow, as was later confirmed in other studies [23]. In subsequent studies it was shown that antibodies exert stereochemical control [8,15]. The k_{cat} values were low, and rate accelerations as compared with the uncatalysed reactions were about 1000-fold [2,3].

The rationale behind the first reactions that were catalysed by antibodies was that the observed rate acceleration is due to stabilization of the transition state of the reaction. The contribution of transition state stabilization to catalysis can be estimated from the ratio of the affinity constants of the antibody for the substrate and transition state [16,23,24]. Information about the former can be obtained from the Michaelis constant and about the latter from studies on inhibition by the transition-state analogue.

Comparing the rate enhancement with the kinetic constants reveals that the rate enhancement in most instances can be explained by stabilization of the transition state. There are a few exceptions [8,10,11]. Antibody NPN43C9 showed a rate enhancement of 1.5×10^5 for the hydrolysis of a *p*-nitrophenyl 4-acylaminophenylacetyl ester, which was almost 1000 times greater than would be expected if only stabilization of the transition state were to play a role [11]. More detailed investigations of this abzyme [25] revealed that the reaction proceeds through a multi-step kinetic sequence. No covalently bound intermediate could be detected. Recently, it was established that another antibody catalysed a transesterification reaction via a ping-pong mechanism with induced fit [26]. Furthermore, evidence for the existence of a covalent intermediate was presented.

From the currently available information, it can be concluded that catalysis by antibodies bears resemblances to catalysis by enzymes. In both instances binding of substrate precedes conversion into an activated complex that turns into product. Amino acid residues in the combining site can contribute to the rate accelerations.

NEW DEVELOPMENTS

Eliciting antibodies against a transition state analogue has proved to be a valid approach, but it suffers from a number of drawbacks: first, the transition state of a reaction must be known; second, it must be possible to synthesize a stable analogue, that has to be sufficiently immunogenic; third, although the preparation of hybridomas has become a well established technique, the selection of cell lines is still very tedious. Usually only a fraction of the obtainable cell lines can be screened, so the full potential of the antibodies cannot be explored. Methods have been developed for the large-scale culture of hybridoma cells, but the costs of antibody production remain high.

Hapten design

The first abzymes were directed against transitions-state analogues. Rate enhancements obtainable by this procedure are generally limited to a factor of 10^3. To improve the catalytic performance, new approaches to hapten design were desired. Because in enzymes amino acid residues are involved in catalysis (e.g., general acid or base catalysis), it was attempted to introduce such groups into the antibody combining site by designing haptens that both resemble closely the structure of the transition state analogue and possess an oppositely charged group. The groups of Schultz [12] and Lerner [27,28] reported that this was succesful.

Another approach to the design of haptens is

based on inducing antibodies that act as entropy traps for the reaction, i.e., they bring reactive groups together in the proper conformation. Examples of such behaviour are the chorismate mutase reaction (Claissen rearrangement) [29–31], the Diels–Alder reactions [13,14] and the photochemical reaction of methyl *trans*-4-cinnamate [32]. Iverson and Lerner [33] have shown that it is possible to obtain antibodies that can hydrolyse a peptide by binding both a cofactor (a metal-trien complex in this instance) and a substrate (the peptide).

Modification of antibodies

Antibodies provide a binding pocket that specifically binds the hapten used to elicit them. If this is a transition state analogue, they might catalyse a reaction. The rate of the reaction can be enhanced by the presence of a catalytic group in the combining site. If such a group is not present, it can be introduced. Two approaches have been described: by chemical modification, or by site-directed mutagenesis. Pollack et al. [34] have explored both methods. The starting material was the Fab fragment of an 2,4-dinitrophenol-binding antibody, which did not show turn over of the substrates offered. Chemical modification was achieved by introduction of a free thiol function near the combining site. The proper positioning of this handle was ensured by using a cleavable dinitrophenol affinity label. The derivatized Fab was capable of accelerating the thiolysis of a dinitrophenylcoumarin ester. In further studies [35], this modification was followed by the attachment of an imidazole to the thiol handle, resulting in cleavage of the offered substrates.

Site-directed mutagenesis was used to impart catalytic activity to an antibody previously not active [36], and to improve the catalytic properties of the phosphorylcholine-binding antibody, of which the catalytic properties were described in [3]. In the latter instance [37], two amino acid residues that had previously been shown to be involved in hapten binding were changed, and in one case this improved the k_{cat} of the reaction eightfold. The other residue turned out to be essential for catalysis.

For the exertion of catalytic activity it is not necessary to express a complete antibody; Fab or Fv suffice. These fragments still consist of two chains, which are not always synthesized in the required ratio by the host cells. To circumvent this problem, single-chain antibodies have been prepared, where the variable regions of both chains are connected by a linker peptide [38,39]. The resulting single-chain antibodies had the same specificity and affinity as the parent monoclonals. Similarly, a single-chain catalytic antibody exhibited the same kinetic parameters as the monoclonal from which it was derived [40].

Future developments in this area will probably involve the introduction of properly positioned catalytic groups in the combining site, e.g., the catalytic triad of proteases, or binding sites for metals or other cofactors [41,42].

Antibody cloning

Modification of antibodies by site directed mutagenis was first carried out in hybridoma cells [43,44]. More recently, methods were developed for the expression and synthesis of functional antibodies and antibody fragments in bacterial cells, [45,46], yeast [47] and plants [48,49]

In the early 1980s it was attempted to clone and express antibodies in bacterial cells. Cabilly *et al.* [50] were the first to report the synthesis of complete heavy and light chains in *Escherichia coli*. Even when both chains were expressed in the same cell, no antigen binding activity could be observed; in vitro reconstitution was necessary to obtain functional antibodies. Also when a single-chain antigen-binding fragment was expressed, denaturation and refolding were necessary [38,39]. However if secretion into the periplasmic space took place [45,46], functional antigen binding fragments were synthesized by *E. coli*. Skerra and Plückthun [45] expressed V_H and V_L fragments that were assembled correctly, whereas Better et al. [46] expressed a functional mouse-human chimeric Fab fragment that contained the variable regions from a mouse monoclonal antibody and the constant regions of a human IgG_1 antibody. Translocation to the periplasmic space could also be used to produce functional single-chain antibodies [51].

New screening methods

Using the existing method for the preparation of monoclonal antibodies, only a few hundred different monoclonals are obtained, whereas in theory the immune system is capable of generating at least 10^6 different antibodies. With the appropriate primers, mRNA for V_H can be used directly from the spleen for amplification by the polymerase chain reaction. A cDNA library was created [52] for both heavy- and light-chain fragments. Subsequently, a combinatorial library was constructed in phage λ [53]. This method allowed the rapid screening for antigen binding of about 10^6 phage plaques. Further improvement of the screening procedure was made by fusing the antibody protein to phage surface proteins [54–56].

POTENTIAL APPLICATIONS OF CATALYTIC ANTIBODIES

Catalytic antibodies combine the properties of enzymes and antibodies. For applications they will have to compete with both, and prove themselves superior. In their favour is that they can be designed to catalyse reactions for which no suitable enzyme or chemical catalyst is available, and that they are very specific. Their main drawback is the fact that they are difficult to obtain. The design of a hapten is not trivial, selection of cell lines that produce catalytically active antibodies is time consuming and the large-scale production of antibodies is still expensive, although progress in this area is rapid. As fields of application one can discern industry, medicine and analysis.

Application of abzymes as large-scale biocatalysts will be hampered by their cost. Another drawback is their generally low activity. In favour of catalytic antibodies is their exquisite substrate specificity and their stability. The similarity in structure facilitates the development of general procedures for both biocatalyst engineering and medium engineering. Therefore catalytic antibodies might find application in a few conversions with a high added value. It is also worth mentioning that one can envisage the development of antibodies with very specific proteolytic activities, that can be used in analogy with restriction enzymes to cut and paste peptides into new enzymes.

For analytical purposes, the cost of antibodies is less prohibitive. Here, their specificity will be the main advantage over enzymes, and their catalytic activity the advantage over antibodies.

The most important application of antibodies might be found in medicine. The major problem connected with the use of both antibodies and enzymes is the respons of the immune system to these foreign proteins. A large research effort is being put into the masking of epitopes on proteins and into humanizing antibodies from other origins. Medical research has yielded many creative ideas for the therapeutic use of antibodies, e.g., single-chain Fv fragments [39] and immunotoxins. Combination of the properties of antibodies with those of enzymes might lead to the development of a new class of medicines.

REFERENCES

1 T.R. Cech and B.L. Bass, Annu. Rev. Biochem., 55 (1986) 599.
2 A. Tramontano, K.D. Janda and R.A. Lerner, Science, 234 (1986) 1566.
3 S.J. Pollack, J.W. Jacobs and P.G. Schultz, Science, 234 (1986) 1570.
4 W.P. Jencks, Catalysis in Chemistry and Enzymology, McGraw-Hill, New York, 1986, p. 288.
5 G. Gallacher, C.S. Jackson, C.M. Topham, M. Searcey, B.C. Turner, G.T. Badman and K. Brocklehurst, Biochem. Soc. Trans., 18 (1990) 600.
6 G. Köhler and C. Milstein, Nature, 256 (1975) 495.
7 D.S. Tawfik, R.R. Zemel, R. Arad-Yellin, B.S. Green and Z. Eshhar, Biochemistry, 29 (1990) 9916.
8 K.D. Janda, S.J. Benkovic and R.A. Lerner, Science, 244 (1989) 437.
9 J. Jacobs, P.G. Schultz, R. Sugasawara and M. Powell, J. Am. Chem. Soc., 109 (1987) 2174.
10 A. Tramontano, A.A. Ammann and R.A. Lerner, J. Am. Chem. Soc. 110 (1988) 2282.
11 K.D. Janda, D. Schloeder, S.J. Benkovic and R.A. Lerner, Science, 241 (1988) 1188.
12 K.M. Shokat, C.J. Leumann, R. Sugasawara and P.G. Schultz, Nature, 338 (1989) 269.
13 D. Hilvert, K.W. Hill, K.D. Nared and M.-T.M. Auditor, J. Am. Chem. Soc., 111 (1989) 9261.
14 A.C. Braisted and P.G. Schultz, J. Am. Chem. Soc., 112 (1990) 7430.
15 A.D. Napper, S.J. Benkovic, A. Tramontano and R.A. Lerner, Science, 237 (1987) 1041.

16 S.J. Benkovic, A.D. Napper and R.A. Lerner, Proc. Natl. Acad. Sci. USA, 85 (1988) 5355.
17 K.D. Janda, R.A. Lerner and A. Tramontano, J. Am. Chem. Soc., 110 (1988) 4835.
18 K.M. Shokat, C.H. Leumann, R. Sugasawara and P.G. Schultz, Angew. Chem., 100 (1988) 1227.
19 A.G. Cochran and P.G. Schultz, J. Am. Chem. Soc., 112 (1990) 9414.
20 C. Lewis, T. Kramer, S. Robinson and D. Hilvert, Science, 253 (1991) 1019.
21 R.A. Lerner, S.J. Benkovic and P.G. Schultz, Science, 252 (1991) 659.
22 S. Paul, D.J. Volle, M.J. Powell and R.J. Massey, J. Biol. Chem., 265 (1990) 11910.
23 K.D. Janda, J.A. Ashley, T.M. Jones, D.A. McLeod, D.M. Schloeder, M.I. Weinhouse, R.A. Lerner, R.A. Gibbs, P.A. Benkovic, R. Hilhorst and S.J. Benkovic, J. Am. Chem. Soc., 113 (1991) 291.
24 B.S. Green and D.S. Tawfik, Trends Biotechnol., 7 (1989) 304.
25 S.J. Benkovic, J.A. Adams, C.L. Borders, Jr., K.D. Janda and R.A. Lerner, Science, 250 (1990) 1135.
26 P. Wirsching, J.A. Ashley, S.J. Benkovic, K.D. Janda and R.A. Lerner, Science, 252 (1991) 680.
27 K.D. Janda, M.I. Weinhouse, D.M. Schloeder and R.A. Lerner, J. Am. Chem. Soc., 112 (1990) 1274.
28 K.D. Janda, M.I. Weinhouse, T. Danon, K.A. Pacelli and D.M. Schloeder, J. Am. Chem. Soc., 113 (1991) 5427.
29 D.Y. Jackson, J.W. Jacobs, R. Sugasawara, S.H. Reich, P.A. Bartlett and P.G. Schultz, J. Am. Chem. Soc., 110 (1988) 4841.
30 D. Hilvert, S.H. Carpenter, K.D. Nared and M.-T.M. Auditor, Proc. Natl. Acad. Sci. U.S.A., 85 (1988) 4953.
31 D. Hilvert and K.D. Nared, J. Am. Chem. Soc., 110 (1988) 5593.
32 A. Balan, B.P. Doctor, B.S. Green, M. Torten and H. Ziffer, J. Chem. Soc. Chem. Commun, (1988) 106.
33 B.L. Iverson and R.A. Lerner, Science, 243 (1989) 1184.
34 S.J. Pollack, G.R. Nakayama and P.G. Schultz, Science, 242 (1988) 1038.
35 S.J. Pollack and P.G. Schultz, J. Am. Chem. Soc., 111 (1989) 1929.
36 E. Baldwin and P.G. Schultz, Science, 245 (1989) 1104.
37 D.Y. Jackson, J.R. Prudent, E.P. Baldwin and P.G. Schultz, Proc. Natl. Acad. Sci U.S.A., 88 (1991) 58.
38 J.S. Huston, D. Levinson, M.M. Mudgett-Hunter, M.S. Tai, J. Novotny, M.N. Margolies, R.J. Ridge, R.E. Bruccoleri, E. Haber, R. Crea and H. Oppermann, Proc. Natl. Acad. Sci. U.S.A., 85 (1988) 5879.
39 R.E. Bird, K.D. Hardman, J.W. Jacobson, S. Johnson, B.M. Kaufman, S.M. Lee, T. Lee, S.H. Pope, G.S. Riordan and M. Whitlow, Science, 242 (1988) 423.
40 R.A. Gibbs, B.A. Posner, D.R. Filpula, S.W. Dodd, M.A.J. Finkelman, T.K. Lee, M. Wroble, M. Whitlow and S.J. Benkovic, Proc. Natl. Acad. Sci. U.S.A., 88 (1991) 4001.
41 V.A. Roberts, B.L. Iverson, S.A. Iverson, S.J. Benkovic, R.A. Lerner, E.D. Getzoff and J.A. Tainer, Proc. Natl. Acad. Sci. U.S.A., 87 (1990) 6654.
42 J.A. Tainer and V.A. Roberts, Nature, 348 (1990) 589.
43 D. Rice and D. Baltimore, Proc. Natl. Acad. Sci. U.S.A., 79 (1982) 7862.
44 V.T. Oi, S.L. Morrison, L.A. Herzenberg and P. Berg, Proc. Natl. Acad. Sci. U.S.A., 80 (1983) 825.
45 A. Skerra and A. Plückthun, Science, 240 (1988) 1038.
46 M. Better, C.P. Chang, R.R. Robinson and A.H. Horwitz, Science, 240 (1988) 1041.
47 A.H. Horwitz, C.P. Chang, M. Better, K.E. Hellstrom and R.R. Robinson, Proc. Natl. Acad. Sci. U.S.A., 85 (1988) 8678.
48 A. Hiatt, R. Cafferkey and K. Bowdish, Nature, 342 (1989) 76.
49 K. During, S. Hippe, F. Kreuzaler and J. Schell, Plant Molecular Biology, 15 (1990) 281.
50 S. Cabilly, A.D. Riggs, H. Pande, J.W. Shively, W.E. Holmes, M.Rey, L.J. Perry, R. Wetzel and H.L. Heyneker, Proc. Natl. Acad. Sci. U.S.A., 81 (1984) 3273.
51 R. Glockhuber, M. Malia, I. Pfitzinger and A. Plückthun, Biochemistry, 29 (1990) 1362.
52 L. Sastry, M. Alting-Mees, W.D. Huse, J.M. Short, J.A. Sorge, B.N. Hay, K.D. Janda, S.J. Benkovic and R.A. Lerner, Proc. Natl. Acad. Sci. U.S.A., 86 (1989) 5728.
53 W.D. Huse, L. Sastry, S.A. Iverson, A.S. Kang, M. Alting-Mees, D.R. Burton, S.J. Benkovic and R.A. Lerner, Science, 246 (1989) 1275.
54 A.S. Kang, C.F. Barbas, K.D. Janda, S.J. Benkovic and R.A. Lerner, Proc. Natl. Acad. Sci. U.S.A., 88 (1991) 4363.
55 J. McCafferty, A.D. Griffiths, G. Winter and D.J. Chiswell, Nature, 348 (1990) 552.
56 H.R. Hoogenboom, A.D. Griffiths, K.S. Johnson, D.J. Chiswell, P. Hudson and G. Winter, Nucleic Acids Res., 19 (1991) 4133.
57 I. Roitt, J. Brostoff and D. Male, Immunology, Gower Medical, London, 2nd edn., 1989.
58 P.M. Colman, Adv. Immunol., 43 (1988) 99.

Analytica Chimica Acta, 279 (1993) 135–140
Elsevier Science Publishers B.V., Amsterdam

Measurements of nitric oxide in biological materials using a porphyrinic microsensor

T. Malinski, Z. Taha, S. Grunfeld, A. Burewicz and P. Tomboulian
Department of Chemistry, Oakland University, Rochester, MI 48309 (USA)

F. Kiechle
W. Beaumont Hospital, Royal Oak, MI 48072 (USA)

(Received 12th October 1992; revised manuscript received 9th December 1992)

Abstract

The application and optimization of a microsensor for in situ measurements of nitric oxide (NO) in biological systems are described. The sensor (diameter 0.5–0.8 μm), exhibiting a response time better than 10 ms and a detection limit of 10 nM, consists of several layers of p-type semiconducting polymeric porphyrin and cation exchanger (Nafion) deposited on a thermally-sharpened carbon fiber. The sensor has been applied to studies of NO release from a single endothelial cell in a pulmonary artery, as well as for the determination of NO in blood.

Keywords: Biosensors; Nitric oxide; Porphyrinic microsensor

Nitric oxide (NO) has been shown recently to be an important bioregulatory molecule in physiological processes [1,2]. Although the total understanding of NO functions is incomplete, the NO radical clearly accounts for the activity of the endothelium-derived relaxing factor (EDRF) [3], acts as a neurotransmitter [4], prevents platelet aggregation [5], and is a major defense molecule of immune cells [6] against tumor cells [7] and intracellular bacteria [6]. Several pathological processes, such as acute hypertension [8], diabetes [9], ischaemia [10], and atherosclerosis [11], are associated with abnormalities of EDRF. In addition to its bioregulatory functions, excess concentrations of NO have been implicated as a major factor in a number of disease processes such as septic shock [12], the destruction of insulin-producing cells [13], Parkinson's disease [14], and Alzheimer's dementia [14].

Despite great interest in studying NO release, all the current methods used for its detection are indirect, relying on measurements of secondary species, such as nitrate removed from biological systems. Nitric oxide release is usually measured by a bioassay, chemiluminescence, and UV–visible spectroscopy. None of these methods can be applied to in vivo or in vitro measurements, and all require chemical pretreatment of the sample. Recently we have published preliminary results obtained by a newly developed amperometric /voltammetric sensor for selective determination of NO in situ in single cells, exhibiting the required detection limit at the sub-femtogram level [15]. The sensor described is based on the catalytic electrochemical oxidation of NO on a specifically designed p-type semiconducting porphyrinic electrode. In this paper we report data that further characterize the sensor, along with

Correspondence to: T. Malinski, Department of Chemistry, Oakland University, Rochester, MI 48309-4401 (USA).

evaluation of its performance in different biological materials.

EXPERIMENTAL

Reagents and materials

Tetrakis(3-methoxy-4-hydroxyphenyl)nickel(II) porphyrin (Fig. 1) was synthesized as previously described [16]. Celion G50–300 carbon fibers (BASF) with a diameter of 6 μm were used. Beeswax with 10% rosin was used to coat the electrodes. Reagents used were of Suprapure quality (Ultrex, J.T. Baker).

Porcine pulmonary arteries were obtained fresh from the slaughterhouse. After removal of blood, the pulmonary artery was placed in a petri dish containing DMEM cell culture media (Fisher). The artery was cut into strips, with each placed into a petri dish containing fresh cell culture media. A differential pulse voltammetry (DPV) and an amperometric measurement were obtained at 37°C. Bradykinin (Sigma) was then added to the pulmonary artery strip; an NO signal was observed approximately 10 s after the addition bradykinin. Human blood was collected into a syringe containing an anticoagulant (ACD). The serum and plasma were seperated by centrifugation. A DPV measurement was obtained followed by an amperometric measurement. Authentic NO was then added to each of the above systems to characterize the decay in nitric oxide concentration in each of the samples.

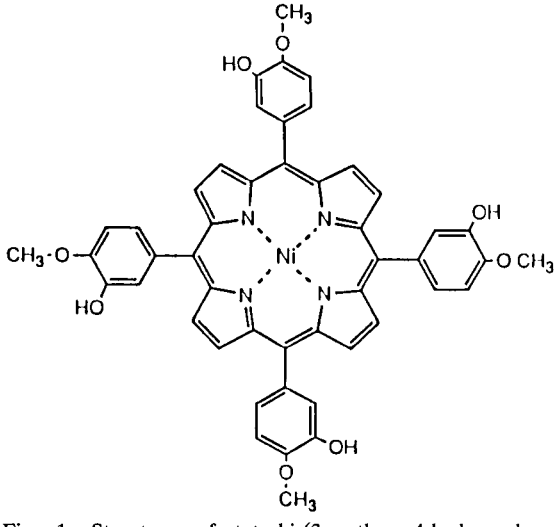

Fig. 1. Structure of tetrakis(3-methoxy-4-hydroxyphenyl)-nickel(II) porphyrin, NiTMHPP.

Apparatus

A three-electrode system in a quartz cell was used for the porphyrin film formation by electrode deposition, and for NO determination by DPV using the sharpened carbon fiber as the working electrode. The auxiliary and reference electrodes were platinum wire and a saturated calomel electrode (SCE), respectively.

A PAR Model 264A polarographic analyzer with a PAR Model 181 current-sensitive preamplifier were used for DPV and for amperometry. The DPV was recorded with a PAR Model 9002A X-Y recorder. The amperometric signal was recorded with a Houston Omniscribe strip chart recorder.

Microelectrode sensor fabrication and modification

The microsensor was produced by threading a carbon fiber through a pulled end of a capillary with 1-cm length of the fiber left protruding. The glass fiber electrode interface was sealed with a nonconductive epoxy and a copper lead was inserted in the opposite end, sealed with silver epoxy. The single fiber electrode was thermally sharpened using a propane microburner, coated with molten beeswax–rosin mixture, and sharpened again. The active surface had a length of 2–6 μm with a fiber diameter of approximately 0.5–0.8 μm.

The polymeric film is deposited from a 5×10^{-4} M monomeric tetrakis(3-methoxy-4-hydroxyphenyl)nickel(II) porphyrin, NiTMHPP, with Ni as central metal, using continuous scan cyclic voltammetry from -0.2 to 1.2 V. The electrode was then coated with Nafion (Aldrich).

RESULTS AND DISCUSSION

Optimization of the carbon fiber microelectrode

Carbon fibers with diameters of 6–8 μm are sharpened to 0.5–0.8 μm in order to avoid cell

membrane rupture during the implantation process. A carbon fiber was sharpened following a procedure described previously [17] using a microburner. Subsequently, the sharpened fiber was immersed in melted beeswax–rosin mixture and kept at a controlled temperature for 5–15 s. After cooling to room temperature, the electrode was resharpened. An electrode obtained by this procedure has several features important for single cell measurement applications, including a smaller diameter but longer sharpened tip. The resulting electrode is a slim cylinder with a small diameter rather than a short taper.

The classical procedure for fabricating microelectrodes by inserting a carbon fiber into a glass microcapillary followed by polishing cannot be applied since the electrode dimensions are not appropriate. The diameter of the electrode includes the glass in addition to the fiber, making it too large for insertion into single cells with diameters smaller than 10 μm. Since the electroactive area is limited to the circular disk of the exposed electrode tip, and the current (analytical signal) is directly proportional to the surface area, it is important to make this area as large as possible for the smallest possible diameter. Since the ratio, R, of surface area of a cone-shaped electrode to that of a disk electrode is b/r (b is the slant height of the cone and r is the radius of the cone or disk), and for a typical electrode dimensions of $r = 0.25$ μm and $b = 5$ μm, the surface area of the cone-shaped electrode will be twenty times that of the disk electrode, so the resulting analytical signal will also be higher by this same factor. Generally, the electrode length should be less than a cell thickness; however, electrodes can be implanted into flat cells from any convenient angle making this restriction less critical.

Multiple electrodes (an electrode array) for studies of NO release in large cells and tissues were constructed in the disk form using a glass microcapillary or encapsulation with polyoxyphenylene [18]. Electrochemical deposition of polyoxyphenylene from 2-allylphenol and ammonium hydroxide dissolved in mixture of butylcellosolve, water, and methanol produces an insulating material (after heating at 150°), with 2–4 μm thickness, high resistivity, and high mechanical stability. The Celion fibers used in these studies are mechanically stronger than fibers with circular cross-section, but the Celion are more difficult to encapsulate in a glass capillary because of their irregular shape. Both the polymeric insulation used for the disk electrode and the wax–rosin insulation used for cone-shaped electrode increase the mechanical strength of these fibers noticeably for a 2 μm thick encapsulation.

Deposition of the polymeric porphyrin

Good catalytic properties as well as its conductivity of the porphyrinic film on the fiber electrode are crucial for obtaining a low detection limit in the NO determination. Deposition of NiTMHPP film can be achieved at constant potential of 0.8–0.9 V, or using a continuous scan of the potential from −0.2 V to 0.9–1.2 V. The films obtained with a continuous potential scan have 2–5 times better catalytic properties toward NO oxidation than films obtained at constant potential. There is a good correlation between the catalytic properties of the film for oxidation of water, and the oxidation of NO.

A continuous scan cyclic voltammogram (Fig. 2) shows the growth pattern observed for NiTMHPP, and clearly indicates film formation on the surface of the carbon fiber. Peak Ia is observed only in the first scan, while peak IIa decreases significantly after the third scan. Film formation occurs only after the second oxidation process. A new redox couple (peaks IIIa, c) appears and increases after each voltammetric scan. Peaks Ia and IIa are due to oxidation of two 3-methoxy-4-hydroxyphenyl substituents in the α' and γ' positions on the porphyrin ring. The oxidation of these two substituents, followed by polymerization, has been described previously [16]. Peaks IIIa and c are due to the redox reaction of the Ni(II)/Ni(III) couple in the polymeric film. Reversibility of this couple depends on pH, the process of film formation (film morphology), and the carbon fiber surface. No correlation has been found between the reversibility of the Ni(II)/Ni(III) reaction, and the catalytic properties for NO oxidation. An important criterion for evaluating catalytic properties of the film is a negative shift of potential for water oxidation

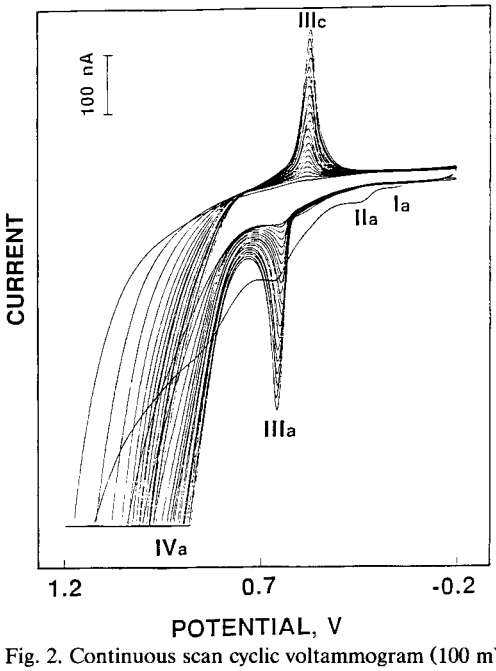

Fig. 2. Continuous scan cyclic voltammogram (100 mV s^{-1}) of NiTMHPP obtained on carbon fiber electrode in 0.1 M NaOH.

(peak IVa), usually about 200 mV compared to that observed on uncovered carbon fiber. When a polymeric NiTMHPP electrode is transferred to 0.1 M NaOH, only peaks IIIa, IIIc and peak Va are observed. Charge transferred in the process IIIc can be used to calculate surface coverage with poly-NiTMHPP film. The surface coverage of 0.9–1.4 nmol cm^{-2} is optimal for catalytic oxidation of NO. Nitric oxide is oxidized on polymeric NiTMHPP at pH 7.4 in three electron transfers (ECE process) to form sequentially NO^+, NO_2^-, and finally NO_3^-.

The polymeric NiTMHPP is covered with Nafion in order to stabilize NO^+ and prevent its further oxidation to NO_3^-, as well as to prevent the diffusion of NO_2^- from the bulk solution to porphyrinic film; NO_2^- is the most common interferent in biological systems containing NO. Nafion, a cation exchanger, hinders diffusion of anions to polymeric NiTMHPP while the neutral NO radical can diffuse easily through the Nafion film. However, the current due to NO oxidation on polymeric NiTMHPP covered with Nafion decreases as a function of the Nafion film thickness. Therefore, coverage with Nafion film should be optimized in order to achieve the best possible detection limit which requires a thinner layer of the Nafion, while simultaneously providing a sufficient barrier against diffusion of NO_2^- which

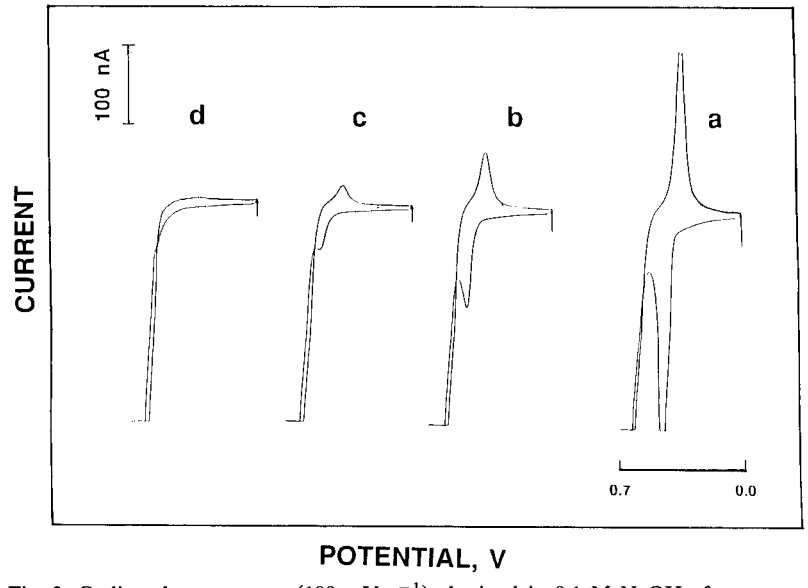

Fig. 3. Cyclic voltammograms (100 mV s^{-1}) obtained in 0.1 M NaOH after sequential coating of poly-NiTMHPP with Nafion. (a) Uncoated poly-NiTMHPP; (b) coated by dipping electrode for 5 s in 1.25% Nafion and dried for 5 min; (c) after second coating; other conditions the same as b; (d) after third coating; other conditions the same as b.

requires a thicker Nafion film. Current due to the Ni(II)/Ni(III) reaction can be used to test the integrity of the Nafion film. Oxidation of Ni(II) to Ni(III) in the film occurs only if a diffusion of the HO^- counter ion into the film is possible. Because a Nafion film with sufficient thickness and without pinholes will prevent HO^- diffusion, a lack of Ni(II)/Ni(III) couple in the voltammogram obtained in 0.1 M NaOH is a good method to verify film integrity. Figure 3 shows cyclic voltammograms obtained for this same poly-NiTMHPP film covered with Nafion film of different thicknesses, obtained after sequential coating by dipping the carbon fiber for 5 s in 1.25% (aqueous ethanol solution) Nafion. Each coat of the Nafion decreases Ni(II) and Ni(III) peaks by a factor of about 3 (Fig. 3). Also, the separation between peaks IIIc and IIIa increases from 102 mV for an uncoated electrode, to 126 and 136 mV, after one and two coatings with Nafion, respectively. The thickness of Nafion obtained after three coatings (total 15 s) is sufficient to prevent diffusion of small anions even at the high concentration gradient. Sensors were further tested for their response to nitrite in a buffer solution of pH 7.4. When there is no response to 20 μM NO_2^-, a concentration 1–2 orders of magnitude higher than expected in biological systems, a sufficient Nafion coating is assumed.

NO release from a single endothelial cell

The sensor was used to measure NO release from a single endothelial cell in the pulmonary artery. A strip of pulmonary artery in cell culture medium was monitored under an inverted microscope. The microsensor was placed on the surface of endothelial cell membrane. After injection of bradykinin (2 nmol) into the medium near the endothelium cell, release of NO was observed using the amperometric method (Fig. 4). The release of NO 8 s after the injection of bradykinin was indicated on the amperogram by a sharp increase in current. A maximum NO concentration on the cell membrane, 490 ± 30 nM, was observed after about 30 s. This surface concentration is very similar to the 450 ± 40 nM concentration observed on endothelial cell membrane from porcine aorta [15]. Injection (after 160 s) of L-arginine, one of the substrates in nitric oxide synthetase, increases the NO concentration from 300 to 540 nM.

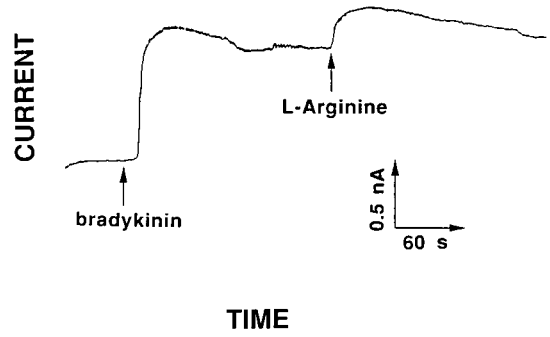

Fig. 4. Amperometric detection of NO in situ by microsensor on the membrane of a single endothelial cell of porcine pulmonary artery.

Determination of NO in blood

The lifetime of 40 μM of NO in human blood was determined by differential pulse voltamme-

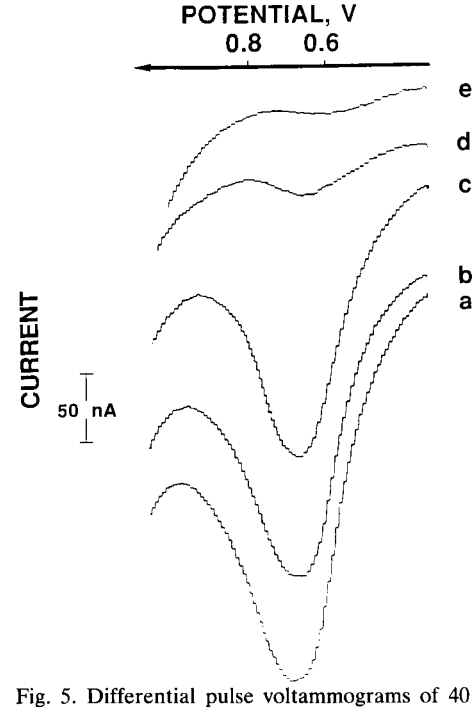

Fig. 5. Differential pulse voltammograms of 40 μM NO injected in blood (3 ml): (a) 60 s; (b) 180 s; and (c) 250 s after injection of NO; (d) after 5 s of stirring; (e) background. Time is reported at the peak maximum.

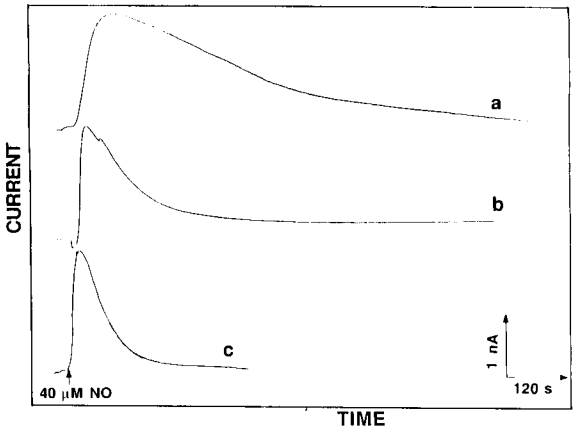

Fig. 6. Amperometric monitoring of NO concentration decay starting with an initial NO concentration 40 μM in: (a) blood serum; (b) blood plasma; (c) blood.

try. NO was injected into 3 ml of blood 20 s after the blood was taken. Voltammograms are shown in Fig. 5, with time reported at the peak maximum. NO was injected in close proximity to the sensor. A decrease of current with time is due to two processes: diffusion of NO into bulk solution, and chemical reaction of NO with blood components. Under static conditions (no stirring), the decay of NO in blood is suprisingly slow. After 250 s, the NO concentration around the sensor is about 20 μM. However, with slow stirring of blood for 5 s (about 80 rpm), this concentration decreased to less than 3 μM. A sensor operating in the amperometric mode was used for continuous monitoring of NO concentration in blood serum, blood plasma, and whole blood (Fig. 6). After an injection of NO by microsyringe into a 3 ml sample (final concentration of NO 40 μM), a typically amperometric rapid current increase was observed, decreasing with time due to diffusion and the chemical reaction of NO. Both processes are slowest in blood serum. In blood plasma, the decrease of NO concentration around the sensor was intermediate between those observed for blood serum and blood.

This work was supported in part by a grant from William Beaumont Hospital Research Institute.

REFERENCES

1 S. Moncada, R.M.J. Palmer and E.A. Higgs, Pharmacol. Rev., 43 (1991) 109.
2 J. Collier and P. Vallance, Br. Med. J., 302 (1991) 297.
3 R.M.J. Palmer, A.G. Ferrige and S. Moncada, Nature, 327 (1987) 526.
4 T.J. O'Dell, R.D. Hawkins, E.R. Kandel and O. Arancio, Proc. Natl. Acad. Sci. USA, 88 (1991) 11285.
5 M.W. Radomski, R.M.J. Palmer and S. Moncada, Proc. Natl. Acad. Sci. USA, 87 (1990) 5193.
6 J.B. Hibbs, Jr., Z. Vavrin and R.R. Tainton. J. Immunol., 138 (1987) 550.
7 J.B. Hibbs, Jr., R.R. Tainton, Z. Vavrin and E.M. Rachlin, Biochem. Biophys. Res. Commun., 157 (1988) 87.
8 L. Linder, W. Kiowski, F. Buhler and T.F. Lusher, Circulation, 81 (1990) 1762.
9 H.H.H.W. Schmidt, T.D. Warner, K. Ishii and F. Murand, Science, 255 (1992) 721.
10 P.M. Vanhoute, J. Cardiovas. Pharmacol., 16 (1990) s15.
11 R.C. Freiman, G.G. Mitchell, D.D. Halsted, M.L. Armstrong and A.G. Harrison, Cir. Res., 58 (1986) 783.
12 D.D. Rees, S. Celleck, R.M.J. Palmer and S. Moncada, Biochem. Biophys. Res. Commun., 197 (1990) 541.
13 I.D.G. Durate, A.K. Sen and F.A. Sunahara, Br. J. Pharm., 94 (1988) 463.
14 S. Moncada, R.M.J. Palmer and E.A. Higgs, Biochem. Pharmacol., 38 (1989) 1709.
15 T. Malinski and Z. Taha, Nature 358 (1992) 676.
16 T. Malinski, A. Ciszewski, J. Bennett, J. Fish and L. Czuchajowski, J. Electrochem. Soc., 138 (1991) 208.
17 T. Malinski, F. Bailey, J.R. Fish and F. Kiechle, Anal. Chim. Acta, 249 (1991) 35.
18 K. Potje-Kamloth, J. Janatai and M. Josowicz, Ber. Bunsenges. Phys. Chem., 93 (1989) 1480.

Analytica Chimica Acta, 279 (1993) 141–147
Elsevier Science Publishers B.V., Amsterdam

Reusable fiber-optic-based immunosensor for rapid detection of imazethapyr herbicide

R.B. Wong

American Cyanamid Company, P.O. Box 400, Princeton, NJ 08543–0400 (USA)

N. Anis and M.E. Eldefrawi

University of Maryland School of Medicine, 655 West Baltimore Street, Baltimore, MD 21201–1559 (USA)

(Received 1st October 1992; revised manuscript received 15th December 1992)

Abstract

Imazethapyr is a herbicide belonging to the imidazolinone class of compounds. It is the active ingredient of a commercial herbicide PURSUIT®. Polyclonal antibodies have been prepared in rabbits and sheep which specifically recognize this class of imidazolinone compounds. Using the immune rabbit serum, an enzyme-linked immunosorbent assay (ELISA) has been developed for the entire class of commercial imidazolinone herbicides including imazaquin, imazapyr, imazethapyr and imazamethabenz methyl. The quantitation of imidazolinones in soil requires a certain amount of sample pretreatment, thus the through-put is not ideal. A simpler immunoassay method for screening large amount of soil samples economically would be useful. Taking the sheep polyclonal immune serum, we used a fluorescent immunoassay employing optical fiber and fluorescence (US Patent 4,582,809, 1986), to assay for imazethapyr. Purified sheep antibody was immobilized on quartz fibers. A mixture of fluorescein-labelled imazethapyr analog and free imazethapyr was presented to the fiber for direct competition of the antibody binding sites or displacement of a previously fluorescein labelled fiber. The response time for the detection of imazethapyr ranged from seconds to minutes. The sensitivity of the assay was 1 nM. This binding of the fluorochrome to the fiber was reversible by washing with a phosphate buffered saline. Multiple measurements were easily processed with a single fiber over the course of several hours. Analysis of imazethapyr residue in soil can be accomplished by subjecting a clarified soil extract solution directly for analysis without further treatment. The crossreactivity data indicates that the assay is apparently specific for the imidazolinone class of compounds.

Keywords: Biosensors; Herbicides; Imazethapyr; Immunosensor

Imazethapyr is a herbicide belonging to the imidazolinone class of compounds. It is effective in weed control by virtue of its ability to inhibit branched-chain amino acid biosynthesis [1]. The most effective use of imidazolinone herbicides depends on the knowledge of the metabolism of these compounds in different plants as well as the residual level of compound in the soil [2]. Soil residue analysis by ELISA has been developed [3]. The method requires some pretreatment of the soil extract before processing by ELISA. An alternate detection method for the ELISA system such as evanescent-excited fluorescence [4], piezoelectric oscillation [5,6], and surface plasmon resonance [7], or through a silicon sensor-based pH detector [8,9] may be useful approaches for the development of a simpler assay method for processing large quantities of soil samples.

We used a fiber optic evanescent fluorosensor as described by Rogers et al. [10] for the development of the imazethapyr immunosensing system. In this communication, we demonstrate an antibody sensor using immune sheep antibody immobilized on quartz fibers. Since fluorescein-linked

Correspondence to: R.B. Wong, American Cyanamid Company, P.O. Box 400, Princeton, NJ 08543–0400 (USA).

imazethapyr analog bound to antibody generates signals, imazethapyr can be quantified by affecting dissociation or association of fluorescent signal on the fiber with a dynamic concentration range of 10^{-3} to 10^{-9} M. This immunosensor system is fast, requires a small sample volume, and is quite transparent to sample matrix, thus requires minimum sample preparation. Another important feature of the sensor is that it is reusable.

EXPERIMENTAL AND RESULTS

Reagents

Polyclonal antibody was generated in sheep using an imidazolinone compound conjugated to bovine serum albumin [11]. The IgG fraction, purified by passing the serum through a protein A column was used to coat quartz fibers for the assay. Analytical grade imidazolinone compounds were synthesized at the American Cyanamid Co. All other agrochemicals were commercial products. The fluorescent tag was prepared by reacting 5-formyl imazapyr with 5({[2-(carbohydrazino)methyl]thio}acetyl)aminofluorescein to form the fluorescein hydrazino methylene imazapyr (FHMI) as shown in Fig. 1.

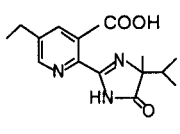

imazethapyr

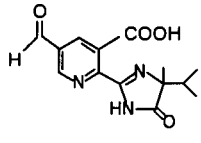

5-formyl imazapyr

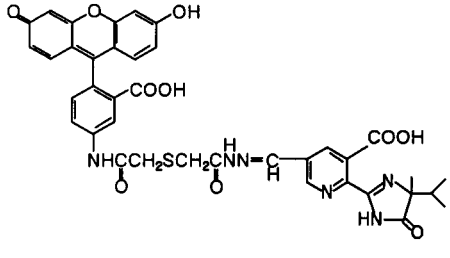

fluorescein hydrazino methylene imazapyr (FHMI)

Fig. 1. Structures of imazethapyr, 5-formylimazapyr, the analog compound for fluorescein label preparation and fluorescein hydrazino methylene imazapyr (FHMI).

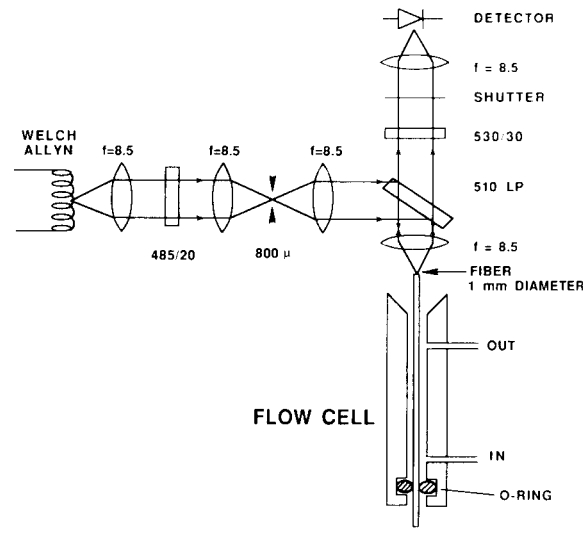

Fig. 2. Schematic drawing of the optical system.

Instrumentation

The portable fluorometer described by Rogers et al. [12], and manufactured by ORD (North Salem, NH) was used to measure the fluorescence signal. Quartz fibers (60 mm × 1 mm diam.) with polished ends were purchased from ORD. The fiber optic immunosensor made use of the evanescent wave effect by exciting a fluorophore bound within the evanescent zone as described by Block and Hirschfeld [13]. A portion of the resultant fluorophore emission trapped in the wave guide, was transmitted back up the fiber and detected after transmission through 510 LP and 530/30 nm filter. The flow cell had a volume of 46 μl which was exchanged every 12 s at a flow-rate of 0.23 ml/min. Figure 2 shows a schematic drawing of the instrument.

Determination of antibody and FHMI concentration used

FHMI (50 nM) in PBS bound non-specifically to quartz fibers as measured by total internal

fluorescence. However, addition of a 0.1% casein in the perfusate eliminated this non-specific signal. When control sheep IgG was immobilized on the fiber, a very small base-line signal was observed when perfused with FHMI. When FHMI was added to a fiber coated with anti-imidazolinone antibody, a strong signal was generated. This indicated that the binding of the FHMI was specific for the antibody. Figure 3 demonstrates the dependence of signal on the FHMI concentration infused and shows the concentration dependent signal generation by varying the amount of antibody immobilized on the fiber. The optimal concentrations of 25 nM FHMI was used for all perfusions, while 25 μg/ml antibody was used for immobilization..

Format of immunoassay

The cartoon in Fig. 4 describes the two modes where the analyte imazethapyr can be quantified. Association mode allows imazethapyr to be added with the FHMI tag and compete for the antibody binding sites on the fiber as the solution is perfused through the chamber. This results in a dose dependent inhibition of signal binding. Dissociation mode prepared the fiber first by attaching a steady-state amount of FHMI before the analyte imazethapyr is introduced. The fluorescent signal is reduced as a result of the binding of the non-fluoresent imazethapyr. The does responses are presented in Figs. 5 and 6. In the association mode (Fig. 5) the effective dose range of imazethapyr was from 0.1 to 100 μM. For the dissociation mode of the assay (Fig. 6), fluorescence reaches a steady state level in approximately 5 min. If imazethapyr was added to the perfusion solution after steady state fluorescence was established, reduction of fluorescence signal was almost immediate. A concentration dependent displacement of 0.001–100 μM of imazethapyr was observed.

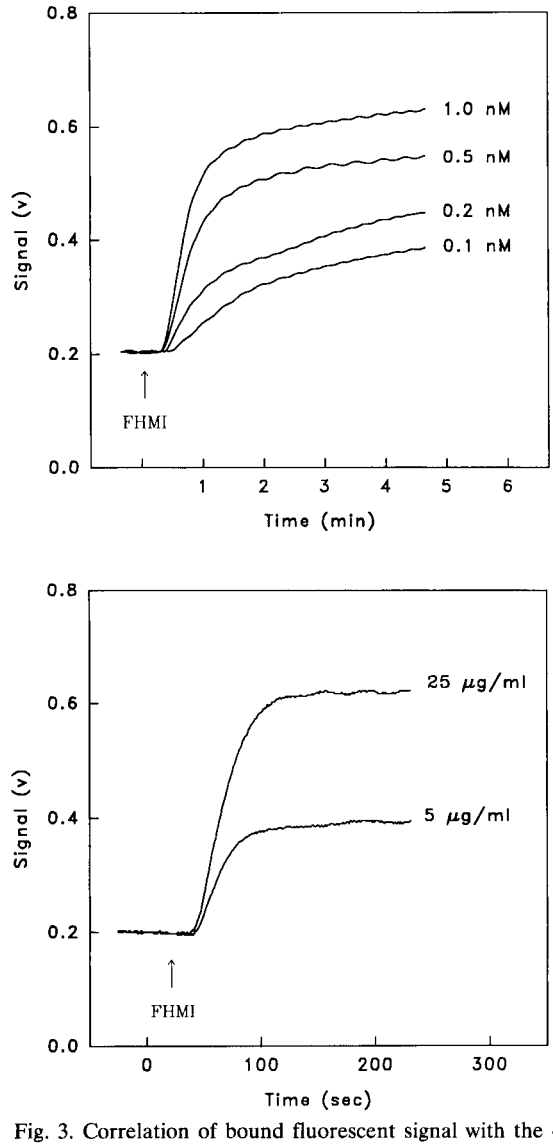

Fig. 3. Correlation of bound fluorescent signal with the concentration of the FHMI (top). Fibers were immobilized with a 25 μg/ml antibody. Solutions of FHMI which varied from 0.1 nM to 10 nM in PBS casein were perfused. Dependence of signal on the concentration of antibody immobilized on the fiber (bottom). A solution of 25 nM FHMI in PBS casein (0.1%) was perfused throughout.

Reusability of the fiber optic sensor

One of the most significant features of this sensor is the ability to use the same sensor for multiple measurements without significant loss of sensitivity. This is due to reversible binding of both FHMI and imazethapyr to the antibody coating the fiber. A single antibody coated fiber was perfused until a steady-state equilibrium was reached. Then, a perfusate containing 1 μM free imazethapyr was introduced. A reduction in fluo-

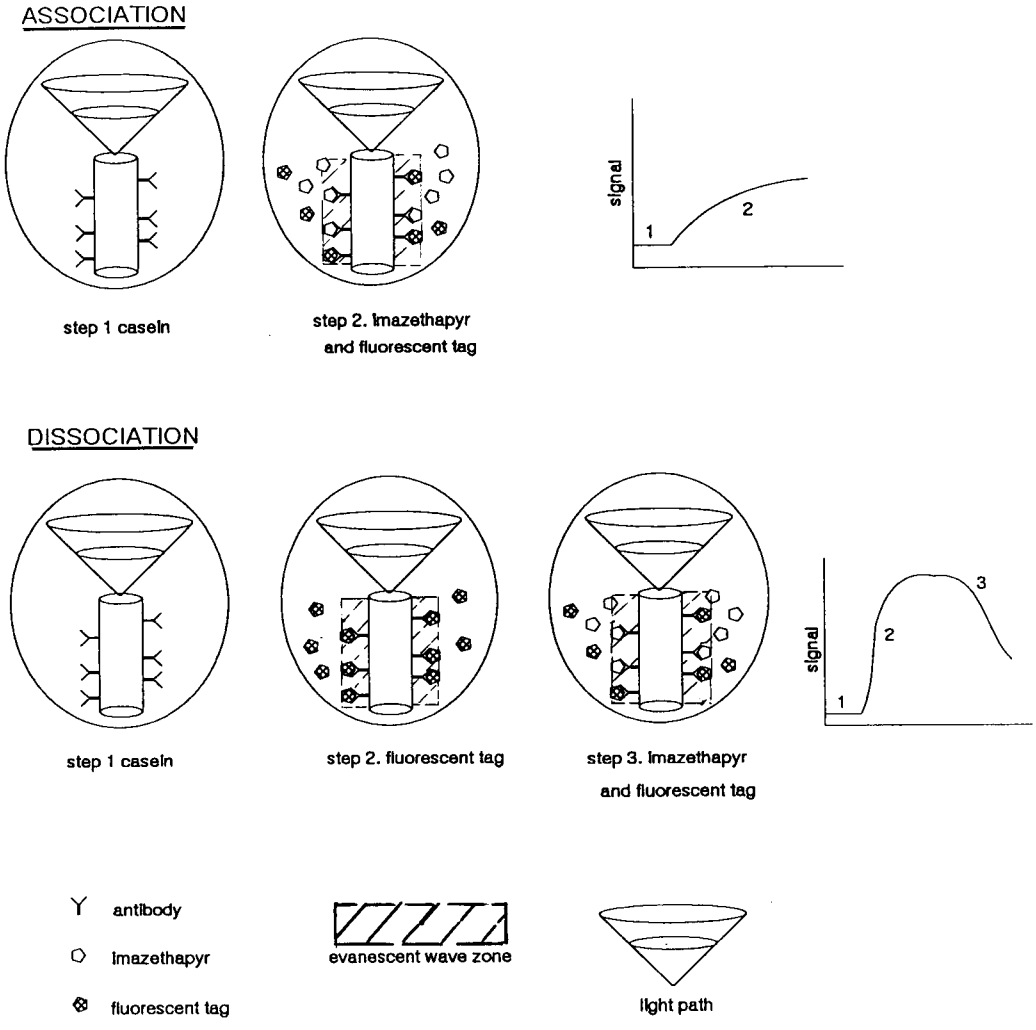

Fig. 4. Assay format: (top) association mode; (bottom) dissociation mode.

rescent signal was observed almost immediately due to the displacement of FHMI from the fiber by free imazethapyr (Fig. 7). When free imazethapyr was removed from the perfusate, the optical signal reversed to its steady-state level. In several examples, single fibers were used to obtain multiple measurements over a span of several hours.

Specificity of the fiber optic sensor

The effect of six agrochemicals (Fig. 8) on the immunosensor was investigated. Three of the compounds: imazapyr, imazaquin, and imazamethabenz methyl belong to the same imidazolinone class. The others: chlorimuron ethyl, sethoxydim, and primisulfuron are herbicides with different chemical structures. When 10 μM concentrations of the compounds were added to the perfusion solution after a steady-state binding of the FHMI was established, the three imidazolinone compounds displaced FHMI from the quartz fiber, whereas the three unrelated chemicals did not (Fig. 9). These results indicate the generic nature and specificity of the polyclonal antibody for detecting imidazolinone herbicides [11].

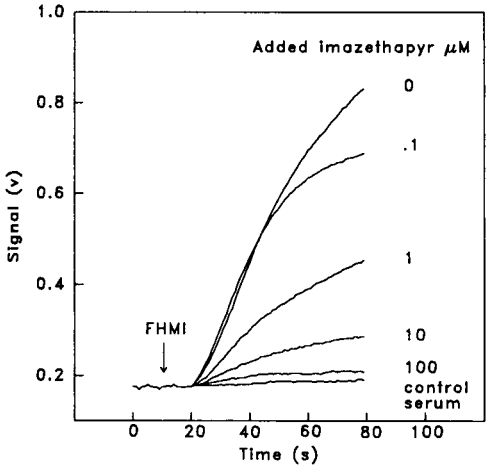

Fig. 5. Inhibition of FHMI association by imazethapyr. Varying concentrations of imazethapyr were added to the perfusion solution (25 nM FHMI in PBS caesin). Each perfusion solution reacted with a new antibody coated fiber. All the fibers were prepared on the same day.

Detection of imazethapyr in untreated soil extracts

Two types of soil (Plano and Sassafras) with different organic matters and clay content were extracted in water at a soil to water ratio of 1 : 1.

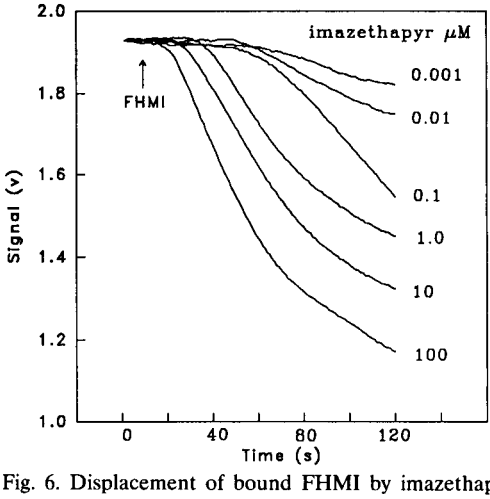

Fig. 6. Displacement of bound FHMI by imazethapyr. A 25 nM FHMI in PBS casein perfusion solution was used to establish a steady state level of fluorescence. After the steady state level was reached, the perfusate was changed to contain different concentrations of imazethapyr (0.001 to 100 μM). The decrease in fluorescence is measured in seconds.

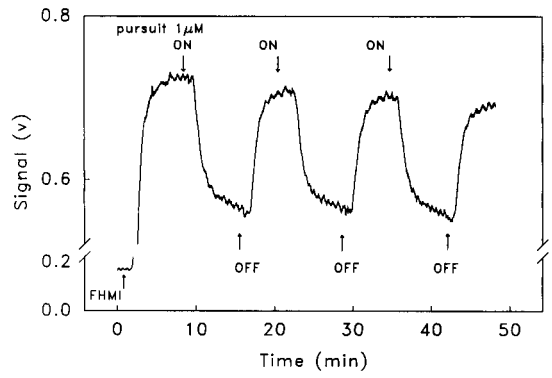

Fig. 7. Reusability of the fiber sensor. A 25 nM FHMI in PBS casein was perfused to reach a steady state of binding (about 5 min), at the point indicated as "ON", 1 μM imazethapyr was introduced in the perfusate. As considerable amount of FHMI was displaced, the perfusion solution was switched back to 25 nM FHMI alone (indicated as "OFF"). The ON and OFF process was repeated.

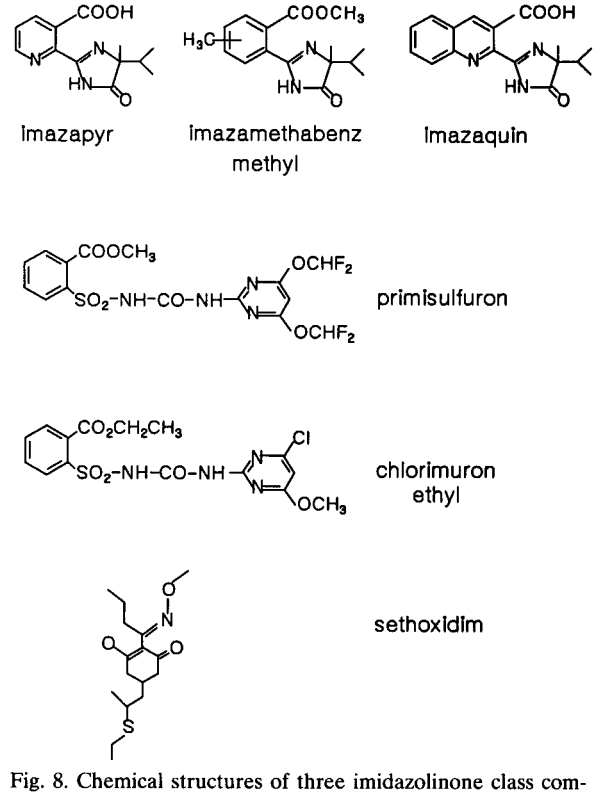

Fig. 8. Chemical structures of three imidazolinone class compounds and three non-imidazolinone agrochemicals used to demonstrate the specificity of the fiber optic sensor.

After sedimenting the particles and filtering through a 0.45-μm filter, the extracts were neutralized with 1/10 the volume of 10X PBS buffer and subjected to assay. The perfusion solution was prepared in the soil extraction instead of the PBS and dose response curves with imazethapyr were established. The dose response curves for imazethapyr present in PBS and the two soil extracts were superimposable (Fig. 10), indicating that the sensor system is quite transparent to matrix in the samples.

Conclusions

A fiber optic evanescent fluorosensor was successfully used for the detection of imazethapyr herbicide in buffered solution and in soil extracts. An IgG fraction of a polyclonal antibody was immobilized on the fiber and direct competitive binding of FHMI and free imzethapyr was monitored by total internal fluorescence transmitted through the optic fiber. The dose response curves obtained from either the binding or the displacement modes indicated that the assay sensitivity was better in the displacement mode (0.001 μM for displacement and 0.1 μM for binding). The reversibility of binding of both FHMI and imazethapyr suggests that this immunosensor may be useful for large sample handling for screening purposes. Automation of the assay system can also be envisioned. Since the samples are perfused through the flow-cell, thus, a short interaction time existed on the fiber probe, allowing the material with the highest affinity for the immobilized antibody be bound to the sensor. Matrix materials, which may present problems in a normal ELISA where incubation time is prolonged, may have a minimal effect in this system. This evanescent-excited fluorescence sensor offers the advantage of speed, sensitivity, and matrix transparency.

One of us (R.B.W.) would like to thank Dr. J. Finn for providing the 5-formyl imazapyr, Dr. J. Rittenburg of AgriDiagnostics Associates for producing the antibody, Drs. G. Asato and A. Lee

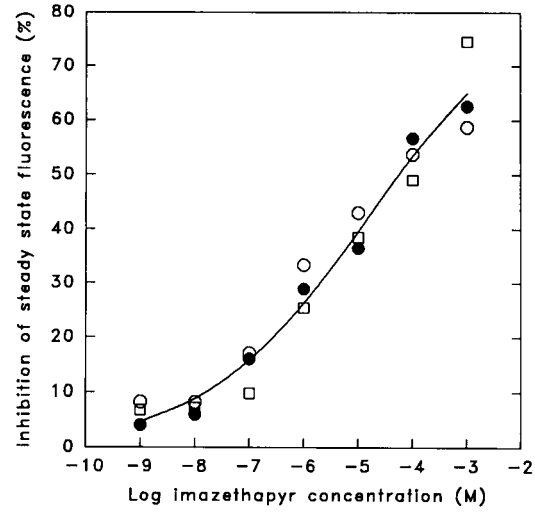

Fig. 10. The matrix transparency of the fiber sensor. Soils Plano and Sassafras were extracted with water at 1:1 ratio (v/w). The extracts were centrifuged at 1700 *g* for 10 min. The clear supernatant was adjusted to neutral pH by the addition of 1/10 the volume of 10X PBS buffer. After filtering through a 0.45-μm filter, the soil extraction solutions were used in place of PBS to prepare the perfusion solutions. FHMI displacement format was used to obtain the dose responses with imazethapyr. Each plot of% inhibition of the soil extracts [Plano (●) and Sassafras (○)] and PBS buffer (□) against imazethapyr concentrations represent an average of two measurements.

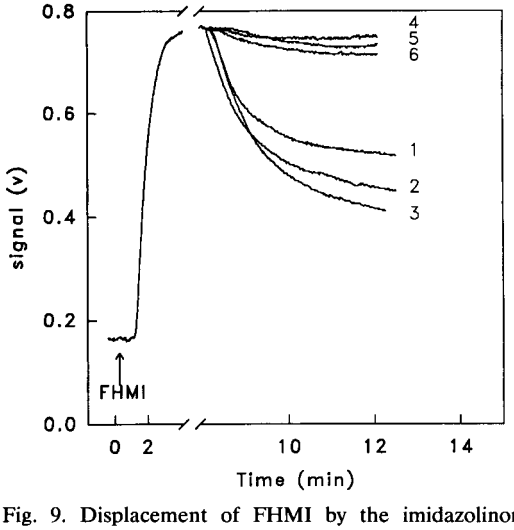

Fig. 9. Displacement of FHMI by the imidazolinone and non-imidazolinone compounds. 25 nM of FHMI in PBS casein was perfused to reach a steady state before a solution of 1 μM compound in the perfusate was added. The graphs 1, 2 and 3 depict imazamethabenz methyl, imazapyr and imazaquin respectively, and 4, 5 and 6 represent chlorimuron ethyl, primisulfuron and sethoxidim, respectively.

for support of the project, and Y. Roman for technical assistance. This research was supported in part by US Army contract DAAA-15-89-C-0007 (M.E.E.).

REFERENCES

1 D.L. Shaner, P.C. Anderson and M.A. Stidham, Plant. Physiol., 76 (1984) 545.
2 D.L. Shaner and N.M. Mallipudi, in D.L. Shaner and S.L. O'Conner (Eds.), The Imidazolinone Herbicides, CRC Press, Boca Raton, FL, 1991, p. 91.
3 D.R. Stocker, J.H. Rittenburg, G.D. Grothaus, R.B. Wong and Y. Roman, 203rd National Meeting of the American Chemical Society, San Francisco, CA, 1992, AGRO 210.
4 J.D. Andrade, R.A. Vanwagenen, D.E. Gregonis, K. Newby and J.N. Lin, IEEE Trans. Electron. Devices, 32 (1985) 1175.
5 E. Prusak-Sochaczewski and J. Luong, Anal. Lett., 23 (1990) 401.
6 L. Radjakovic, V. Ghaemmaghami and M. Thompson, Anal. Chim. Acta, 217 (1989) 111.
7 L.G. Fagerstam, in J.J. Villafranca (Ed.), Techniques in Protein Chemistry II, Academic Press, New York, 1990, p. 65.
8 J.D. Olson, P.R. Panfili, R. Armenta, M.B. Femmel, H. Merrick, J. Gumprz, M. Goltz and R.F. Zuk, J. Immunol. Methods, 134 (1990) 71.
9 K.R. Rogers, J.C. Fernando, R.G. Thompson, J.J. Valdes and M.E. Eldefrawi, Anal. Biochem., 202 (1992) 111.
10 K.R. Rogers, C.J. Cao, J.J. Valdes, A.T. Eldefrawi and M.E. Eldefrawi, Fundamental and Applied Toxicology, 16 (1991) 810.
11 R.B. Wong and Z.H. Ahmed, J. Agric. Food Chem., 40 (1992) 811.
12 K.R. Rogers, J.J. Valdes and M.E. Eldefrawi, Anal. Biochem., 182 (1989) 353.
13 M.J. Block and T.B. Hirschfeld, US Pat. 4,582,809 (1986).

Analytica Chimica Acta, 279 (1993) 149–153
Elsevier Science Publishers B.V., Amsterdam

Biosensor monitoring of blood lactate during open-heart surgery

Marika Kyröläinen, Håkan Håkanson, Rolf Ekroth and Bo Mattiasson

Department of Biotechnology, Chemical Centre, Lund University, P.O. Box 124, S-221 00 Lund (Sweden)

(Received 1st October 1992; revised manuscript received 4th January 1993)

Abstract

An on-line monitoring system for lactate in blood is described. The system consists of a sampling unit allowing dilution at the sampling point, a sample treatment unit for dialysis of the sample and an enzyme reactor with immobilized lactate oxidase. A Clark electrode is used as transducer. The enzyme preparation shows high storage stability and good operational stability. The system was used, during and after open-heart surgery, to follow fluctuation in the concentrations of L-lactate in blood being pumped to and from the brain. A small difference of approximately 0.3–0.5 mM was monitored.

Keywords: Biosensors; Enzymatic methods; Blood; Enzyme reactor; Lactate; Surgery

During open-heart surgery, the patient is connected to a heart and lung machine. The circulation of the blood is carefully surveyed in order to ensure a sufficient oxygen supply in the body. At present there is no possibility of continuously determining whether the oxygen supply to the organs of the body is actually sufficient during these circumstances. This limitation would be circumvented by continuous monitoring of a metabolite which reflects the oxygen supply. L-lactate is such a metabolite and an on-line monitoring system for blood L-lactate has been developed. A measure of adequate oxygen supply is the so-called arterial/venous difference (A/V difference) which can be calculated if the concentration of L-lactate is monitored in both arterial blood and venous blood of a body organ. A limited oxygen supply is indicated by a change in the A/V difference.

Correspondence to: M. Kyröläinen, Department of Biotechnology, Chemical Centre, Lund University, P.O. Box 124, S-221 00 Lund (Sweden).

The monitoring system is a continuous flow system that consists of a sampling and a sample-handling unit connected to an enzyme column and a suitable transducer [1]. L-Lactate is converted by means of immobilized lactate oxidase and the oxygen consumption is registered with a Clark electrode.

EXPERIMENTAL

Materials

Lactate oxidase from *Peddicoccus* species (32 U mg^{-1}) and L-lactate calibration solution (1 mol l^{-1}) were obtained from Boehringer (Mannheim, Germany). Catalase from bovine liver (44 000 U mg^{-1}, 90 mg ml^{-1}) and porous glass (pore size 50 nm, particle diameter 0.13–0.21 mm) were purchased from Sigma (St. Louis, MO). All other chemicals were of analytical reagent grade.

Immobilization of enzymes

Preparations of alkylamine glass and aldehyde glass were made according to the procedure of

Weetall [2]. In a typical preparation, 0.6 g (dry weight) of activated glass was used for the immobilization of 6.3 mg of lactate oxidase (200 U). The enzyme was dissolved in 2.0 ml of 50 mM sodium–potassium phosphate buffer (pH 7.0) containing 0.9% (w/v) sodium chloride, and was added to the activated glass. The mixture was placed on a blood mixer and incubated at room temperature for coupling to take place. After 3 h, 60 μl of catalase (44 000 U mg^{-1}, 90 mg ml^{-1}) were added and the coupling was allowed to continue. The co-immobilization of catalase was carried out in order to improve the enzyme stability and to increase the measuring range. After another 2 h, 40 mg of cyanoborohydride were added to reduce the Schiff bonds formed, thus stabilizing the coupling [3]. The mixture was left at room temperature for 1 h and was then placed in a cold room for 19 h.

The enzyme preparation was washed with coupling buffer and then 10 ml of 1.0 M ethanolamine (adjusted to pH 7.7 with 6 M hydrochloric acid) were added. This step was intended to block the excess aldehyde groups [3]. The reaction was allowed to continue for 2 h in the cold room before the enzyme preparation was washed with ultrapure water obtained from a Milli-Q system (Millipore) and thereafter with coupling buffer. The enzyme preparation was finally packed into small columns (30 mm × 4.0 mm, i.d.) and stored in coupling buffer containing 0.02% (w/v) sodium azide at 4°C when not in use.

Instrumentation

The instrumentation used for sampling and on-line analysis of lactate was a commercially available system designed for continuous measurements of blood glucose (Gambro, Lund, Sweden) [1]. The system was slightly modified in order to be used as lactate monitor. The flow sheet in Fig. 1 explains the basic principle of the system.

The sampling probe consists of a coaxial tube with the inner tube about 2 mm shorter than the outer tube. Heparin solution (200 U ml^{-1}) is pumped through the outer compartment of the coaxial tube at a flow-rate of 3–4 ml h^{-1}. The heparin solution is mixed with the blood sample

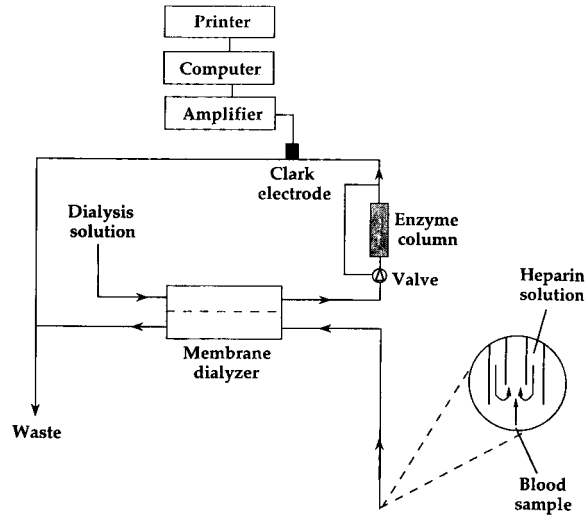

Fig. 1. Flow scheme of the analytical system.

at the tip of the catheter and the mixture is sucked into the inner tubing at a flow-rate of 6 ml h^{-1}. In this way blood clotting is prevented and no leakage from the sampling system occurs. The sample is pumped to a small dialyser where lactate passes through the dialysis membrane [Cuprophane (Enka, Germany) molecular weight cut-off 5000–10000]. A dialysis solution [50 mM sodium–potassium phosphate buffer (pH 7.0) containing 0.9% (w/v) sodium chloride] is pumped at the permeate side of the membrane at a flow-rate of 60–70 ml h^{-1}. The permeate flow is then passed through the enzyme column where lactate is converted by means of immobilized lactate oxidase and catalase according to the reaction:

$$\text{L-lactate} + O_2 \xrightarrow{\text{lactate oxidase}} \text{pyruvate} + H_2O_2$$

$$2H_2O_2 \xrightarrow{\text{catalase}} O_2 + 2H_2O$$

The oxygen concentration is registered with a Clark electrode. The flow passes through the column for 60 s and then a valve switches to a position where the column is by-passed for 30 s. The difference in the oxygen level of a solution which has passed and by-passed the enzyme column corresponds to the amount of lactate in the sample. The computer in the monitor converts this difference into a concentration. The system is calibrated by feeding a calibration solution (5.5

mM L-lactate in dialysis solution) instead of blood through the system.

Enzyme response

The linearity and the operational stability of the monitoring system were investigated by measurements of standard solutions of L-lactate in coupling buffer. Blood samples from a blood bank were thereafter analysed according to the same procedure in order to establish whether blood influenced the enzyme response [4].

Stability of the enzyme response

The stability of the enzyme response was investigated in three ways. Enzyme columns were stored for 230 days after initial testing and then tested intermittently over a period of 50 days. Other enzyme preparations were tested over a period of 50 days without prior storage. The enzyme response was also tested as operational stability. The lactate concentration of a standard solution was monitored during a total of 7.5 h.

Patient monitoring

The first measurements of blood L-lactate in a human using the on-line monitoring system were carried out on a female volunteer. The blood L-lactate level was monitored during physical exercise on a test bicycle and during the recovery period after the exercise. Blood samples were taken for off-line analyses [4].

The possibility of measuring the A/V difference of the brain was investigated. The L-lactate level in venous blood from the brain was monitored during open-heart surgery. During this time the patient was connected to the heart and lung machine for about 1 h. Off-line analyses of arterial blood samples were performed by the hospital staff. The patient was transferred to the intensive care unit after surgery and L-lactate monitoring was continued. The L-lactate level was monitored in both arterial and venous blood of the brain with two parallel analytical systems. The total monitoring time was about 7.5 h.

RESULTS AND DISCUSSION

Immobilized lactate oxidase combined with polarographic sensors was studied. The storage stability of the immobilized enzyme preparation showed good performance even after 280 days of storage in wet conditions in the presence of sodium azide at 4°C (Fig. 2). From this test it was not possible to measure a half-life, but it is clear that storage during controlled coditions causes no problems.

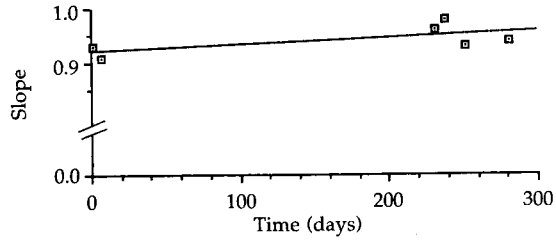

Fig. 2. Enzyme response as a function of storage time. ⊡ = Slope of calibration line.

The operational stability was also tested. As shown in Fig. 3, more than 250 samples caused no decrease in response when operating at 2.0 mM, a concentration of relevance to the medical application studied. More extensive studies on the stability of the enzyme columns involved repeated measurements of calibration solutions to create calibration graphs. Also here, high stability was observed. The first tendencies of a lowered response at higher concentrations (> 5 mM) appear after 30 days of storage and six repeated assay series (42.5 monitoring hours).

Analysis of blood samples has previously been shown to be convenient because of the sampling system and the dialysis step. The enzyme column is thus well protected from particulate matter and

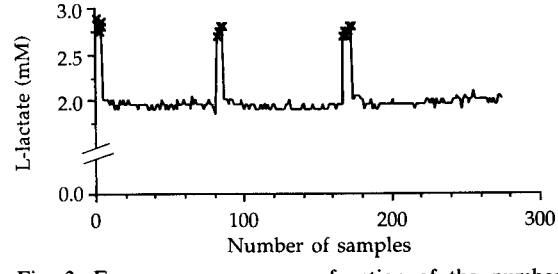

Fig. 3. Enzyme response as a function of the number of samples. Solid line = concentration of L-lactate (mM) in sample solution; × = concentration of L-lactate (mM) in standard solution.

macromolecules that could interfere. Biosensors for lactate based on lactate oxidase have been described on several occasions recently. Most of the work has focused on fermentation monitoring [5] but medical applications have also been discussed [6–8].

Lactate is a good indicator of oxygen supply to peripheral parts of the body. In an earlier investigation we studied the effect of physical exercise on the concentration of L-lactate in the blood [4]. Also in medical care, information about L-lactate concentration in the circulation gives useful information about the condition of the patient.

The present investigation dealt with open-heart surgery. Here, the patient is attached to a heart and lung machine and the body temperature is externally controlled. It is of utmost importance to keep a good control of the oxygen supply to the body and especially to the brain during such surgical processes. When no continuous monitoring was possible, off-line samples were analysed for content of blood gases and of lactate. The level of lactate has proved to be an important indicator. By analyzing arterial and venous blood it is possible to obtain an estimation of the condition of the organ under study.

The concentration of L-lactate in venous blood of the brain during open-heart surgery and off-line analyses of arterial blood are shown as a function of time in Fig. 4. The level of L-lactate in the venous blood increased when the patient was connected to the heart and lung machine but then remained stable. The slow warming procedure of the patient was started about 30 min before the heart- and lung machine was turned off. The blood L-lactate level decreased to the original value when the patient was disconnected from the heart and lung machine.

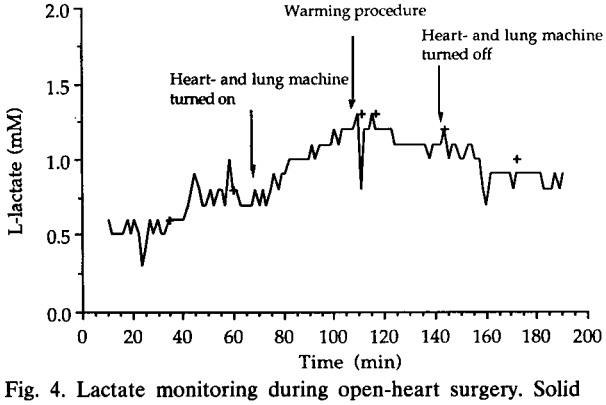

Fig. 4. Lactate monitoring during open-heart surgery. Solid line = concentration of L-lactate (mM) in venous blood from the brain, registered on-line; + = concentration of L-lactate (mM) in arterial blood to the brain, off-line analyses.

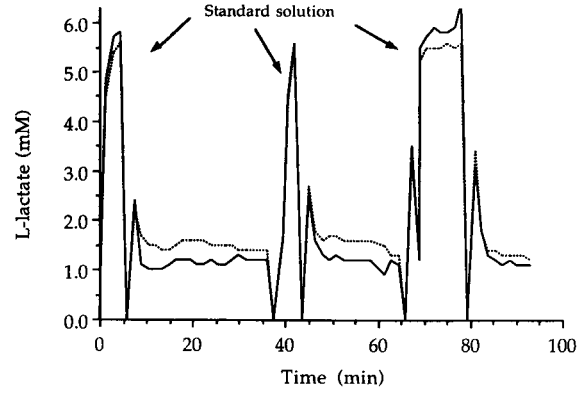

Fig. 5. Lactate monitoring during the recovery period after open-heart surgery. Dotted line = concentration of L-lactate (mM) in arterial blood from the brain, registered on-line; solid line = concentration of L-lactate (mM) in venous blood from the brain, registered on-line.

Figure 5 shows the L-lactate level in arterial and venous blood of the brain as a function of time after surgery. The calibration solution was analysed intermittently in order to see if there was a deviation between the two monitoring systems. An A/V difference ($lactate_{artery} - lactate_{vein}$) in the range 0.3–0.5 mM was noted. The measurements were performed in order to investigate the possibility of detecting an A/V difference and not to obtain an absolute value of the difference. It is the existence of an increase or a decrease in the A/V difference rather than the actual value that is of interest. The brain is believed to have a great capacity to consume blood L-lactate and should therefore normally have a positive A/V difference. A decrease in the A/V difference indicates lactate production, which is correlated with an insufficient oxygen supply.

The differences observed between arterial and venous blood are small, which places demands on the reliability and stability of the analytical sys-

tem used. Off-line sampling becomes hazardous from this point of view, as sample handling is difficult to standardize fully. When operating with fully automated continuous analytical systems, much better reliability is achieved and therefore such subtle differences may also be studied. It is important in this case to stress the need to be able to calibrate on-line, without disconnecting the patient, as a small baseline drift may quench the subtle differences studied. The use of the biosensor system in this case extended our knowledge of the well being of the patient undergoing treatment. This example is by no means unique and one can expect many similar studies in the future.

The on-line monitoring system developed for blood L-lactate is a valuable tool for measurements where metabolic processes causes rapid changes in the L-lactate level. The sampling unit also makes it possible to monitor blood L-lactate in situations where it is difficult or impossible to take off-line samples.

Support from the National Swedish Board of Technical and Industrial Development is gratefully acknowledged.

REFERENCES

1 H. Håkanson, Methods Enzymol., 137 (1988) 319.
2 H.H. Weetall, Methods Enzymol., 44 (1976) 134.
3 P. Thavarungkul, H. Håkanson, O. Holst and B. Mattiasson, Biosensors Bioelectron., 6 (1991) 101.
4 H. Håkanson, M. Kyröläinen and B. Mattiasson, Biosensors Bioelectron., in press.
5 K. Schügerl, Anal. Chim. Acta, 213 (1988) 1.
6 B.A. Petersson, Anal. Chim. Acta, 209 (1988) 231.
7 M. Mascini, F. Mazzei, D. Moscone, G. Calabrese and M.M. Benedetti, Clin. Chem., 33 (1987) 591.
8 G. Palleschi, M. Mascini, L. Bernardi, G. Bombardieri and A.M. DeLuca, Anal. Lett., 22 (1989) 1209.

Analytica Chimica Acta, 279 (1993) 155–161
Elsevier Science Publishers B.V., Amsterdam

Introduction to the dielectric estimation of cellular biomass in real time, with special emphasis on measurements at high volume fractions

Chris L. Davey, Hazel M. Davey and Douglas B. Kell [a]

Department of Biological Sciences, University of Wales, Aberystwyth, Dyfed SY23 3DA (UK)

Robert W. Todd

Aber Instruments, Science Park, Cefn Llan, Aberystwyth, Dyfed SY23 3AH (UK)

(Received 1st October 1992; revised manuscript received 28th December 1992)

Abstract

The equations that describe the magnitude of the β-dielectric dispersion of biological cell suspensions are introduced. It is then demonstrated how this magnitude can be used to monitor cellular biomass concentrations in real time. These equations are then shown accurately to describe experimental data obtained over a wide range of cell sizes and volume fractions.

Keywords: Cell suspensions; Dielectric estimations

The on-line and real-time measurement of the biomass content of industrial fermentations has long been an area of interest for the development of novel sensing devices. The problems encountered are usually considerable, however. Not only is the biomass often filamentous rather than being discrete spheres or rods but it can also occur as pellets rather than as a uniform suspension. The medium is frequently poorly defined, with a large amount of non-biomass solids which can give a high optical density even prior to inoculation. The fermentors are often aerated and this creates problems of bubbles adding significant noise to the measurements. In addition it is normally the measurement of biomass (as opposed to necromass) that is of interest, and so the sensing device must be able to distinguish the two. Here we show how the dielectric method of measuring biomass can deal with most of these problems. In addition we illustrate the effects of high cellular volume fractions on the linearity of the method.

Correspondence to: C.L. Davey, Department of Biological Sciences, University of Wales, Aberystwyth, Dyfred SY23 3AH (UK).
[a] Also at Aber Instruments.

Electric fields, capacitance and cell suspensions

For the purposes of this paper a very simplified and intuitive description of the processes involved will be presented. Reviews of the full theory can be found, e.g., in Refs. 1 and 2.

The application of an electric field to a suspension of cells in an aqueous ionic solution is illustrated in Fig. 1. The electric field can be considered as a force field that pushes electrical charges along, in this case the ions in the solution. It runs from the positively to the negatively charged electrode and pushes the positive ions in the direction of the field and the negative ions in

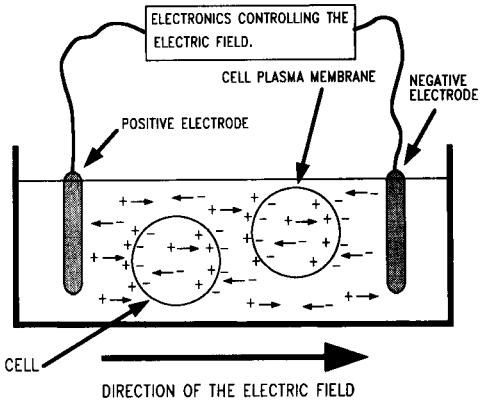

Fig. 1. The effect an applied electric field has on a suspension of biological cells. The ions are shown as point charges.

the opposite direction. As can be seen from the figure, many of the ions both inside and outside the cells can move only so far before they bump into the cell's plasma membranes and are prevented from moving any further. The result of this is that there develops a charge separation or polarisation at the poles of the cells. The capacitance of the suspension (measured in Farads, F) gives a measure of the extent of these field-induced polarisations. As there is a large amount of charge polarisation in the suspension in Fig. 1 then one may expect its capacitance to be high. Further, as the volume fraction of cells increases the amount of membranes polarised increases and so the capacitance of the suspension increases further. It is by the measurement of the capacitance of the suspension that one monitors the biomass content [3]. (It is also worth mentioning that the electrodes themselves can display a substantial and frequency dependent capacitance; artefacts of this type are minimised by using a 4-terminal measurement [4].)

A 4-terminal machine that monitors biomass via the radiofrequency electrical capacitance has been developed and commercialised by Aber Instruments (Science Park, Aberystwyth) and is called the Biomass Monitor (BM, formerly called the Bugmeter). It is the theory of how this machine measures biomass that forms the basis of this paper.

Frequency of an electric field and its effect on the capacitance of a cell suspension

So far the field has only been shown going in one direction. Of course one can reverse the field direction. If one does this then the only effect of the field reversal is to change the polarity of the polarisations of the cells but not their magnitude. As capacitance gives a measure of the magnitude of the field induced polarisations then changing the field direction does not change the capacitance of the suspension per se.

One can of course change the rate at which the field changes direction. The number of times the field changes direction per second is measured by its frequency (Hz). Frequency has a marked effect on the capacitance of a cell suspension, because the ions moving up to and polarising the plasma membranes take a finite time to reach them. Figure 2 shows the typical polarisation induced across a cell as the frequency of the electric field is increased. Also shown is how the capacitance of the suspension changes. At frequency (a) on Fig. 2 the field frequency is low and so a lot of ions have time to reach the plasma membranes and polarise them before the field changes direction and moves the ions the oppo-

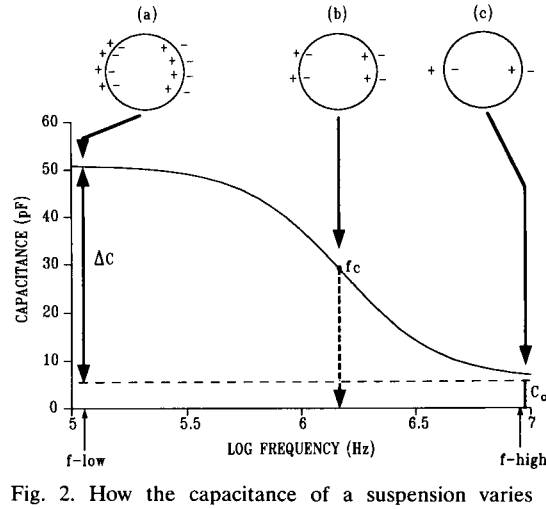

Fig. 2. How the capacitance of a suspension varies with frequency. Also shown are three cells from a suspension like Fig. 1 at a (a) low, (b) medium and (c) high frequency with respect to the β-dispersion. For convenience the induced polarisations of the plasma membranes are shown only with the field going in one direction (left to right). See the text for a full discussion of the annotation on this figure.

site way. Thus the capacitance of the cell suspension is high. At higher frequencies (b on the figure) fewer ions have time to reach the membranes and so the extent of the induced transmembrane polarisation is less and the capacitance of the suspension is also lower. At very high frequencies (c on the figure) very few ions have time to move to and polarise the membranes before the field changes direction, and so the induced membrane polarisation is very small. At these frequencies the cell's contribution to the capacitance of the suspension is very small and one just measures the background capacitance of the medium (mainly due to water dipoles).

From Fig. 2 it is seen that the capacitance of the suspension goes from a high low-frequency plateau (maximal cell polarisation, Fig. 2a) to a low high-frequency plateau (minimal cell polarisation, Fig. 2c). This fall in capacitance of a suspension due to the loss of induced membrane polarisation with increasing frequency is called the β-dispersion. The residual high frequency capacitance due to the medium is called C_∞ and the height of the low-frequency plateau above this is the ΔC (capacitance increment) of the β-dispersion. The frequency when the fall in capacitance is half completed (i.e. the frequency when capacitance equals $C_\infty + (\Delta C/2)$ is called the critical frequency (f_c).

As one is aiming to measure the biomass content of a cell suspension then one needs to see what effect this has on the β-dispersion curve shown in Fig. 2. Figure 3 shows the β-dispersion of cell suspensions with different biomass contents. The figure shows that the f_c is not changed by the biomass content, nor is C_∞. What does change as a function of biomass content is the magnitude of ΔC, which increases as the biomass content does. Thus the problem of measuring the biomass content of a cell suspension reduces to one of measuring the magnitude of the ΔC of the β-dispersion [3].

Effect of necromass and non-biomass material on the biomass measurements

So far it has been stated that one can measure the biomass content of a suspension using dielectric means, and by the measurement of the ΔC of

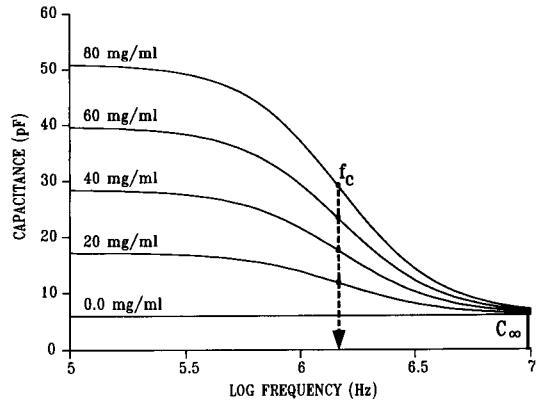

Fig. 3. The effect of increasing biomass concentrations (in mg wet weight ml^{-1}) on the β-dispersion of a cell suspension. See the text for a full discussion.

the β-dispersion in particular, but no justification for this statement has been given. If the cells in a suspension have badly ruptured plasma membranes then the ions in the solution just move through the holes in the membranes and fail to cause polarisation of the membranes even at low frequencies. Thus dead cells do not have a significant β-dispersion (i.e., a ΔC). Thus if one uses the ΔC of the β-dispersion to measure the biomass content of a cell suspension one can expect to measure only cells with intact plasma membranes (i.e., living cells) as opposed to ruptured (dead) cells [5].

Since the basis for biomass measurement via the ΔC of the β-dispersion depends on the polarisation of the plasma membranes by the application of an electric field one can expect, and indeed finds, that the mechanism works for intact cells of any size and shape.

If non-biomass solids, oil droplets or gas bubbles are present in the medium then their effect on the ΔC of the β-dispersion must be considered. The ions in a growth medium either travel straight through the non-biomass material if it is permeable to ions or just move round them if it is not. In neither case are significant charge polarisations produced (since they have no plasma membranes) and so these materials will not produce a significant ΔC term. Thus non-biomass materials are not expected to contribute to the

ΔC of the β-dispersion in a real fermentation medium.

If the volume fraction of the non-biomass material is very high then it may contribute in a negative sense to the β-dispersion curve. This is because one is replacing a finite volume fraction of polarisable material (cells and water) with non-polarisable material (non-biomass solids, oil, bubbles etc). The effect of this is to reduce C_∞, as the volume fraction of water has been reduced. ΔC is also reduced because one has reduced the volume fraction of biomass present.

Measurement of the ΔC of the β-dispersion for the estimation of cellular biomass

Earlier it was stated that the problem of biomass measurement reduces to one of the estimation of the ΔC of the β-dispersion. Thus one needs a convenient means of measuring ΔC during a fermentation. There are two ways of achieving this. Figure 2 showed a β-dispersion and marked on it were two spot frequencies labelled f-low and f-high. The capacitance at f-high is approximately equal to C_∞ whilst that at f-low approximately equals $(C_\infty + \Delta C)$. Thus one can see that if one measures the capacitance at f-high and f-low "simultaneously", and then subtracts the capacitance at f-high (C_∞) from that at f-low $(\Delta C + C_\infty)$ one gets ΔC, which is what is related to the biomass concentration. This is the principle of dual-frequency biomass measurements. The second method of estimating ΔC, and hence biomass concentration, uses the capacitance at f-low alone. At zero biomass concentration the capacitance at f-low equals C_∞ (see Figs. 2 and 3); thus one can measure the capacitance of the medium at f-low prior to inoculation and then back off this capacitance to zero (i.e., set C_∞ to zero). This means that any change in capacitance at f-low during a fermentation must reflect changes in ΔC and hence biomass concentration. This is how single-frequency biomass measurements work.

For a real fermentation one normally produces a calibration curve of ΔC (estimated by single- or dual-frequency measurements) versus biomass concentration (e.g., as dry weight). Figure 4 is such a calibration curve for a yeast. Dual- and

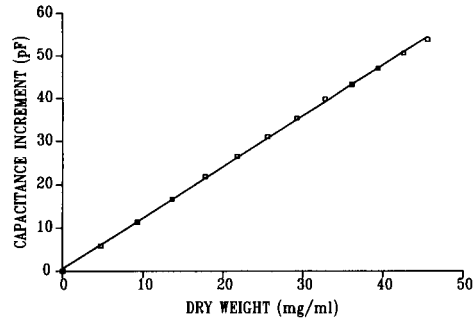

Fig. 4. A calibration curve of ΔC (capacitance increment), as judged by single frequency measurements (f-low = 0.4 MHz, cell constant = 78 m^{-1}), versus mg dry weight ml^{-1}. The linear regression fit had a gradient of 1.179, a Y-intercept of 0.547 and an r^2 of 0.9995.

single- frequency measurements using a Biomass Monitor (BM) have been successfully used to monitor the biomass concentrations in a variety of systems [6]. These include bacterial and yeast cultures [3,7,8], bacterial biofilms [9], cultured cells [10], immobilized cells [11] and filamentous cells in liquid and solid substrate fermentations [12,13]. Mishima et al. [14] have studied 2-terminal capacitance measurements as a method for biomass estimation, apparently in ignorance of the above work.

Capacitance and relative permittivity

To consider the relationship between the ΔC of the β-dispersion and the structure of the cells in the suspension giving rise to it, one cannot work easily with capacitances. The reason for this is that capacitance is a macroscopic measurement that depends on the geometry of the electrodes used. For biomass measurements this is fine because the electrode geometry remains constant. However for physical calculations the need to adjust the capacitances read to allow for the electrode geometry is an inconvenience. Thus one requires a way of quoting capacitances so that they are independent of the geometry of the electrodes. To do this one converts capacitance to relative permittivity (ϵ'). Just like capacitance, ϵ' gives a measure of the extent of the polarisations induced in a material by the application of an electric field. The capacitance (C in Farads) of a

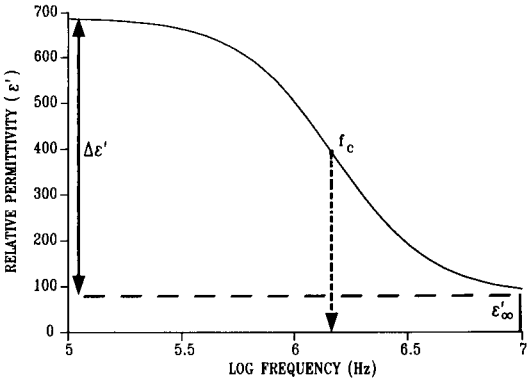

Fig. 5. The data of Fig. 2 (cell constant 120 m^{-1}) converted to ϵ' using Eqn. 1. The annotations on the figure are discussed in the text.

material is related to the equivalent relative permittivity (ϵ') by:

$$\epsilon' = C(k/\epsilon_0) \quad (1)$$

ϵ_0 is the permittivity of free space and is a constant with a value of 8.854×10^{-12} F m^{-1}. k is known as the cell constant and has units of m^{-1}, reflecting the geometry of the electrodes. The important point is that electrodes of different geometries (different k values) will record different capacitances for the same cell suspension, but will all produce the same ϵ' value.

Relative permittivity (ϵ') of a cell suspension in the region of the β-dispersion

From Eqn. 1 it is clear that the relative permittivity of a material (e.g., a suspension) is equal to the capacitance multiplied by a constant for a given electrode system of (k/ϵ_0). Taking this into account then a β-dispersion plot like Fig. 2 is reflected in the permittivity plot of Fig. 5. ΔC becomes $\Delta\epsilon'$ (dielectric increment) and C_∞ becomes ϵ'_∞; all that has happened is that the capacitance terms have been multiplied by (k/ϵ_0) to convert them to ϵ' values. The f_c is the same in both plots. The formula that relates the magnitude of $\Delta\epsilon'$ (and hence the ΔC) to the properties of the biological cells in the suspension is:

$$\Delta\epsilon' = (9PrC_m)/4\epsilon_o \quad (2)$$

Here P (which is unitless) is the volume fraction of cells present (i.e., the volume of material bounded by a plasma membrane, per unit volume of suspension), r is the radius of the nominally spherical cells from the cell centre to the plasma membrane (in metres) and Cm is the plasma membrane capacitance per unit of membrane area (F m^{-2}). This gives a measure of the ability of the plasma membrane to store charge. For biological systems C_m typically has a value of 0.01 F m^{-2}.

For a given cell suspension, r and C_m are constant and ϵ_0 is a physical constant anyway. Thus a plot of $\Delta\epsilon'$ versus cellular volume fraction is a straight line of gradient $(9rC_m/4\epsilon_0)$. This relationship explains why ΔC is linearly proportional to biomass concentration.

$\Delta\epsilon'$ (and ΔC) of the β-dispersion at high volume fractions

Equation 2 holds only for "low" volume fractions, in which the electric field impinging on a given cell in the suspension has not been distorted by the cells around it. At high volume fractions this does not apply, and a plot of $\Delta\epsilon'$ vs. volume fraction begins noticeably to plateau out (at say $P > 0.15$, i.e., approximately 150 mg wet weight ml^{-1}). From the point of view both of academic studies on cell structure (e.g., estimating C_m using Eqn. 2) and the industrial measurement of biomass concentrations, one needs to be able to model and compensate for this loss of linearity.

Schwan and Morowitz [15] suggested a modification to Eqn. 2 that allowed for this non-linearity at high volume fractions (P):

$$\Delta\epsilon' = (9rC_m)/(4\epsilon_0) \cdot P/[1 + (P/2)]^2 \quad (3)$$

This is Eqn. 2 with the additional term $1/[1 + (P/2)]^2$ that models the non-linearity at high values of P. This additional factor depends only on the volume fraction of cells present and is independent of the cell radius. Although this equation is potentially of great use, it had never been checked thoroughly with real cells. By making careful and independent measurements of P (by two different methods), r and $\Delta\epsilon'$ for a number of bacterial and yeast suspensions, we have recently shown that this equation does indeed hold true over a wide range of cell sizes and volume

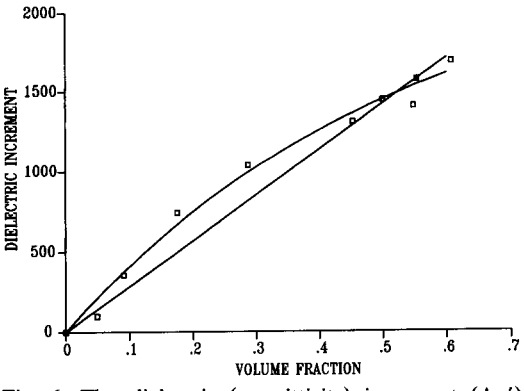

Fig. 6. The dielectric (permittivity) increment ($\Delta\epsilon'$) as a function of volume fraction for Distillers Co. Distillery yeast. The straight and curved lines are for the best fits of Eqns. 2 and 3 respectively to the data using non-linear least squares fitting. See Ref. 16 for a full description.

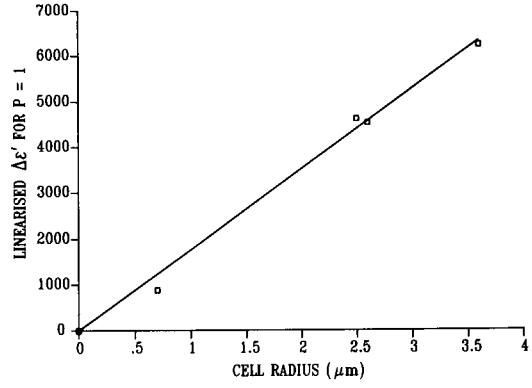

Fig. 8. A plot of $\Delta\epsilon'$ as linearised for a volume fraction of 1 vs. the radius of the cells used. Data are shown for one bacterial strain (Micrococcus luteus) and three strains of the yeast Saccharomyces cerevisiae (DCL Baker's and Distillery yeasts, and a strain called BB 11). See Ref. 16 for details.

fractions [16]. Figure 6 shows how the $\Delta\epsilon'$ varies as a function of volume fraction for a strain of the yeast *Saccharomyces cerevisiae*. Also shown on the plot are the least squares fits of Eqns. 2 and 3 to the data (see Ref. 16 for full experimental details). For both fits $\Delta\epsilon'$ and P were measured for the cell suspensions used and so the fits were achieved by iteration of the $(9rC_m/4\epsilon_o)$ terms in each equation. Equation 3 produced a visually as well as a statistically better fit to the data than did Eqn. 2.

Equation 3 can be modified by replacing all the volume fraction terms P by $V_{sp}C_n$. Where V_{sp} is the specific enclosed volume of the cells (i.e., the volume enclosed by the plasma membranes of the cells, per unit biomass) in ml (mg dry weight)$^{-1}$. C_n is the dry weight of the cells in mg ml^{-1}. That the correction factor for the nonlinear relationship between $\Delta\epsilon'$ and P is indeed independent of the cell radius has the important and useful consequence that a simple calibration curve of dielectric increment vs. dry weight or cell numbers permits one to determine the specific enclosed volume of the strain of interest, i.e., the volume enclosed by the cytoplasmic membranes of the cells per unit biomass (Fig. 7).

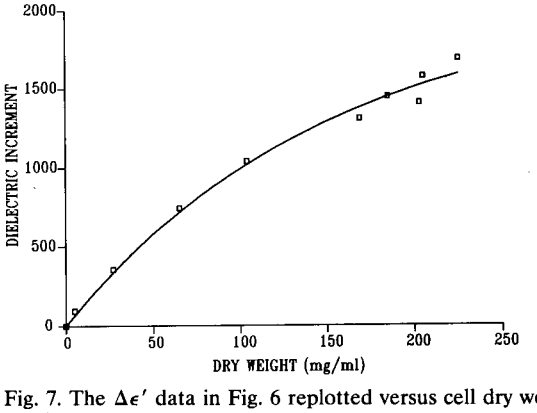

Fig. 7. The $\Delta\epsilon'$ data in Fig. 6 replotted versus cell dry weight ml^{-1}. The curve on the plot is the non-linear least squares best fit of Eqn. 3 with $V_{sp}C_n$ replacing the P terms. See the text for details. The best fit for V_{sp} was 3.5 ml mg^{-1}.

From Eqn. 2 one would expect that a plot of $\Delta\epsilon'$ per unit volume fraction (either measured at low P or linearised) vs. the cell radius to give a straight line. This is shown in Fig. 8.

Conclusions

This paper has discussed the theory behind how the Aber Instruments Biomass Monitor measures biomass concentrations. In addition data were presented to demonstrate that the $\Delta\epsilon'$ (ΔC) of the β-dispersion, which is what is measured by the BM to monitor biomass, is linear with volume fraction to very high levels. At concentrations where linearity is lost it is shown that this is predictable using a simple equation that can be implemented as part of a linearising routine.

This work is supported by the Science and Engineering Research Council, UK, Aber Instruments Ltd. and FT Applikon Ltd., under the terms of the LINK scheme in Biochemical Engineering.

REFERENCES

1 K.R. Foster and H.P. Schwan, CRC Crit. Rev. Biomed. Eng., 17 (1989) 25.
2 C.L. Davey and D.B. Kell, in Treatise on Bioelectrochemistry, Vol. VI, Birkäuser, Zürich, 1993, in press.
3 C.M. Harris, R.W. Todd, S.J. Bungard, R.W. Lovitt, J.G. Morris and D.B. Kell, Enz. Micr. Technol., 9 (1987) 181.
4 D.B. Kell, in A.P.F. Turner, I. Karube and G.S. Wilson (Eds.), Biosensors; Fundamentals and Applications, Oxford University Press, Oxford, 1987, p. 427.
5 N. Stoicheva, C.L. Davey, G.H. Markx and D.B. Kell, Biocatalysis, 2 (1989) 245.
6 D.B. Kell, G.H. Markx, C.L. Davey and R.W. Todd, Trends Anal. Chem., 9 (1990) 190.
7 C.A. Boulton, P.S. Maryan and D. Loveridge, in Proc. 22nd European Brewing Convention, Zürich, 1989, p. 653.
8 L.E. Ferris, C.L. Davey and D.B. Kell, Eur. Biophys. J., 18 (1990) 267.
9 G.H. Markx and D.B. Kell, Biofouling, 2 (1990) 211.
10 G.H. Markx, C.L. Davey, D.B. Kell and P. Morris, J. Biotechnol., 20 (1991) 279.
11 G.J. Salter, D.B. Kell, L.A. Ash, J.M. Adams, A.J. Brown and R. James, Enzym. Micr. Technol., 12 (1990) 419.
12 C.L. Davey, W. Penaloza, D.B. Kell and J.N. Hedger, World J. Microbiol. Biotechnol., 7 (1991) 248.
13 R. Fehrenbach, M. Comberbach and J.O. Pêtre, J. Biotechnol., 23 (1992) 303.
14 K. Mishima, A. Mimura, Y. Takahara, K. Asami and T. Hanai, J. Ferment. Bioeng., 72 (1991) 291.
15 H.P. Schwan and H.J. Morowitz, Biophys. J., 2 (1962) 395.
16 C.L. Davey, H.M. Davey and D.B. Kell, Bioelectrochem. Bioenerg., 28 (1992) 319.

Analytica Chimica Acta, 279 (1993) 163–166
Elsevier Science Publishers B.V., Amsterdam

Application of fast atom bombardment mass spectrometry for the analysis of biologically active compounds

L. Fourie

Department of Chemistry, Potchefstroom University for CHE, 2520 Potchefstroom (South Africa)

K.J. van der Merwe, P. Swart and S.S. de Kock

Department of Biochemistry, University of Stellenbosch, 7600 Stellenbosch (South Africa)

(Received 14th October 1992; revised manuscript received 19th February 1993)

Abstract

A fast atom bombardment (FAB) mass spectrometric method for structural studies on phenolic aziridines and their open-chain precursors is described. It was found that the presence of free phenolic groups put limitations on the FAB ionisation method previously described for the study of acetylated aziridines. A new method for structure confirmation of phenolic aziridines and their precursors is described in which thioglycerol is used for in situ derivatization as well as a FAB matrix.

Keywords: Mass spectrometry; Aziridines

The shrub *Salsola tuberculatiformis* Botsch, occurring in the Keetmanshoop district of Namibia, was used by the Kalahari Bushmen for contraceptive purposes. It was previously reported that extracts of this plant inhibit the estrous cycle of laboratory animals [1].

During an investigation into the isolation and identification of active principals involved, it was found that the active compounds were extremely labile and easily decomposed autocatalytically. Biochemical assays, based on the inhibition of adrenal steroidogenic enzymes, by these compounds eventually led to the isolation, in microquantities [2], of a single active fraction called S2.

S2 is a highly unstable fraction and in the presence of water quickly decomposes into the weakly active synephrine (**1**). Whereas acetylation of synephrine led to the stable triacetate [**2**, $m/z = 273$ electron impact (EI) ionisation], acetylation of S2 under identical conditions yielded an unstable monoacetate (**3**, $m/z = 191$ EI ionisation). The fragmentation pattern observed for the latter compound corresponded with that of the acetylated aziridine **3**, subsequently synthesized in our laboratory and confirmed with nuclear magnetic resonance (NMR) spectroscopy. These results strongly suggest the presence of 2-(4-hydroxyphenyl)-1-methylaziridine in S2.

Aziridines as well as their protonated forms, the aziridinium ions, are highly reactive compounds which can be formed in situ by chemical [3] or thermal cyclization of ethylamino precursors with a good leaving group R_4 on carbon 2 as shown in Fig. 1. This is a reversible reaction since the aziridine ring can be opened again by nucleophilic attack by R_4^- acting as a nucleophile.

In order to try to distinguish whether acetylated S2 contained the aziridine (**3**), its corresponding open-chain precursor, or a mixture of both, acetylated precursors (**4e–h**) and their cy-

Correspondence to: L. Fourie, Department of Chemistry, Potchefstroom University for CHE, 2520 Potchefstroom (South Africa).

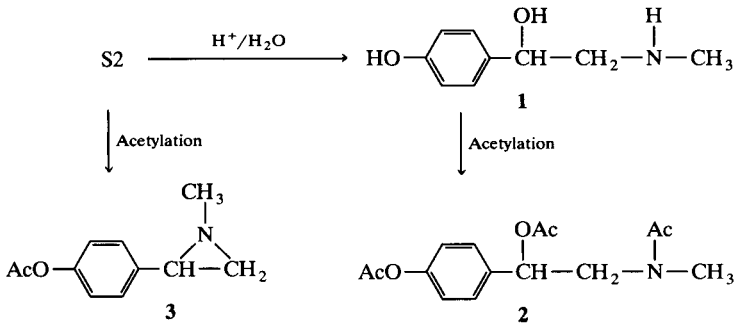

Fig. 1. Reaction scheme for the formation of synephrine (**1**), synephrine triacetate (**2**) and acetylated S2 (**3**).

clized counterparts (**5**e–h) were synthesized in our laboratory and fully characterized by NMR spectroscopy. When these compounds were studied using EI ionisation, it was noticed that the open-chain precursors did not show their true molecular ions, but instead the M^+ peaks of the corresponding cyclized aziridines. When the same acetylated compounds were investigated using fast atom bombardment (FAB) [4] ionisation, both the open-chain precursors (**4**) and the aziridines (**5**), showed their respective true molecular ion peaks $[M + H]^+$, at the calculated m/z values. FAB ionisation therefore enabled us to distinguish between these very labile interconvertible compounds and to prove unequivocally that acetylated S2 is an aziridine and not an open-chain precursor [5].

Since the possibility existed that the aziridine in acetylated S2 might have been formed as an artefact during acetylation of S2, our mass spectrometric studies were extended to include phenolic precursors related to S2. For this purpose compounds **4**a–d (Fig. 2) were synthesized in our laboratory and studied by using FAB mass spectrometry.

EXPERIMENTAL

The syntheses of compounds **4**a–d were undertaken by methods described in the literature [6]. Structures were verified using ^1H and ^{13}C NMR. All mass spectra were recorded on a VG70-70E mass spectrometer fitted with an Ion

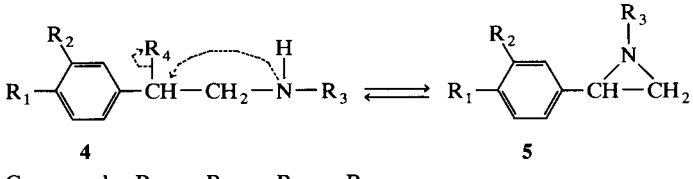

4 **5**

Compound	R_1	R_2	R_3	R_4
a	OH	H	H	Br, Cl
b	OH	H	CH_3	Br, Cl
c	OH	OH	H	Br
d	OH	OH	CH_3	Br
e	OAc	H	H	Br, Cl
f	OAc	H	CH_3	Br, Cl
g	OAc	OAc	H	Br
h	OAc	OAc	CH_3	Br

Fig. 2. Chemical structures of aziridine precursors (**4**) and their corresponding aziridines (**5**).

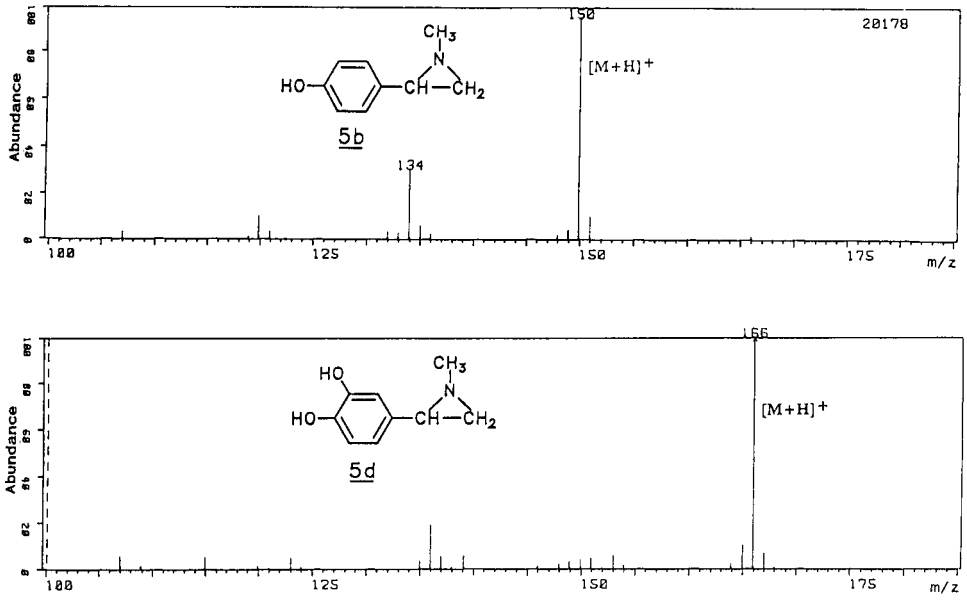

Fig. 3. FAB mass spectra of cyclized analogues (5a–d).

Tech saddle field gun (Ion Tech, Teddington) employing xenon as bombardment gas (8 kV, 1 mA). The mass spectrometer was operated in the positive ion mode (6 kV) and the magnetic analyzer scanned at 5 s per decade over the mass range 500–100 Da. All mass spectral data were acquired and processed on a VG2035 data system.

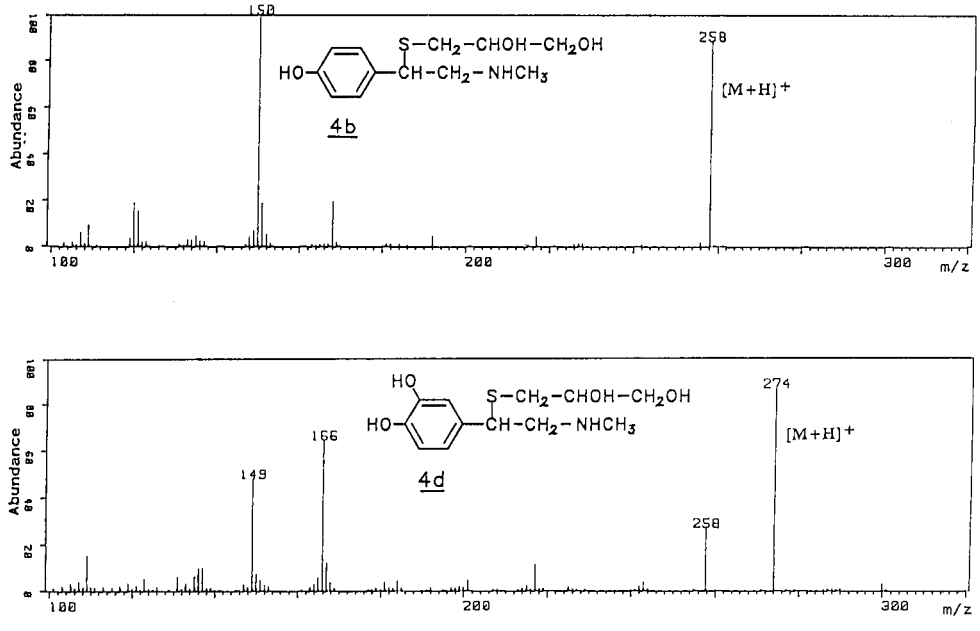

Fig. 4. Mass spectra of chemical adducts of the open-chain precursors 4b and 4d formed during FAB ionisation using thioglycerol matrix.

Glycerol and thioglycerol [7] obtained from Fluka were used as matrix compounds and standard VG stainless steel targets used for ionisation.

RESULTS AND DISCUSSION

The results obtained with compounds **4**a–d clearly indicated that, in contrast to our previous experience with the acetylated compounds [5], FAB ionisation no longer yielded the true molecular ions of the phenolic precursors (**4**a–d), but instead showed the $[M + H]^+$ peaks of the corresponding aziridines (**5**a–d). Typical mass spectra are given in Fig. 3. These studies demonstrated the influence of the free phenolic group on the chemical behaviour of these aziridines and their precursors, indicating the limitations of the previously reported method [5] in the study of the phenolic analogues.

A major problem in the investigations of the active compounds occurring in the Salsola plant, is their extreme instability. Since the chemical origin of this instability is now established, attempts were made to prepare stabilized derivatives of these compounds. Aziridines or precursors which could give rise to aziridines, show a high reactivity towards thiol containing compounds. For this reason, we have made use of a thiol containing probe [8] in the investigations of S2. The idea therefore arose to substitute glycerol with thioglycerol as the FAB matrix compound to induce the in situ derivatization [9] of the phenolic aziridine, or its precursor, directly on the target of the FAB ion source. A similar method to confirm the structures of labile organic hydrates by using a glycerol/cesium iodide matrix, have been reported previously [10].

The FAB mass spectra, in all cases, displayed prominent peaks corresponding to the $[M - Br/Cl + \text{thioglycerol}]^+$ chemical adducts. The chemical structures and typical mass spectra are given in Fig. 4.

The speed, ease and simplicity of this combined derivatization and ionisation procedure will undoubtedly be of great significance for the study of the naturally occurring oral contraceptives in *Salsola Tuberculatiformis* Botsch.

Aziridines are seldomly found in nature, but are important in medicinal chemistry where they function as reactive intermediates in the mechanism of action of several synthetic drugs. These drugs, which include the nitrogen mustards commonly used for the treatment of cancer [11], are utilized as so-called prodrugs which cyclize from open-chain precursors to corresponding aziridines, which then act as the active alkylating agents.

Conclusion

This study demonstrates that the FAB method previously described for the study of acetylated aziridines and their precursors cannot be applied to the study of their un-acetylated analogues. A new method in which thioglycerol is employed for the in situ derivatization and ionisation matrix is described as a valuable method for the mass spectral study of aziridines and their open-chain precursors.

The authors herewith acknowledge financial support by the South African Medical Research Council and the Foundation for Research Development.

REFERENCES

1 P.A. Basson, J.A. Morgenthal, R.B. Billbrough, J.L. Marais, S.P. Kruger and J.L. de B. van der Merwe, Onderstepoort J. Vet. Res., 36 (1969) 59.
2 P. Swart. Ph.D Thesis, Department of Biochemistry, University of Stellenbosch, Stellenbosch (1986).
3 K.N. Campbell, B.K. Campbell, J.F. McKenna and E.P. Chaput, J. Org. Chem., 8 (1948) 102.
4 M. Barber, R.S. Bordoli, R.D. Sedgwick and A.N. Tyler, Nature (London), 293 (1981) 270.
5 K.J. van der Merwe, S.S. de Kock, P. Swart and L. Fourie, Biol. Mass Spectrom., 21 (1992) 672.
6 A. Albert, Heterocyclic Chemistry, Athlone Press, London, 1959.
7 J.L. Gower, Biomed. Mass Spectrom., 12 (1985) 191.
8 M. Bretschneider, Mh. Chem., 78 (1948) 82.
9 K. Vekey and L.F. Zerilli, Org. Mass Spectrom., 26 (1991) 939.
10 F.J.C. Martins, A.M. Viljoen, L. Fourie, M. Coetzee and P.L. Wessels, Tetrahedron, 47 (1991) 9215.
11 P. Calabresi and R.E. Parks, L.S. Goodman and A. Gilman (Eds.), The Pharmacological Basis of Therapeutics, Macmillan, New York, 4th edn., 1970, pp. 1348–1356.

Analytica Chimica Acta, 279 (1993) 167–177
Elsevier Science Publishers B.V., Amsterdam

Spectral analysis of interactions between proteins and dye ligands

J. Hubble

School of Chemical Engineering, University of Bath, Claverton Down, Bath (UK)

A.G. Mayes and R. Eisenthal

Department of Biochemistry, University of Bath, Claverton Down, Bath (UK)

(Received 1st October 1992; revised manuscript received 30th November 1992)

Abstract

Interactions between the triazine dye Cibacron Blue F3GA and the protein lysozyme have been investigated by monitoring the characteristic spectral shift which accompanies the binding phenomenon. This technique, which is both quick and convenient, allows determination of apparent dissociation constants, and in the case of supported dyes, the fraction of total dye available for protein binding. In this paper, this approach has been used to compare experimental results obtained with both free and dextran coupled dye allowing the effects of dye conjugation to be quantified in the absence of diffusional limitations seen with insoluble supports. In addition to equilibrium studies, changes in absorbance have also be used to follow binding kinetics using a "stopped flow" system. Results obtained indicate that dextran-supported dye molecules over a range of dye/dextran ratios show a constant ration of dye availability, but show a decrease in dissociation constant with increased loading. Kinetic studies show the feasibility of applying a standard saturation model to the dye–protein interaction where free dye is used. However, in the case of dextran-supported dyes a model which takes account of dye stacking is required to describe adequately the results obtained.

Keywords: Kinetic analysis; Cibacron Blue F3GA; Dyes; Lysozymes; Proteins

A detailed investigation of the binding interactions observed with affinity adsorbents based on porous beaded supports is greatly complicated by the effects of diffusional limitations on the observed kinetics of binding [1]. To assess the consequences of ligand immobilisation on binding phenomena in the absence of these limitations it is possible to use soluble supports such that binding occurs in a continuous liquid phase [2]. In such a system, providing the viscosity is not excessive, there will be negligible mass transfer limitations, and kinetic and equilibrium binding results can be compared with those obtained for free ligands. Hence soluble systems can be used to provide a quantitative assessment of the effects of ligand immobilisation on the intrinsic kinetics of the interaction.

Measurement of ligand–protein binding by spectrophotometry is a well established technique [3–5], and is attractive as it can be applied to equilibrium and kinetic measurements with equal facility [6]. The signal obtained results from a spectral shift caused by a change in the environment of either the ligand or the protein when binding occurs. This change can be monitored either in titration (i.e., equilibrium) experiments or kinetic studies.

Correspondence to: J. Hubble, School of Chemical Engineering, University of Bath, Claverton Down, Bath (UK).

The method has been widely used for the measurement of binding of triazine dyes to proteins; in most cases Cibacron Blue F3GA has been the ligand of choice. However, other dyes have also been found to give spectral shifts suggesting that the technique should be widely applicable [7,8].

In a previous report we showed that spectral titration can be used to compare interactions of both free and supported dye with the protein lysozyme [6]. The results obtained demonstrated the potential of the technique but highlighted problems caused by the stacking interactions known to occur between planar dye molecules in close proximity [9,10]. Dye stacking can have two significant effects on the results obtained from spectral studies. The first arises from the difference in extinction coefficient between stacked and unstacked dye. The second arises from the effect of stacking on dye availability for binding. In this paper we consider these effects in more detail paying particular attention to the assessment of binding kinetics.

THEORY

Equilibrium experiments

No dye stacking. Difference spectra are obtained when dye or dye–dextran conjugate is titrated with increasing concentrations of a protein with which it can bind. The spectral shift can be related to changes in the fractional saturation of the adsorbent. In the case of dextran-coupled dye, calculation is complicated by the presence of conjugated dye which is in an orientation that precludes binding. For this reason the conjugated dye is divided into two populations: (i) available, D_a and (ii) unavailable, D_u. For the simplest case where dye stacking is insignificant the observed absorbance of a dye–dextran conjugate preparation (measured at 595 nm) can be expressed in terms of the absorbtion coefficient for free dye and the sum of D_a and D_u:

$$A_{595} = e_f(D_a + D_u) \quad (1)$$

where e_f is the absorption coefficient of uncomplexed dye.

The introduction of lysozyme into the system leads to two competing effects on the observed absorbance: (i) a lowering of the uncomplexed dye concentration; and (ii) formation of a dye–protein complex which has a modified absorption coefficient (e_b).

The observed absorbance can be described by:

$$A_{595} = e_f[(D_a - D_b) + D_u] + e_b D_b \quad (2)$$

where D_b is the concentration of complexed dye.

In practice the relative concentrations of D_a and D_u will not be known in advance of the titration, and may vary between different batches of adsorbent. To overcome this problem the difference in absorbance between solutions of equal dye concentration with and without lysozyme are determined. Hence subtraction of Eqn. 1 from Eqn. 2 gives:

$$\Delta A_{595} = D_b(e_b - e_f) \quad (3)$$

The D_b term may be substituted by an appropriate binding expression, containing terms in K_d and the total concentrations of protein and "available" dye. Assuming binding is reversible the dissociation constant for binding can be written:

$$K_d = \frac{(D_a - D_b)(L_t - D_b)}{D_b} \quad (4)$$

where L_t is the total concentration of added lysozyme.

Solving Eqn. 11 for D_b gives the physically significant root:

$$D_b = \tfrac{1}{2}\Big[(D_a + K_d + L_t) - \sqrt{(D_a + K_d + L_t)^2 - 4D_aL_t}\Big] \quad (5)$$

This expression can be substituted into Eqn. 3 to give the following expression relating the change in A_{595} to K_d, D_a and e_b.

$$\Delta A_{595} = (e_b - e_f)\tfrac{1}{2}\Big[(D_a + K_d + L_t) + \sqrt{(D_a + K_d + L_t)^2 - 4D_aL_t}\Big] \quad (6)$$

Equation 6 can be fitted to experimental data using non-linear regression to provide least

squares estimates of e_b, e_f, D_a and K_d. Having obtained an estimate of the available dye concentration (D_a) the number of dye moieties per conjugate molecule participating in binding can be calculated from the product of the loading (dye to dextran ratio) and the ration of D_a to total dye.

Dye stacking systems. For systems where stacking cannot be ignored these relationships have to be modified to account for this effect. The simplest assumption that can be made is that stacking represents a reversible dimerisation with a dissociation constant defined by:

$$K_s = \frac{(D_a - 2D_s)^2}{D_s} \tag{7}$$

where K_s is the dissociation constant for stacking and D_s is the stacked dye concentration.

Solving Eqn. 7 for D_s gives the physically significant root:

$$D_s = \frac{\left[4D_a + K_s - \sqrt{K_s(8D_a + K_s)}\right]}{8} \tag{8}$$

Assuming that the dye population that is unavailable for binding is also unavailable for stacking, the absorbance of a dye solution where stacking occurs can be written as:

$$A_{595} = e_f[(D_a - 2D_s) + D_u] + e_s D_s \tag{9}$$

where e_s is the extinction coefficient for stacked dye.

Substitution of D_s in Eqn. 9 using Eqn. 8 gives an expression which relates absorbance to dye concentration. In the case of free dye D_u will equal zero and D_a will equal the total dye concentration such that this relationship can potentially be used to determine e_s and K_s from absorbance/concentration data obtained over an extended concentration range.

When protein is introduced into the system the absorbance will change depending on the concentration of bound complex formed (D_b) and the extinction coefficient (e_b). Modifying Eqn. 9 accordingly gives:

$$A_{595} = e_f[(D_a - 2D_{s1} - D_b) + D_u] + e_s D_{s1} + e_b D_b \tag{10}$$

where D_{s1} is the concentration of stacked dye which is redefined to account for D_b:

$$K_s = \frac{(D_a - 2D_{s1} - D_b)^2}{D_{s1}} \tag{11}$$

In this case the physically meaningful root is given by:

$$D_{s1} = \tfrac{1}{8}\left\{4(D_a - D_b) + K_s - \sqrt{K_s[8(D_a - D_b) + K_s]}\right\} \tag{12}$$

Subtraction of the two Eqns. 9 and 10 relating absorbance to dye concentration gives an expression describing the absorbance change:

$$\Delta A_{595} = D_b(e_b - e_f) + 2e_f(D_{s1} - D_s) + e_s(D_s - D_{s1}) \tag{13}$$

The description of the dye–protein interaction is again complicated by the occurrence of dye stacking where the definition of K_d must be modified:

$$K_d = \frac{(D_a - 2D_{s1} - D_b)(L_t - D_b)}{D_b} \tag{14}$$

Equation 14 results in a cubic expression for D_b which is no longer amenable to simple algebraic solution. However, as we know that the physically meaningful root must lie between 0 and the smaller of L_t or D_a, evaluation of D_b is easily accomplished numerically using a bisection algorithm. Hence Eqns. 8, 12, 13 and 14 can be combined to predict ΔA_{595} as a function of D_a, K_s, K_d, e_s, e_b, and e_f. As described earlier e_s and e_f can be determined independently from absorbance/concentration data for free dye, and so D_a, K_s, K_d, and e_b remain to be estimated from a least squares fit to experimental binding data.

Kinetic experiments

No stacking assumption. Kinetic studies can be conducted with both free dye and dye–dextran conjugate. In this case it is necessary to formulate an integrated rate equation which describes the variation of D_b as a function of time. Used in conjunction with Eqn. 3 this integrated rate equation can be used to describe the time dependent

absorbance change observed as a result of the dye–protein interaction. For the simple case when stacking is ignored:

$$\frac{dD_b}{dt} = k_1[(D_a - D_b)(L_t - D_b) - K_d D_b] \quad (15)$$

where k_1 is the "on" constant and $K_d = k_2/k_1$. This equation can be analytically integrated to give an expression relating D_b to time:

$$D_b = \{(bb - sx)(bb + sx) - (bb + sx) \times (bb - sx)\ e^{t \cdot sx}\}\{2k_1[e^{t \cdot sx}(bb - sx) - (bb + sx)]\}^{-1} \quad (16)$$

where $bb = -k_1(K_d + D_a + L_t)$; $sx = [bb^2 - 4k_1(K_d + D_a + L_t)]^{1/2}$; and t = time. This expression can be substituted into Eqn. 3 to give the final equation which relates change in absorbance at 595 nm to time. However, although this expression gave a good fit to data obtained between the interaction of lysozyme with free dye, a systematic deviation between predicted and experimental results showed that this simple rate model was unable to describe adequately the data obtained with dye–dextran conjugates, which appear to indicate a combination of rapid initial reaction with a subsequently slower approach to equilibrium.

A possible explanation of this inadequacy is that the experimental data represents the sum of two coupled processes. It has been shown that the kinetics of dye/dye stacking interactions can influence the apparent kinetics of the interaction of dye and macromolecule [11]. Hence the rapid initial phase of the interaction could represent interaction of macromolecule with unstacked dye, while the subsequent reaction would be limited by the rate of 'destacking' of the interacting dye molecules. In a simplified form this can be described mathematically by a slight modification to Eqn. 15 and the introduction of a second differential equation to describe the stacking interaction (again assumed to be a dimerisation).

$$\frac{dD_b}{dt} = k_1[(D_a - D_b - 2D_{s1})(L_t - D_b) - K_b D_b] \quad (17)$$

$$\frac{dD_s}{dt} = k_3[(D_a - D_b - 2D_{s1})^2 - K_s D_{s1}] \quad (18)$$

where k_3 is the formation constant for stacking, $K_s = k_4/k_3$, and D_{s1} the concentration of stackeddye (stacking assumed to be a dimerisation).

In our previous study non-linear least squares estimates of these parameters were obtained by using a fourth order Runge-Kutta routine to solve Eqns. 17 and 18 numerically over the reaction time course. These results in combination with Eqn. 3 were used to predict the observed progress curves. Although this approach gave a much improved fit, it proved impossible to reconcile estimates of K_d and D_a obtained from kinetic and equilibrium data.

A more rigorous analysis of the stacking effect requires that Eqns. 17 and 18 be used in conjunction with Eqns. 8 and 13 such that the consequences of stacking on both optical density and binding interactions are quantified.

MATERIALS

Lysozyme (grade VI from chicken egg white), dextran of nominal average molecular weight 5×10^5 (termed 5D), and dextran of nominal molecular weight 2×10^6 (termed 20D) were obtained from Sigma (Poole). Cibacron Blue 3G was purchased from Ciba (Manchester). All other reagents were of analytical grade and were purchased from British Drug Houses (Poole).

METHODS

Preparation of Cibacron Blue–dextran conjugates

Dextran–dye conjugates of different dye–dextran ratios were prepared and characterised using methods described previously [2,6]. Gel filtration experiments showed that no low molecular weight material of high absorbance was present in the conjugate solutions. This indicated that the free dye was separated from that bound to dextran by the preparation method. Similar analysis showed that no release of dye occurred over a two-month

storage period and that the conjugates were stable two months after production.

Spectral titration

Equilibrium studies. Sample and reference cuvettes each containing a solution of approximately 70 μM (with respect to dye) conjugate in 10 mM Tris, 50 mM NaCl (pH 8.0) were equilibrated at 25°C in a Cecil 272 spectrophotometer with a thermostated cuvette holder. Small volumes of 5 mM lysozyme solution were added to the sample cuvette and equal volumes of buffer added to the reference cuvette. The contents of the cuvettes were mixed in situ using small plastic paddles which could be left in the cuvettes without obstructing the light path. The absorbance difference was measured at 595 nm after each addition of lysozyme. Lysozyme concentrations in the range 0–250 μM were used. All conjugate solutions were normalised for total dextran content by adding underivatised dextran of the appropriate molecular weight to adjust the concentration of dextran to that of the one with the lowest dye to dextran ratio used in the titrations.

Kinetic studies. Reaction kinetics were followed using a stopped flow apparatus with associated computerised data capture Model SF51 (Hi-Tech Scientific, Salisbury). Solutions of dye or dye–dextran conjugate, and lysozyme were made up at twice the required final concentration and loaded into the two syringes of the apparatus. Injection was carried out using a pneumatic ram which achieved very efficient mixing and consequently small dead times. Data was captured by a PC fitted with a rapid (1 MHz) analogue-to-digital conversion card and stored and displayed using software supplied with the instrument. Readings were taken at intervals over the time scale 0–2 s for most runs except for free dye mixed with lysozyme where the time scale was increased to 100 s for some runs.

Laser light scattering measurements

These were carried out using an Oros Instruments M801 molecular size detector which used a technique based on photon correlation spectroscopy. Essentially the rate of movement of molecules in solution is used to calculate their effective diffusion coefficient, which is in turn used to estimate their molecular weight. Solutions of underivatised dextran of different molecular weights and dye dextran conjugates were filtered through 0.2-μm filters to remove dust particles etc. Samples were injected into the sampling cell of the instrument through a 0.2-μm filter and at least 10 readings taken for each conjugate tested. From the data the mean diffusion coefficient D_T was determined. A calibration graph constructed with the underivatised dextran samples was then used to calculate an apparent molecular weight for each conjugate tested. Samples were measured in distilled water and in 1 M NaCl solution.

RESULTS

The objective of the experimental programme was to establish the relationship between binding capacity and kinetics and the dye to dextran ratio in conjugates prepared at different ligand loadings. To this end a series of both kinetic and equilibrium experiments was conducted and the data obtained interpreted in terms of the relationships developed in the theory section. It has been shown that equilibrium studies aimed at using spectral titration to quantify the interaction of free dye with lysozyme are not feasible due to

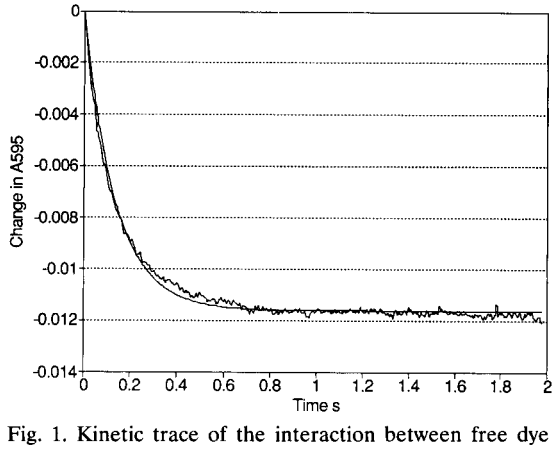

Fig. 1. Kinetic trace of the interaction between free dye (35 μM) and lysozyme (500 μM). The curve was generated using a non-linear least squares fit (see Theory).

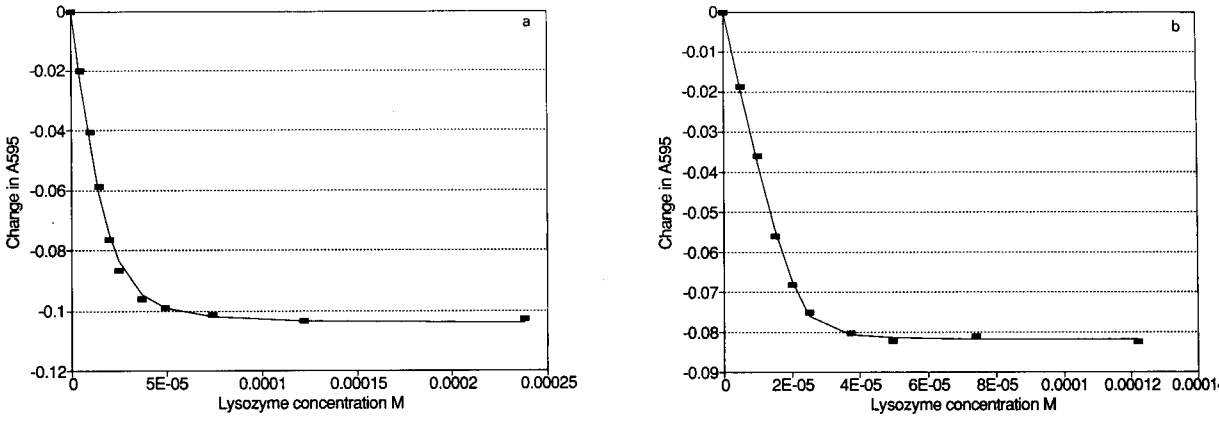

Fig. 2. Change in equilibrium absorbance as a function of lysozyme concentrations. (a) 20D10 conjugate (83 μM); (b) 5D5 conjugate (75 μM).

the formation of aggregates which mask the spectral changes arising from the dye–protein interaction. Stopped flow experiments have shown that this effect becomes apparent some seconds after the adsorption interaction is complete. Figure 1 shows results obtained from such an experiment conducted with free dye and lysozyme. The smooth line is the least squares fit obtained using Eqns. 17, 18 and 10. In this and all other runs data were fitted to models in which all the parameters were adjustable to allow direct comparison with the estimates obtained.

In the case of dye–dextran conjugates both equilibrium and kinetic experiments are possible as aggregation is not apparent over the range of protein and dye concentrations used. However, this effect can be seen with more highly substituted dextrans used at high lysozyme concentrations. Equilibrium experiments were conducted with conjugates based on 5×10^5 Dalton dextran (5D series) and 2×10^6 Dalton dextran (20D series). The experimental data were fitted to Eqns. 5, 9 and 10 to give estimates of K_d, K_s, D_a, e_s, e_b and e_f. Figure 2a and b shows typical fits

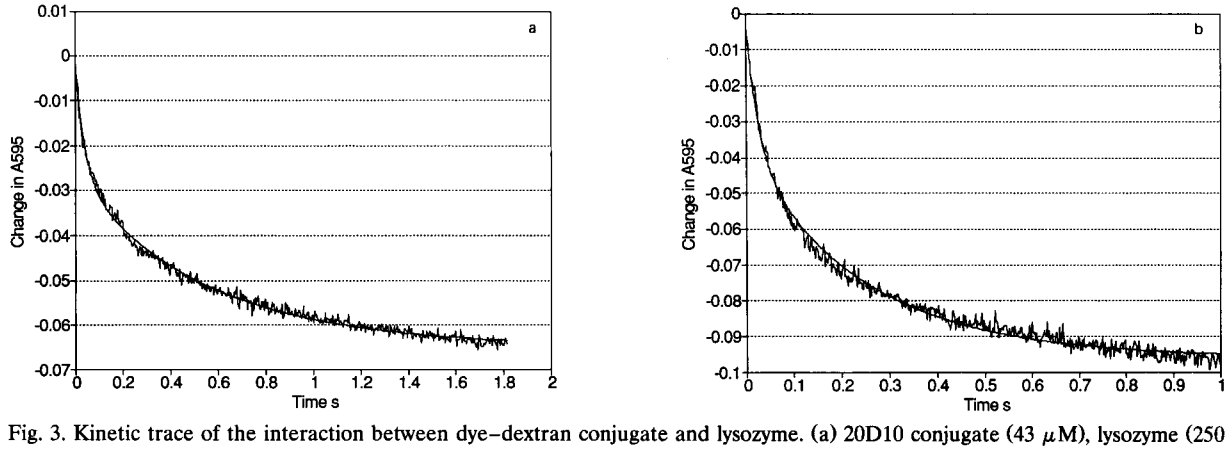

Fig. 3. Kinetic trace of the interaction between dye–dextran conjugate and lysozyme. (a) 20D10 conjugate (43 μM), lysozyme (250 μM); (b) 5D5 conjugate (51 μM), lysozyme (250 μM). The curve was generated using a non-linear squares fit (see Theory).

TABLE 1

Values for the diffusion coefficients of various dextran standards and dye–dextran conjugates in distilled water determined by laser light scattering measurements

(The diffusion coefficients are quoted with dimensions of $m^2\ s^{-1} \times 10^{13}$. The MW values of the conjugates were calculated from the regression line through the linear portion of a log MW against log D_T calibration graph using the data from the dextran standards)

Dextran standards			Dye–dextran conjugates			
MW (10^3)	Mean D_T	S.D. (n)	Code	Mean D_T	S.D. (n)	MW (10^3)
40	498	8.5(16)	5D1	142	6.0(13)	586 [a]
70	383	3.3(11)	5D3	155	4.1(20)	480
124	312	7.7(13)	5D5	165	7.6(17)	438
480	155	2.2(14)	5D8	179	19.9(19)	362
2000	141	6.2(11)	5D10	234	20.6(14)	204

[a] Extrapolated value.

obtained to an example from each dextran series. The sum of squares of residuals was similar for all data sets.

Kinetic experiments were conducted using both conjugate series and the results fitted to Eqns. 17, 18 and 10 as for the free dye. Typical results are shown in Fig. 3a and b where again examples are provided for each conjugate series. All results up to this point were obtained using a lysozyme concentration of 2.5×10^{-4}M. To investigate the influence of protein concentration a series of experiments were conducted at different concentration values using a single conjugate preparation. The results obtained are shown in Fig. 4.

Molecular weight and diffusion coefficient values obtained for both conjugate ranges using the Oros machine are shown in Table 1. Although reaction stoichiometry predicts that conjugate molecular weight should increase with increasing dye–dextran loading, the results obtained suggest

TABLE 2

Summary of best fit parameter estimates obtained from equilibrium studies

	5D1	5D3	5D5	5D8		
Loading	7	27	53	124		
D_a (10^{-5})	1.2	1.7	2.4	2.1		
n	1.1	6.2	17	39		
K_d (10^{-5})	2.1	0.56	0.04	0.05		
K_s (10^{-5})	1.5	4	32	14		
e_s (10^3)	4.23	3.54	6.13	3.35		
e_b (10^4)	1.01	1.02	0.97	1.02		
e_f (10^4)	1.18	1.18	1.2	1.2		
	20D2	20D3	20D4	20D7	20D9	20D10
Loading	14	28	54	133	196	263
D_a (10^{-5})	1.1	1	1.1	1.8	1.7	1.9
n	2.1	3.7	8.1	26	39	60
K_d (10^{-5})	1.6	1.3	1.1	0.7	0.52	0.32
K_s (10^{-5})	0.26	0.47	0.77	2	2.6	1.7
e_s (10^3)	5.68	2.27	1.72	4.27	2.09	8.89
e_b (10^4)	1	1.09	0.98	1	1.02	1.07
e_f (10^4)	1.2	1.2	1.2	1.2	1.19	1.22

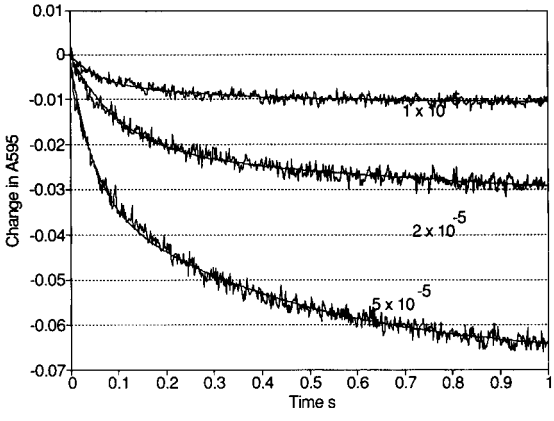

Fig. 4. Kinetic trace of the interaction between the 5D5 conjugate (51 μM) and lysozyme at a range of concentrations.

that the converse is true. It would appear that this apparent anomaly is the result of dye stacking effects leading to compaction of the conjugate molecules. This effect would be more pronounced in the more highly substituted preparations and would result in the lower diffusion coefficients that are observed.

DISCUSSION

In deriving the theoretical relationships used in this study the aim was to take account of the interactions which are known to occur and their consequences. Hence in addition to the high affinity interaction of protein with dye, there is also the possibility of dye/dye stacking interactions which result in significant changes in the apparent extinction coefficient, and the probability that in dye–dextran conjugate preparations not all dye will be accessible for binding. In taking account of these phenomena a number of simplifying assumptions have been made, and the simplest possible mechanism for the stacking interaction has been employed. However, even with these simplifications the number of parameters is large, and so taken in isolation a single good fit to a set of data provides little evidence to support the validity of the model.

It is apparent from the data presented that the modelling approach is capable of giving excellent fits to the data obtained from any one single experiment, but the critical factor is the consistency of the parameter estimates obtained and their plausibility in the light of independently determined estimates obtained using independent techniques. The parameter values obtained are shown in Table 2 for equilibrium studies, and Table 3 for kinetic studies.

Comparison of the values obtained from the different experiments shows that all give a similar value for the extinction coefficient for unstacked dye of 12000 M^{-1} (mean 11960, S.D. 87). This value is in good agreement with literature values reported for the molar extinction coefficient of

TABLE 3

Summary of best fit parameter estimates obtained from kinetic studies

	5D1	5D3	5D5	5D8
k_1 (10^3)	2.53	4.26	6.38	2.82
k_3 (10^5)	8.1	5	2.3	2.6
K_d (10^{-4})	21	7.7	4.9	6.7
K_s (10^{-5})	1.5	1.7	4.4	3.1
D_a (10^{-5})	2.6	2.5	3.5	2.5
n	3.8	13	36	67
e_s (10^3)	4.4	3.9	2.7	2.8
e_b (10^4)	1.08	1.07	1.12	1.1
e_f (10^4)	1.19	1.2	1.18	1.2
	20D2	20D6	20D10	Free dye
k_1 (10^3)	2.65	2.98	4.4	4.23
k_3 (10^5)	7.8	3.3	3.7	–
K_d (10^{-3})	2.2	0.92	0.61	1.2
K_s (10^{-5})	2.3	3.8	3	–
D_a (10^{-5})	2.3	2.5	2.5	–
n	6.7	12	153	–
e_s (10^3)	2.3	4.1	3.9	–
e_b (10^4)	1.15	1.02	1.05	1.08
e_f (10^4)	1.2	1.2	1.2	1.2
5D5 series				
Lysozyme (μM)	50	20	10	
k_1 (10^3)	9.6	4.6	37	
k_3 (10^5)	1.9	1.7	17	
K_d (10^{-5})	220	4.8	7.8	
K_s (10^{-5})	2.8	1	0.07	
D_a (10^{-5})	2.5	2	1	
n	26	21	10	
e_s (10^3)	4	3.1	1.5	
e_b (10^3)	7.7	9.7	8.1	
e_f (10^4)	1.3	1.2	1.18	

Cibacron Blue (13000 M^{-1})[12]. It is interesting to note that these values are significantly higher than the estimates we obtained in our earlier study (9000–9800 M^{-1})[6] where the stacking effect was not quantified. As expected the values of both stacked and protein bound dye are markedly lower than this value. With the exception of experiments conducted at non saturating lysozyme concentration the estimated values of e_b lie in the range 9700–11000 (mean 10470, S.D. 490) which are within the range of experimental error. Values obtained for the extinction coefficient of stacked dye show greater variation (2000–9000, mean 3900, S.D. 1708) but still show little evidence of systematic variation. This finding is consistent with the model assumptions which would not suggest that the values of these parameters should be dependent of dye to dextran ratio. The fact that the estimates are in the main similar for both kinetic and equilibrium data is also reassuring.

Estimates of available dye concentrations also show little variation from preparation to preparation. The value of n (the maximum number of dye moieties per conjugate molecule capable of participating in binding) as a function of loading is shown in Fig. 5 for the 5D series, with the 20D series showing a similar trend. The figure of 30% availability for the equilibrium results is consistent with the results of our earlier studies using gel permeation techniques to assess binding capacities where a constant 30% dye availability was indicated irrespective of loading studied. However, kinetic studies suggest a higher availability which requires explanation.

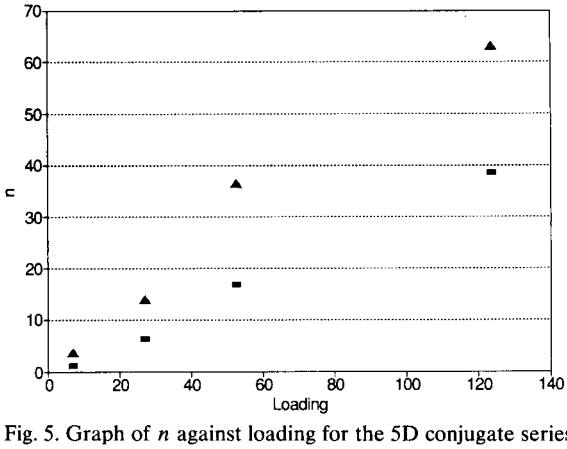

Fig. 5. Graph of n against loading for the 5D conjugate series. ▲, Kinetic estimates; ■, equilibrium estimates.

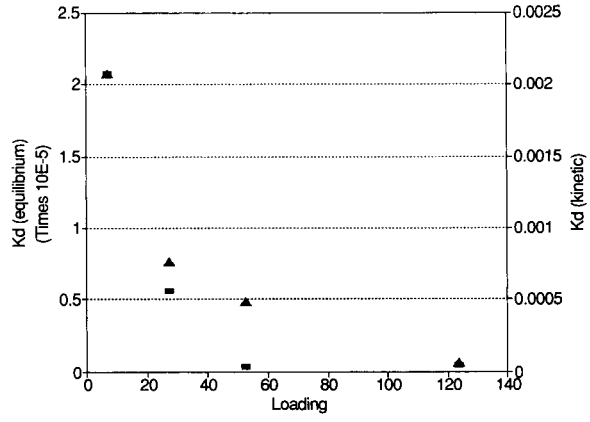

Fig. 6. Graph of K_d against loading for the 5D conjugate series. ▲, Kinetic estimates; ■, equilibrium estimates.

The remaining parameters are the kinetic and equilibrium constants which describe the dye–protein and dye stacking interactions. In this case parameter values would not be expected to be constant across a range of preparations of varying dye to dextran ratio. Our previous studies have suggested that K_d should decrease with increasing dye to dextran ratio, and a similar effect might be expected for stacking interactions where stacking might be enhanced by the closer proximity of adjacent dye molecules. In fact the results do suggest that K_d values decrease with loading (Fig. 6). Again, while the trends are similar there is not a good agreement between the magnitude of the estimates of K_d obtained from kinetic studies with those obtained from equilibrium determinations. These discrepancies cannot be explained in terms of the model formulated in the theory section. However there are some plausible possibilities which can be considered.

(i) The results obtained from our earlier gel permeation studies [2] suggested that there are two classes of interaction between lysozyme and Cibacron Blue. Both show saturation phenomena, but may be distinguished on the basis of their half saturation constants. It is probable that the spectral changes described in this report are a conse-

quence of the higher affinity interactions, and that the lower affinity "non specific" interactions are not directly quantified by this technique. Although not directly apparent in spectral titration studies low affinity binding effects could lead to changes in ligand availability on a timescale longer than those employed for the kinetic studies and hence might explain the lower D_a estimates obtained from equilibrium results. Similarly the K_d values obtained from equilibrium spectral changes are 4–10 fold lower than those from gel permeation studies providing further evidence for this effect.

(ii) It is possible that the interaction of protein with ligand is a two-stage process with the complex undergoing a transitional change between an initial and a stabilised state. Given that the transitional change is an equilibrium process and that the extinction coefficients of the two forms are identical it can be shown algebraically that this would lead to a higher value for the apparent K_d in the case of kinetic experiments.

The value of the stacking constant K_s again appears to show little systematic variation with ligand loading. However, results obtained from the molecular size analyzer suggest that degree of ligand loading significantly affects the size of the resultant complex and it may be that this complicates the effect of ligand/ligand proximity on the apparent value of K_s.

The results obtained at non saturating lysozyme concentrations are internally consistent. Values predicted for e_f are similar to those obtained at saturating concentrations. However, there is the suggestion that both e_s, K_s and D_a may be dependent on lysozyme concentration. This may be a consequence of lower lysozyme concentrations leading to less disruption of the stacking interaction. However, this is not accounted for in the present model, and if true would suggest that a minimum driving concentration is necessary to effect destacking.

Conclusions

The model proposed is capable of giving a good fit to both kinetic and equilibrium data obtained from spectral titration data. The values of the parameters obtained show agreement with values obtained using alternative experimental approaches. Mainly the parameter values are consistent between data sets. Where they are not, the deviation can potentially be explained in terms of relatively simple extensions to the original assumptions. While more extensive data are required to evaluate statistically the performance of the model, it would appear that it is capable of giving reasonable prediction over a range of conditions.

If correct the model suggests that ligand density can have a profound effect on the kinetics of binding as well as the equilibrium capacity of a affinity adsorbent based on the Cibacron Blue ligand.

The authors thank the SERC for support through Grant No. GR/F/90967, and a studentship for A.G.M. We also wish to thank the Institute of Food Research, Reading, for the loan of equipment essential for the kinetic work reported in this study.

LIST OF SYMBOLS

D_a Dye concentration available for binding (M)
D_b Concentration of complexed dye (M)
D_s Concentration of stacked dye (M)
D_u Dye concentration unavailable for binding (M)
K_d Dissociation constant for dye–lysozyme complex (M)
K_s Dissociation constant for stacked dye (M)
L_t Total lysozyme concentration (M)
k_1 Forward rate constant for dye–lysozyme complex formation (l mol^{-1} s^{-1})
k_2 Backward rate constant for dye–lysozyme complex formation (s^{-1})
k_3 Forward rate constant for stacking (l mol^{-1} s^{-1})
k_4 Backward rate constant for stacking (s^{-1})
n Number of dye molecules per dextran molecule participating in binding
t Time (s)
e_b Optical absorption coefficient for dye–lysozyme complex (l mol^{-1} cm^{-1})

e_s Optical absorption coefficient for stacked dye (l mol^{-1} cm^{-1})

e_f Optical absorption coefficient for free dye (l mol^{-1} cm^{-1})

REFERENCES

1 S.L. Fowell and H.A. Chase, J. Biotechnol., 4 (1986) 355.
2 A.G. Mayes, J.D. Moore, R. Eisenthal and J. Hubble, Biotechnol. Bioeng., 36 (1990) 1090.
3 S.T. Thompson and E. Stellwagen, Proc. Natl. Acad. Sci., 73 (1976) 361.
4 S. Subramanian, Arch. Biochem. Biophys., 216 (1982) 116.
5 G. Johansson and M. Joelsson, J. Chromatogr., 537 (1991) 219.
6 A.G. Mayes, J. Hubble and R. Eisenthal, Biotechnol. Bioeng, 40 (1992) 1263.
7 Y.D. Clonis, CRC Crit. Rev. Biotechnol., 7 (1988) 263.
8 T. Skotland, Biochim. Biophys. Acta, 659 (1981) 312.
9 M.M. Federici, P.B. Chock and E.R. Stadtman, Biochemistry, 24 (1985) 647.
10 E. Stellwagen and Y.-C. Liu, in I.M. Chaiken (Ed.), Analytical Affinity Chromatography, CRC Press, Boca Raton, FL, 1987, p. 170.
11 J. Aubard, M.A. Schwaller, A. Adenier and G. Dodin, in M.A. Vijayalakshmi and O. Bertrand (Eds.), Protein Dye Interactions: Developments and Applications, Elsevier, New York, 1989.
12 G.K. Chambers, Anal. Biochem., 83 (1976) 551.
13 C.R. Lowe and J.C. Pearson, Methods Enzymol., 104 (1984) 97.

Analytica Chimica Acta, 279 (1993) 179–183
Elsevier Science Publishers B.V., Amsterdam

Oxyheamoglobin degradation and radiolysis analysed by Mössbauer and positron annihilation techniques

M.I. Oshtrakh and E.A. Kopelyan

Division of Applied Biophysics, Ural Polytechnical Institute, Sverdlovsk 620002 (Russian Federation)

V.A. Semionkin

Faculty of Experimental Physics, Ural Polytechnical Institute, Sverdlovsk 620002 (Russian Federation)

(Received 1st October 1992)

Abstract

Mössbauer and positron lifetime spectra were measured for samples of fresh concentrated human oxyhaemoglobin solution, during its incubation for 2 weeks at room temperature and after its γ-irradiation. Oxyhaemoglobin degradation and radiolysis were monitored by Mössbauer spectrometry. Positron annihilation data are discussed in the light of the Mössbauer results.

Keywords: Raman spectrometry; Blood; Haemoglobin; Mössbauer spectrometry; Oxyhaemoglobin; Positron annihilation; Radiolysis

Mössbauer spectrometry and positron annihilation are useful techniques for the study of various species. Their application in biological and medical research could reveal information about the electronic structure of iron, microstructural variations, micromolecular structure and biochemical processes.

This paper presents preliminary results of a positron annihilation study of human haemoglobin solution in combination with Mössbauer spectrometry. Positron lifetime spectra have been measured previously only for lyophilized haeme proteins [1], and showed that positron annihilation parameters are influenced by different protein molecular structures. In this first study concentrated human oxyhaemoglobin solution was chosen in order to examine its degradation under non-sterile conditions and its radiolysis by γ-rays.

Correspondence to: M.I. Oshtrakh, Division of Applied Biophysics, Ural Polytechnical Institute, Sverdlovsk 620002 (Russian Federation).

EXPERIMENTAL

Human oxyhaemoglobin (HbO_2) in physiological saline (0.9% NaCl) was kindly provided by the Institute of Blood Transfusion of the All-Russian Haematological Scientific Centre (Moscow). Oxyhaemoglobin solution was prepared by a reported method [2] and then concentrated to ca. 38% (w/v) of protein and stored in liquid nitrogen. The oxyhaemoglobin solution was incubated under non-sterile conditions for 2 weeks at room temperature. Samples were taken for simultaneous measurements of Mössbauer and positron lifetime spectra immediately before incubation began and then after ca. 60, 140 and 310 h. Oxyhaemoglobin radiolysis was done using γ-rays with an average energy of 9 MeV produced by Microtron M-20 electron beam interaction with a steel converter. Oxyhaemoglobin irradiation was effected at doses of ca. 16, 26 and 33 kGy, then Mössbauer and positron lifetime spectra were measured.

TABLE 1

Mössbauer parameters of incubated human oxyhaemoglobin solution samples

Sample No.	Incubation time (h)	δ [a] (mm s^{-1})	ΔE_Q [a] (mm s^{-1})	S [c] (%)	Compound
1	0	0.264	2.083	100	HbO_2
2	64	0.964	2.397	94	Hb
		0.261 [b]	2.089 [b]	6	HbO_2
3	141	0.937	2.319	95	Hb
		0.262 [b]	2.090 [b]	5	MetHb
4	309	0.925	2.303	56	Hb
		0.260	2.132	31	MetHb
		0.762	0.561	9.8	X
		0.427	1.077	3.2	Haemochromes

[a] Experimental errors were ±0.016–0.017 mm s^{-1}. [b] Fixed parameters. [c] S = Relative area.

Mössbauer spectra of frozen solutions were measured with a standard constant acceleration spectrometer using 511 channels of a multi-channel analyser. The velocity resolution was 0.016–0.017 mm s^{-1} per channel. A 3.6×10^9 Bq ^{57}Co(Pd) source was used at room temperature. The haemoglobin samples were contained in a cryostat at 87 K. Details of the Mössbauer spectral measurements have been published previously [3,4]. Mössbauer spectra were fitted by a least-squares procedure using a Lorentzian line shape. Isomer shifts are given with respect to α-Fe at 295 K.

Positron lifetime spectra were measured using a conventional fast–fast coincidence spectrometer. A 2×10^6 Bq ^{22}Na source was made by evaporation from a carrier-free 1 M HCl solution on polyether film (3.6 μm) and covered with the same film. The time resolution with the ^{22}Na source was ca. 380 ps. The positron lifetime spectra of haemoglobin solution were measured at room temperature for 1.5 h with total count rates about 5×10^5 and a time scale of 20.2 ps per channel. Lifetime spectra were fitted using three components by the POSITRONFIT program [5].

RESULTS AND DISCUSSION

Parameters of the Mössbauer spectra of incubated oxyhaemoglobin solution samples are given in Table 1. Using the values of the isomer shifts, δ, quadrupole splittings, ΔE_Q, and relative areas, S, the possible iron-containing compounds and their abundance in solution were determined. It was found that ca. 60 h of incubation of oxyhaemoglobin led to HbO_2 deoxygenation and 94% of deoxyhaemoglobin (Hb) was observed. Samples incubated for ca. 140 h also contained 95% Hb; however, it is considered that the additional component in the Mössbauer spectrum could be related to the formation of low-spin methae-

TABLE 2

Positron annihilation lifetimes in incubated human oxyhaemoglobin solution samples [a]

Sample No.	Incubation time (h)	τ_2 (ns)	I_2 (%)	τ_3 (ns)	I_3 (%)
1	0	0.440 ± 0.002	86.9 ± 0.2	1.98 ± 0.05	13.1 ± 0.2
2	64	0.360 ± 0.005	64.6 ± 1.1	1.78 ± 0.03	17.6 ± 0.3
3	141	0.355 ± 0.004	68.8 ± 1.3	1.99 ± 0.04	17.3 ± 0.2
4	309	0.400 ± 0.004	77.5 ± 1.3	2.08 ± 0.06	17.9 ± 0.3

[a] ± Values are standard deviations from computer fitting procedures (calculated errors) for each partial least-squares parameter. These standard deviations are deviations of theoretical spectrum from experimental one.

moglobin–H_2O (MetHb) in this instance whereas the previous sample contained a residual amount of HbO_2 [the ΔE_Q and δ values for HbO_2 and the low-spin MetHb (see Table 1 in ref. 4) were close]. Further incubation led to an increase in MetHb owing to oxidation and to the formation of haemochromes [low-spin six-coordinated iron(II)–haeme complexes] and an unusual high-spin iron(II) compound X. Based on the Mössbauer results it was concluded that the initial HbO_2 solution was converted during incubation into Hb owing to bacterial growth and then was partly oxidized with low-spin MetHb formation and degraded with a total abundance of 13% of haemochromes and unknown component X. These data were used further for the analysis of the positron lifetime parameters.

Parameters of the positron lifetime spectra (lifetimes τ_i, intensities I_i) of the initial HbO_2 solution and incubated solutions are given in Table 2. The best fit was obtained for three-component analysis with the short-lived component fixed at 125 ps. A full unconstrained three-component fit of the initial sample spectrum gave two similar intermediate-lived components with unreasonably high intensities of opposite signs. It seemed that there was no short-lived component in this spectrum. Therefore, to compare the results for different samples I_1 for the initial HbO_2 solution was fixed at 0.01 (this value is considerably less than the statistical errors for the intensities). The changes in the relative intensities for all time components were observed. The intensity of the intermediate-lived I_2 component decreased with progress of the deoxygenation process and then increased again with partial oxidation of deoxyhaemoglobin. In contrast, the intensity of the long-lived component I_3 increased during incubation of HbO_2 solution. The short-lived component had almost the opposite tendency to that of the intermediate-lived component.

It is known that the short-lived component is attributable to the annihilation of *para*-positronium (*p*-Ps) and positronium–molecular species, the intermediate-lived component is attributable to the direct annihilation of positrons (e^+) and e^+–molecular species and the long-lived component is attributable to *ortho*-positronium (*o*-Ps) annihilation in free volume holes [6]. Therefore, it was concluded that during the deoxygenation process in solution the proportion of direct e^+ annihilation decreased whereas that of *p*-Ps annihilation increased. The proportion of direct e^+ annihilation increased again with MetHb formation and partial protein destruction. It is believed that the effect of bacterial growth in haemoglobin solution on the positron annihilation parameters was not significant because no correlation could be found between bacterial

TABLE 3

Mössbauer parameters of γ-irradiated human oxyhaemoglobin solution

Sample No.	Irradiation dose (kGy)	δ [a] (mm s^{-1})	ΔE_Q [a] (mm s^{-1})	S [b] (%)	Compound
1	0	0.264	2.083	100	HbO_2
2	16.5	0.266	2.155	58.9	HbO_2
		1.022	2.155	12.8	Hb
		0.097	0.651	10.4	X_1
		0.202	1.677	17.9	X_2
3	26.5	0.283	2.453	25.6	HbO_2
		1.028	2.384	30.8	Hb
		0.053	0.771	21.3	X_1
		0.236	1.878	22.3	X_2
4	33.0	0.227	2.091	18.1	HbO_2
		0.946	2.303	67.1	Hb
		0.082	0.821	14.8	X_1

[a] Experimental errors were ± 0.016–0.017 mm s^{-1}. [b] S = Relative area.

TABLE 4

Positron annihilation parameters of γ-irradiated human oxyhaemoglobin solution

Sample No.	Irradiation dose (kGy)	τ_2 (ns)	I_2 (%)	τ_3 (ns)	I_3 (%)
1	0	0.440 ± 0.002	86.9 ± 0.2	1.98 ± 0.05	13.1 ± 0.2
2	16.5	0.380 ± 0.005	66.5 ± 1.1	1.96 ± 0.05	15.4 ± 0.3
3	26.5	0.390 ± 0.005	63.8 ± 1.0	2.05 ± 0.05	15.1 ± 0.2
4	33.0	0.365 ± 0.005	64.4 ± 1.1	1.92 ± 0.04	17.3 ± 0.3

growth and changes in the intensities of positron lifetime components. Therefore, if these changes could be related to haemoglobin molecules in solution mainly, the conformational states of haemoglobin should be taken into account. It is assumed in this case that the presence of liganded (R state) haemoglobin in solution (HbO_2 or MetHb) led to an increase in the direct annihilation of e^+ and e^+–R state haemoglobin complexes. This may be caused by the different quaternary structure of the R and unliganded T states of haemoglobin [7] and, therefore, by the different surface amino acid residues and changes in their interactions with ions in solution.

The changes in the long-lived component could be a result of a slight increase in the number of free volume holes after HbO_2 deoxygenation where *o*-Ps pick-off annihilation occurs. The decrease in the τ_3 value for sample incubated for 60 h indicated the lower average radius of the free volume holes. Then τ_3 increased again to its initial value. These results may be explained by the different internal packing of haemoglobin globules in the R and T states. (This decrease could not be explained by the chemical quenching of *o*-Ps because an increase in the amounts of possible quenchers with incubation would cause an additional decrease in τ_3, but this was not observed.)

Parameters of the Mössbauer spectra of γ-irradiated oxyhaemoglobin solution are given in Table 3 and clearly show the deoxygenation process during γ-irradiation with a decrease in HbO_2 content and an increase in Hb content. Deoxygenation of HbO_2 solution could be a result of photodissociation, as was observed earlier for γ-irradiated HbO_2 in red blood cells [4]. However, in this work the deoxygenation process was observed at lower irradiation doses than previously [4]. Two additional components, X_1 and X_2, were found in the Mössbauer spectra of γ-irradiated HbO_2 solution. The parameters of component X_2 are close to those of hemichromes [low-spin six-coordinated Fe(III)–haeme complexes] and $MetHbOH^-$, in agreement with previous results [4]. On the other hand, component X_1 could not be identified. Also, only two additional components were found instead of the three found previously [4]. It is assumed that these differences are related to the different samples (HbO_2 in red blood cells and in solution) and the different energies of the γ-rays (ca. 9 and ca. 15.5 MeV).

The lifetime parameters for γ-irradiated samples are given in Table 4. As can be seen, there were no reliable changes in the long-lived lifetimes τ_3 with irradiation dose, whereas I_3 increased. Therefore, it was concluded that there were no long-lived free radical products of radiolysis in solution. A decrease in τ_2 with irradiation dose was observed together with a decrease in the intensity I_2. The increase in the *o*-Ps intensity I_3 was probably due to an increase in the relative amount of Hb in the solution and to the formation of compounds X_1 and X_2. The changes in the relative amounts of the various compounds might also influence the τ_2 value owing to the formation of different e^+–molecular complexes.

Comparison of the positron lifetime results for non-sterile degradation and radiolysis of HbO_2 solution showed similar tendencies of the behaviour of I_3. This could be related to the deoxygenation process. The behaviour of the intermediate-lived parameters (τ_2, I_2) appeared to be different for degradation and radiolysis of HbO_2

solution. This shows the differences in protein destruction for the two processes because of the formation of different compounds.

Conclusion

These Mössbauer and positron annihilation results demonstrate that non-sterile incubation of HbO_2 solution and sterile radiolysis by γ-rays led to the deoxygenation of HbO_2 and the formation of products of protein destruction. However, these products appeared to be different for HbO_2 destruction by incubation and by radiolysis.

The authors thank A.L. Berkovsky for preparing the concentrated oxyhaemoglobin solution. This work was supported by Grant F-21-5 from the State Comittee on Science and High Schools of the Russian Federation.

Note added in proof

The non-identified components X and X_1 which were previously found in our Mössbauer spectra gave rise to the question: were these real new compounds or our errors? Further verification of these data showed the presence of an error related with the contribution of the ^{57}Fe nuclei of the beryllium window Be(^{57}Fe) of the scintillator detector to the Mössbauer spectra. Usually, Mössbauer parameters of the Be(^{57}Fe) were fixed during spectra fitting [3,4]. Unfortunately, in this case the value of the isomer shift for the Be(^{57}Fe) was taken with respect to sodium nitroprusside instead of α-Fe. The correct fitting of Mössbauer spectra showed disappearence of these components. However, recalculated Mössbauer parameters of other components and their variations during degradation and radiolysis were not changed significantly. So, the revised data did not affect above results and discussion except "unusual" components X and X_1 which should be excluded from consideration.

The component X_2 gave rise to a more important question because it could also be a result of the asymmetry of the absorption lines shape for HbO_2 Mössbauer spectra (see [3]). These further results will be discussed elsewhere.

REFERENCES

1 P.C. Jain, R.R. Jain, and P. Joshi, Indian J. Biochem. Biophys., 11 (1974) 340.
2 A.A. Kozlov, A.L. Berkovsky, I.L. Smirnova, N.A. Gorbunova and T.A. Balakina, Russ. Pat., 1205910A (1985).
3 M.I. Oshtrakh and V.A. Semionkin, FEBS Lett., 208 (1986) 331.
4 M.I. Oshtrakh and V.A. Semionkin, Radiat. Environ. Biophys., 30 (1991) 33.
5 P.J. Kirkegaard and M. Eldrup, Comput. Phys. Commun., 7 (1974) 401.
6 Y.C. Jean, Microchem. J., 42 (1990) 72.
7 M.F. Perutz, G. Fermi, B. Luisi, B. Shaanan and R.C. Liddington, Acc. Chem. Res., 20 (1987) 309.

Analytica Chimica Acta, 279 (1993) 185–192
Elsevier Science Publishers B.V., Amsterdam

Preservation of shelf life of enzyme based analytical systems using a combination of sugars, sugar alcohols and cationic polymers or zinc ions

Timothy D. Gibson and John N. Hulbert

Department of Biochemistry and Molecular Biology, University of Leeds, Leeds LS2 9JT (UK)

John R. Woodward

Yellow Springs Instruments Inc., Yellow Springs, OH 45387 (USA)

(Received 1st October 1992; revised manuscript received 14th January 1993)

Abstract

The shelf life of enzyme based analytical systems to measure ethanol and hydrogen peroxide has been enhanced using neutral dextrans and combinations of cationic polymers or zinc ions and a sugar or sugar alcohol. Dry enzyme preparations of alcohol oxidase with these stabilisers retained 80–100% enzyme activity over periods of up to 2 months when thermally stressed at 37°C whilst controls in the absence of stabilisers lost 74% of the initial activity over 7 days at 37°C. The sugar alcohol, lactitol and the cyclic polyalcohol, inositol gave the highest stabilisation effect in conjunction with the cationic polymers diethylaminoethyl (DEAE)-dextran and Gafquat 755N. A combination of zinc ions and lactitol, has also been used to stabilise horseradish peroxidase at very low enzyme concentrations. Full activity was retained for 10 days at 37°C in the presence of stabiliser whilst unstabilised enzyme lost 64% of the initial activity under the same conditions. The use of the stabiliser combinations has found application in promotion of the shelf life of diagnostic alcohol kits and neutral, unsubstituted dextrans have been tested in the production of an ethanol kit based on alcohol oxidase.

Keywords: Enzymatic methods; Polymers; Sugars; Zinc

The use of enzymes in analytical applications has become a well known and acceptable method, as they have a number of significant advantages over conventional analytical chemistry in that they confer specificity, sensitivity and that they operate under mild analytical conditions.

One major disadvantage of enzyme based assays is that the enzyme component is often unstable, which may lead to degeneration of the reagent during storage and spurious results. To overcome this tendency, various methods have been used to increase the stability of enzymes including immobilisation [1], chemical modification by crosslinking [2], polymer grafting or substitution reactions [3], physical entrapment or encapsulation in polymer matrices or membranes [4] and the addition of chemicals to the enzyme preparation [5–7].

Enzyme preparations for use in analytical methods are often supplied in a dry stabilised form, using a combination of chemical additives to promote stability. This approach allows long

Correspondence to: T.D. Gibson, Department of Biochemistry and Molecular Biology, University of Leeds, Leeds LS2 9JT (UK).

term storage and ease of transport between supplier and end user.

Using a combination of a sugar alcohol, lactitol and the cationic polymer DEAE–dextran, we have previously reported the successful stabilisation of a range of enzymes including alcohol oxidase and horseradish peroxidase and applied the method to produce analytical systems (test kits and biosensors) to measure alcohol [8–10].

Comparitive studies on the stabilisation of alcohol oxidase have been carried out using lactose, sucrose, inositol or maltitol in place of lactitol and also the effect of replacing DEAE-dextran with unsubstituted dextrans, Gafquat 755N (a copolymer of vinylpyrollidone and quaternised methyl methacrylate) or zinc ions as reported by Carpenter et al. [11].

Also reported are the results obtained from the dry stabilisation of a range of other enzymes including; malate dehydrogenase, choline oxidase, galactose oxidase, glycerol 3-phosphate oxidase, lactate dehydrogenase, uricase, glucose 6-phosphate dehydrogenase and hexokinase.

In every case the dry storage stability of the test enzymes was enhanced when compared to results obtained in the absence of the stabilisers.

EXPERIMENTAL

Materials

Alcohol oxidase from *Hansenula polymorpha*, galactose oxidase from *Dactylium dendroides* and alcohol test kits were obtained from Leeds Biochemicals; horseradish peroxidase (Type HRP-4) was obtained from Biozyme, choline oxidase, glycerol 3-phosphate oxidase, malate dehydrogenase and lactate dehydrogenase were all obtained from Sigma; uricase (from yeast) was a gift from Enzymatix; glucose 6-phosphate dehydrogenase and hexokinase were gifts from Genzyme.

Lactitol was a gift from Cortecs (Deeside) and diethylaminoethyl (DEAE)–dextran was obtained from Pharmacia; Gafquat 755N solution was a gift from GAF Europe (Guildford); uric acid, glucose 6-phosphate, DL-lactic acid (hemicalcium salt), adenosine triphosphate (ATP), DL-malic acid, β-nicotinamide adenine dinucleotide (NAD), glycerol-3-phosphate, choline chloride and D-galactose were obtained from Sigma; 4-aminoantipyrine was obtained from Aldrich. *N*-Ethyl-*N*-(2-hydroxy-3-sulphopropyl)-*m*-toluidine was obtained from Leeds Biochemicals. All other chemicals were obtained from BDH–Merck.

Enzyme drying and stability testing

The protocols reported by Gibson et al. [8] were followed, these are outlined below. Fresh solutions of enzyme were prepared in suitable buffers and kept at 4°C until used. Aliquots of enzyme solution were mixed with phosphate buffer and combinations of the stabilisers to give final concentrations of 5% (w/v) unsubstituted dextran, sugar or sugar alcohol, 1% (w/v) DEAE–dextran (or Gafquat 755N, 1%, v/v) and 0.9 mM zinc sulphate in a volume of 1–2 ml. Controls contained buffer and enzyme solution

TABLE 1

Enzyme drying compositions
(The enzymes were dissolved in the buffer solutions together with buffered stabiliser solutions before drying for 4 h under vacuum at 35°C. When dry the enzymes were stored desiccated at 37°C for accelerated degradation testing)

Enzyme	Buffer	pH	Buffer concentration (mM)
Alcohol oxidase	Phosphate	7.0	100
Choline oxidase	Tris–HCl	8.0	30
Glycerol 3-phosphate oxidase	Phosphate	7.0	30
Galactose oxidase	Phosphate	7.0	10
Malate dehydrogenase	Phosphate	8.0	25
Lactate dehydrogenase	Phosphate	7.0	10
Glucose 6-phosphate dehydrogenase	Phosphate	7.0	100
Hexokinase	Phosphate	7.0	100
Uricase	Phosphate	7.87	20

only, the composition of each enzyme drying system is shown in Table 1.

Aliquots (100 μl) were dispensed into the base of 4 ml disposable polystyrene cuvettes and dehydrated under vacuum (0.1 mbar) using a Gallenkamp vacuum oven set at a temperature of 30°C. The chamber of the oven contained 500 g of fresh silica gel and the drying procedure was carried out for a total of 4 h. When drying was completed the dry enzyme preparations were stored in airtight plastic sandwich boxes containing silica gel. (Uricase, glucose 6-phosphate dehydrogenase and hexokinase were all freeze-dried overnight in a Chemlab freeze drier, with the chamber held at room temperature.)

The stability of the dry enzyme preparations was measured by monitoring the accelerated degradation of the dry enzyme preparations at 37°C. The incubations were carried out in the presence of silica gel as it was found that damp preparations of enzymes were inactivated rapidly even with the stabiliser combinations present.

Ethanol test reagents were prepared as described in Gibson et al. [8] except that the stabiliser combination was replaced by unsubstituted dextran (molecular weight 10000). The reagents were compared after storage at 4°C and 37°C using ethanol standards to develop the tests, according to the data sheets of the standard ethanol test kits supplied by Leeds Biochemicals.

Assay methods

For alcohol oxidase, malate dehydrogenase, choline oxidase, glycerol 3-phosphate oxidase, galactose oxidase and horseradish peroxidase the standard assay procedures described in Gibson et al. [8] were followed. For horseradish peroxidase the procedure was modified by replacement of the 4-hydroxybenzene sulphonic acid (Na salt) with the more sensitive colour reagent, *N*-ethyl-*N*-(2-hydroxy-3-sulphopropyl)-*m*-toluidine in conjunction with 4-aminoantipyrine.

In the case of uricase, glucose 6-phosphate dehydrogenase, and hexokinase the enzyme assay methods given by the manufacturers were followed, whereas for lactate dehydrogenase the assay given by Wahlfeld [12] was used.

RESULTS AND DISCUSSION

Horseradish peroxidase stabilisation

Previous studies with alcohol oxidase and other enzymes indicated that a combination of DEAE–

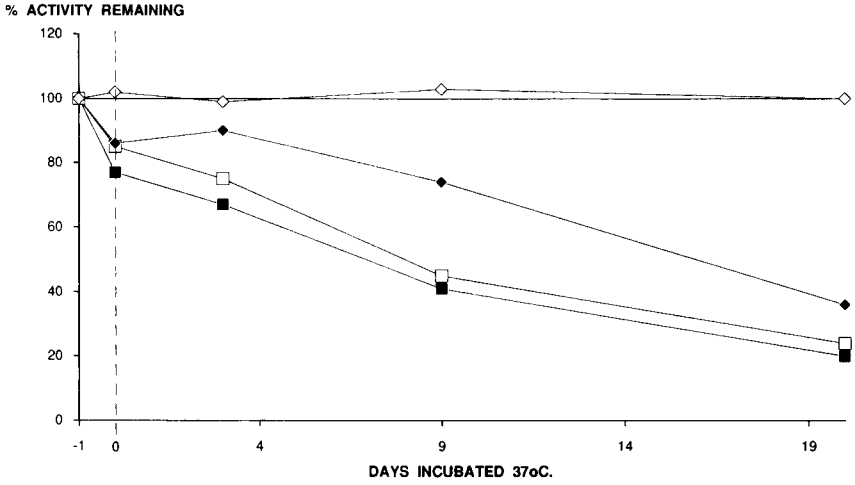

Fig. 1. Horseradish peroxidase was stabilised by using Gafquat 755N (1% v/v) and lactitol (5% w/v). The enzyme concentration was 1.25 units ml^{-1}, (4.6 $\mu g\,ml^{-1}$). The buffer used for drying was sodium phosphate pH 8.0, (200 mM). Kinetic assays were carried out in sodium phosphate pH 7.0, (100 mM) containing 4-aminoantipyrine (0.4 mM) and the sodium salt of *N*-ethyl-*N*-(2-hydroxy-3-sulphopropyl)-*m*-toluidine (10.0 mM). Key to symbols: ■ = No stabilisers; □ = Gafquat 755N; ◆ = lactitol; ◇ = lactitol/Gafquat 755N; ——— = 100% activity.

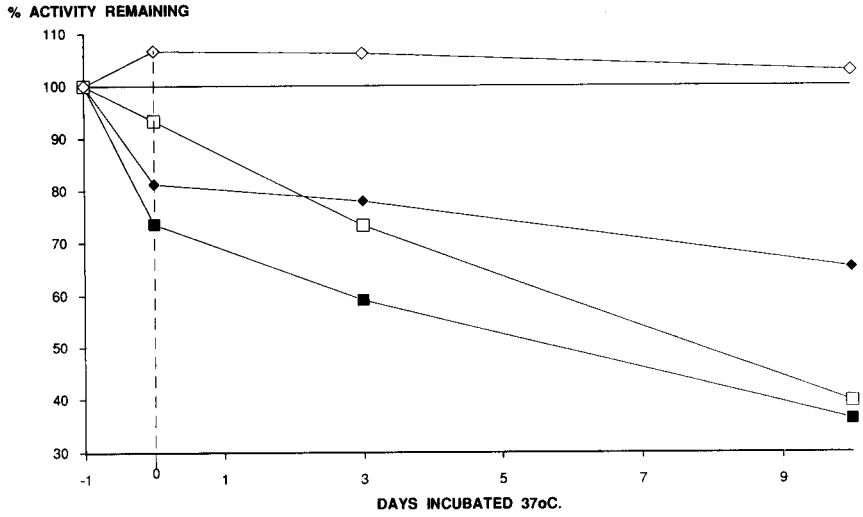

Fig. 2. Horseradish peroxidase was stabilised by using a combination of zinc ions (0.9 mM) and lactitol (5% w/v). The enzyme concentration was 1.25 units ml^{-1}, (4.6 $\mu g ml^{-1}$). The buffer used for drying was sodium phosphate pH 8.0, (200 mM). Kinetic assays were carried out in sodium phosphate pH 7.0, (100 mM) containing 4-aminoantipyrine (0.4 mM) and the sodium salt of *N*-ethyl-*N*-(2-hydroxy-3-sulphopropyl)-*m*-toluidine (10.0 mM). Key to symbols: ■ = No stabilisers; □ = zinc ions; ◆ = lactitol; ◇ = lactitol/zinc ions; ——— = 100% activity.

dextan and lactitol stabilised the enzyme activity to thermal stress at 37°C [8–10]. The present studies reported here extend this work to include the alternative cationic polymer Gafquat 755N and zinc ions in conjunction with lactitol as stabilisers, the results for horseradish peroxidase are shown in Figs. 1 and 2.

The type of response observed is similar to that obtained when using DEAE–dextran and lactitol [8] which gives evidence that the important effect of the polymer species employed is due to the charge of the polymer and not necessarily its structure, the structures of DEAE–dextran and Gafquat 755N are shown in Fig. 3. DEAE–dextran is derived from a naturally occurring polysaccharide composed of repeating units of glucose linked with α-(1–6)- bonds and a smaller number of α-(1–3)-branch points, the diethylaminoethyl substituent groups are chemically formed on the 2 position of the glucose units giving the molecule an overall positive charge in solution. The occurrence of the "tandem" groups in the molecule ensures that the structure remains ionised at all pH values as the pK_a is reported to be about 14 for the quaternary amino group, the other groups have pK_a values of 9.2 (tertiary amino group directly substituted) and 5.5 (tertiary amino group "tandem" substituted). Gafquat 755N is wholly synthetic, being formed from a combination of vinylpyrollidone and dimethylaminoethyl methacrylate reacted together to give a copolymer having pendant quaternary amino groups, pK_a about 14. As before the polymer is always ionised at pH values under 14, however the higher proportion of quaternary amino groups in relation to DEAE–dextran means that Gafquat is a stronger cation.

This effect of charged combinations of stabilisers has also been seen when zinc ions were used in conjunction with a range of sugars in the stabilisation of rabbit phosphofructokinase by Carpenter et al. [11]. The present results using zinc ions and lactitol to stabilise horseradish peroxidase show a similar increase in the enzyme stability on drying. Again the evidence points towards the importance of the electrostatic charge contributed by the zinc ions to the overall stabilisation effect.

Further work is in progress to determine the response of alcohol oxidase to these stabilisers, this will be reported later after complete evaluation.

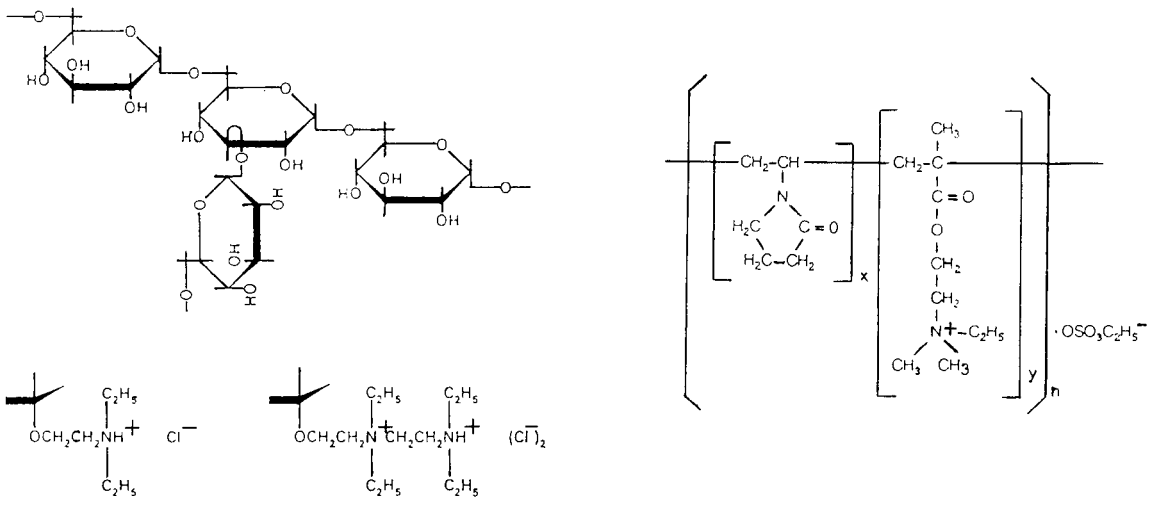

Fig. 3. The molecular structure of dextran is shown above. The 2 position of the polysaccharide backbone is derivatised with diethylaminoethyl groups to give DEAE-dextran, molecular weight 500 000. Direct attachment produces a tertiary amino derivative, whilst "tandem" attachment produces a quaternary as well as a tertiary amino group. "Tandem" groups are present in a 2:1 ratio over the single groups. The structure of Gafquat 755N is also shown. This is a synthetic quaternary polymer of molecular weight about 1 000 000.

Alternative sugars and sugar alcohols

The effect of replacing lactitol with a number of related sugars in the DEAE-dextran/alcohol oxidase system is shown in Fig. 4. In contrast to the charged molecule contribution where structure appears to be less important to the overall stabilising effect, the stucture of the sugars or sugar alcohols used seems to be important for

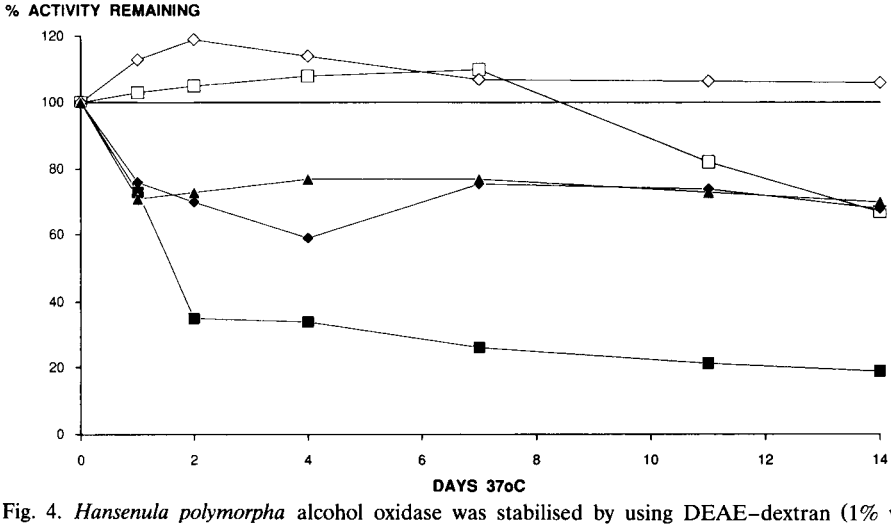

Fig. 4. *Hansenula polymorpha* alcohol oxidase was stabilised by using DEAE-dextran (1% w/v) in combination with lactose, sucrose, inositol or maltitol (5% w/v). The buffer used for drying was sodium phosphate pH 7.0, (100 mM throughout except 10 mM for maltitol) Kinetic assays were carried out in sodium phosphate buffer pH 7.0 (100 mM) containing horseradish peroxidase 2.0 units ml^{-1}, 4-aminoantipyrine (0.4 mM) and 4-hydroxybenzene sulphonic acid Na salt (25.0 mM). Key to symbols: ■ = No stabilisers; □ = DEAE-lactose; ♦ = DEAE-sucrose; ◇ = DEAE-inositol; ▲ = DEAE-maltitol; ——— = 100% activity.

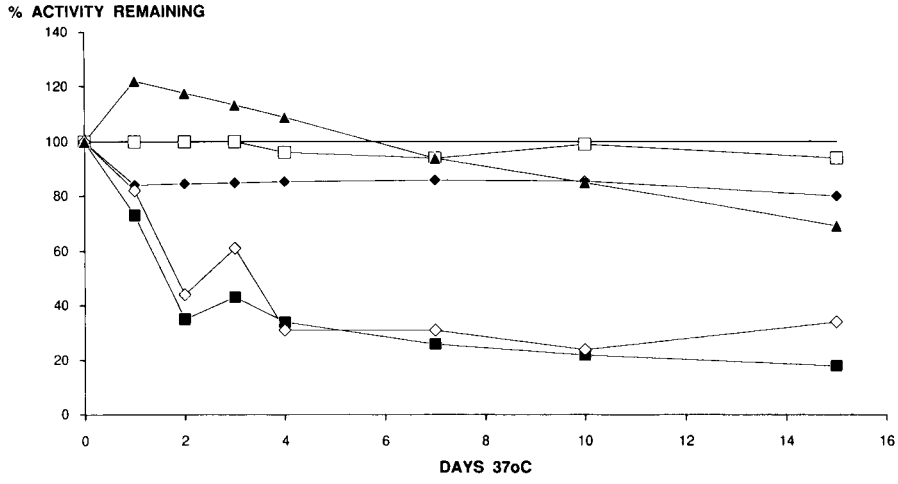

Fig. 5. *Hansenula polymorpha* alcohol oxidase was stabilised by two different unsubstituted neutral dextrans (5% w/v). Also for comparison, the results obtained fron DEAE–dextran and dextran sulphate are shown. The buffer used for drying was sodium phosphate pH 7.0, (100 mM). Kinetic assays were carried out in sodium phosphate buffer pH 7.0 (100 mM) containing horseradish peroxidase 2.0 units ml^{-1}, 4-aminoantipyrine (0.4 mM) and 4-hydroxybenzene sulphonic acid Na salt (25.0 mM). Key to symbols: ■ = No stabilisers; □ = dextran (medical grade); ♦ = Dextran T500; ◇ = DEAE–dextran; ▲ = dextran sulphate; ——— = 100% activity.

stability to be conferred. This observation has been reported by various workers using a number of different enzymes and methods of stabilisation [5–7,9,13,14]. The best two stabilising combinations shown in Fig. 4 are lactose and inositol with DEAE–dextran. Inositol has been found to stabilise alcohol oxidase in the absence of DEAE–dextran (unpublished results) so it is not suprising that it confers stability in this format. Lactitol (4-*O*-β-D-galactopyranosyl-D-glucitol) is itself prepared from lactose (4-*O*-β-D-galactopyranosyl-D-glucose) and is therefore structurally related. Maltitol (4-*O*-α-D-glucopyranosyl-D-glucitol) differs in that the bond between the sugar residues is α rather than β, effectively orientating the glucitol residue downwards relative to the pyranose ring rather than upwards. The effect of this molecular orientation is to reduce the stabilisation effect by 30% as shown in Fig. 4, similarly sucrose (β-D-fructofuranosyl-α-D-glucose) having an α bond also shows an approximate 30% loss of activity.

TABLE 2

Comparison of ethanol reagents stored at 37°C and 4°C

(Duplicate sets of ethanol reagents were stored desiccated at 4°C and 37°C to assess the loss of enzyme activity over 18 days incubation. The results shown above were obtained by measuring the rate of colour formation at 25°C at the different ethanol concentrations shown. Assay conditions given in the data sheets for standard ethanol kits obtained from Leeds Biochemicals were used in all cases)

Ethanol concentration (mg l^{-1})	Absorbance (500 nm min^{-1})		Activity lost (%)
	Storage at 4°C	Storage at 37°C	
200	0.0175	0.014	20.0
500	0.0425	0.035	17.6
1000	0.0875	0.0725	17.1

TABLE 3

Dry stability of enzymes using lactitol and diethylaminoethyl (DEAE)–dextran
(The control results were obtained using enzyme preparations without the stabilisers. Assay procedures for the enzymes listed were carried out as reported in Refs. 8 and 12 or from the enzyme data sheet supplied by the manufacturer)

Enzyme	Enzyme activity remaining (%)		
	Initial	After thermal stress	days at 37°C
Malate dehydrogenase			
Control	14.0	2.0	20
With stabilisers	114.0	96.0	20
Choline oxidase			
Control	63.3	3.9	15
With stabilisers	97.7	80.6	15
Galactose oxidase			
Control	117.0	38.0	16
With stabilisers (inositol) [a]	125.0	117.0	16
Glycerol 3-phosphate oxidase			
Control	110.0	59.7	15
With stabilisers	98.2	111.3	15
Lactate dehydrogenase			
Control	64.0	46.0	54
With stabilisers	81.0	69.0	54
Uricase			
Control	82.0	26.0	15
With stabilisers	91.0	100.0	10
Glucose 6-phosphate Dehydrogenase			
Control	34.3	23.6	16
With stabilisers	94.1	100.4	16
Hexokinase			
Control	57.1	38.9	21
With stabilisers	71.0	71.1	21

[a] Inositol was used instead of lactitol with galactose oxidase, as lactitol was found to be a substrate for the enzyme.

Unsubstituted dextrans

The effect of using unsubstituted dextrans in place of DEAE–dextran and lactitol has been carried out at pH 7.0 in phosphate buffer, the results are shown in Fig. 5. The anionic polymer, dextran sulphate was included for comparitive purposes. It can be seen that the cationic DEAE–dextran (molecular weight 500 000) has little effect on the dry stability of alcohol oxidase at pH 7.0 whereas the unsubstituted dextrans (500 000 molecular weight) have a significant stabilising effect. This is presumably connected to the positive charge on the dextran molecule.

Dextran sulphate, being negatively charged does not show the same effect but initially over the first few days of incubation actually shows an increased stabilisation effect over the neutral dextran molecules. The difference in results of the two unsubstituted dextrans was thought to be due to the relative purity of the preparations, one being a medical grade product and the other not. The success of this trial led to the use of the unsubstituted dextran being tested in the ethanol test kits reported by Gibson et al. [8].

Ethanol test kits

The results obtained for test reagents stabilised using neutral dextran as stabiliser for alco-

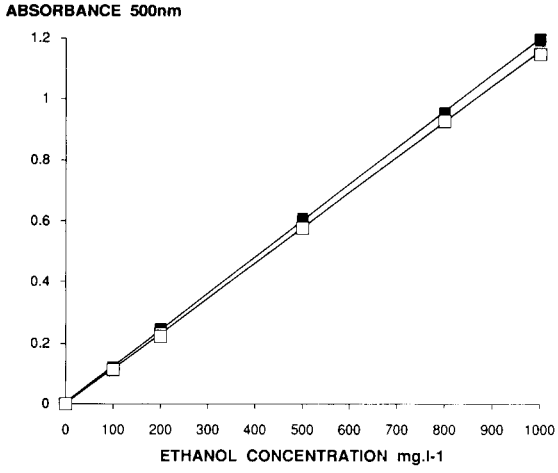

Fig. 6. Ethanol standard curves were constructed using ethanol reagents that were incubated at (■) 4°C and (□) 37°C. The linearity of the response to ethanol was not affected after 18 days incubation using the reaction conditions of the standard ethanol kits supplied by Leeds Biochemicals, (37°C for 20 min).

hol oxidase and horseradish peroxidase are shown in Table 2 and Fig. 6. Table 2 compares the relative rates of colour development from reagents stored at 4°C and 37°C for 18 days. The results from those stored at elevated temperature were consistently lower by 17–20% when compared to results from those stored at 4°C, indicating some loss of enzyme activity.

The results in Fig. 6 show the standard curves obtained from both sets of reagents using the incubation conditions of standard test kits (37°C for 20 min). The absolute response is slightly lower for the reagents stored at 37°C but the linearity is unaffected for the reaction conditions used.

Stabilisation of other enzymes

The stabilisation of a range of other enzymes are shown in Table 3. The enzymes were stabilised using the DEAE–dextran and lactitol combination and stressed at 37°C as before. The results clearly indicate that the stabilising combination has an effect in all cases, sometimes dramatically so. A more moderate response is noticed for lactate dehydrogenase and hexokinase which may indicate an alternative combination of stabilisers may be more effective for these enzymes. Initial experiments indicate that a combination of an anionic polymer and lactitol may confer greater stability on dried lactate dehydrogenase.

REFERENCES

1 P.V. Sundaram, Enz. Microb. Technol., 4 (1982) 290.
2 V.P. Torchilin and K. Martinek, Enz. Microb. Technol., 1 (1979) 74.
3 J.J. Marshall, TIBS, April (1978) 79.
4 K. Martinek, A.M. Klibanov, V.S. Goldmacher and I.V. Berezin, Biochim. Biophys. Acta, 485 (1977) 1.
5 K. Hellman, D.S. Miller and K.A. Cammack, Biochim. Biophys. Acta, 749 (1983) 133.
6 M. Asther and J.-C. Meunier, Enz. Microb. Technol., 12 (1990) 902.
7 W.N. Ye, D. Combes and P. Monsan, Enz. Microb. Technol., 10 (1988) 498.
8 T.D. Gibson, I.J. Higgins and J.R. Woodward, Analyst, 117 (1992) 1293.
9 T.D. Gibson, J.R. Woodward, J.N. Hulbert, S.M. Parker and I.J. Higgins, Biosensors'92 Conference Proceedings, Elsevier, Amsterdam, 1992, p. 163.
10 T.D. Gibson and J.R. Woodward, in P.G. Eldman and J. Wang (Eds.), Biosensors and Chemical Sensors, American Chemical Society, Washington, DC, 1992, Chap. 5, p. 40.
11 J.F. Carpenter, L.M. Crowe and J.H. Crowe, Biochim. Biophys. Acta., 923 (1987) 109.
12 A.W. Wahlfeld, in H.U. Bergmeyer (Ed.) Methods in Enzymic Analysis. Volume III. Oxidoreductases, Section 2.2.2, Verlag Chemie, Weinheim, 1989, p. 126.
13 R.F. Bernier and F.J. Stutzenberger, J. Biotechnol., 7 (1988) 293.
14 J.F. Back, D. Oakenfull and M.B. Smith, Biochemistry, 18 (1979) 5191.

PUBLICATION SCHEDULE FOR 1993

	S'92	O'92	N'92	D'92	J	F	M	A	M	J	J	A
Analytica Chimica Acta	267/1 267/2	268/1 268/2	269/1 269/2	270/1 270/2	271/1 271/2	272/1 272/2 273/1–2	274/1 274/2	275/1–2 276/1 276/2	277/1 277/2	278/1 278/2	279/1 279/2	280/1 280/2
Vibrational Spectroscopy		4/1			4/2		4/3	5/1		5/2		5/3

INFORMATION FOR AUTHORS

Manuscripts. The language of the journal is English. English linguistic improvement is provided as part of the normal editorial processing. Authors should submit three copies of the manuscript in clear double-spaced typing on one side of the paper only. *Vibrational Spectroscopy* also accepts papers in English only.

Abstract. All papers and reviews begin with an Abstract (50–250 words) which should comprise a factual account of the contents of the paper, with emphasis on new information.

Figures. Figures should be prepared in black waterproof drawing ink on drawing or tracing paper of the same size as that on which the manuscript is typed. One original (or sharp glossy print) and two photostat (or other) copies are required. Attention should be given to line thickness, lettering (which should be kept to a minimum) and spacing on axes of graphs, to ensure suitability for reduction in size on printing. Axes of a graph should be clearly labelled, along the axes, outside the graph itself. All figures should be numbered with Arabic numerals, and require descriptive legends which should be typed on a separate sheet of paper. Simple straight-line graphs are not acceptable, because they can readily be described in the text by means of an equation or a sentence. Claims of linearity should be supported by regression data that include slope, intercept, standard deviations of the slope and intercept, standard error and the number of data points; correlation coefficients are optional.

Photographs should be glossy prints and be as rich in contrast as possible; colour photographs cannot be accepted. Line diagrams are generally preferred to photographs of equipment.

Computer outputs for reproduction as figures must be good quality on blank paper, and should preferably be submitted as glossy prints.

Nomenclature, abbreviations and symbols. In general, the recommendations of the International Union of Pure and Applied Chemistry (IUPAC) should be followed, and attention should be given to the recommendations of the Analytical Chemistry Division in the journal *Pure and Applied Chemistry* (see also *IUPAC Compendium of Analytical Nomenclature, Definitive Rules*, 1987).

References. The references should be collected at the end of the paper, numbered in the order of their appearance in the text (*not* alphabetically) and typed on a separate sheet.

Reprints. Fifty reprints will be supplied free of charge. Additional reprints (minimum 100) can be ordered. An order form containing price quotations will be sent to the authors together with the proofs of their article.

Papers dealing with vibrational spectroscopy should be sent to: Dr J.G. Grasselli, 150 Greentree Road, Chagrin Falls, OH 44022, U.S.A. Telefax: (+1-216) 2473360 (Americas, Canada, Australia and New Zealand) or Dr J.H. van der Maas, Department of Analytical Molecule Spectrometry, Faculty of Chemistry, University of Utrecht, P.O. Box 80083, 3508 TB Utrecht, The Netherlands. Telefax: (+31-30) 518219 (all other countries).

0003-2670/93/$06.00

This issue is printed on acid-free paper.

PRINTED IN THE NETHERLANDS

Chromatography of Mycotoxins

Techniques and Applications

edited by **V. Betina**

Journal of Chromatography Library Volume 54

This work comprises two parts, Part A: Techniques and Part B: Applications. In Part A the most important principles of sample preparation, extraction, clean-up, and of established and prospective chromatographic techniques are discussed in relation to mycotoxins. In Part B the most important data, scattered in the literature, on thin-layer, liquid, and gas chromatography of mycotoxins have been compiled. Mycotoxins are mostly arranged according to families, such as aflatoxins, trichothecenes, lactones etc. Chromatography of individual important mycotoxins and multi-mycotoxin chromatographic analyses are also included. Applications are presented in three chapters devoted to thin-layer, liquid, and gas chromatography of mycotoxins.

Contents:

PART A. TECHNIQUES.

1. Sampling, Sample Preparation, Extraction and Clean-up *(V. Betina).* Introduction. Sampling and Sample Preparation. Sample Extraction and Clean-up. Illustrative Example. Conclusions.

2. Techniques of Thin Layer Chromatography *(R.D. Coker, A.E. John, J.A. Gibbs).* Introduction. Clean-up Methods. Normal Phase TLC. Reverse-phase TLC (RPTLC). High Performance Thin Layer Chromatography (HPTLC). Preparative TLC. Detection. Quantitative and Semi-Quantitative Evaluation. Illustrative Examples. Conclusions.

3. Techniques of Liquid Column Chromatography. *(P. Kuronen).* Introduction. Sample Pretreatment. Column Chromatography. Mini-Column Chromatography. High-Performance Liquid Chromatography. Conclusions.

4. Techniques of Gas Chromatography *(R.W. Beaver).* Introduction. Resolution in Gas Chromatography. Extracolumn Resolution. Conclusions.

5. Emerging Techniques: Immunoaffinity Chromatography *(A.A.G. Candlish, W.H. Stimson).* Introduction. Immunoaffinity Chromatography Theory. Practical Aspects and Instrumentation. Sample Preparation. Illustrative Examples.

6. Emerging Techniques: Enzyme-Linked Immunosorbent Assay (ELISA) as Alternatives to Chromatographic Methods *(C.M. Ward, A.P. Wilkinson, M.R.A. Morgan).* Introduction. Principles of ELISA. Sample Preparation. Instrumentation and Practice. Illustrative Examples. Conclusions.

PART B. APPLICATIONS.

7. Thin-Layer Chromatography of Mycotoxins *(V. Betina).* Introduction. Aflatoxins. Sterigmatocystin and Related Compounds. Trichothecenes. Small Lactones. Macrocyclic Lactones. Ochratoxins. Rubratoxins. Hydroxyanthraquinones. Epipolythiopiperazine-3,6-diones. Tremorgenic Mycotoxins. Alternaria Toxins. Citrinin. α-Cyclopiazonic Acid. PR Toxin and Roquefortine. Xanthomegnin, Viomellein and Vioxanthin. Naphtho-γ-pyrones. Secalonic Acids. TLC of Miscellaneous Toxins. Multi-Mycotoxin TLC. TLC in Chemotaxonomic Studies of Toxigenic Fungi. Conclusions.

8. Liquid Column Chromatography of Mycotoxins *(J.C. Frisvad, U. Thrane).* Introduction. Column Chromatography. Mini-Column Chromatography. High Performance Liquid Chromatography. Informative On-line Detection Methods. Conclusions.

9. Gas Chromatography of Mycotoxins *(P.M. Scott).* Introduction. Trichothecenes. Zearalenone. Moniliformin. Alternaria Toxins. Slaframine and Swainsonine. Patulin. Penicillic Acid. Sterigmatocystin. Aflatoxins. Ergot Alkaloids. Miscellaneous Mycotoxins. Conclusions.

Subject Index.

1993 xiv + 440 pages
Price: US $ 180.00 / Dfl. 315.00
ISBN 0-444-81521-X

ORDER INFORMATION

For USA and Canada
ELSEVIER SCIENCE PUBLISHERS
Judy Weislogel,
P.O. Box 945
Madison Square Station,
New York, NY 10160-0757
Fax: (212) 633 3880

In all other countries
ELSEVIER SCIENCE PUBLISHERS
P.O. Box 211,
1000 AE Amsterdam
The Netherlands
Fax: (+31-20) 5803 705

US$ prices are valid only for the USA & Canada and are subject to exchange rate fluctuations; in all other countries the Dutch guilder price (Dfl.) is definitive. Customers in the European Community should add the appropriate VAT rate applicable in their country to the price(s). Books are sent postfree if prepaid.

ELSEVIER
SCIENCE PUBLISHERS

0003-2708(19930701)279:1;1-U